

PROCEEDINGS

20th International Conference on Harmful Algae

"HAB Science and Human Well-being"

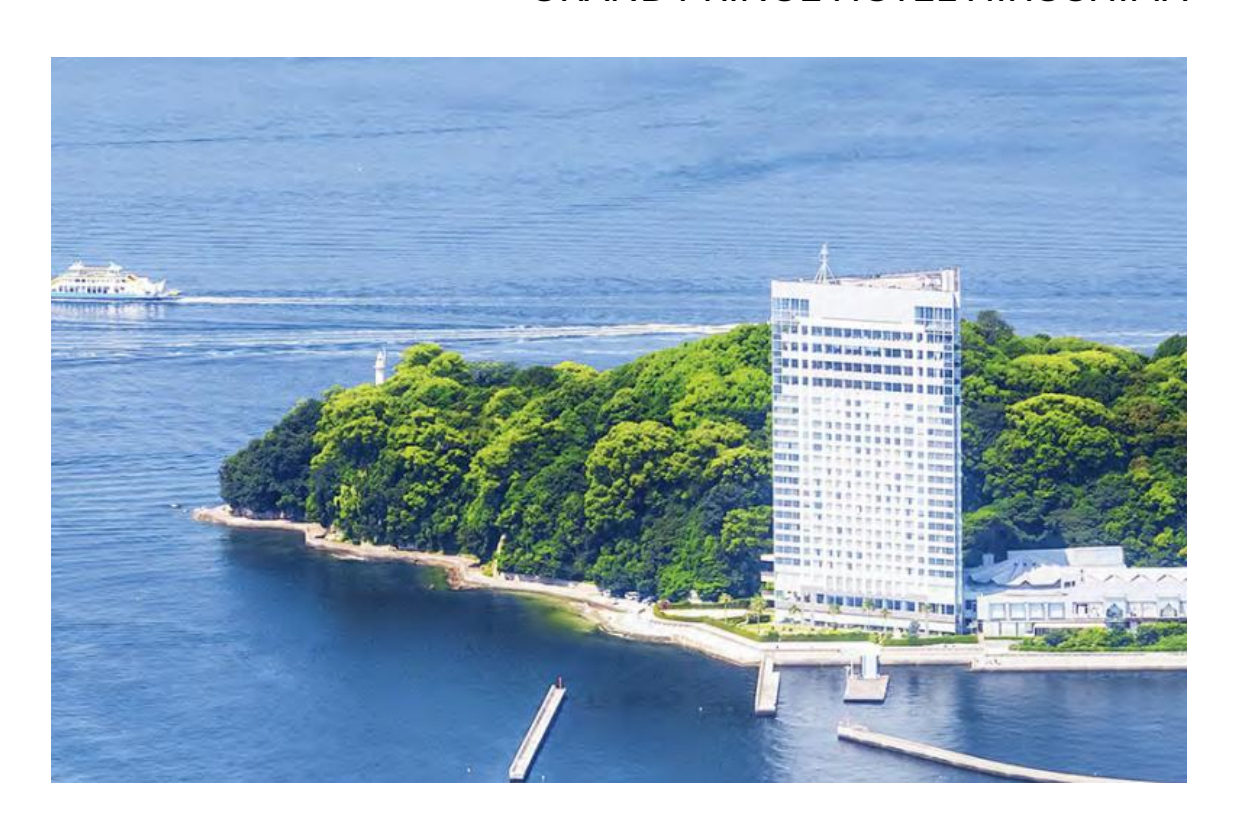






November 2023

GRAND PRINCE HOTEL HIROSHIMA



SPONSORS ACKNOWLEDGMENTS

The Organizing Committee wishes to warmly thank the following companies for their support and contribution:

PLATINUM PARTNER



GOLD PARTNERS



Genetics of Toxin Production and Prediction

SILVER PARTNERS









OTHER PARTNERS

Restar Communications Corporation
Hinomarusangyou Corporation
Satake Corporation
Plantbio Co., LTD
Am-Lab Inc.
Laboratory of Aquatic Science Consultant Co.,LTD.
Kyokko Trading Co., LTD
Regional-Design Co., LTD
JFE West Japan GS Co., LTD
JEOL LTD

SUPPORTING ORGANIZATIONS

Hiroshima University The Japanese Society of Fisheries Science The Plankton Society of Japan The Oceanographic Society of Japan The Japanese Society of Phycology **Japanese Society of Fisheries Oceanography** Japanese Society of Microbial Ecology Society of Genome Microbiology, Japan **Japan Fisheries Research and Education Agency Prefectural University of Hiroshima International EMECS Center** Research Institute for Seto Inland Sea **Hiroshima Prefecture** Hatsukaichi City **Hiroshima City Higashihiroshima City Hiroshima Convention & Visitors Bureau** Fisheries Agency Ministry of the Environment, Japan Ministry of Health, Labour and Welfare, Japan "The International Society for the Study of Harmful Algae" (ISSHA)

PREFACE

As the global outbreak of the novel coronavirus (COVID-19) has finally calmed down, we are delighted to welcome participants to the 20th International Conference on Harmful Algae (ICHA 2023) in Hiroshima, Japan, from November 5–10, 2023. This marks the first in-person ICHA in five years, bringing together more than 500 participants from 40 countries to exchange knowledge, foster collaborations, and advance research on harmful algal blooms (HABs). The Local Organizing Committee (LOC) and the Scientific Committee (SC) of ICHA 2023 extend our sincere gratitude to the International Society for the Study of Harmful Algae (ISSHA) executives and all participants for their support and cooperation in making this event a reality. Organizing ICHA 2023 came with its challenges, as the LOC navigated the lingering effects of the COVID-19 pandemic and rising global costs. Given these circumstances, we greatly appreciate the understanding and support of ISSHA members in adapting to an exclusively in-person format, despite our initial plans for a hybrid meeting.

Japan has a deep-rooted connection with its coastal environment, a relationship encapsulated by the concept of "Sato-Umi," where human interactions with marine ecosystems have historically enhanced biological productivity and biodiversity. In alignment with this philosophy, the theme of ICHA 2023, "HAB Science and Human Well-being," reflects our commitment to advancing scientific understanding of HABs while promoting their effective management for the benefit of society, fisheries, and ecosystem health. Our goal is to exchange relevant scientific knowledge, enabling better predictions of HAB occurrences, improved mitigation strategies, and a deeper understanding of their ecological and socio-economic impacts.

The scientific program of ICHA 2023 showcases the latest advancements in HAB research, featuring an Opening Lecture, nine Plenary Lectures by distinguished experts, 216 oral presentations, 199 poster presentations, and 45 ignite talks spanning 16 key research themes, including:

- Ecology
- Biology and Biogeography
- Community/Species Interactions
- Taxonomy
- Microbiomes and Omics
- o Prediction and Modeling
- Monitoring and Mitigation
- Ciguatera and Benthic-, Ichthyotoxic- and Cyanobacterial HABs
- o Toxins, Biosynthesis and Detection Methods
- Toxicology
- Surveillance and Management
- o HABs in a Changing World
- Socio-Economic Impacts and Emerging Issues

A significant highlight of ICHA 2023 was the panel discussions and special sessions dedicated to HAB mitigation, new monitoring technologies, and interdisciplinary approaches to tackling the challenges posed by HABs. These sessions facilitated interactive discussions among researchers, industry representatives, and policy advisors, enabling knowledge transfer and the development of innovative solutions.

In addition to the rich scientific program, ICHA 2023 provided an opportunity to experience Hiroshima's historical and cultural heritage, reminding us of the importance of environmental stewardship and sustainable development. Social events, including guided cultural tours, networking receptions, and the conference banquet, provided a warm and welcoming environment for participants to strengthen professional relationships and build new collaborations. The success of ICHA 2023 would not have been possible without the dedication of numerous individuals and organizations. We extend our deepest appreciation to Dr. Wayne Litaker, former ISSHA President, for his tremendous support over the past year, as well as to our sponsors, scientific steering committees, session chairs, and peer reviewers, whose contributions were essential in maintaining the quality and integrity of the conference proceedings. We are also sincerely grateful for the generous support from international organizations, government agencies, private sponsors, and local institutions, along with the tireless efforts of the local organizing committee, volunteers, and technical staff, all of whom ensured the seamless execution of this event.

This proceedings volume includes 30 peer-reviewed contributions, covering a wide range of HAB-related topics, from fundamental research on HAB biology and toxin biosynthesis to applied studies on HAB monitoring, mitigation, and management strategies. We hope that these contributions will serve as a valuable resource for researchers, practitioners, and decision-makers, providing new insights into the complexities of HABs and supporting the development of effective mitigation and policy measures.

As we celebrate the achievements of ICHA 2023, we also look ahead to the 21st International Conference on Harmful Algae (ICHA 2025), which will be hosted in Punta Arenas, Chile. We extend our deepest gratitude to all participants for their dedication, enthusiasm, and commitment to advancing HAB research and management. The discussions, collaborations, and innovations shared at this conference will undoubtedly shape the future of HAB science and contribute to sustainable solutions for addressing harmful algal blooms worldwide.

We look forward to continuing these vital conversations and collaborations at ICHA 2025, and we hope to see you all again as we strive to further our understanding of HABs and their impact on marine and freshwater ecosystems.

With sincere appreciation,

Ichiro Imai

Chair of ICHA 2023 Hiroshima, Japan

COMMITTEES

LOCAL ORGANIZING COMMITTEE

Akira Ishikawa

Mie University

Fumito Maruyama

Hiroshima University

Goh Nishitani

Tohoku University

Ichiro Imai, Chair

Hokkaido University

Kanako Naito

Prefectural University of

Hiroshima

Kazuhiko Koike, Vice Chair

Hiroshima University

Keizo Nagasaki

Kochi University

Kenji Tarutani

Japan Fisheries Research and

Education Agency

Masao Adachi

Kochi University

Mitsunori Iwataki

University of Tokyo

Natsuko Nakayama

Japan Fisheries Research and

Education Agency

Ryoji Matsushima

Japan Fisheries Research and

Education Agency

Satoshi Nagai, Vice Chair

Japan Fisheries Research and

Education Agency

Setsuko Sakamoto

Japan Fisheries Research

and Education Agency

Shigeru Itakura

Okabe Co., Ltd.

Shizuka Ohara

Hiroshima University

Takashi Kamiyama

Japan Fisheries Research and

Education Agency

Toshiyuki Suzuki, Vice Chair

Japan Fisheries Research and

Education Agency

Yoichi Miyake

Japan Fisheries Research and

Education Agency

Yuji Tomaru

Japan Fisheries Research and

Education Agency

SCIENTIFIC COMMITTEE

Akihiro Tuji

National Museum of Nature

and Science

Akira Miyazono

Hokkaido Research

Organization

Hirotaka Kitaguchi

Fukuyama University

Ho-Dong Park

Shinshu University

Albert Valdish Manuel

Japan Fisheries Research and Education Agency

Atsushi Mitsutani

Fukuyama University

Atsushi Yamaguchi

Hokkaido University

Goh Onitsuka

Japan Fisheries Research and Education Agency

Hajime Uchida

Japan Fisheries Research and Education Agency

Haruo Yamaguchi

Kochi University

Hiroshi Shimada

Hokkaido Research Organization

Kunihiro Okano

Akita Prefectural University

Koki Yuasa

Japan Fisheries Research and Education Agency

Masafumi Natsuike

Hokkaido Research Organization

Masaki Fujita

Hokkaido University

Masayuki Satake

University of Tokyo

Naoki Yoshie

Ehime University

Naoyoshi Nishibori

Shikoku University

Kanako Ishikawa

Lake Biwa Environmental Research Institute

Kazumi Wakita

Tokai University

Kazutaka Miyahara

Hyogo Prefectural Technology Center for Agriculture, Forestry and Fisheries

Kazuyoshi Miyamura

Oita Prefectural Agriculture, Forestry and Fisheries Research Center

Kei Kimura

Saga University

Keigo Yamamoto

Research Institute of Environment, Agriculture and Fisheries, Osaka Prefecture

Ken-Ichiro Ishii

Seed Bank Co. Ltd.

Tadashi Matsubara

Japan Fisheries Research and Education Agency

Taisuke Ohtsuka

Lake Biwa Museum, Shiga Prefecture

Takafumi Yoshida

Northwest Pacific Region Environmental Cooperation Center

Tetsuya Nishikawa

Hyogo Prefectural Technology Center for Agriculture, Forestry and Fisheries

Tomohiro Nishimura

Japan Fisheries Research and Education Agency

Toshiya Katano

Tokyo University of Marine Science and Technology

Yasuhiro Yamasaki

National Fisheries University

Nobuharu Inaba

Public Works Research

Institute

Ryuichi Watanabe

Japan Fisheries Research and

Education Agency

Shigeru Sato

Kitasato University

Shoko Ueki

Okayama University

Yutaka Okumura

Japan Fisheries Research and

Education Agency

Yohei Shimasaki

Kyushu University

Yuichi Hayami

Saga University

Yuichiro Yamada

Kitasato University

Yuko Cho

Tohoku University

INTERNATIONAL ADVISORY BOARD

Allan Cembella

Germany

Ana Amorim

Portugal

Andrew Turner

United Kingdom

Arjun Verma

Australia

Aurelia Tubaro

Italy

Beatriz Reguera

Spain

Bernd Krock

Germany

Carolin Peter

Sweden

Christina Marampouti

Netherlands

Christine Band Schmidt

Mexico

Christopher Bolch

Australia

Christopher Gobler

United States

Chui Pin Leaw

Malaysia

Donald M. Anderson

United States

Elin Lindehoff

Sweden

Esther Garcés

Spain

Gustaaf Hallegraeff

Australia

Hans Paerl

United States

Helene Hegaret

France

Henrik Enevoldsen

Denmark

lan Jenkinson

China

Ichiro Imai

Japan

Ingrid Sassenhagen

Germany

Jiangtao Wang

China

Keith Davidson

United Kingdom

Leonardo Guzmán

Chile

Dedmer van de Waal

Netherlands

Lorena Durán Riveroll

Mexico
Luiz Mafra
Brazil

Marie-Yasmine Dechraoui Bottein

France

Marta Estrada

Spain

Mitsunori Iwataki

Japan

Nina Lundholm

Denmark
Paulo Vale
Portugal
Philipp Hess

France
Po Teen Lim
Malaysia

Lisa Campbell

United States

Santiago Fraga

Spain

Satoshi Nagai

Japan

Seung Ho Baek

Rebyblic of Korea

Shauna Murray

Australia

Steffaney Wood

United States

Tim Harwood

New Zealand

Uwe John

Germany

Vera L. Trainer

United States

Wayne Litaker

United States

EDITORS

Ichiro Imai

Ryoji Matsushima

Satoshi Nagai

Goh Nishitani

Setsuko Sakamoto

Toshiyuki Suzuki

REVIEWERS

Ana Amorim

Donald M. Anderson

Christine J. Band-Schmidt

Christopher J. Bolch

Luis M. Botana

Lisa Campbell

Allan D. Cembella

Yuko Cho

Keith Davidson

Marta Estrada

Masaki Fujita

Gustaff Hallegraeff

Philipp Hess

Nobuharu Inaba

Ian R. Jenkinson

Uwe John

Toshiya Katano

Bernd Krock

Chui Pin Leaw

Nina Lundholm

Luiz L. Mafra Jr.

Christina Marampouti

Marina Montresor

Masafumi Natsuike

Tomohiro Nishimura

Shizuka Ohara

Yutaka Okumura

Goh Onitsuka

Beatriz Reguera

Setsuko Sakamoto

Masayuki Satake

Yohei Shimasaki

Shoko Ueki

Paulo Vale

Kazumi Wakita

Jiangtao Wang

Haruo Yamaguchi

Keigo Yamamoto

Yasuhiro Yamasaki

TABLE OF CONTENTS

Taxonomy

Epibenthic dinoflagellates from the southern Gulf of California
Ciguatera and Benthic HABs
Measuring diel migration in lab cultures of <i>Gambierdiscus</i>
Ostreopsis cf. ovata trends in the Conero Riviera (northern Adriatic Sea) over 14 years25
Stefano Accoroni, Francesca Neri, Marika Ubaldi, Tiziana Romagnoli, Cecilia Totti
Biology and Biogeography
Current status of expansion of HAB species in Hokkaido, northern Japan, with special reference to large-scale dispersal of <i>Karenia mikimotoi</i> via ocean current system
Hiroshi Shimada, Masatoshi Sato, Akiyoshi Shinada, Daichi Arima, Tomoaki Yasunaga, Makoto Kanamori, Hiroshi Kuroda, Setsuko Sakamoto, Ichiro Imai
HABs in a Changing World
Analysis of surface harmful algal blooms in the Tropical Mexican Pacific: A remote sensing approach33
Sinuhé Hernández Márquez, María Eugenia Zamudio-Resendiz, María Luisa Núñez-Resendiz, Felipe Omar Tapia Silva, Kurt Martin Dreckmann, Abel Sentíes
Effects of ocean acidification on the growth and domoic acid production of the diatom <i>Pseudo-nitzschia multiseries</i> from the California Current System37 William P. Cochlan, Christopher E. Ikeda, Brian D. Bill, Vera L. Trainer, Charles G. Trick

Prediction and Modeling

Application of a quantitative molecular methods to characterize abundance and distribution of Alexandrium cysts for NOAA's HAB Forecasting.......41 Cheryl Greengrove, Steve Kibler, Julie Masura, Julie Matweyou, Courtney Hart, Mark Vandersea, Tyler Harman

Toxicology

Ecology

Monitoring and Mitigation

Impact of drought and wildfires in recent trends of Diarrhetic Shellfish Toxins in

the period 2001-2023
Investigation of Limit of Detection and Quantification for digital PCR assays: the case study of <i>Azadinium spinosum</i> (Dinophyceae) in Irish waters69 Nicolè Caputo, Dave Clarke, Francesca Cucchi, Fiona Kavanagh, Luca Mirimin
Using particle size distribution (PSD) to automate imaging flow cytobot (IFCB) data quality in coastal California, USA
In-situ segmentation and post-processing of phytoplankton image data suitable for an autonomous surface vehicle
A mini-review on environmentally friendly strategies against HABs81 Ichiro Imai, Keigo Yamamoto, Nobuharu Inaba
Toxins, Biosynthesis and Detection Methods
Branched-chain fatty acids in 7- <i>O</i> -acyl okadaite esters from bivalves85 Paulo Vale, Hajime Uchida, Toshiyuki Suzuki
New azaspiracid analogues produced by <i>Azadinium spinosum</i> isolated from Japanese coastal waters89
Mayu Ozawa, Hajime Uchida, Satoshi Numano, Ryuichi Watanabe, Ryoji Matsushima, Hiroshi Oikawa, Kazuya Takahashi, Mitsunori Iwataki, Toshiyuki Suzuki
Toxin analysis of Kareniaceae cultures isolated from the northern coastal waters
in Japan

The magical mystery tour that is the Dinoflagellate sterolysin biosynthesis some assembly (correction) required
Allen R. Place, Ernest P Williams, Saddef Haq, Tsevtan R. Bachvaroff
Microbiomes and Omics
Translational costs and regulation in <i>Amphidinium carterae</i> : Insights from synchronized cultures with a novel quantification method
Diversity of HABs from the Texas coast (Gulf of Mexico) with a focus on extreme events: a full length 18S rDNA metabarcoding approach
Microbiomes of <i>Gambierdiscus lewisii</i> from the Great Barrier Reef, Queensland, Australia
Genomics and eco-active organic matter in the oceans: the roles of harmful and other algae, with emphasis on physical effects
Surveillance and Management
Citizen science participation can increase the coverage and speediness in harmful microalgae blooms detection
Performance of high-throughput microfluidic real-time qPCR technology for the simultaneous detection of six <i>Alexandrium</i> species in environmental samples
Francis Butler, Luca Mirimin

Biotoxins profile in mussels of the Northern Adriatic Sea in the last decade (2012-2022): major contamination events and correlation with toxic phytoplankton...125 Giorgia Zoffoli, Franca Guerrini, Laura Pezzolesi, Monica Cangini, Sonia Dall'Ara, Silvana Vanucci, Rossella Pistocchi

Epibenthic dinoflagellates from the southern Gulf of California

A.E. Ramos-Santiago^{1*}, I. Leyva-Valencia^{1,2}, C.J. Band-Schmidt¹, Y.B. Okolodkov³

¹Instituto Politécnico Nacional, Centro Interdisciplinario de Ciencias Marinas (IPN-CICIMAR), Av. Instituto Politécnico Nacional s/n, Col. Playa Palo de Santa Rita, La Paz, Baja California Sur, 23079, Mexico;
 ²Secretaría de Ciencia, Humanidades, Tecnología e Innovación (SECIHTI); Instituto Politécnico Nacional, Centro Interdisciplinario de Ciencias Marinas (IPN-CICIMAR), Av. Instituto Politécnico Nacional s/n, Col. Playa Palo de Santa Rita, La Paz, Baja California Sur, 23079, Mexico;
 ³Instituto de Ciencias Marinas y Pesquerías, Universidad Veracruzana (ICIMAP-UV), Mar Mediterráneo 314, Fracc. Costa Verde, Boca del Río, Veracruz, 94294, Mexico.

*corresponding authors' emails: cbands@ipn.mx; ileyvav@ipn.mx

Abstract

The ecological role of epibenthic dinoflagellates in shallow ecosystems consists of their participation in matter and energy transfer between sediments and the water column. The aim of this study was to perform the morphological identification of epibenthic dinoflagellates isolated from the southern Gulf of California. Samples were collected in Bahía Concepción, Bahía de La Paz, and Ensenada de La Paz. Dinoflagellate cells were isolated from macroalgal samples collected at depths of < 10 m and from horizontal tows that were carried out in shallow water (< 2 m). Currently, at IPN-CICIMAR, 34 strains of epibenthic dinoflagellates isolated between 2015 and 2022 are cultured under varying conditions. They were maintained at salinities of 32, 34 and 36, temperatures of 24 °C and 30 °C, and a light/dark cycle of 12 h:12 h, with an illumination of 150 μmol E m⁻² s⁻¹ in modified K and GSe media. The strains were identified by light and scanning electron microscopy as 13 species from the genera Amphidinium, Coolia, Ostreopsis, Gambierdiscus, Prorocentrum, Symbiodinium and Vulcanodinium. In this study, only short light microscopy descriptions are provided. The morphological characteristics obtained by light microscopy allowed the identification of Coolia malayensis; however, most strains were tentatively identified to species level with the information provided by this tool. In some cases, interspecific morphological differences are subtle (e.g., between Prorocentrum cassubicum and Prorocentrum norrisianum), making it difficult to identify species based only on morphological characteristics. Therefore, the combination of morphological and molecular tools is needed for accurate species identification.

Keywords: cultures, epibenthic dinoflagellates, morphology, Gulf of California, Mexico.

https://doi.org/10.15027/0002041256

Introduction

Epibenthic dinoflagellates are associated mainly with shallow waters. They are distributed in tropical, subtropical, and temperate zones. Their habitats include macroalgae, seagrasses, mangroves, floating detritus, sand, mud, dead corals, and marine animals, mainly invertebrates. A total of 242 marine benthic dinoflagellate species from 63 genera are known (Hoppenrath *et al.*, 2023).

The current morphological and molecular taxonomy of epibenthic dinoflagellates is complex due to the species with similar morphological and

molecular characteristics. Some common species complexes are: *Coolia monotis*, *Gambierdiscus toxicus*, *Prorocentrum rhathymum* and *Ostreopsis ovata* (Gómez *et al.*, 2017; Ramos-Santiago *et al.*, 2022; Hoppenrath *et al.*, 2023). Therefore, identification to species level requires the inclusion of morphological and molecular traits.

Epibenthic dinoflagellates can produce benthic harmful algal blooms (BHAB). BHAB may be overlooked because of our inability to see them from the water surface, unlike pelagic blooms caused by planktonic species. These events can potentially have negative consequences for aquatic ecosystems, the economy, and human health

(Moreira-González et al., 2021). Some genera include toxic species: Amphidinium Claperède & Lachmann, Gambierdiscus R. Adachi & Y. Fukuyo, Coolia Meunier, Prorocentrum Ehrenberg, Ostreopsis J. Schmidt, and Vulcanodinium E. Nézan & N. Chomérat.

Materials and Methods

Study area and field work

Samples were taken from nine sites: one site in Bahía Concepción, five sites in Bahía de La Paz (La Gaviota Island and El Sauzoso, Las Parcelas, and El Tecolote beaches) and three sites in the Ensenada de La Paz. Various macroalgal species, and sediments were obtained by free diving or SCUBA at depths of < 10 m. In shallow water (< 2 m) horizontal tows were taken with a 10 μ m mesh phytoplankton net.

Isolation and culture

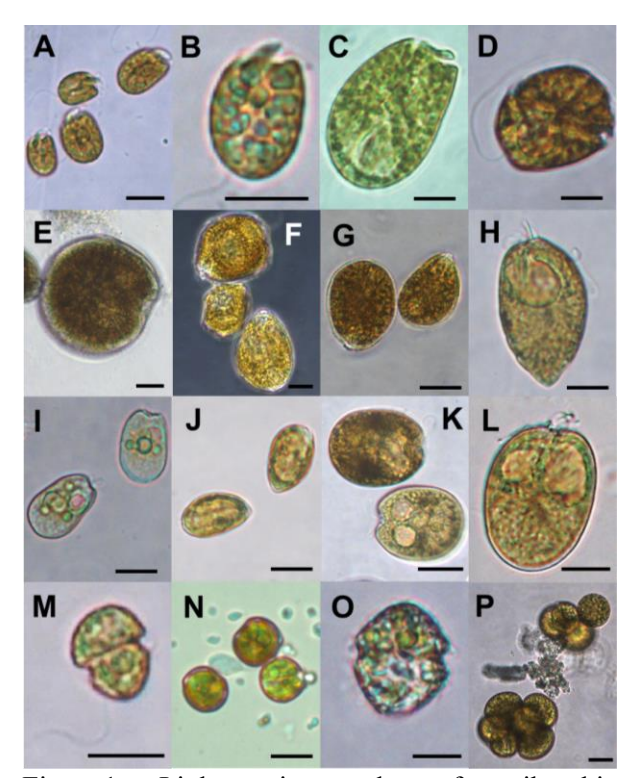
Vegetative dinoflagellate cells were isolated under an inverted microscope Carl Zeiss AXIO Vert.A1. Dinoflagellates were separated by capillary action in small drops of K medium (Keller *et al.*, 1987) and modified GSe medium (Bustillos-Guzmán *et al.*, 2015). A gradual scale-up was performed until cultures with a volume of 20 mL were obtained. The strains were maintained at salinities of 32, 34 and 36, temperatures of 24 °C and 30 °C, under a 12 h:12 h light/dark cycle with an illumination of 150 μmol E m⁻² s⁻¹.

Results and Discussion

The morphology of 34 strains of epibenthic dinoflagellates was described; 13 species of seven genera were identified: *Amphidinium*, *Coolia*, *Gambierdiscus*, *Ostreopsis*, *Prorocentrum*, *Symbiodinium* and *Vulcanodinium*. General morphological features of live cells observed under light microscopy are described below (Fig. 1).

Two species of the order Amphidiniales were identified. *Amphidinium carterae* Hulburt (Fig. 1A-B) is a naked dinoflagellate, with asymmetrical, ventrally oval, and dorsoventrally flattened cells (Ramos-Santiago, 2023). The epicone is asymmetrical, crescent-shaped, deflected to the left-upward; the cell is broadest in the median line. Chloroplasts are numerous and yellow-green. Pyrenoid is central, ring-shaped. No pusules were observed. *Amphidinium* cf. *operculatum* Claparède

& Lachmann (Fig. 1C) is ovoid to ellipsoidal in ventral view. The epicone is asymmetrical, triangular, and deflected to the left in ventral view. The hypocone is convex on the right side, almost straight on the left side and broadly rounded in the posterior part; the cell is broadest below the median line. No pusules or pyrenoids were observed.



epibenthic Light micrographs of dinoflagellates from the southern Gulf California. A-B) Amphidinium carterae. C) Amphidinium cf. operculatum. D) malayensis. E) Gambierdiscus carpenteri. F) Ostreopsis cf. lenticularis. G) Ostreopsis cf. ovata. H) Prorocentrum koreanum. I) Prorocentrum cf. cassubicum. J) Prorocentrum triestinum. K) Prorocentrum concavum. L) Prorocentrum rhathymum. M-N) Symbiodinium natans-clade A, and O-P) Vulcanodinium rugosum. Scale bar: 10 um in A-D, H-J, L, O; 20 um in E-G, K, P.

From the order Gonyaulacales, species of *Coolia*, *Gambierdiscus* and *Ostreopsis* were identified. *Coolia malayensis* Leaw, P.-T. Lim & Usup (Fig. 1D) is rounded and has anteroposteriorly compressed cells (Ramos-Santiago *et al.* 2022). The epitheca is slightly smaller than the hypotheca. The cingulum is deeply excavated, descending, and displaced one cingulum width. Chloroplasts are numerous, semicircular, golden-green. *Gambierdiscus carpenteri* cells (Fig. 1E) are

anteroposteriorly compressed, lenticular (Ramos-Santiago *et al.*, 2024). Chloroplasts are numerous, brown-green.

Table 1. Cell sizes of epibenthic dinoflagellate species from the southern Gulf of California. N: Number of measured cells.

Species	Length	Width	
Species	(µm)	(µm)	
Amphidinium	12.9–14.4	9.5-10	
carterae	(N=66)	9.3-10	
A. cf. operculatum	29.5–36.9	25.4–21.3	
A. Cl. operculatum	(N=40)	23.4–21.3	
Coolia malayensis	25–38.1	21.6–33.7	
Cootta matayensis	(N=174)	21.0-33.7	
Gambierdiscus	58-94.9	84.3-90.5	
carpenteri	(N=47)	84.3-90.3	
Ostreopsis cf.	56.8-83.2	46 – 67.2	
lenticularis	(N=69)	40 - 07.2	
O. cf. ovata	43.4–59.6	28.2–44	
O. Cl. Ovala	(N=67)	28.2 -44	
Prorocentrum	35.4–42.5	18.3–30.5	
koreanum	(N=107)	16.5- 50.5	
P. cf. cassubicum	16.9–20	10.7–12.9	
1. Cl. cassuoteam	(N=38)	10.7-12.7	
P. triestinum	19.7–21.8	10–11.9	
1. II testinum	(N=35)		
P. concavum	41.5–45.5	34.2-41.8	
1. concavam	(N=77)	34.4-41.6	
P. rhathymum	25.8–32.7	18.7–23.3	
1. mainyman	(N=189)	10.7-23.3	
Symbiodinium natans-	9.7–12.1		
clade A (mobile	(N=69)	6.2–9	
stage)	(11 07)		
Vulcanodinium	20.9–26.5		
rugosum (mobile	(N=33)	18–23	
stage)	(14-33)		

Two morphotypes of *Ostreopsis* were observed. The large-celled morphotype was identified as *Ostreopsis* cf. *lenticularis* Y. Fukuyo (Fig. 1F). Cells were lenticular, more or less oval in ventral/dorsal view, with a colorless and pointed ventral zone. Chloroplasts are numerous, greenbrown. The small-celled morphotype was identified as *Ostreopsis* cf. *ovata* Y. Fukuyo (Fig. 1G) (Ramos-Santiago, 2023). Cells show the typical *Ostreopsis* droplet or teardrop shape (Hoppenrath *et al.*, 2023). Chloroplasts are numerous and yellow-brown. One to two pusules were observed in both *Ostreopsis* species.

Five species of the order Prorocentrales were identified from macroalgae and surrounding water (Ramos-Santiago 2023). Prorocentrum koreanum M.-S. Han, S.Y. Cho & P. Wang (Fig. 1H) shows heart-shaped and pyriform cells. In the anterior part, 1 to 3 pusules were observed. Chloroplasts are numerous, green-brown. The periflagellar zone is wide and shallow. It has a straight, winged apical spine, directed forward. No pyrenoid was observed. This species is considered planktonic; however, it is recurrent in samples of benthic substrates and has therefore been considered for this Prorocentrum cf. cassubicum M.A. Faust & S.L. Morton cells (Fig. 1I) are oval to oblong and asymmetrical. Chloroplasts are numerous, greenyellow, peripheral. Pyrenoid is central, ring-shaped. The periflagellar area is V-shaped. There are 1 to 3 pusules near the periflagellar area. Cells lack a developed apical spine. Prorocentrum triestinum J. Schiller cells (Fig. 1J) are asymmetrical, with a broadly rounded anterior end and a posterior area with a pointed posterior end. Pusule is located in the anterior part. Chloroplasts are green-yellowbrown, elongated, with multiple lobules, peripheral. No pyrenoid was observed. The species differs from a morphologically similar P. redfieldii Bursa in the cell shape and the size of the apical spine, which is shorter in P. triestinum (Tillmann et al., 2021). The species is usually planktonic; however, it was also isolated from coralline turfs in New Zealand (Rhodes & Smith, 2019). Prorocentrum concavum Y. Fukuyo (Fig. 1K) has broad, oval, symmetrical, dorsoventrally flattened cells, with 2 to 3 pusules near the periflagellar area. Chloroplasts are golden-brown. The pyrenoid is central, ring-shaped. Prorocentrum rhathymum A.R. Loeblich III, Sherley & R.J. Schmidt cells (Fig. 1L) are asymmetrical, oval to oblong, with rounded margins. One to two pustules are present in the anterior part. Chloroplasts are green-brown. The periflagellar area is broadly U-shaped. The apical spine is poorly developed.

Two strains were identified as *Symbiodinium natans*-clade A from the order Suessiales (Ramos-Santiago *et al.*, 2025). The group showed two stages, one of them with mushroom-shaped mastigote cells (Fig. 1M). The epicone is slightly larger than the hypocone. Brownish reticulate chloroplasts are located at the periphery of the cells. Pyrenoid is almost central. Cells of the other stage are non-motile, coccoid (Fig. 1N).

Vulcanodinium rugosum Nézan & Chomérat from the order Peridiniales has vegetative cells with numerous green-brown chloroplasts. The cells have a conical epitheca and truncated apex (Fig. 1O) (Ramos-Santiago, 2023). Cells of non-motile stage are spherical, smooth, grouped in pairs or forming clusters of many daughter cells (Fig. 1P).

Acknowledgements

We thank A. Evhelin-Mendez of the University of Tennessee (Knoxville, TN, USA) and Marcia M. Gowing (Seattle, WA, USA) for improving the English style. This study was financed with the projects CONAHCyT A1-S-14968, CONAHCyT PRONAII, PRONACES SSyS 319104 and the institutional project SIP-2024-0544. A.E.R.S. received a scholarship of CONAHCyT (1151607) and from BEIFI (B210365). C.J.B.S. is a COFAA and BEIFI recipient.

References

- Bustillos-Guzmán, J. J., Band-Schmidt, C. J., Durán-Riveroll, L. M., Hernández-Sandoval, F. E. *et al.* (2015). Paralytic toxin profile of the marine dinoflagellate *Gymnodinium catenatum* Graham from the Mexican Pacific as revealed by LC-MS/MS. Food Addit. Contam. Part A, 1-14.
- Gómez, F., Qiu, D., Lin, S. (2017). The synonymy of the toxic dinoflagellates *Prorocentrum mexicanum* and *P. rhathymum* and the description of *P. steidingerae* sp. nov. (Prorocentrales, Dinophyceae). J. Eukaryot. Microbiol. 64(5), 668-677.
- Hoppenrath, M., Chomérat, N., Horiguchi, T., Murray, S. A. *et al.* (2023). Marine benthic dinoflagellates their relevance for science and society. 2nd ed. E. Schweizerbart'sche Verlagsbuchhandlung (Nägele u. Obermiller) and Senckenberg Gesellschaft für Naturforschung, Stuttgart, Germany, 376 pp.
- Keller, M. D., Selvin, R. C., Claus, W., Guillard, R. R. L. (1987). Media for the culture of oceanic ultraplankton. J. Phycol. 23, 633-638.
- Moreira-González, A. R., Comas-González, A., Valle-Pombrol, A., Seisdedo-Losa, M. *et al.* (2021). Summer bloom of *Vulcanodinium rugosum* in Cienfuegos Bay (Cuba) associated to

- dermatitis in swimmers. Environ. Sci. Technol. Lett. 757, 143782.
- Ramos-Santiago, A. E., Band-Schmidt, C. J., Leyva-Valencia, I., Muñoz-Ochoa, M. *et al.* (2022). Análisis morfológico y molecular de *Coolia malayensis* (Dinophyceae) y efectos de extractos de la macroalga *Dictyota dichotoma* (Phaeophyceae) en su crecimiento. CICIMAR Oceánides 1(37), 1-20.
- Ramos-Santiago, A. E. (2023). Taxonomía morfológica y molecular de dinoflagelados epibentónicos del Golfo de California. Master thesis. Instituto Politécnico Nacional, Centro Interdisciplinario de Ciencias Marinas, La Paz, B.C.S. Mexico, 199 pp.
- Ramos-Santiago, A. E., Band-Schmidt, C., Leyva-Valencia, I., Fernández-Herrera, L. *et al.* (2024). *Gambierdiscus carpenteri* (Dinophyceae) from Bahía de La Paz, Gulf of California: morphology, genetic affinities, and mouse toxicity. Bot. Mar. 67(4), 309-324.
- Ramos-Santiago, A. E., Leyva-Valencia, I., Okolodkov, Y. B., & Band-Schmidt, C. J. (2025). Morphological and molecular characterization of the free-living *Symbiodinium natans*-clade A (Dinophyceae) from Bahía de La Paz, Gulf of California. Cienc. Mar. 51.
- Rhodes, L., Smith, K.F. (2019). A checklist of the benthic and epiphytic marine dinoflagellates of New Zealand, including Rangitāhua/Kermadec Islands. N. Z. J. Mar. Freshwater Res. 53(2): 258-277.
- Tillmann, U., Beran, A., Gottschling, M., Wietkamp, S. et al. (2022). Clarifying confusion Prorocentrum triestinum J. Schiller and Prorocentrum redfieldii Bursa (Prorocentrales, Dinophyceae) are two different species. Eur. J. Appl. Physiol. 57(2), 207-226.

Measuring diel migration in lab cultures of Gambierdiscus

Jens Wira^{1*}, Allen R. Place¹, Wayne Litaker², Patricia Tester³

¹ Institute of Marine and Environmental Technology, University of Maryland Center of Environmental Sciences, Baltimore, Maryland, USA. E-mail: jwira@umces.edu
 ² CSS, Inc, under contract from NOAA, 101 Pivers Island Rd, Beaufort, NC 28516, USA
 ³ Ocean Tester LLC, 295 Dills Point Road, Beaufort, NC 28516, USA
 *corresponding author's email: jwira@umces.edu

Abstract

Gambierdiscus is a genus of large epibenthic dinoflagellates of interest as the causative agents of ciguatera poisoning. Little is known about their swimming behavior and how that affects sampling and monitoring efforts for environmental populations. Pelagic dinoflagellates frequently exhibit diel vertical migration behaviors, but whether benthic dinoflagellates exhibit analogous diel migration (DM) patterns has not yet been established. The presence of DM might affect important sampling and monitoring efforts of cells like Gambierdiscus, as well as trophic toxin transfer models if systematic shifts in cell locations occur. In this work, we demonstrate a framework for observing the swimming behavior and diel patterns in the lateral movement of multiple species of Gambierdiscus in cultures, inferring their vertical movement off the surface, and show marked differences in the diel patterns exhibited between species. This differentiation in the timing of movements, when viewed in the light of varying toxin levels among species, may have implications on toxin monitoring from environmental samples.

Keywords: Gambierdiscus, ciguatera poisoning, diel migration, artificial substrate, machine vision

https://doi.org/10.15027/0002041257

Introduction

Gambierdiscus is a genus of large epibenthic dinoflagellate found in tropical and sub-tropical regions. Species in this genus are of interest because some produce a suite of potent neurotoxins known as ciguatoxins (CTXs). As marine species graze on Gambierdiscus, CTXs enter the food chain, reaching elevated levels in higher trophic level fish and shellfish. Consumption of these contaminated seafoods often results in mild to severe gastrointestinal. cardiovascular. neurological symptoms termed ciguatera poisoning.

Monitoring *Gambierdiscus* abundance in the wild is essential for assessing the risk of their potential impact on human health. Environmental population estimates involve sampling the benthos, but the lack of homogeneity of the benthic environment leads to high variability in cell density estimates, even when adjacent macrophyte hosts are sampled. Previous work has estimated that as many as 10 replicates may be required in low

density populations for an acceptably low sampling variance (Taylor and Gustavson, 1986). Given the lack of understanding as to any preference for specific algal substrates, studies have rightly focused on comparing only estimates taken from conspecific or similar hosts, with the understanding that this does not reflect the ground-truth cell abundance (Lobel et al., 1988; Nishimura et al., 2018; Tester et al., 2022).

Using artificial substrates to collect cells from diverse substrates is a promising sampling method, that involves the deployment of plastic or fiberglass mesh screens into the environment, collecting the samplers and then enumerating the cells that colonize the substrate after a fixed period of time (Tester et al., 2014). However, it is not known if the behavior of *Gambierdiscus* affects the use of such sampling methods.

One example of how behavior affects location, and by extension informs our ability to sample *Gambierdiscus*, is the diel vertical migration (DVM) patterns of many pelagic dinoflagellate species, where over the course of a 24-hour day they localize to different depths (Hasle, 1950). In addition, DVM is one of many evolutionary strategies used to improve the competitive fitness of many pelagic plankton (Baek et al., 2009; Kamykowski et al., 1998; Roman et al., 1988). Similar diel movement (DM) patterns may occur in benthic dinoflagellates but have yet to be demonstrated. Any significant diel movement behavior could affect population estimates depending on the time-of-day samples are collected. Time-integrated sampling methods collecting cells over sufficient time periods can be used to integrate any such abundance variations caused by DM patterns (Tester et al., 2014).

To better understand the species-specific behavior of *Gambierdiscus*, we developed a low-cost, modular framework using computer vision techniques to observe the movement patterns of benthic cells in culture over multiple diel cycles. In this work we demonstrated the use of techniques for the quantification of motility for four species of *Gambierdiscus* and the differences in their diel patterns and responses to light.

Materials and Method

Cell Culturing and Experimental Conditions: Cultures of four species of Gambierdiscus were provided by Chris Holland of NOAA, G. belizianus (CCMP399), G. caribaeus (CCMP1651), G. carolinianus (Kenny6), and G. excentricus (Pulley Ridge). Cells were raised in K33 media, and maintained at 27°C on a 12-hour light:dark photoperiod at 75 µmol m⁻² s⁻¹ of full spectrum light. For experiments, cells were acclimated for two days by transferring 2 ml of culture into 15 ml of fresh media in untreated T25 culture flasks and maintained at experimental conditions. Cell behavior was recorded at a data rate of 0.2 FPS.

Data acquisition:

For video recording, hardware and cultures were mounted on a T-frame constructed of 2020 aluminum t-slot extrusion rails. Two Basler Pulse 2592x1944 px (5 MP) USB3.0 color cameras (Basler puA2400-14um) were placed on a single movable arm on the frame, and samples platforms were mounted above. 3D-printed holders were used to attach the cameras and platforms for the sample volumes to the t-slot frame. A 3D rendering of the setup is found in Fig. 1.

Lighting for the day period was provided by a dimmable photography LED Panel (Viltrox) with a Color Rendering Index of 95+ mounted onto the frame above the samples. For the dark periods, samples were illuminated using red light by a low power programmable LED strip wrapped around a pipe and mounted within a half-pipe reflector capped with a diffuser sheet. Red light (630 nm peak) was chosen based on the absorption spectra of Amphidinium carterae, another benthic dinoflagellate, and evidence of a blue light cryptochrome driving the division circadian rhythm in Karenia brevis (Hotos and Bekiari, 2023; Stephanie A. et al., 2007). Light measurements in this setup did not exceed 1 µmol m⁻² s⁻¹. Lighting was synchronized to the camera acquisition setup via a 12V relay module (SainSmart) controlled via serial over USB.

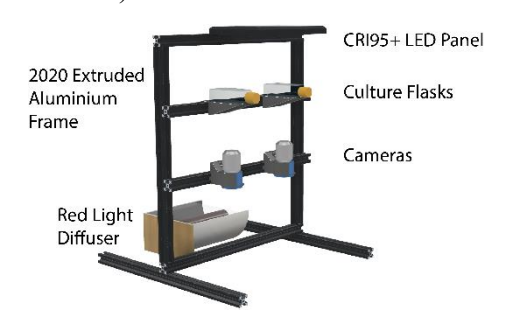


Fig. 1. 3D rendering of experimental setup showing the different components mounted to a 2020 aluminium t-slot T-frame.

The cameras were mounted with a 25 mm F1.8 C-Mount lens (Serounder) with a minimum working distance of 0.25 m. A 10 mm C-Mount spacer was added, bringing the minimum working distance to approximately 0.11 m. Using this optical setup, the minimum field of view (FOV) of 25.0 mm x 15.5 mm. With a sensor size of 5.7 x 4.3 mm and pixel pitch of 2.2 μ m, this resulted in an optical magnification of approximately 0.25X and a pixel size of 8 μ m.

Image acquisition and lighting conditions were controlled via a MATLAB live script that allowed for programmed photoperiods and imaging schedules, as well as synchronization of the acquisition parameters to different lighting conditions. The script controls camera acquisition parameters via the GenTL interface. It is a generic programming interface standard for machine vision cameras that allows adaptation other camera brands.

All parts used were readily available, and the cost of the above-mentioned setup excluding the computer for recording did not exceed \$700 in 2021. The majority of the cost was for two Basler Pulse cameras. All remaining parts were purchased off the shelf from large online retailers.

Data Analysis:

The processing and analysis of video microscopy data is an ongoing and active field of research (Zimmer et al., 2006). To transform the videos into a form of data that is amenable for analysis, objects in the video usually have to be segmented from the background, and detected objects in consecutive frames are linked together and assigned to individuals (Zimmer et al., 2006).

Segmentation of cells was carried out using a semantic segmentation deep learning model. Different models were trained for either the day or night period, both of which were trained similarly. Each frame of each video was passed through the corresponding day or night neural network model, which generates a binary mask for cell and background pixels. The binary masks were then processed to identify and segment individual blobs. Doublet blobs were further processed classified using an SVM algorithm trained on features such as shape, eccentricity, size, and aspect ratio, to identify blobs that contained multiple cells. Finally, those objects were split using a watershed algorithm, and final cell centroids are determined. MATLAB 2023B implementations of the above algorithms and methods were used.

Cell tracking was performed by matching cell positions across frames by solving the linear assignment problem, with a cost matrix based on the Euclidian distance between points in consecutive frames, while also employing a memory window, which enabled tracking of cells that sporadically drop out of view due to a variety

of reasons such as random noise (Kuhn, 1955). The resulting trajectories were then smoothed by applying a locally estimated scatterplot smoothing (LOESS) on the X and Y coordinates of the cell positions across time before use in analysis.

For quantifying behavior, the population average movement speed of cells was calculated by determining the distance traveled by a cell along the substrate surface (plane of focus) between frames and averaging across all cells being tracked. Many cells moving along the surface could be tracked for up to 12-hours. When the trajectories being tracked suddenly terminated this was scored as cells leaving the substrate surface and entering the water column (i.e. leaving the focal plan and no longer trackable). The two metrics were then correlated by fitting a mixed linear model with ARIMA autocorrelation using R's nlme package. All data processing and analyses were carried out in R and MATLAB.

Results and Discussion

All four species studied displayed distinct DM patterns in lateral swimming speeds, with maximal movements associated with L:D and D:L transitions (Fig. 2). The exact timing of these lateral swimming speed peaks relative to the transitions, as well their magnitude, were species-specific. *G. carolinianus* showed the greatest spike in lateral swimming speed during the L:D transition and *G. belizeanus* during D:L transitions.

A linear mixed effects model indicated the periods when maximal swimming occurred corresponded with those when the greatest number of truncated tracks were observed (p<0.01). This indicates cells were detaching from the substrate and entering the water column primarily occurred during periods when maximal lateral movement was occurring.

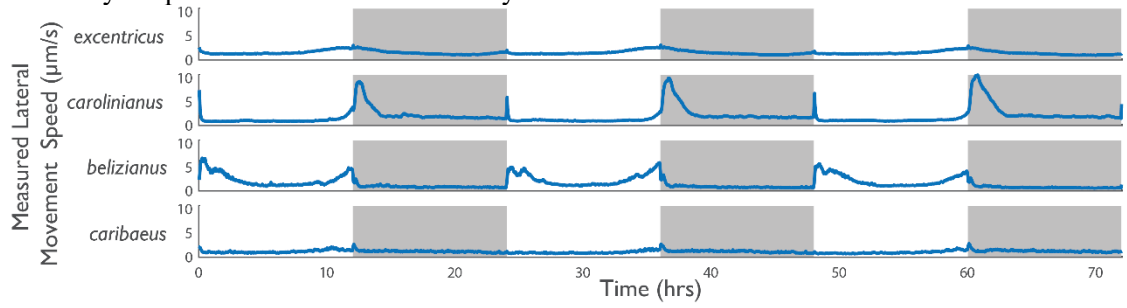


Fig. 2. Variations in swimming speed along the flask surface exhibited by four species of *Gambierdiscus* species over three diel periods (72 h). White areas indicate lights turned on (L) and gray areas the dark (D) periods. A smoothing window was applied for clarity.

The data plotted in Fig. 3 showed the relationship between the proportion of the cell population entering the water column and swimming speed along the surface was also species-specific. Higher swimming speeds were sometimes, but not always associated with greater detachment from the substrate surface. The different responses might be related to different ecology of the cells, but discussion is outside the scope of this study.

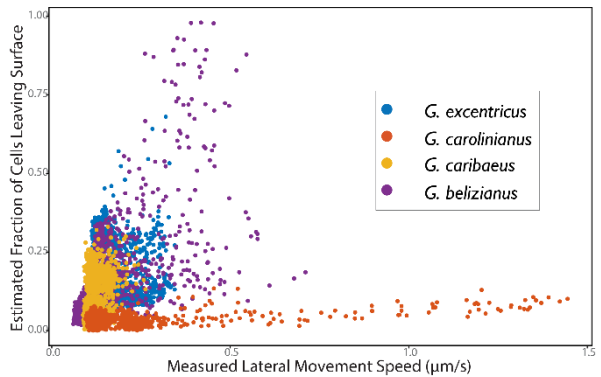


Fig. 3. Scatter plot showing the measured lateral swimming speed of cells correlates to the fraction of cells entering the water column, as estimated by the number of truncated tracks divided by the mean number of tracks in a 10-minute window.

In summary, the results demonstrate a successful framework for studying the swimming ecology and diel behavior of Gambierdiscus cells in culture. Our initial results hint at different diel lateral movement schedules and movements versus swimming patterns among the species, as well as DVM patterns which were inferred from their lateral movement on the culture surface. Future work will seek to directly measure the DVM of Gambierdiscus in culture. These observations help account for why a 24 h incubation period is required to obtain good Gambierdiscus cell abundance estimated using the screen collection method (Tester et al. 2022). It should also be noted, the current study was conducted in a non-turbulent environment. The degree to which currents and turbulence in the field will affect behavior patterns and subsequent dispersion patterns is unknown. Tester et al (2014) found a good correlation among Gambierdiscus cell densities on screen sampling devices and nearby macrophytes during field experiments indicating that at least for the dominant species effective dispersion rates are similar. Further work is needed to determine the range of intraspecies variations in diel swimming behavior and to understand if these behaviors occur in the field. Such information could be used to inform sampling strategies and reduce the sampling effort or the 24-hour integration time.

Acknowledgements

The authors gratefully acknowledge Chris Holland for the provision of the *Gambierdiscus* strains used in this study, and the MEES program and NOAA's National Centers for Coastal Ocean Science for assistance in participation of ICHA 2023.

References

Baek, S.H., Shimode, S., Shin, K., Han, M.-S., Kikuchi, T., (2009). Harmful Algae 8, 843–856.

Hasle, G.R., (1950). Oikos 2, 162.

Hotos, G., Bekiari, V., (2023). International Journal of Plant Biology 14, 879–895.

Kamykowski, D., Milligan, E.J., Reed, R.E., (1998). Journal of Plankton Research 20, 1781–1796.

Kuhn, H.W., (1955). Naval Research Logistics 2, 83–97.

Lobel, P.S., Anderson, D.M., Durand-Clement, M., (1988). The Biological Bulletin 175, 94–101.

Nishimura, T., Tawong, W., Sakanari, H., Ikegami, T., Uehara, K., Inokuchi, D., Nakamura, M., Yoshioka, T., Abe, S., Yamaguchi, H., Adachi, M., (2018). Plankton and Benthos Research 13, 46–58.

Roman, M.R., Ashton, K.A., Gauzens, A.L., (1988). Hydrobiologia 167, 10.

Stephanie A., B., E. Starr, H., Erik E., S., Frances M., V.D., (2007). Journal of Phycology 43, 509–518.

Taylor, F., Gustavson, M., (1986). Proceedings of the 7th. International Diving Science Symposium. Padova, Italy. CMAS, University of Padua, Italy. pp. 95–111.

Tester, P.A., Kibler, S.R., Holland, W.C., Usup, G., Vandersea, M.W., Leaw, C.P., Teen, L.P., Larsen, J., Mohammad-Noor, N., Faust, M.A., Litaker, R.W., (2014). Harmful Algae 39, 8–25.

Tester, P.A., Litaker, R.W., Soler-Onís, E., Fernández-Zabala, J., Berdalet, E., (2022). Harmful Algae 120, 102351.

Zimmer, C., Zhang, B., Dufour, A., Thebaud, A., Berlemont, S., Meas-Yedid, V., Marin, J.-C.O., (2006). IEEE Signal Processing Magazine 23, 54–62.

Ostreopsis cf. ovata trends in the Conero Riviera (northern Adriatic Sea) over 14 years

Stefano Accoroni^{1,2}, Francesca Neri¹, Marika Ubaldi¹, Tiziana Romagnoli¹, Cecilia Totti^{1,3}

¹Dipartimento di Scienze della Vita e dell'Ambiente, Università Politecnica delle Marche, Via Brecce Bianche, 60131 Ancona, Italy.

²Fano Marine Center, The Inter - Institute Center for Research on Marine Biodiversity, Resources and Biotechnologies (FMC), Viale Adriatico 1/N, 61032 Fano, Italy.

³Consorzio Interuniversitario per le Scienze del Mare, CoNISMa, ULR Ancona, Ancona, Italy. *corresponding author's email: s.accoroni@univpm.it

Abstract

Harmful blooms of the toxic dinoflagellate *Ostreopsis* cf. *ovata* have been a recurrent phenomenon along the Mediterranean rocky coasts in the last decades. Since their first records, there has been a widespread belief that the extension of this dinoflagellate well-known in tropical areas to higher latitudes was due to the global warming and the general rise of seawater temperature. Blooms of *Ostreopsis* cf. *ovata* along the Conero Riviera (northern Adriatic Sea) occur between the end of the summer and the beginning of the autumn since 2006. *Ostreopsis* cf. *ovata* abundance data collected from its first record to nowadays were analyzed to better define the interannual trend of this phenomenon and its possible linking to certain climate change predictors. A significant increasing trend in the magnitude of *Ostreopsis* phenomenon was observed up to year 2012, then a stabilization at relatively low values was observed. This trend does not follow the incessant increase in water temperature observed during the last three decades in Adriatic Sea, but rather recalls that of an invasive species, although the provenience of *O. cf. ovata* in the Mediterranean Sea is still unresolved. Even if the *Ostreopsis* bloom in this area seems to slightly lessen in the last decade, *Ostreopsis* abundances still reach values up to 10^3 cells cm⁻² which could be harmful to human health.

Keywords: benthic dinoflagellates, global warming, harmful algae, time series, toxic algae

https://doi.org/10.15027/0002041258

Introduction

Benthic dinoflagellate species of the genus *Ostreopsis* produce toxins mostly belonging to palytoxin (PITX) analogues (Medina-Pérez *et al.*, 2023).

Growth, and abundance of benthic HAB dinoflagellates are largely temperature driven, and the biogeographic distribution is expected to shift in response to climate induced changes as ocean temperature rise provided that other species-specific requirements can be met (Kibler *et al.*, 2015).

Ostreopsis species were initially reported in tropical areas, and only later in temperate latitudes (Parsons *et al.*, 2012). In tropical areas they show

higher diversity, but lower cell maxima (10^5 cells g^{-1} fw) than in temperate latitudes (up to 10^6 cells g^{-1} fw). Especially in the Mediterranean coasts, *Ostreopsis* blooms (mostly caused by *O*. cf. *ovata*, although *O*. cf. *siamensis* and *O. fattorussoi*, have also been identified, Penna *et al.* 2012) are a phenomenon of great concern due to their impact on human health (Berdalet *et al.*, 2022).

In the Mediterranean Sea, *O.* cf. *ovata* blooms appeared as a sudden upsurge around the 2000's, followed the next years by an expansion to the currently known range for the species and a relative stability the last following decade, providing the most evident case of range expansion and increased impact over time in this area (Zingone *et al.*, 2021). This apparent sudden range expansion and impact of species of the same genus was also observed in

New Zealand and other temperate areas of the world (Parsons et al., 2012). However, no clear increase of species abundances has been reported since the 2000 outburst, while the abovementioned range expansion has also coincided with a dramatic increase in monitoring programs and research projects focused on benthic microalgae (Zingone et al., 2021). Several authors have discussed the link between climate change and harmful benthic microalgae: although some authors suggest that the predicted higher temperatures and greater number of high temperature days should stimulate more intense Ostreopsis blooms in the future (Tester et al., 2020), others suggest that the trend observed in the Mediterranean Sea recalls that of an invasive species rather than that of a species favored by a temperature increase (Zingone et al., 2021).

The aim of this study was to investigate trends in *Ostreopsis* cf. *ovata* abundance in a hot-spot area for *Ostreopsis* blooms, i.e. the Conero Riviera, north Adriatic Sea (Mangialajo *et al.*, 2011), gathering data from its first record, in 2007, to 2021. The results of this study will help to better define whether if the increasing, stabilizing or decreasing trends of *Ostreopsis* blooms are linked to climate change predictors.

Materials and Method

The study was carried out in the Conero Riviera (Ancona, N Adriatic Sea), at the Passetto station (43°37′09″N, 13°31′54″E) characterized by a rocky bottom and shallow depths.

Sampling of *Ostreopsis* cf. *ovata* was conducted weekly from July to November (i.e. covering the entire seasonal bloom period) in 2007, 2009, 2010, 2011, 2012, 2013, 2014, 2015, 2019 and 2021, mainly on macroalgae, with a frequency of 14 samples per year. Following the method described by Accoroni *et al.* (2024), fragments of macroalgal thalli were collected in three replicates at a depth of 0.5 m and, once in laboratory, treated to dislodge the epiphytic cells. *Ostreopsis* abundances were estimated using an inverted microscope equipped with phase contrast, in counting chambers according to the Utermöhl sedimentation method. The final data were expressed as cells cm⁻² of macroalga.

Surface temperature and salinity were measured with a CTD. Water samples for nutrient analysis (NO₃, NO₂, NH₄, PO₄ and Si(OH)₄) were collected in polyethylene bottles (50 mL) near the sampled substrata, immediately filtered through GF/F Whatman filters (Ø 25 mm) and stored in triplicate in 4 mL polyethylene bottles at -22 °C until analysis conducted, using an Autoanalyzer QuAAtro Axflow following the colorimetric method by Strickland and Parsons (1972).

Statistical analyses were performed using the R software (R Core Team 2021). Ts (Time-series objects) and decompose functions from the stats package were used to create the time series (with a frequency of 14 samples per year) of O. cf. ovata abundances and to decompose it in its seasonal, trend and irregular components. A change point analyses to detect a structural change point was performed with methods and functions belonging to the F statistics and generalized fluctuation tests (Zeileis et al., 2003). Furthermore, cpt.mean from the changepoint package (Killick and Eckley, 2014) was used to assess a change point in the mean, setting method as AMOC (at most one change). Once the change point was determined, the trend before and after this point was assessed fitting a linear model, using generalized least squares, as this method allows correlation of the error. The Generalized Least Squares function from the nlme package was used to fit linear models using generalized least squares (Pinheiro et al., 2023). Time series of data of water temperature, DIN, PO₄ and N/P were decomposed in their seasonal, trend and irregular components, considering an additive structure. The ts and decompose functions of the stats R package were used to create the time series and to decompose it in its seasonal, trend and irregular components. The Mann-Kendall tests for the detection of trends were performed on the time series after subtracting the seasonal component, to avoid the effect of the seasonality on the trends (McLeod, 2022).

Results and Discussion

Blooms of *O.* cf. *ovata* have been constantly reported along the Conero Riviera since 2007 as well as symptoms of human suffering, seafood contamination and increased mortality of other organisms (Totti *et al.*, 2010; Accoroni *et al.*, 2022).

Generally, each year the first cell detection on benthic substrata occurred in late July/early August, the maximum abundances in early autumn (end of September/early October), and the bloom decline by the end of October/early November (Fig. 1).

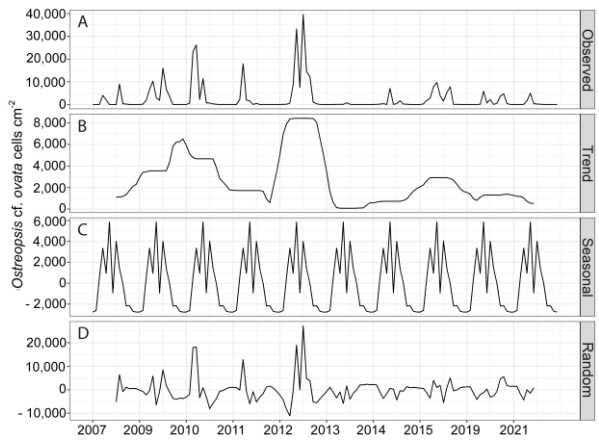


Fig. 1. Decomposition of (A) the *O.* cf. *ovata* time series in its (B) trend, (C) seasonal and (D) random components.

The times series of *O*. cf. *ovata* showed the typical blooming behaviour of the species in the study area as highlighted by the strong seasonal signal (Fig. 1C), which remained constant through the series. However, a change in the annual maximum can be observed, as shown by the trend component (Fig. 1B). First, an increasing trend can be observed (up to year 2010), followed by a slight decrease and a strong increase in 2012. After this strong peak, a decline can be observed.

The structural change point (p<0.05) in the *Ostreopsis* cf. *ovata* time series was estimated to be on 15th October 2012; all the used statistical methods separated the series into two partitions, showing a significant increasing trend (p<0.05) and no trend before (beginning of the series-October 2012) and after the change point (October 2012-end), respectively (Fig. 2).

Regarding the environmental parameters, the time series decomposition of water temperature, DIN, PO_4 and N/P highlighted the typical strong seasonal behaviour of the physico-chemical parameters and significant increasing and decreasing trends of water temperature (tau = 0.32, p<0.001, Mann-Kendall test) and PO_4 (tau = -0.24, p<0.001, Mann-Kendall test), respectively. No significant trends were observed for DIN.

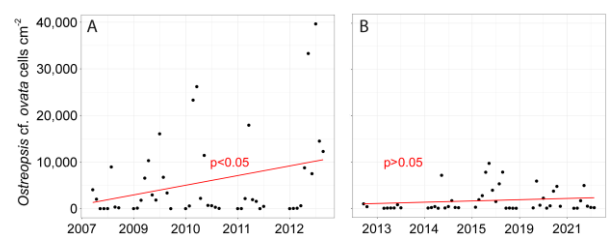


Fig. 2. Generalized least squares time series regression for the period (A) before and after (B) the changepoint (15/10/2012).

The increasing trend in the magnitude of the Ostreopsis phenomenon observed from its first record to 2012, and the following stabilization to relatively low values, does not follow the uninterrupted increasing trends observed in water temperature during the last three decades. Therefore, in this Mediterranean area, the rising of water temperature does not seem to be related to an increase in Ostreopsis blooms. Ostreopsis did not even show any earlier bloom initiation time as suggested for other Mediterranean areas (Fricke et al., 2018), as blooms have been observed each year in late July - August. This could be explained considering that the start of the bloom in this area is linked to the onset of two synchronous optimal conditions, i.e. optimal temperature and nutrient availability (Accoroni et al., 2015). Therefore, even in the case that global warming promoted an early bloom initiation, it would be limited in this area until late July-August, i.e., the time when optimal N and P levels occur. This nutrient constraint is irrespective of the rising temperature of the last years.

The trend observed in this study suggests that O. cf. ovata in this area may be an alien species as proposed by Zingone et al. (2021). Simberloff and Gibbons (2004) observed that an invasive alien species often shows a phase of sudden increase in the new area followed by a decline, probably due to competition or other biological interactions or to some unidentified effects.

Phylogenetic studies do not resolve this issue, as identical strains of *O*. cf. *ovata* are found in the SW Atlantic (Brazil) and Mediterranean Sea are also recorded in W Pacific (Japan), suggesting that W Pacific *O*. cf. *ovata* might have been introduced into the Mediterranean and/or Atlantic ocean, or *vice versa* (Sato *et al.*, 2011).

Walsh et al. (2016) proposed two possible scenarios for the establishment of an invasive species population and first outbreak timing: i) an invasive species establishment after some introduction events and becomes abundant soon after passing a detection level; ii) the establishment and the out-break are separated in time; as a result, the established population is detected much later. In the Mediterranean Sea, did Ostreopsis bloom soon after it was introduced, or was there an existing, below-detection-levels population that bloomed later due to some sort of trigger? Fraga et al. (2012) suggested that it is possible that the enhancing of the Ostreopsis phenomenon observed in the first years since its first records could have been caused by a phase shift in benthic microalgae communities due to anthropogenic or natural environmental change. The mass mortalities of benthic invertebrates recorded as a consequence of the exceptional 2003 heatwave could have affected non-identified potential predators of Ostreopsis, and a potential cascade effect led to an increase in Ostreopsis populations.

In conclusion, contrarily to what is generally thought about the relationship between global warming and the occurrence of *Ostreopsis* blooms in temperate areas, in the northern Adriatic Sea, the two phenomena do not seem to be related.

Although the site of origin of *O*. cf. *ovata* in the Mediterranean Sea is still unresolved, the hypothesis about the allochthonous character of the species in that region is supported by the trend analyses of *O*. cf. *ovata* abundances reported in this study.

References

- Accoroni, S., Glibert, P.M., Pichierri, S., Romagnoli, T., *et al.* (2015). Harmful Algae 45, 14–25.
- Accoroni, S., Ubaldi, M., Bacchiocchi, S., Neri, F., et al. (2022). J. Mar. Sci. Eng. 10, 1402
- Accoroni, S., Neri, F., Ubaldi, M., Romagnoli, T., *et al.* (2024). Mar. Biol. 171, 10.
- Berdalet, E., Pavaux, A.-S., Abós-Herràndiz, R., Travers, *et al.* (2022). Harmful Algae 119, 102320.
- Fraga, S., Rodriguez, F., Bravo, I., Zapata, M., *et al.* (2012). Cryptogam. Algol. 33, 171–179.
- Fricke, A., Pey, A., Gianni, F., Lemée, R., et al.

- (2018). Mar. Pollut. Bull. 131, 552–564.
- Kibler, S.R., Tester, P.A., Kunkel, K.E., Moore, S.K., *et al.* (2015). Ecol. Modell. 316, 194–210.
- Killick, R. and Eckley, I.A. (2014). Stat. Softw. 58.
- Mangialajo, L., Ganzin, N., Accoroni, S., Asnaghi, V., et al. (2011). Toxicon 57, 408–420.
- McLeod, A.I., (2022) Kendall: Kendall Rank Correlation and Mann-Kendall Trend Test. R package version 2.2.1.
- Medina-Pérez, N.I., Cerdán-García, E., Rubió, F., Viure, L., et al. (2023). Toxins 15, 188.
- Parsons, M.L., Aligizaki, K., Bottein, M.-Y.D., Fraga, S., *et al.* (2012). Harmful Algae 14, 107–129.
- Penna, A., Fraga, S., Battocchi, C., Casabianca, S., et al. (2012). Cryptogam. Algol. 33, 153–163.
- Pinheiro, J., Bates, D., R Core Team, 2023. nlme: Linear and Nonlinear Mixed Effects Models. R package.
- Sato, S., Nishimura, T., Uehara, K., Sakanari, H., et al. (2011). PLoS One 6.
- Simberloff, D. and Gibbons, L. (2004). Biol. Invasions 6, 161–172.
- Strickland, J.D.H. and Parsons, T.R. (1972). A practical handbook of seawater analysis. Bull. 167, 2nd Ed. Supply Serv. Canada, Ottawa; Canada 310 pp.
- Tester, P.A., Litaker, R.W., Berdalet, E. (2020). Harmful Algae 91, 101655.
- Totti, C., Accoroni, S., Cerino, F., Cucchiari, E., *et al.* (2010). Harmful Algae 9, 233–239.
- Walsh, J.R., Munoz, S.E., Vander Zanden, M.J. (2016). Ecosphere 7, e01628.
- Zeileis, A., Kleiber, C., Krämer, W., Hornik, K. (2003). Comput. Stat. Data Anal. 44, 109–123.
- Zingone, A., Escalera, L., Aligizaki, K., Fernández-Tejedor, M., *et al.* (2021). Harmful Algae 102, 101843.

Current status of expansion of HAB species in Hokkaido, northern Japan, with special reference to large-scale dispersal of *Karenia mikimotoi* via ocean current system

Hiroshi Shimada^{1*}, Masatoshi Sato², Akiyoshi Shinada³, Daichi Arima⁴, Tomoaki Yasunaga⁴, Makoto Kanamori⁵, Hiroshi Kuroda⁶, Setsuko Sakamoto⁷, Ichiro Imai⁸

- ¹ Kushiro Fisheries Research Institute, Hokkaido Research Organization (HRO), 2-6 Hama-cho, Kushiro, Hokkaido 085-0024, Japan.
- ² Wakkanai Fisheries Research Institute, HRO, 4-5-15 Suehiro, Wakkanai, Hokkaido 097-0001, Japan.
- ³ Salmon and Freshwater Fisheries Research Institute, HRO, 3-373 Kita-Kashiwagicho, Eniwa, Hokkaido 061-1433, Japan
 - ⁴ Central Fisheries Research Institute, HRO, 238 Hamanaka-cho, Yoichi, Hokkaido 046-8555, Japan. ⁵ Headquarters, HRO, Kita 19 Nishi 11, Kita-ku, Sapporo, Hokkaido 060-0819, Japan.
 - ⁶ Kushiro Field Station, Fisheries Resources Institute, Japan Fisheries Research and Education Agency (FRA), 116 Katsurakoi, Kushiro, Hokkaido 085-0802, Japan.
- ⁷ Fisheries Technology Institute, FRA, 2-17-5 Maruishi, Hatsukaichi, Hiroshima 739-0452, Japan. ⁸ Graduate School of Fisheries Science, Hokkaido University, 3-1-1 Minato-cho, Hakodate, Hokkaido 041-8611, Japan.

*corresponding author's email: shimada-hiroshi@hro.or.jp

Abstract

To reveal the recent situation of the expansion of HAB species around Hokkaido, northern Japan, we investigated the past occurrences of HAB events since 1970s. Several HAB species were newly detected after 2013 as well as the toxic dinoflagellates *Alexandrium catenella* (Group I) and *Dinophysis* spp., that produce shellfish toxins. Notorious red tide species *Chattonella marina*, *Karenia mikimotoi* and *Margalefidinium polykrikoides*, and toxic species *Ostreopsis* sp. and *Prorocentrum lima* had been newly recorded in 2010s. These species are supposed to be introduced to the west coast of Hokkaido from western Japan via the Tsushima Warm Current system. In autumn 2021, the harmful red tide caused by *Karenia selliformis* occurred on the Pacific coast of eastern Hokkaido, and the death of large amounts of fishery species (e.g., sea urchin *Strongylocentrotus intermedius*, chum salmon *Oncorhynchus keta* and sea snail *Neptunea* spp.) were related to this HAB event. The harmful event is assumed to be caused by the introduction of *K. selliformis* from the offshore area of north Pacific via ocean current systems. It is necessary to elucidate geographical distribution of HAB species and to monitor further expansion of HAB species via ocean current system in subarctic regions where new HAB species are at risk of expansion.

Keywords: HAB species, harmful red tide, expansion, ocean current, climate change, marine heatwave.

Introduction

The occurrences of HAB events have been reported since 1970's around Hokkaido, northern Japan (Shimada 2021). Though the occurrences of paralytic shellfish toxin (PST) and diarrheic shellfish toxin (DST) were mainly recorded until 2000's, the expansion of HAB species became to be noticed on the background of climate change after 2010's (Shimada 2021). Especially, two historical HAB events regarded to be the first record of harmful red tides due to *Karenia mikimotoi* in northern Japan in Hakodate Bay in autumn of 2015 (Shimada et al. 2016a) and large

harmful red tides due to *K. selliformis* along the Pacific coast of Hokkaido in autumn 2021 (Iwataki et al. 2022). In this paper, the recent situation of expansion of HAB species around Hokkaido are described with the special reference to large-scale dispersal of *Karenia mikimotoi* via ocean current system.

Materials and Method

To clarify the recent situation of expansion of HAB species, the records of red tide occurrences during 1970's-2000's and the reports of occurrences of HAB species after 2010's along the coast of

Hokkaido were summarized referring Shimada et al. (2016a), Shimada et al. (2016b) and Shimada (2021).

Table1 Date and period of survey at each sampling station in northern Japan with detection results of *K. mikimotoi*

Survey/station	Period of survey	Date or period(station) of detection of K. mikimotoi	Detection method
Area-wide occurrence			
St.1-16 (Japan Sea/	May 29-Jun.7, Jul.24-Aug.2, Oct.5-7, 2017	Jul.24, 2017(St.1) LAMP	
Tsugaru Strait)	May 28-Jun.7, Jul.23-29, Oct.2-5, 2018	Jul.23(St.6), Oct.2(St.4), Oct.3, 2018(St.8, St.11)	
	May 27-Jun.12, Jul.23-Aug.5, Oct.1-4, 2019	May 27(St.2), Jun.12(St.14), Jul.23(St.2, St.4, St. 6), Oct.1(St.1, St.3, St.5, St.7), Oct.3, 2019(St.16)	
St.17-26	Jul.25, 2017	(Not detected in 2017) LAMP	
(Okhotsk Sea)	Jul.23-24, 2018	(Not detected in 2018)	
	Jul.29-30, 2019	Jul.30, 2019(St.21, St.23, St.26)	
Seasonal dynamics			
St.H (Hakodate)	Jan.13, 2016-Dec.18, 2019 (conducted 1-4 times a month)	Aug.9, 2016-Jan.4, 2017 Aug.28-Oct.24, 2017 Jun.20-Dec.11, 2018 Jul.25-Sep.25, 2019	LAMP/ LM observation
St.Y (Yoichi)	Jan.4, 2016-Dec.27, 2019 (conducted every weekdays)	Nov.2-3, 2016 (Not detected in 2017) Sep.21-Oct.9, 2018 Jul.16-Oct.3, 2019	LAMP/ LM observation

To reveal the dispersal of the harmful red tide of K. mikimotoi, area-wide surveys conducted at 26 sampling stations were Tsushima/Tsugaru/Soya warm current area during every May-October of 2017-2019 (Table 1, Fig. 1). Collected materials on the polycarbonate filter (Whatman Nuclepore, pore size: 3 µm) of surface seawater samples (500 mL) at each station were provided for the molecular identification for K. mikimotoi using the LAMP method (Kitatsuji et al. 2019). Simultaneously, to elucidate the dynamics of K. mikimotoi occurrences, the seasonal distribution was monitored at two coastal stations (Hakodate and Yoichi, Table 1, Fig. 1) during 2016-2019. Surface seawater samples (1 L) collected at each sam

pling station were divided into two subsamples (each 500 mL) one for the molecular identification (LAMP method) and the second one for direct counting of K. mikimotoi using an inverted light microscope (Nikon, Diaphot TMD or Olympus, IX70) after x100-1000 concentration using a Nuclepore filter. Surface seawater temperature and salinity were measured using CTD instrument (JFE Advantec, RINKO-Profiler ASTD102) or mercury thermometer and hydrometer (Shimada et al. 2016b). The transportation of the harmful dinoflagellate K. mikimotoi were examined using particle tracking experiment based on the ocean model JADE2 (Ito et al. 2018) and the occurrence information of K. mikimotoi off the northern coast of Kyusyu in 2015 (Satomichi et al. 2016).

The biological information and the hypothesis scenario of the occurrence of the huge harmful red

tides of *K. selliformis* in the Pacific coast of Hokkaido in 2021 autumn were described referring Kuroda et al. (2021) and Iwataki et al. (2022).

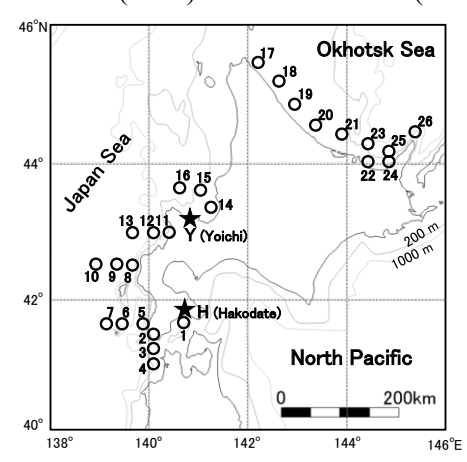


Fig. 1 Map showing sampling stations for monitoring of *K. mikimotoi* of the area-wide surveys (open circles) and the seasonal dynamics surveys (closed stars) respectively during 2016-2019.

Results and Discussion

Until 2000s, the significant HAB events were only the occurrences of PST and DST caused by the toxic dinoflagellates Alexandrium catenella (Group I) and *Dinophysis* spp. in Hokkaido, while the red tides due to common species had been recorded with no damage to fisheries (Shimada 2021). However, several HAB species were newly detected after 2010s, the notorious red tide species Chattonella marina. Margalefidinium polykrikoides, K. mikimotoi and K. selliformis (Fig. 2), and the toxic species Ostreopsis sp. and Prorocentrum lima (Fig. 2) had been newly recorded (Sato et al. 2011, Shimada et al. 2016b, Shimada 2021, Iwataki et al. 2022).

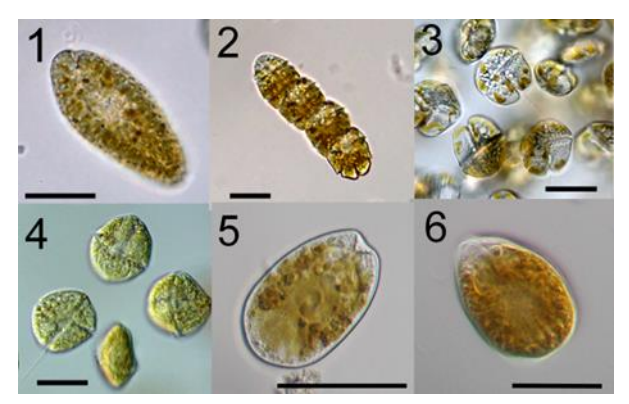


Fig. 2 Photomicrographs showing the notorious red tide organisms and toxic dinoflagellates newly recorded in Hokkaido after 2010's.

1: Chattonella marina, 2: Margarefidinium polikrikoides, 3: Karenia mikimotoi, 4: K. Selliformis, 5: Prorocentrum lima, 6: Ostreopsis sp. (scale bar: 30 μm) Area-wide surveys revealed that *K. mikimotoi* occurred widely in the Tsushima/Tsugaru/Soya Warm Current water (Table 1, Fig. 3). Seasonal dynamics of cell densities of *K. mikimotoi* at the two coastal stations (Hakodate and Yoichi, Fig. 4) suggested that *K. mikimotoi* occurred almost every year mainly during summer-autumn when the SST was increasing above 20 °C.

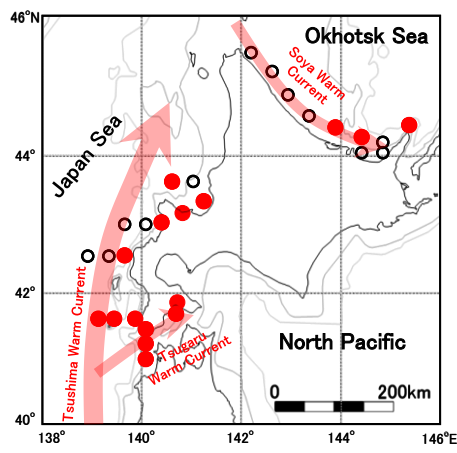


Fig. 3 Distribution of *K. mikimotoi* around Hokkaido during 2016-2019. Red closed circles indicate stations of *K. mikimotoi* occurrence by the area-wide surveys and the seasonal dynamics surveys using the molecular biological method (LAMP). Open black circles indicate non-detection of *K. mikimotoi*.

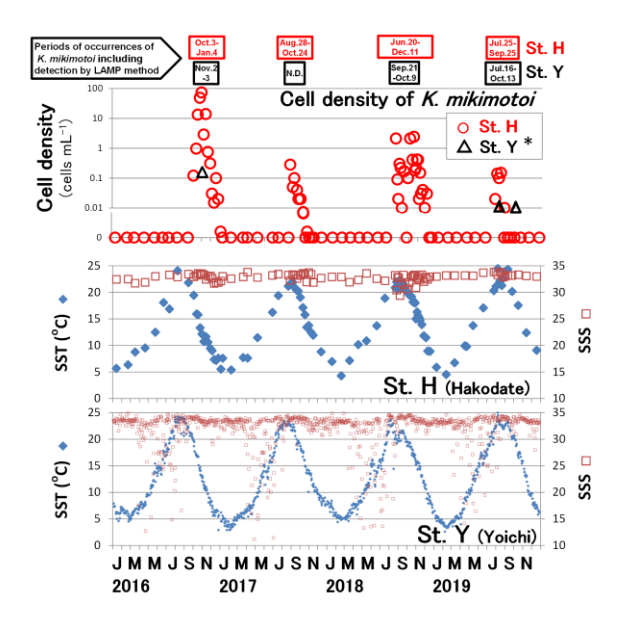


Fig. 4 Seasonal dynamics of cell densities of *K. mikimotoi* at St.H and St.Y (above), sea surface temperature and salinity at St.H (middle) and St.Y (below) with information of the periods of *K. mikimotoi* occurrences during 2016-2019.

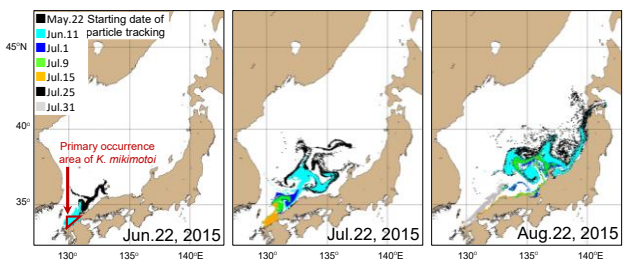


Fig. 5 Particle tracking experiment (1 m depth, 1-3 months after the first tracking) using the ocean model (JADE2) and the occurrence information of *K. mikimotoi* in 2015 reported by Satomichi et al. (2016).

The results of particle tracking experiment using the ocean model JADE2 strongly suggested that *K. mikimotoi* were transported from the northern coast of Kyushu (western Japan) to Hokkaido that took a few months (Fig. 5) in 2015 when the harmful red tides occurred in Hakodate Bay, southern Hokkaido. These results were able to explain rationally on the bloom dynamics of *K. mikimotoi* red tides in the autumn of 2015 reported by Shimada et al. (2016a) and Kakumu et al. (2018). Similarly, most of the warm-water HAB species could be assumed to be introduced to the west coast of Hokkaido from western Japan via the Tsushima/Tsugaru/Soya Warm Current system. It is important to monitor the warm-water

system. It is important to monitor the warm-water HAB species frequently (once a month at least) in the warm current area.

In the autumn 2021, the huge harmful red tide due to *K. selliformis* (Fig. 2) occurred on the Pacific coast of eastern Hokkaido (Iwataki et al. 2022), and great amounts of fishery species (e.g., sea urchin *Strongylocentrotus intermedius*, chum salmon *Oncorhynchus keta* and sea snail *Neptunea* spp.) were killed by the HAB event. The harmful event was assumed to be caused by the introduction of *K. selliformis* via ocean current systems (e.g. Oyashio Current, Coastal Oyashio), after the appearance/disappearance of the marine heat wave (MHW) in the western North Pacific from July to August 2021 (Kuroda et al. 2021, Yamaguchi et al. 2022).

Our results suggest that the large-scale expansions of HAB species is supposed to be caused by the ocean current systems. It is necessary to elucidate geographical distribution of HAB species and to monitor further expansion of HAB species via ocean current systems in subarctic regions such as Hokkaido, considering the upcoming issue on the climate change and the expansion of HAB species in the world (Dale et al. 2006, Gobler et al. 2017, Gobler 2020).

^{*} Regarding St.Y, symbols for 0 (cells L^{-1}) values are omitted because only 3 times the occurrence of *K. mikimotoi* were found by microscope observations.

Acknowledgements

A part of present study is financially supported by the Fisheries Agency of Japan. We are grateful to staff of the Oshima Fisheries Technical Guidance Office and the captains and crews of the R/V Hokuyo Maru and the R/V Kinsei Maru for kindly helping with the sampling *in situ*.

References

- Dale, B., Edwards, M., Reid, P.C. (2006). In: Granéli, E., Turner, J.T. (eds.) Ecology of Harmful Algae. Springer, Berlin. Climate change and harmful algal blooms. pp. 367-378.
- Gobler, C.J., Doherty, O.M, Hattenrath-Lehmann, T.K., Griffith, A.W., Kang, Y., Litaker, R.W. (2017) Ocean warming since 1982 has expanded the niche of toxic algal blooms in the North Atlantic and North Pacific oceans. PNAS 114, 4975-4980.
- Gobler, C.J. (2020) Climate change and harmful algal blooms: Insights and perspective. Harmful Algae 91, 101731.
- Ito, S., Tsujino, H., Miyazawa, Y., Hirose, N., Komatsu, K., Yoshie, N. (2018) In: Jang C.J. and Curchitser E. (eds.) 5. Regional high-resolution ocean models in the western North Pacific and its marginal seas. PICES Scientific Report 54, pp. 44-55.
- Iwataki, M., Lum, M.W., Kuwata, K., Takahashi, K., Arima, D., Kuribayashi, T., Kosaka, Y., Hasegawa, N., Watanabe, T., Shikata, T., Isada, T., Orlova, T.Y., Sakamoto, S. (2022) Morphological variation and phylogeny of *Karenia selliformis* (Gymnodiniales, Dinophyceae) in an intensive cold-water algal bloom in eastern Hokkaido, Japan. Harmful Algae 114, 102204.
- Kakumu, A., Morita, K., Shimada, H., Yamaguchi, A., Imai, I. (2018) First detection of the noxious red tide dinoflagellate *Karenia mikimotoi* and bloom dynamics in 2015 and 2016 in Hakodate Bay, Hokkaido, northern Japan. Bull. Plankton Soc. Japan 65, 1-11.
- Kitatsuji, S., Shikata, T., Sakamoto, S., Nakayama, N., Nagai, K., Onitsuka, G., Tada, K. (2019) Detection of harmful algae grazed by *Noctiluca scintillans* by lamp method. Journal of Fisheries Technology 12, 23-29.

- Kuroda, H., Azumaya, T., Setou, T., Hasegawa, N. (2021) Unprecedented outbreak of harmful algae in Pacific coastal waters off southeast Hokkaido, Japan, during late summer 2021 after recordbreaking marine heatwaves. J. Mar. Sci. Eng. 9, 1335.
- Sato, S., Nishimura, T., Uehara, K., Sakanari, H., Tawong, W., Hariganeya, N., Smith, K., Rhodes, L., Yasumoto, T., Taira, Y., Suda, S., Yamaguchi, H., Adachi, M. (2011) Phylogeography of *Ostreopsis* along West Pacific Coast, with Special Reference to a Novel Clade from Japan. PLoS One 6, e27983.
- Satomichi, N., Ezaki, O., Sugino, K., Katayama, Y. (2016) The red tides of *Karenia mikimotoi* in the Chikuzen-kai during the summer of 2015. Bull. Fukuoka Fisheries Mar. Technol. Res. Cent. 26, 83-91 (in Japanese).
- Shimada, H. (2021) Long-term fluctuation of red tide and shellfish toxin along the coast of Hokkaido (Review). Sci. Rep. Hokkaido Fish. Res. Inst. 100, 1-12.
- Shimada, H., Kanamori, M., Yoshida, H., Imai, I. (2016a) First record of red tide due to the harmful dinoflagellate *Karenia mikimotoi* in Hakodate Bay, southern Hokkaido, in autumn 2015. Nippon Suisan Gakkaishi 82, 934-938.
- Shimada, H., Sakamoto, S., Yamaguchi, M., Imai, I. (2016b) First record of two warm water HAB species *Chattonella marina* (Raphidophyceae) and *Cochlodinium polykrikoides* (Dinophyceae) on the west coast of Hokkaido, northern Japan in summer 2014. Reg. Stud. Mar. Sci. 7, 111—117.
- Sildever, S., Kawakami, Y., Kanno, N., Kasai, H., Shiomoto, A., Katakura, S., Nagai, S. (2019) Toxic HAB species from the Sea of Okhosk detected by a metagenetic approach, seasonality and environmental drivers. Harmful Algae 87, 101631.
- Yamaguchi, A., Hamao, Y., Matsuno, K., Iida, T. (2022) Horizontal distribution of harmful redtide *Karenia selliformis* and phytoplankton community along the Pacific coast of Hokkaido in autumn 2021. Bull. Jpn. Soc. Fish. Oceanogr. 86, 41-49.

Analysis of surface harmful algal blooms in the Tropical Mexican Pacific: A remote sensing approach

Sinuhé Hernández Márquez^{1*}, María Eugenia Zamudio-Resendiz², María Luisa Núñez-Resendiz³, Felipe Omar Tapia Silva⁴, Kurt Martin Dreckmann³, Laura Margarita Márquez Valdelamar⁵, Abel Sentíes³.

¹Doctorado en Ciencias Biológicas y de la Salud, Universidad Autónoma Metropolitana, México; ²Laboratorio de Fitoplancton Marino y Salobre, Departamento de Hidrobiología, Universidad Autónoma Metropolitana, Iztapalapa, México; ³Laboratorio de Macroalgas Marinas y Salobres, Departamento de Hidrobiología, Universidad Autónoma Metropolitana, Iztapalapa, México; ⁴ Laboratorio de Geomática Aplicada, Departamento de Hidrobiología, Universidad Autónoma Metropolitana, Iztapalapa, México; ⁵Instituto de Biología, Universidad Nacional Autónoma de México

*Corresponding author's email: shmbart1@gmail.com

Abstract

In this study, an integrated approach utilizing satellite technology and field data was employed to monitor Harmful Algal Blooms (HABs) in the Tropical Mexican Pacific (TMP). The 2019 research used the Surface Algal Bloom Index (SABI) algorithm on Modis-Aqua sensor data via Google Earth Engine, pinpointing significant occurrences of HABs in February, August, and October, especially in Banderas Bay, Acapulco Bay, and the Gulf of Tehuantepec. This approach was further enriched by comparative analysis with UAMITPacific microalgae collection samples, incorporating advanced microscopy and molecular phylogenetic techniques for precise taxonomic identification. A notable aspect of this study was the new bloom record of Helicotheca tamesis and Eutreptiella sp., adding to the significance of these observations. The findings provide vital insights for managing HABs and safeguarding marine and coastal resources, emphasizing the importance of focused monitoring during critical months for effective environmental management. This study not only demonstrates the impact of environmental factors such as ocean currents on HAB dynamics but also highlights the effectiveness of integrating various scientific methods. This approach is crucial in offering comprehensive insights into marine ecosystem health and aiding in the protection of crucial marine and coastal environments from the effects of HABs.

Keywords: Google Earth Engine, Diversity, Taxonomic.

https://doi.org/10.15027/0002041260

Introduction

In the Tropical Mexican Pacific (TMP), the study of Harmful Algal Blooms (HABs) faces a significant challenge due to inadequate monitoring. Unlike the better-researched Temperate Pacific and transition zones, where the proximity to research facilities allows for constant observation, the TMP's remoteness has led to a limited and fragmented understanding of HABs dynamics. (Meave et al. 2018) This knowledge gap has also contributed to economic losses, negatively affecting shellfish industries, including clam and oyster farms in coastal areas (Cortés-Lara et al. 2022). To address these issues, this research uses satellite technology to study HABs in the TMP, offering a novel approach to overcome the geographical regions and logistical barriers in environmental monitoring (Awaldi 2010).

The primary objective of this study is to analyze satellite-derived HABs data at the TMP, focusing on areas exceeding 1 km², and to validate these findings through a comparative analysis with samples from the UAMITPacific microalgae collection (Meave and Zamudio, specifically collected in 2019. This method aims not only to test the effectiveness of satellite technology for HAB monitoring, but also to identify the specific organisms involved in these blooms. By employing this dual approach, the study is expected to provide a more comprehensive understanding of HAB occurrences in the TMP.

Materials and Method

Remote perception

This research used the programming capabilities of Google Earth Engine in to access and manipulate satellite data from the Modis-Aqua sensor, specifically targeting HABs spanning 1 km². After data acquisition, a customized version of the Surface Algal Bloom Index (SABI) algorithm, proposed by Alawadi (2010), was applied. This adaptation included a strategic focus on specific spectral bands to enhance analysis, as illustrated in Figure 1. This methodological approach allowed for a detailed examination of the spatial and temporal distribution of HABs in the targeted area.

$$SABI = \frac{X_{NIR} - X_R}{X_B + X_G}$$

XR= B1,645 nm; XNIR= B2,869 nm; XB= B3,469 nm; XG= B4,555 nm

Eq. 1. SABI Equation, where "B" denotes the modified band number used from MODIS-Aqua.

After this, data post-processing was conducted using the Geographic Information System (GIS) software QGIS and GRASS GIS. QGIS was instrumental in providing detailed visualization and spatial analysis, while GRASS GIS offered robust capabilities for the processing of both raster and vector data.

Specific diversity data

For the assessment of specific diversity, the Utermöhl method (1931) was employed, tailored to the specific regions identified on the 2019 maps. This approach involved the collection of surface-level samples using the Van Dorn bottle sampling technique.

Taxonomic identification

For taxonomic identification, an array of microscopy techniques to analyze fine morphology was employed. These techniques included electron microscopy, bright-field optical microscopy, and fluorescence microscopy. Additionally, for select organisms, molecular phylogenetic analyses were conducted to further elucidate their taxonomic classification.

Results and Discussion

A schematic map of currents was obtained to examine the relationship with HABs, considering the annual cycle (Fig. 1).

In 2019, an analysis using the SABI algorithm identified specific months merged per day with a high incidence of HABs: February (Fig. 2), August (Fig. 3), and October (Fig. 4). In February, HABs were detected in both Banderas Bay, Nayarit, and Acapulco Bay, Guerrero, Mexico. Subsequently, in

August, HABs predominated in Acapulco Bay, and in October, they were observed in the Gulf of Tehuantepec. This temporal pattern highlighted the variability and geographic distribution of HABs in these key marine regions of Mexico.

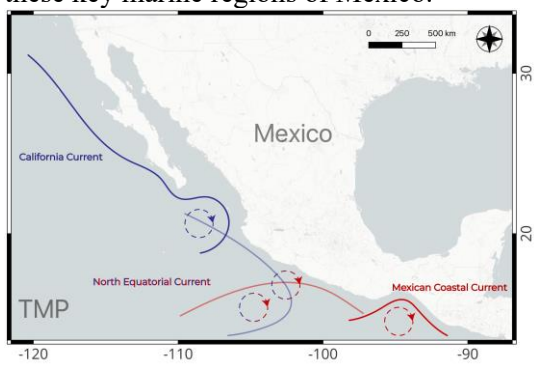


Fig. 1 Schematic map of marine currents in Mexico

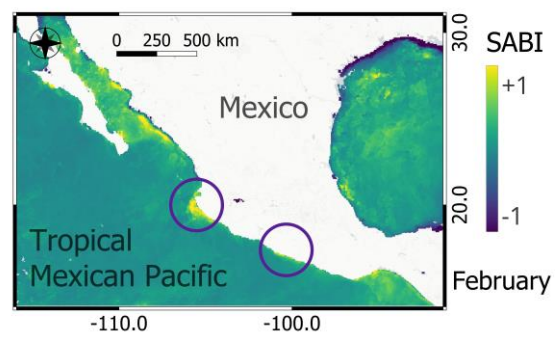


Fig. 2. SABI map of February 2019, circulating Banderas Bay and Acapulco Bay, value of 0.1-1=Bloom, ≤0=No Bloom.

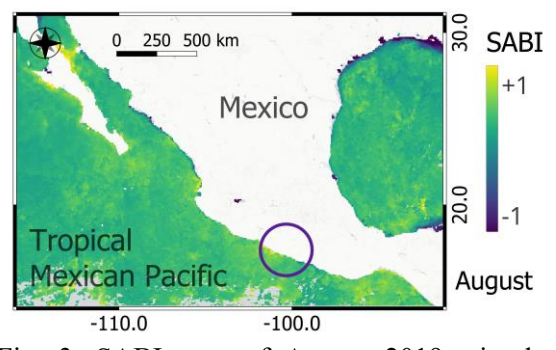


Fig. 3. SABI map of August 2019, circulating Acapulco Bay, value of 0.1-1=Bloom, ≤0=No Bloom.

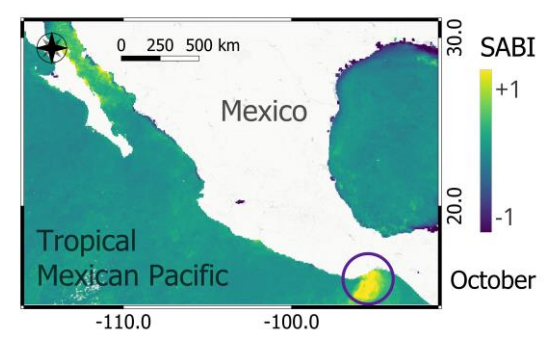


Fig. 4. SABI map of October 2019, circulating Tehuantepec Gulf, value of 0.1-1=Bloom, ≤0=No Bloom.

Case 1: Banderas Bay, Nayarit, Mexico

In February 2019, two significant organisms were identified in the study, conducted in the bay. The first, Margalefidinium polykrikoides, was observed in concentrations of 7245 x 10⁶ cells/L, which aligns with the findings of Cortés-Lara et al. (2004, Similarly, Gymnodinium 2014, 2018). catenatum was detected at a density of 5651 x 10⁶ cells/L, corroborating the observations by Cortés-Lara et al. in 2011 and 2017. These occurrences are influenced bv the notably environmental conditions of the bay, including the influx of untreated sewage and the impact of tourism. Additionally, the phenomenon is further intensified by the interaction of the California Current and the Mexican Coastal Current to Norecuatorial, leading to a unique convergence of factors that exacerbate the prevalence of HABs in the region.

Case 2: Acapulco Bay, Guerrero, México

In February 2019, a study in Acapulco Bay identified several key phytoplankton species. *Karenia longicanalis* was found at 3872 x 10⁶ cells/L, aligning with the findings of Meave & Zamudio (2018). Similar correlations were observed for *Levanderina fissa* at 1738 x 10⁶ cells/L, *Akashiwo sanguinea* at 4410 x 10⁶ cells/L, and *Grammatodinium* sp. at 2531 x 10⁶ cells/L, the latter consistent with Escarceaga-Bata et al. (2023). August 2019 in the bay showed *Miryonecta rubra* at 3558 x 10⁶ cells/L (Cortés-Altamirano et al. 1995), *Lingulodinium polyedra* at 4682 x 10⁶ cells/L, and *Gounyaulax spinifera* at 891 x 10⁶ cells/L, both in agreement with Meave & Zamudio (2018).

October 2019 marked significant discoveries: *Pseudo-nitzschia* spp. at 26 x 10⁶ cells/L and *Chaetoceros* at 681 x 10⁶ cells/L, both matching Meave & Zamudio (2018), and notably,

Helicotheca tamesis (Fig. 5A) at 3298 x 10⁶ cells/L, a new bloom record.

Eutreptiella sp. (Fig. 5D) at 56 x 10⁶ cells/L, a new bloom record and a new record from México considering all the country.

The identification of *H. tamesis* and *Eutreptiella* sp. as a HAB is particularly important as it contributes to our understanding of ecosystem dynamics and potential threats to marine life and human health. These findings underscore the prevalence of HABs in Acapulco Bay during these months, a phenomenon significantly influenced by the convergence of ocean currents. The interaction between these currents, particularly during temperature-induced upwelling events, creates conditions conducive to these blooms, highlighting the complex interplay of environmental factors in this region.

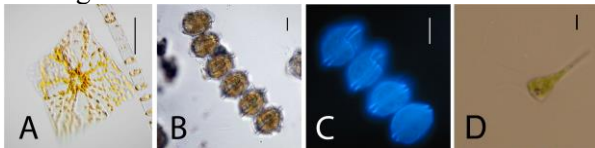


Fig. 5. A) Helicotheca tamesis, B) Pyrodinium bahamense, C) Alexandrium sp. D) Eutreptiella sp.

Case 3: Tehuantepec Gulf

In October 2019, research conducted in the Gulf of Tehuantepec revealed significant occurrences of red tide. Although absolute abundance data were not available, crucial photographic records were obtained. Species identified during these events included Pyrodinium bahamense (Fig. 5B), corroborating Alonso-Rodríguez et al. (2015), and Alexandrium sp. (Fig 5C), aligning with Band-Schmidt et al. (2011). The Gulf of Tehuantepec was notably identified as the area with the most extensive algal bloom, as illustrated in Figure 4. Furthermore, this bloom is directly influenced by the onset of the North Equatorial Current, which transforms into the warm Mexican Coastal Current. This interaction highlights the significant impact of ocean currents on the timing and magnitude of red tide events in the Gulf, underscoring the complex interplay between marine environmental factors and algal bloom dynamics in this region.

The findings are significant because monitoring through GIS, as this study demonstrates, reveals that HABs do indeed occur at least at the surface level. This validates the method despite criticisms regarding its limitations, such as the inability to identify specific species. Nonetheless, it remains an important discovery as it assists local

populations in safeguarding and potentially relocating their cultures.

Conclusions

Firstly, the research conducted across various regions in the TMP in 2019, underscores the significant influence of environmental and oceanographic factors on the prevalence and distribution of HABs. Particularly, regions such as Banderas Bay and Acapulco Bay demonstrate how the interplay of ocean currents, including the California Current and the North Equatorial Current, directly impacts the occurrence and intensity of HABs. These insights highlight the need for continued monitoring and a deeper understanding of oceanographic dynamics. Such knowledge is essential for the prediction and effective management of HAB outbreaks, which is crucial for the protection of marine ecosystems and the safeguarding of coastal economies, especially those that depend on shellfish industries.

Secondly, the effectiveness of employing satellite technology, complemented by advanced microscopy techniques, has been strongly supported in the identification and analysis of HABs within the TMP. Use of the Surface Algal Bloom Index (SABI) algorithm, coupled with field data from the UAMITPacific microalgae collection, has facilitated accurate identification of bloomforming species and their concentrations. This was particularly evident in the detailed analysis of blooms in Banderas Bay, Acapulco Bay, and the Gulf of Tehuantepec. The success of this integrated approach not only validates the application of remote sensing in the study of HABs, but also reinforces the importance of combining several scientific methodologies to achieve a holistic understanding of these complex marine events.

References

- Alawadi, F. (2010). 'Detection of Surface Algal Blooms Using the Newly Developed Algorithm Surface Algal Bloom Index (SABI)'. Remote Sens. Ocean Sea Ice Large Water Reg. 2010, 7825, 45-58.
- Alonso-Rodríguez, R., Mendoza-Amézquita, E., Velásquez-López, S.A., Seim, J.A., Martínez-Rodríguez, V.M. (2015). 'Florecimientos algales nocivos producidos por *Pyrodinium bahamense* en Oaxaca, México (2009-2010)'. Salud Pública Méx. 57(4), 343-351.
- Band-Schmidt, C.J., Bustillos-Guzmán, J.J., López-Cortés, D.J., Núñez-Vázquez, E., Hernández-Sandoval, F.E. (2011). 'El estado actual del estudio de

- florecimientos algales nocivos en México'. Hidrobiológica 21(3), 381-413.
- Cortés Lara, M.D.C., Cortés Altamirano, R., Sierra-Beltrán, A.P. (2004). 'Presencia de *Cochlodinium catenatum* (Gymnodiniales: Gymnodiniaceae) en mareas rojas de Bahía de Banderas, Pacífico mexicano'. Rev. Biol. Trop. 52, 35-49.
- Cortés-Lara, M., Cupul-Magaña, A.L., Cupul-Velázquez, A.M. (2022). 'Fitoplancton marino de Bahía de Banderas con una revisión de los florecimientos algales nocivos en la región'. Pac. Mex. 9.
- Cortés-Lara, M.C., Cortés-Altamirano, R., Cupul-Magaña, A.L., Rodríguez Nava, L.V., Vega-Villasante, F. (2012). Guía de Florecimientos Microalgales (2000-2011) Causantes de Mareas Rojas en Bahía de Banderas, Jalisco-Nayarit. México: Univ. Guadalajara, 112 pp.
- Cortés-Lara, M.C., Gárate-Lizárraga, I., Cupul-Magaña, A.L., Rodríguez-Troncoso, A.P. (2018). In: Navarro-Olache, L.F., Peynador, C. (Eds.), Memorias del XX Congreso Nacional de Oceanografía, Mérida, Yucatán, México, 18-21 September, pp. 14.
- Escarcega-Bata, A., Zamudio-Resendiz, M.E., Hernández-Rosas, A., Resendiz, M.L.N., Dreckmann, K.M., Sentíes, A. (2023). 'First Record of *Grammatodinium* (Dinophyceae) for the American Eastern Pacific Coast: Morphological, Molecular and Ecological Confirmation'. Eur. J. Protistol. 87, 125942.
- Lee, M.S., Park, K.A., Micheli, F. (2021). 'Derivation of Red Tide Index and Density Using Geostationary Ocean Color Imager (GOCI) Data'. Remote Sens. 13(2), 298.
- Meave del Castillo, M.E., Zamudio-Resendiz, M.E. (2018). 'Planktonic Algal Blooms from 2000 to 2015 in Acapulco Bay, Guerrero, Mexico'. Acta Bot. Mex. (125).
- Meave, M.E. and Zamudio, M.E. (2012). Diversidad y dinámica del fitoplancton marino en la bahía de Acapulco, Guerrero, database project-HJ014. CONABIO, Mexico. http://www.conabio.gob.mx/institucion/cgibin/datos 2.cgi?Letras=HJandNumero=14 (Accessed may 22, 2024).
- Utermöhl, V.H. (1931). Neue Wege in der quantitativen Erfassung des Plankton. (Mit besonderer Berücksichtigung des Ultraplanktons.) Internationale Vereinigung für theoretische und angewandte Limnologie: Verhandlungen, 5 (2), 567-596.

Effects of ocean acidification on the growth and domoic acid production of the diatom *Pseudo-nitzschia multiseries* from the California Current System

William P. Cochlan^{1*}, Christopher E. Ikeda^{1,2}, Brian D. Bill³, Vera L. Trainer⁴, Charles G. Trick⁵

¹Estuary and Ocean Science Center, San Francisco State University, 3150 Paradise Drive, Tiburon, CA 94920, USA;

²Pacific Marine Environmental Laboratory, National Oceanic and Atmospheric Administration, 7600 Sand Point Way NE, Seattle, WA 98115, USA;

³Northwest Fisheries Science Center, National Marine Fisheries Service, National Oceanic and Atmospheric Administration, 2725 Montlake Blvd E, Seattle, WA 98112, USA;

⁴Olympic Natural Resources Center, University of Washington 1455 S. Forks Ave, Forks, WA 98331, USA; ⁵Department of Health and Society, University of Toronto, 1265 Military Trail, Toronto, Ontario M1C 1A4, Canada.

Corresponding author's e-mail: cochlan@sfsu.edu

Abstract

Toxic blooms of the diatom genus *Pseudo-nitzschia* are common in the coastal waters of eastern boundary upwelling systems (EBUS), including those of the California Current System (CCS) off the west coast of the United States, where ocean acidification (OA) is unequivocally observed. However, the relationship between toxic blooms with their elevated domoic acid (DA) concentrations and regions of decreased pH levels is still uncertain and variable. Our laboratory study used unialgal cultures of acclimated *P. multiseries* – a toxigenic species isolated from Monterey Bay, a well-known DA hotspot, to examine this relationship and determine whether ocean acidification promotes more rapid cellular growth and/or increased DA production in response to declining pH under both macronutrient-sufficient and -deficient conditions expected in episodic upwelling regions such as the CCS which exhibits silicate limitation of diatom growth in some areas. Unlike earlier studies with other strains and species of *Pseudo-nitzschia*, OA does not affect the specific growth rate achieved by *P. multiseries*. Although cellular DA levels greatly increase with silicate deficiency, there is no significant relationship with pH, and rates of DA production do not increase at reduced pH levels of 7.94 and 7.82 relative to 8.08 (control). Our results demonstrate the importance of using ecologically-relevant species and suggest that the impacts of OA differ greatly among toxigenic species and their degree of macronutrient sufficiency.

Keywords: ocean acidification, diatoms, Pseudo-nitzschia, domoic acid, macronutrients, carbon dioxide, pH

https://doi.org/10.15027/0002041261

Introduction

Atmospheric concentrations of carbon dioxide (CO₂) have increased dramatically due to fossil fuel combustion, and the ocean has absorbed roughly 30 percent of anthropogenically emitted CO₂ since the Industrial Revolution. Currently, CO₂ is dissolving into the ocean at approximately 20-25 million tons per day (e.g., IPCC, 2014), and this process is driving a steady increase in the partial pressure of CO₂ and a decrease in seawater pH - collectively termed ocean acidification (OA). Projections suggest that by the year 2100, average atmospheric CO₂ will increase between 720-1,020 ppm with the resultant decrease in surface ocean

pH by 0.14-0.32 pH units (IPCC 2014; Le Quéré et al., 2018).

Eastern boundary upwelling systems (EBUS), where CO_2 -rich and nutrient-replete waters upwell to the surface are already experiencing levels of OA not predicted for most surface waters until the end of the century. Toxic blooms of *Pseudo-nitzschia* are common in the coastal waters of EBUS, including those of the California Current System (CCS) off the west coast of the United States (e.g., Trainer et al., 2000), where increased pCO_2 and the accelerated decline in seawater pH has been unambiguously demonstrated (e.g., Feely et al., 2008, 2016; Chavez et al., 2018).

At present, the impacts of OA on the growth and toxigenicity of Pseudo-nitzschia species are variable; controlled culture studies have shown that elevated pCO₂ can result in 2-3 fold increases in cellular DA concentrations in nutrient-limited cultures of P. multiseries (Sun et al., 2011) and P. fraudulenta (Tatters et al., 2012), whereas others have reported cellular DA concentrations of P. multiseries to increase up to 70-fold at elevated, not reduced, pH levels in Japanese and Eastern Canadian strains (Lundholm et al., 2004; Trimborn et al., 2008). The relationship between OA and the specific growth rate achieved by Pseudo-nitzschia species is equally confusing since culture studies have shown that elevated pCO2 can result in increased (Sun et al., 2011; Tatters et al., 2012; Kelly et al., 2023), decreased (Lundholm et al., 2004, Ayache et al., 2021; Wingert and Cochlan, 2021) or no change in specific growth rate (Cho et al., 2001; Ayache et al., 2021) depending on the species of Pseudo-nitzschia and the experimental conditions. In the present study we have addressed this unresolved issue by examining the effects of OA on the growth and production of DA by P. *multiseries* – one of the two most harmful diatoms in the coastal EBUS waters of California.

Materials and Method

A toxigenic strain of Pseudo-nitzschia multiseries (HAB-54, isolated in April, 2019 from northern Monterey Bay CA, USA, by H.A. Bowers) was used in the unialgal batch culture experiments described in this study. Cultures were grown in filter-sterilized (0.2-µm, PolyCap® TC filter, Whatman Corp.) coastal seawater (obtained from Bodega Marine Laboratory, Bodega Bay, CA, USA) and enriched with ESNW medium (Harrison et al. 1980; Berges et al. 2001 and subsequent Corrigendum 2004) as outlined by Cochlan et al. (2008). Enrichments were otherwise unchanged except for the macronutrients: silicic acid, nitrate, and orthophosphate which were added at initial concentrations of 50, 150, and 20 µmol L⁻¹, respectively, to achieve culture biomass levels resembling those commonly observed during intense blooms in the EBUS coastal waters off California, and to ensure that the stationary phase was induced by the depletion of silicic acid. Ambient concentrations of nitrate and phosphate were at levels considered saturating for diatom growth throughout the experiment.

Cultures were grown in acid-cleaned, autoclaved 6.0-L Pyrex[®] glass boiler flasks, maintained at 15° C (± 0.5° C) in temperature-controlled environmental chambers (Sanyo MLR-352H), and continuously stirred at 60 rpm to facilitate the suspension of cells within the 4-L of medium. Cultures were illuminated on a 14:10 h light: dark cycle using white, fluorescent tubes (Mitsubishi FL40SS-W/37). Average photosynthetic photon flux density (PPFD), measured using a 4π collector (QSL-100 Quantum scalar irradiance meter; Biospherical Instruments Inc.) immersed in medium-filled culture vessels, was 200 µmol photons m⁻² s⁻¹. Triplicate cultures were grown at the current (pH = 8.08; approx. global average at the sea surface) and two reduced pH levels (7.94, 7.82). The pH of the cultures was controlled by direct injection of a compressed CO₂/air mixture (15% v/v) into the media, and was monitored with a computer-controlled pH/pCO₂ STAT system (Loligo Systems) to maintain the desired pH levels (± 0.02 pH units) as detailed by Wingert and Cochlan (2021).

Individual 'starter' cultures were first acclimated to the three pH conditions for a minimum of three consecutive growth cycles (each 15-16 days in duration and equivalent to 25-30 generations) and were considered acclimated to a specific pH treatment when exponential growth rates varied less than 10% for a minimum of three consecutive growth cycles. Once acclimated, each starter culture was split into triplicate (n = 3) cultures for the final experimental growth cycle where samples were collected daily to determine concentrations of macronutrients, cells and both particulate (pDA) and dissolved DA (dDA). Cell samples (1.5 mL) were preserved with acidic Lugol's solution (2.5% v/v final concentration) and stored in the dark at ca. 5°C until microscopic enumeration using a 1-mL gridded Sedgewick-Rafter chamber and an inverted microscope (Olympus IX83) equipped with a differential interference contrast system. Specific growth rates were calculated from leastsquares linear regression analysis of 3-4 days of exponential growth once equivalent cell densities (>1,000 cells/mL⁻¹) were reached. Rates were determined from plots of the natural log of cell abundance versus time, using the exponential growth equation (Guillard 1973). Samples (100 mL) collected for DA analysis were taken from each triplicate culture, and gently filtered through membrane filters (0.45-µm pore size, 47-mm diam., MF Millipore[™] membrane filters) and the filters and filtrates stored until analyses. Particulate and dissolved DA concentrations were determined from the sample filters and filtrates, respectively, using an indirect, competitive enzyme-linked immunosorbent assay (PNW cELISA; Eberhart et al., 2012).

Results and Discussion

Decreases in pH, resulting from increased dissolved CO₂ levels, did not affect the specific growth rates (µ) achieved by non-axenic cultures of P. multiseries (strain HAB-54) during their nutrient-replete exponential phase. Cultures maintained at pH 8.08 (control), 7.94, and 7.82 supported average specific growth rates of $1.04 \pm 0.08 \,d^{-1}$, $1.00 \pm 0.01 \,d^{-1}$, and 1.09 \pm 0.16 d⁻¹ respectively, and were statistically indistinguishable when examined with a oneway ANOVA and Tukey's HSD tests (8.08 vs. 7.94: p = 0.868; 8.08 vs. 7.82: p = 0.844; 7.94 vs. 7.82: p = 0.562). This result is in contrast to Sun et al. (2011) who reported elevated growth rates for an Atlantic strain of P. multiseries (ca. 16% increase) in nutrient-replete, semicontinuous cultures maintained at increased pCO₂/low pH (ca. 750 ppm/pH 7.9). Variability in growth response to changing pH among species/strains of Pseudo-nitzschia is now apparent; for example, for *P. australis*, specific growth rates are either unaffected, increase, or decrease with expected future declines in pH (Ayache et al., 2021; Wingert and Cochlan, 2021; Kelly et al., 2023).

Given the toxic threat to marine ecosystems and the commercial, recreational, and sustenance fisheries they support, it is essential to understand whether declines in pH resulting from OA will increase the production of DA by species of the *Pseudo-nitzschia* genus. For *P*. multiseries, although particulate (pDA) and dissolved (dDA) domoic acid were detectable in all of the pH treatments during both the nutrientreplete exponential growth and nutrient-deplete stationary growth phases, ca. 90% of the total DA measured during both phases was found as pDA (data not shown). As expected for this species, total DA (pDA + dDA) increased markedly during the Si-limited stationary phase (Figure 1).

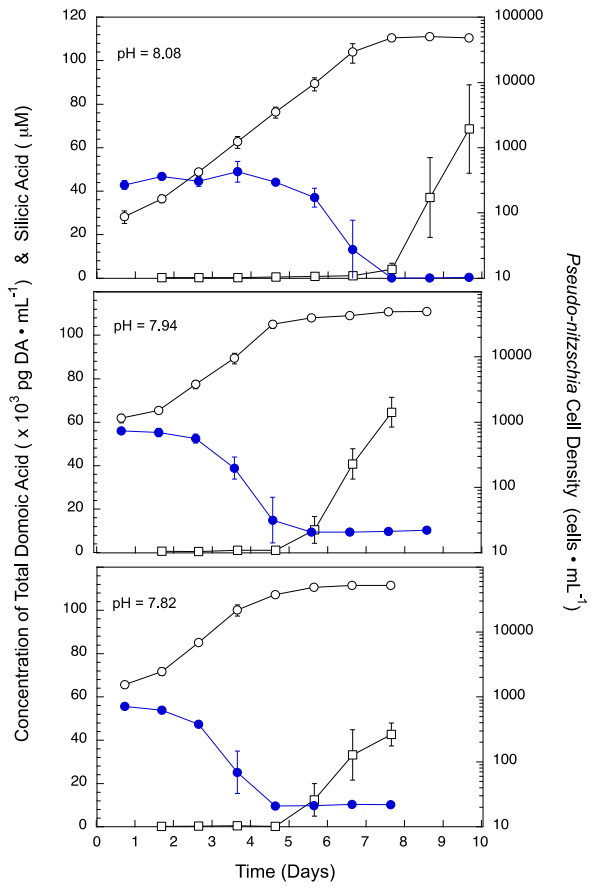


Figure. 1. Ambient concentrations of silicic acid (\bullet), *P. multiseries* cells (\circ) and total DA (pDA + dDA; \square) as a function of time. Values are means of triplicate (n = 3) cultures. Error bars represent ± 1 standard deviation (\pm SD); those not visible are within the size of the symbols.

Unlike a previous OA study conducted with an Atlantic strain of P. multiseries (Sun et al. (2011), we found that DA did not increase with declining pH. The total DA concentrations normalized to cell density did not vary as a result of pH treatment; one-way ANOVAs with Tukey's HSD multiple comparison tests reveal no statistically significant differences between the three pH treatments during both the late exponential phase $(F_{2,8} = 2.45, p = 0.167)$, as well as the three days of Si-limited stationary growth: day 1 ($F_{2.8} = 2.21, p = 0.191$), day 2 ($F_{2.8}$ = 1.47, p = 0.303) and day 3 (F_{2,8} = 4.52, p =0.063). Although the cell-specific concentrations increased with time during the stationary phase (Figure 2), there was no impact of changing pH levels as seen for the P-limited cultures of the Atlantic strain.

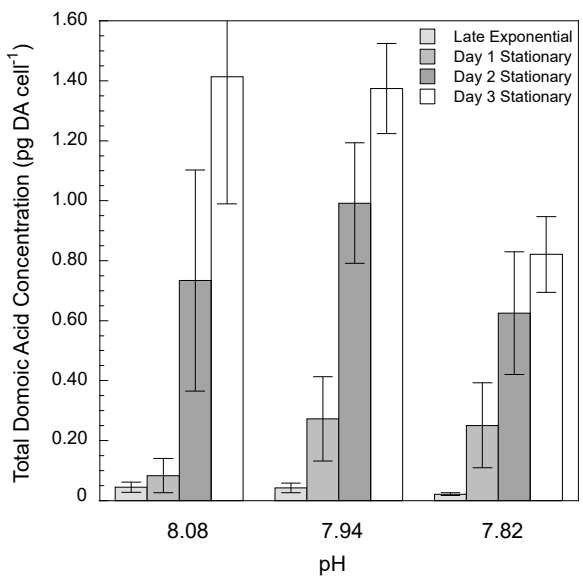


Figure 2. Total DA concentration normalized to cell density as a function of pH during the late exponential phase and three days of Si-limited stationary growth. Values are means of triplicate (n = 3) cultures. Error bars represent ± 1 standard deviation (\pm SD); those not visible are within the size of the symbols.

In the present study, the physiological response of P. multiseries was not associated with pH, but was clearly modulated by macronutrient availability. Here batch cultures were analyzed as they progressed from macronutrient-replete conditions which supported rapid, but pH-invariant specific growth rates and cell-specific DA concentrations, macronutrient-depleted conditions cellular division quickly became minimal, but cellspecific DA concentrations still did not vary with pH. It is clear that increasingly acidic seawater due to rising pCO_2 does not increase the cellular growth rate, nor the production of domoic acid (cellular DA quota) of this strain of *P. multiseries* isolated from the California Current System. As more OA studies are conducted, it is becoming evident that the impacts of OA are not uniform, but vary with species (and strain), and thus geographic-specific isolates from regions of concern must be examined if the results of controlled laboratory studies such as this are employed in models to forecast bloom development and toxicity in natural systems.

Acknowledgements

We thank Ms. Lindsey Metz for her assistance in conducting the experiments presented here. This research was funded by the California Ocean Protection Council (OPC; Prop. 84) administered by California Sea Grant, the California State University Council on Ocean Affairs, Science & Technology (COAST), and the San Francisco Estuary Institute (SFEI). Travel funding was provided by the NOAA Ocean Acidification Program.

References

Ayache, N. et al., (2021). Mar. Environ. Res., 169, 105380.

Berges, J.A. *et al.*, (2002). J. Phycol. 37, 1138-1145 [Correction addition, 40, 619, 2004].

Chavez, F.P. *et al.*, (2018). Deep-Sea Res. Part II 151, 137–146.

Cho et al., (2001). Algae 16, 275-285.

Cochlan *et al.*, (2008). Harmful Algae, 8, 111-118.

Eberhart, B.L., Bill, B.D., Trainer, V.L. (2012). Harmful Algae 19, 39-45.

Feely, R.A. *et al.*, (2008). Science 320, 1,490-1,492.

Feely, R.A. *et al.*, (2016). Estuar. Coast. Shelf Sci. 183, 260-270.

Guillard, R.R.L.(1973). In: Stein, J.R. (ed.), Handbook of Phycological Methods. Culture Methods and Growth Measurements. Cambridge University Press, Cambridge, UK., pp. 289-311.

Harrison, P.J. *et al.*, (1980). J. Phycol. 16, 28-35. International Governmental Panel on Climate Change. (2014). IPCC, Geneva, Switzerland: 1-151.

Kelly, K.J. *et al.*, (2023). Harmful Algae 127, 102467.

Le Quéré *et al.*, (2018). Earth Syst. Sci. Data, 10, 405-448.

Lundholm, N. *et al.*, (2004). Mar. Ecol. Prog. Ser. 273, 1-15.

Sun, J. et al., (2011). Limnol. Oceanogr. 56, 829-840.

Tatters, A.O. *et al.*, (2012). PLoS ONE 7, e32116. Trainer, V.L. *et al.*, (2000). Limnol. Oceanogr. 54, 289-308.

Trimborn, S. *et al.*, (2008). Physiol. Plantarum 133, 92-105.

Wingert, C.J., and Cochlan, W.P. (2021). Harmful Algae 107, 102030.

Application of a quantitative molecular methods to characterize abundance and distribution of *Alexandrium* cysts for NOAA's HAB Forecasting

Cheryl Greengrove^{1*}, Steve Kibler², Julie Masura¹, Julie Matweyou³, Courtney Hart⁴, Mark Vandersea², Tyler Harman²

University of Washington Tacoma, 1900 Commerce Street, Tacoma WA 98402 USA;
 NOAA Beaufort Laboratory,101 Pivers Island Road, Beaufort, NC 28516 USA;
 University of Alaska Fairbanks - Alaska Sea Grant, 118 Trident Way, Kodiak AK 99615 USA;
 University of Alaska Fairbanks - Juneau Center, 17101 Point Lena Loop Road Juneau, AK 99801 USA.

* corresponding author's email: cgreen@uw.edu

Abstract

Alexandrium catenella is a paralytic shellfish poisoning-causing dinoflagellate that overwinters as a resting cyst and germinates into the water column in the spring-summer. Using winter cyst distribution, a Gulf of Maine forecast and an early warning system in Puget Sound, Washington were developed to mitigate human health risks and economic effects of shellfish closures. The current protocol for A. catenella cyst enumeration by fluorescent microscopy is time consuming and requires highly specific training for cyst identification. This MERHAB project, funded by NOAA, includes development of a new quantitative polymerase chain reaction (qPCR) methodology for A. catenella cysts that is being evaluated against the standard microscopy protocol with the goal of producing more rapid and accurate cyst abundance data. Comparison of microscopy- and qPCR-based cyst abundances shows a strong correlation, but quantitative estimates of cysts using the qPCR method tends to overestimate cyst numbers. Assay development showed the importance of using a qPCR standard curve based on cysts instead of a diluted amplicon, necessitating concentration of a large number of A. catenella cysts from the environment at the time of the survey. Furthermore, interannual and regional variability in rDNA gene copy number requires development of a new standard curve for each cyst survey. qPCR standard curves were constructed and compared across three regions using cysts from the Gulf of Maine, Puget Sound and Kodiak, Alaska. To assess temporal variability in rDNA gene copy number, seasonal comparison of qPCR standard curves was completed for Quartermaster Harbor, Puget Sound over one year.

Keywords: Alexandrium catenella, cysts, qPCR, forecast, Gulf of Maine, Puget Sound, Alaska

https://doi.org/10.15027/0002041262

Introduction

NOAA is developing Alexandrium catenella bloom forecast products through the harmful algal bloom Operational Forecasting System (HABOFS) to mitigate human health risks and economic effects of shellfish closures during seasonal blooms of this toxic dinoflagellate along U.S. Atlantic northeast and Pacific northwest coastal states (https://coastalscience.noaa.gov/research/stressor-impacts-mitigation/hab-forecasts/). Alexandrium catenella overwinters as a benthic resting cyst and germinates in the spring (Anderson et al., 2014), making saxitoxin-laden vegetative cells available for filter feeding by shellfish (Cusick and Sayler,

2013). Ingestion of shellfish containing saxitoxin by humans can result in Paralytic Shellfish Poisoning (PSP) (Price *et al.*, 1991). Forecasting efforts hinge on determination of *A. catenella* cyst wintertime abundance at bloom locations.

Previous studies have mapped winter distribution of *A. catenella* cysts in sediments from the Gulf of Maine (GoME; Anderson *et al.*, 2014) and Puget Sound, Washington (PS; Horner *et al.*, 2011; Greengrove *et al.*, 2015) to provide shellfish growers with early warning of potential hotspots for blooms. In addition, sediment cyst surveys in SE Alaska (Tobin *et al.*, 2017) and the Bering and Chukchi Seas (Anderson *et al.*, 2021) indicate high

concentrations of *A. catenella* cysts where there are limited monitoring and forecasting capabilities. The current protocol for cyst enumeration by fluorescent microscopy (Yamaguchi *et al.*, 1995) is laborious, time consuming and requires highly specific training. There is a need to streamline cyst quantification to shorten the turnaround time in advance of the spring bloom season and make the quantification methods consistent across regions.

This project, funded by NOAA's MERHAB program (https://coastalscience.noaa.gov/scienceareas/habs/merhab/), uses sediment samples from the GoME, PS and Kodiak, AK to map regional A. catenella cyst abundances and to conduct interlaboratory comparison of the standard microscopy method for cyst enumeration to check for consistency of counts. These microscopyderived abundances are then compared with those derived using qPCR. The same sediment samples are used to develop and evaluate a qPCR assay for A. catenella cysts. This molecular work builds on species-specific molecular developed over the last two decades (Anderson et al., 1999; Hosoi-Tanabe and Sako, 2006; Erdner et al., 2010; Vandersea et al., 2017). This new method was designed to provide cyst abundance data to HABOFS and other regional marine resource management systems more quickly and consistently than is currently possible with microscopy-based methods. This paper focuses on the comparison of manual microscopy-based cyst counts (Yamaguchi et al., 1995) with the qPCR method in the GoME and examines spatial and temporal differences in qPCR standard curves across the three regions and seasonally over one year in Quartermaster Harbor (QMH), Puget Sound.

Materials and Methods

For the regional analyses, surface sediment samples were collected by Craib corer or Van Veen grab sampler in the GoME at 53 stations in October 2020 and at 47 stations in October 2022; at 47 Puget Sound stations in Jan-Feb 2020; and at 10 Kodiak, Alaska stations in Dec 2020. Sediment for standard curves was obtained from the central Maine cyst seed bed in the GoME (Anderson *et al.*, 2014), from QMH in Puget Sound and in Kalsin Bay near the City of Kodiak, AK. Samples were also collected every other month over a year (2022-

2023) in QMH to evaluate standard curve seasonal variability. The 0-1 cm surface layer was sectioned from Craib cores and retained for processing. The grab samples were sub-sampled from the upper 2 cm of sediment with a plastic scoop. Prior to processing, the sediment samples from the GoME and Alaska were split and subsamples were sent to University of Washington Tacoma (UWT) for duplicate counting as part of the interlaboratory comparison. Samples from PS and Alaska were split and subsamples were sent to the NOAA Beaufort Lab for qPCR method development along with the GoME samples. Samples from the GoME, PS and Alaska were processed and enumerated at each investigator's lab using the standard microscopy method (Yamaguchi et al., 1995). Cyst abundances were mapped using ArcGIS® software (Esri, https://www.esri.com) and microscopybased cyst enumeration results were compared among labs using a t-test (normal data) or Wilcoxon Signed Rank Test (non-normal).

For cyst counting and qPCR, sediment samples were homogenized, and a 5 cm³ subsample was collected for processing. Subsamples were sonicated and sieved to isolate the 20-100 µm cyst fraction after Anderson et al. (2005). Microscopybased cyst enumeration was performed using methods in Yamaguchi et al. (1995). For qPCR, the cyst fraction was concentrated onto a 47 mm, 8 µm NucleoporeTM polycarbonate filter (Cytiva Global Life Science Solutions, Marlborough, MA, USA) and DNA was extracted using the Nucleospin Soil DNA extraction Kit (Takara Bio USA, Inc., San Jose, CA) with lysis buffer SL1 after the manufacturer's protocol. A FastPrep-24 ClassicTM bead beater (MP Biomedicals, Santa Ana, CA, USA) was used to disrupt cysts in each sample at a speed of 6.0 m s⁻¹ for 1 min. The DNA was eluted in 50 µL and qPCR-amplified with a BIO RAD CFX ConnectTM real time system (BIO RAD. Hercules, CA, USA) (Vandersea et al., 2017). The qPCR reaction mix contained SYBR green QuantiNova Probe PCR Master Mix (Qiagen, Germantown, MD, USA) and 1 μL of each DNA extract using a quantification cycle (Cq) after Bustin et al. (2009). A melting curve analysis was performed following thermal cycling to check the specificity of the PCR reactions.

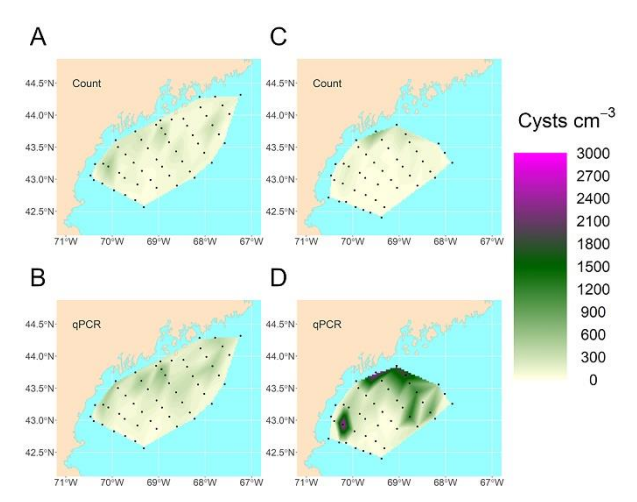


Fig. 1. Gulf of Maine *Alexandrium catenella* manual cyst counts (A, C) and qPCR cyst estimates (B, D) for October 2020 and October 2022 respectively.

Cyst-based qPCR standard curves constructed using microscopy-based counts. A cyst concentrate was first created by processing multiple aliquots of sediment with the methods above, and then using density gradient centrifugation (Richlen et al., 2016) to concentrate the cysts and remove contaminating particulates. Aliquots of the cyst concentrate (1-1,000 cysts) were then DNA extracted for qPCR with identical aliquots for cyst counts. Standard curves were constructed by plotting the quantification cycle (Cq) values vs log transformed cyst concentrations, and linear regression analysis was used to calculate the slope.

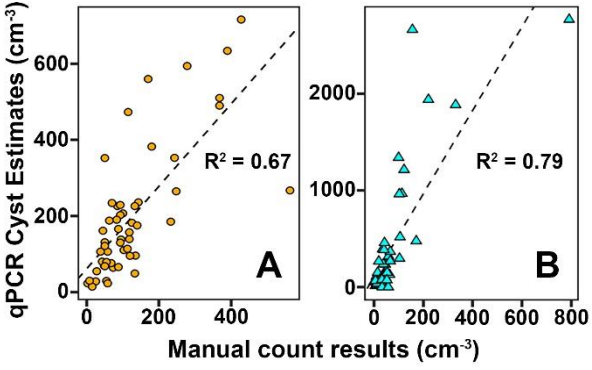


Fig. 2. A) October 2020 and B) October 2022 Gulf of Maine *Alexandrium catenella* cyst correlation analysis between manual counts and qPCR cyst estimates (per cm³). Coefficient of determination (R²).

Results and Discussion

Alexandrium catenella cyst distribution in surface sediments collected from the three regions (over three years) were mapped using the standard microscopy enumeration method from Yamaguchi et al. (1995) that was presented in an earlier proceedings paper (Greengrove et al., 2022). Cysts were present in all three areas (GoME, PS and AK) for all years of the study with Kodiak, Alaska cyst abundances consistently the highest. Here, we compare cyst abundances from the microscopy method with cyst abundance estimates using the qPCR technique for GoME 2020 and 2022 (Figs. 1 & 2). The results show a strong correlation between qPCR assay cyst estimates and manual cyst counts (Fig. 1). However, the qPCR assay method tended to overestimate cyst abundances compared to manual counting methods in some instances (Fig. 2). Cyst-based standard curves were developed so cyst abundance estimates could be determined using qPCR. This assay is an improvement over a previous qPCR assay by Erdner et al. (2010) because we use cyst-based standard curves and not a plasmid-based curve.

Cyst-based standard curves were developed for all three regions (Fig 3A) to assess differences in the Cq that may reflect apparent differences in the number of rDNA gene copies per cyst. The results show cysts from the Gulf of Maine, Puget Sound and Kodiak appear to differ in the number of gene copies per cyst (Fig. 3A), indicating separate qPCR standard curves are likely needed to quantify cyst abundance in each region. To explore the potential effect of seasonal changes on the qPCR standard curve (Fig. 3B), cysts from Quartermaster Harbor in Puget Sound were collected every two months over a year. The results show the Cq can shift over the course of a year (Fig. 3B), indicating a cyst monitoring study at a given location should always be conducted using cysts collected during approximately the same time of year in the same area. These are preliminary results and we hypothesize that these regional and temporal differences may arise from sediment samples containing cysts with different ploidies (i.e., N vs 2N). More cyst microscopy and qPCR data are needed to better understand how year to year variability affects qPCR abundance estimates and if this is related to ploidy differences. So even though cyst-based standard curves are needed for each survey when developing qPCR assays, the qPCR method significantly reduces processing and analysis time for obtaining cyst density estimates. This method may be especially useful for large cyst surveys and could be integrated into HABOFS forecasts results provided a standard curve is created for each survey.

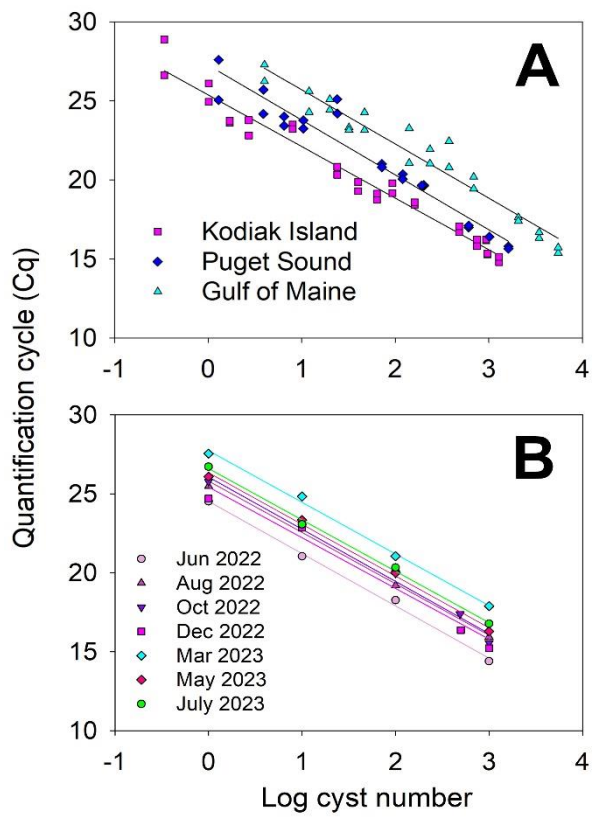


Fig. 3. Comparison of A) Regional cyst-based standard curves for Gulf of Maine, Puget Sound and Kodiak for 2020, and B) Seasonal cyst-based standard curves for Quartermaster Harbor Puget Sound, WA during June 2022 – July 2023.

Acknowledgements

This project is funded by NOAA National Centers for Coastal Ocean Science (NCCOS) MERHAB grant number NA19NOS4780188.

References

Anderson, D.M., Fachon, E., Pickart, R.S., Lin, P., Fischer, A.D., Richlen, M.L., *et al.* (2021). PNAS 118. e2107387118

- Anderson, D.M., Keafer, B.A., Kleindinst, J.L., McGillicuddy Jr., D.J., Martin, J.L., Norton, *et al.* (2014). Deep-Sea Res. II 103, 6-26.
- Anderson, D.M., Kulis, D.M., Keafer, B.A., Berdalet, E. (1999). J. Phycol. 35, 870-83.
- Anderson, D.M., Stock, C.A. Keafer, B.A., Bronzino, A., Nelson, B., Thompson, D.J., *et al.* (2005). Deep Sea Res. II 52, 2522-2542.
- Bustin, S.A., Benes V., Garson J.A., Hellemans J., Huggett J., Kubista M., *et al.* (2009). Clin. Chem. 55, 611-622.
- Cusick, K.D., Sayler, G.S. (2013). Mar. Drugs 11, 991-1018.
- Erdner, D.L., Percy, L., Keafer, B., Lewis, J., Anderson, D.M. (2010). Deep-Sea Res. II 57, 279-287.
- Greengrove, C., Masura, J., Kibler, S., Matweyou, J., Hart, C. (2022) In: Band-Schmidt, C.J. and Rodríguez-Gómez, C.F. (Eds.). Proc.19th International Conf. on Harmful Algae, La Paz, Mexico, pp. 226-231.
- Greengrove, C.L., Masura, J.E., Moore, S.K., Bill, B.D., Hay, L.R., Eldred, K.C., *et al.* (2015). In: MacKenzie, A.L. (Ed.). Proc. 16th International Conf. on Harmful Algae, Wellington, New Zealand, pp. 163-166.
- Horner, R.A., Greengrove, C.L., Davies-Vollum, K.S., Gawel, J.E., Postel, J.R., Cox, A. (2011). Harmful Algae 11, 96-105.
- Hosoi-Tanabe, S., Sako, Y. (2006). Fish. Sci. 72, 77-82.
- Price, D.W., Kizer, K.W., Hansgen, K.H. (1991). J. Shellfish Res. 10, 119-145.
- Richlen, M.L., Zielinski, O., Holinde, L., Tillman, U., Cembella, A., Lyu, Y., Anderson, D.M. (2016). Mar. Ecol. Prog. Ser. 547, 33-46.
- Tobin, E., Eckert, G., Whitehead, C., Sullivan, K. (2017). Alaska Marine Science Symposium, Anchorage, AK, USA, pp. 23-27.
- Vandersea, M.W., Kibler, S.R., Van Sant, S.B., Tester, P.A., Sullivan, K., Eckert, G., *et al.* (2017). Phycologia 56, 303-320.
- Yamaguchi, M., Itakura, S., Imai, I., Ishida, Y. (1995). Phycologia 34, 207-214.

Brevetoxins emergent toxins in France: Evaluation of BTX-3 mouse acute toxicity by oral gavage

Apolline Urman¹, Mathilde Keck¹, Nathalie Arnich², Denis Servent¹, Jordi Molgó^{1*}

¹Université Paris-Saclay, CEA, Département Médicaments et Technologies pour la Santé, Service d'Ingénierie Moléculaire pour la Santé (SIMoS), EMR CNRS 9004, 91191 Gif-sur-Yvette, France. ² French Agency for Food, Environmental and Occupational Health & Safety (ANSES)

*corresponding author's E-mail: jordi.molgo@cea.fr

Abstract

Brevetoxins (BTXs) constitute a family of lipophilic marine phycotoxins produced by the dinoflagellate *Karenia brevis*, but other dinoflagellates are likewise assumed synthesizing BTX-like analogs. BTXs can accumulate in shellfish, fish and diverse marine organisms. Exposure to BTXs in humans may occur mainly by inhalation through aerosolized marine water and potentially by seafood ingestion. BTXs produce the so-called neurotoxic shellfish poisoning (NSP), characterized by neurological, gastrointestinal and/or cardiovascular symptoms. In 2018, BTXs were first detected in mussels from a Mediterranean lagoon in Corsica Island (France). To prevent health risks associated to the consumption of contaminated shellfish, ANSES recommended a guidance level of 180 µg BTX-3 eq/kg shellfish meat, and recommended assessing the BTXs acute oral toxicity in rodents. This study provides information on the acute oral toxicity of BTX-3, the main BTX analog found in shellfish, in male and female mice administered with increasing doses of BTX-3 over a 48-hour observation period. Through our experimental approach, we identified potential starting points that could be used to establish an acute oral reference dose (ARfD) including reductions in body weight, body temperature, and muscle activity.

Keywords: Acute oral toxicity; Brevetoxin-3; Gender differences; Symptomatology; ARfD

https://doi.org/10.15027/0002041263

Introduction

The proliferation of *Karenia brevis* dinoflagellates (red tides) regularly causes harmful impacts on wildlife, human health, and local economies (Flewelling et al., 2005). These negative economic and ecosystem impacts are primarily attributed to the production of brevetoxins (BTXs), and other potentially toxic metabolites, during dinoflagellate blooms (Hort et al., 2021). BTXs are a family of potent liposoluble, thermostable, cyclic polyether marine biotoxins that can accumulate in shellfish, fish, and/or other marine organisms. Like many other marine toxins, they resist cooking and freezing, and they lack a distinctive odor or taste. BTXs bind to voltage-gated sodium channels (Nav) and act as channel modulators in excitable cells and tissues in which the channels are expressed (Konoki et al., 2019; De Lera Ruiz et al., 2015). Perturbation of Nav channel functioning by BTXs causes the NSP (Abraham et al., 2021).

BTX-2 and BTX-3 were first detected in France over 2018-2022 in shellfish samples from the Diana Lagoon by the EMERGTOX network, and correspond to emerging biotoxins (Amzil et al., 2023). BTXs are presently regulated in the United States of America, Mexico, Australia, and New Zealand, but not in France or Europe. The lack of toxicological and epidemiological information to establish maximum shellfish limits led ANSES (French Agency for Food, Environmental and Occupational Health & Safety) to recommend a guidance value of 180 µg BTX-3 eq.kg⁻¹ bw for the presence of BTX in shellfish (Arnich et al., 2021). ANSES also suggested conducting studies focusing on three key areas: i) improving analytical methods for BTX detection, ii) monitoring impacted areas, and iii) assessing the effects of BTX through an acute oral toxicity study in rodents, which was currently lacking in the available literature (ANSES, 2021). Herein, we designed a protocol and investigated the acute oral toxicity of

BTX-3 in male and female mice, taking into account the symptomatology, biological and clinical chemistry parameters.

Materials and Method

BTX-3 (product code: L8902, batch number: 901.122L8902, purity: $\geq 95\%$, and MW: 897.11 g.mol⁻¹) was purchased at Latoxan (Portes-lès-Valence, France), and stored at -20°C. Solutions for administration were freshly prepared in glass bottles with $\leq 5\%$ DMSO for successive dilutions, and the concentrations of BTX-3 used were confirmed by LC-ESI-MS/MS.

The experimental procedure was validated by the local Animal Ethics Committee (CETEA DSV – comité n° 44), and obtained the authorization APAFIS#32015-2021061612169288 v1. Male (n = 30) and female (n = 30) outbred Swiss mice (4-weeks old, were purchased at Janvier Laboratory, St. Berthevin, France).

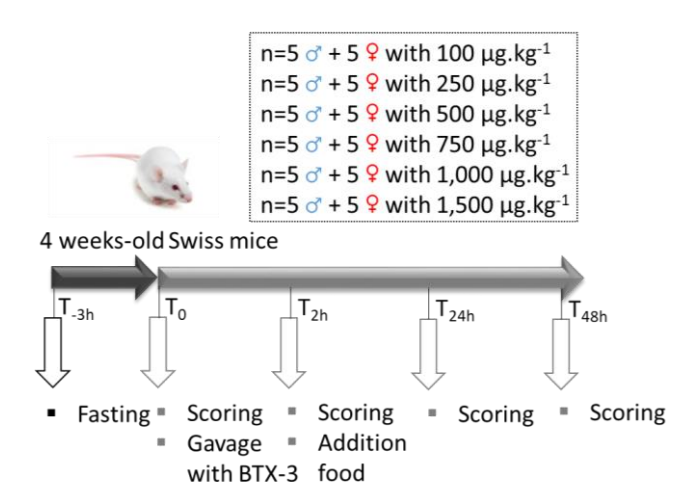


Fig. 1. Doses of BTX-3 studied in mice and the experimental protocol used.

Mice were randomized in sex groups (Fig. 1), before BTX-3 oral gavage with 10 μ L.g⁻¹ (199-312 μ L per mouse) at 6 different doses (100-1,500 μ g.kg⁻¹ bw;) with sterile plastic feeding tubes (20 ga x 38 mm; Phymep, Paris, France). Mice were observed 2 h, 24 h and 48 h after oral administration. At these specified time-points, a scoring system was implemented to assess the critical endpoints outlined in Table 1.

Data are shown as means \pm standard error of the mean. The d'Agostino-Pearson test was used for

Endpoint	Grade 1	Grade 2	Grade 3	Grade 4		
Weight relative to T ₀	< -10%	-10% to -20%	-20% to -30%	> -30%		
Tempe- rature	Normal	> during 24 h	∖ during 48 h	N.A.		
Muscle activity	Normal	Reduced / Mouse in sitting position	Reduced / Crossed front legs / Paralysis of hind legs	Full body stiffening		
Grip test	Success	Failure with attempted collision	Failure without attempted collision	N.A.		
Jaw movement	Normal	Occasional convulsive movements	Repeated convulsive movements	Continuous convulsive movements		
Tremors	No	Occasional	Repeated, but not intense	Repeated & intense		

Table 1. Scoring table. Grade 1 was considered as normal. Grade 2 meant that mouse must be monitored. Grade 3 meant that mouse must be monitored more closely with addition of semiliquid food and heating on mat. If four or more grade 3 parameters were observed, mouse were euthanized. Grade 4 meant that mouse must be euthanized. N.A.: not applicable.

assessing normality. To compare repeated measurements over time, we used the non-parametric mixed-effects model followed by Dunnett's multiple comparisons test. Differences were considered significant if p value was < 0.05. Statistical analyses were done using GraphPad Prism 9 software.

Results and Discussion

The study design was reviewed and approved by ANSES experts. In this study each animal was its own control. We compared each animal to its own basal value at T0, making it easier to detect true treatment effects.

We investigated the effect of a single oral administration in mice with increasing doses of BTX-3 (100 to 1,500 μ g kg⁻¹ bw) during a 48 h observation period. We monitored biological parameters (temperature and body weight) and observed symptomatology (muscular activity, grip test, jaw movements, and tremors) in mice 2 h, 24 h and 48 h after BTX-3 administration (Fig. 2). At these three time points, a scoring system was applied for the critical endpoints listed in Table 1.

It is important to create a scoring table for toxicity evaluation, which would enhance transparency, reproducibility, and standardize the evaluation process.

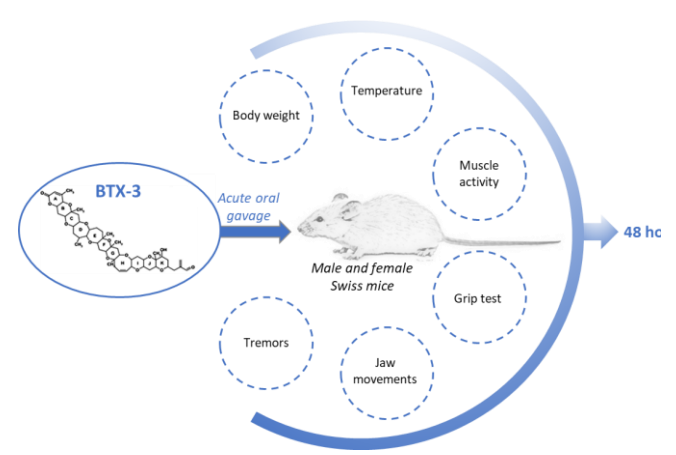


Fig. 2. Schematic representation of parameters evaluated during the experimental procedure.

When assessing the impact of BTX-3 on body weight, female mice showed increased sensitivity. At the dose of 100 µg kg⁻¹ bw, a noticeable weight loss was observed exclusively in female mice 24 h after administration, when compared to before administration (Fig. 3A). This is the first study, performed in both male and female mice, with BTX-3 revealing gender-specific effects of this biological toxin on parameters symptomatology. The role of sex in biomedical studies has often been overlooked, despite evidence of sexually dimorphic effects in some biological studies. Considering both sexes in acute toxicity studies in rodents is essential to ensure a more comprehensive assessment of potential toxic effects, and a more accurate evaluation of health risks, improving the robustness of the results. Sex hormones can influence the metabolism, elimination, and response to toxic substances. From the perspective of extrapolating results to humans, the inclusion of both sexes in preclinical studies is crucial. Sex-specific toxic response in rodents may indicate possible variations in human responses (Karp et al., 2017).

For both genders, BTX-3 induced a rapid, transient, decrease in body temperature (Fig. 3B). Collecting data on body weight and temperature during the observation period is essential and is not done systematically. Variations in body weight and temperature can be sensitive indicators of physiological disturbances, metabolic changes, or other effects related to exposure to the toxin,

bearing in mind that animals of the same species can exhibit significant variations in terms of metabolism, absorption, and elimination of substances.

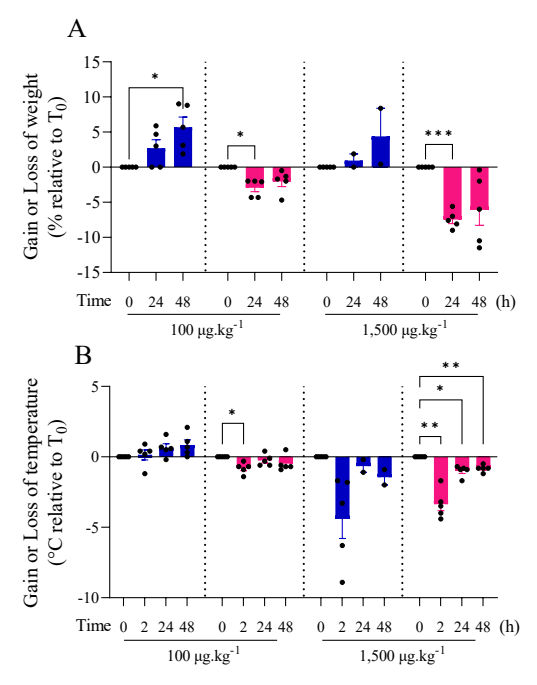


Fig. 3. Gain or loss of weight and temperature after BTX-3 oral administration for 100 and 1,500 μ g.kg⁻¹ bw group over 48 h (male in blue, female in pink). * p < 0.05, ** p < 0.01, *** p < 0.001.

Notably, BTX-3 caused transient reduction in muscle activity in males which manifested by grip test failures, more frequent convulsive jaw movements, and tremors, indicating an increased sensitivity to BTX-3. The onset of symptoms was rapid, occurring within 2 h of administration, and transient, disappearing after 24 h. Table 2 gives NOAEL and LOAL corresponding to the various parameters monitored. At the dose of 1,500 µg kg⁻¹ bw BTX-3 was found more toxic to males. requiring euthanasia in three out of five males just 4 h after administration due to the critical (significant decrease parameters temperature, stiffening of the whole continuous convulsive movements of the jaw, and recurrent tremors). No significant effect of BTX-3 was detected on clinical chemistry parameters whatever the dose administered.

Table 2 summarizes the NOAELs of the following critical endpoints: decrease in body weight, decrease in body temperature, alteration in muscle activity, grip test, jaw movements, and tremors. A benchmark dose lower confidence limit

(BMDL) approach was tested for some endpoints, but the criteria were fulfilled only for muscle activity. BMDL₁₀ were calculated at 448 μg.kg⁻¹ for females and 435 μg.kg⁻¹ for males.

Endpoint	NOAEL	LOAEL			
Decrease in body weight ^a	100 μg.kg ⁻¹ in ♀	250 μg.kg ⁻¹ in ♀			
Decrease in body temperature ^b	NOEL: 100 μg.kg ⁻¹ in ♀	LOEL: 250 µg.kg ⁻¹ in ♀			
Muscle activity	250 μg.kg ⁻¹ in Q 500 μg.kg ⁻¹ in Δ	500 μg.kg ⁻¹ in Q 750 μg.kg ⁻¹ in <i>Δ</i>			
Grip test	500 μg.kg ⁻¹ in ♀	750 μg.kg ⁻¹ in ♀			
Jaw movements	500 μ g.kg ⁻¹ in δ	750 μ g.kg ⁻¹ in $\stackrel{?}{\circlearrowleft}$			
Tremors	$1,000$ $\mu g.kg^{-1}$ in 3	1,500 μ g.kg ⁻¹ in δ			

Table 2. NOAELs and LOAELs identified from this study for critical endpoints. NO(A)EL: No Observed (Adverse) Effect Level; LO(A)EL: Lowest Observed (Adverse) Effect Level

The lowest point of departure would be a NO(A)EL of 100 µg kg-1 bw based on a decrease in body temperature and body weight in females. In a human equivalent dose (HED), this would correspond to 13.44 µg kg⁻¹ bw with a mice body weight of 0.02284 kg (for this group of mice), and a default human body weight of 70 kg, according to the following formula: Human equivalent dose = Animal dose × (Animal weight/Human weight)^{1/4}. To derive an ARfD, the following uncertainty factors would be applied: UFA (interspecies variability) = 2.5 (less than 10 because of the use of an HED), UFH (inter-individuals variability) = 10. The derived ARfD would be 13.44/25 = 0.54 $\mu g kg^{-1} bw = 0.60 \text{ nmol } kg^{-1} bw$. Another potential point of departure would be an alteration in muscle activity, with a NOAEL of 250 µg kg⁻¹ bw in females. In HED, the dose would be 33.92 µg kg⁻¹ bw with a mice body weight of 0.02372 kg (for this group of mice) and a default human body weight of 70 kg. To derive an ARfD, the following uncertainty factors would be applied: UFA = 2.5, UFH = 10. The derived ARfD would be 33.92/25= $1.36 \mu g kg^{-1} bw = 1.52 nmol kg^{-1} bw$. For this endpoint, it was possible to calculate a BMDL₁₀ for males and females. The lowest value was 435 µg kg^{-1} in males. In HED, the dose would be 60.42 µg kg^{-1} bw. The derived ARfD would be 60.42/25 =

 $2.42 \mu g kg^{-1} bw = 2.70 nmol kg^{-1} bw$. Our results, and those recently published (Costas et al., 2023; Barbe et al., 2023) could now be considered by a public health agency in order to establish an official ARfD. Further studies of long-term effects of BTX-3 oral exposure are needed to propose a chronic health-based guidance value.

Acknowledgements

Authors thank the ANSES experts for their comments on the design of this study, and Dr. Anne Thébault for her advice in statistics.

References

- Flewelling, L.J., Naar, J.P., Abbott, J.P., Baden, D.G. *et al.*, (2005). Nature, 435, 755-756.
- Hort, V., Abadie, E., Arnich, N., Dechraoui Bottein, M.-Y. *et al.*, (2021). Mar. Drugs, 19, 656.
- Konoki, K.; Baden, D.G.; Scheuer, T.; Catterall, W.A. (2019) Toxins, 11, 513.
- De Lera Ruiz, M., Kraus, R.L. (2015). *J. Med. Chem.* 58, 7093-7118.
- Abraham, A., Flewelling, L.J., El Said, K.R., Odom, W. et al., Toxicon, 191, 9–17.
- Amzil, Z., Derrien, A., Terre Terrillon, A., Savar. *et al.*, (2023). Mar. Drugs, 21, 435.
- Arnich, N., Abadie, E., Amzil, Z., Dechraoui Bottein. *et al.*, (2021). Mar. Drugs, 19, 520.
- ANSES (2021). Opinion of the French Agency for Food, Environmental and Occupational Health & Safety of 2 March 2021 on the State of Knowledge on Brevetoxins in Shellfish, Data on Toxicity, Occurrence and Brevetoxin-Producing Microalgae (Request No 2020-SA-0020) (in French).
 - https://www.anses.fr/en/system/files/ERCA202 0SA0020EN-b.pdf
- Karp, N., Mason, J., Beaudet, A., Benjamini, Y. *et al.*, (2017). Nat. Commun. **8**, 15475.
- Costas, C., Louzao, M.C., Raposo-García, S., Vale, C. et al., (2023). Food Chem. Toxicol. 182, 114178.
- Barbe, P., Molgó, J., Thai, R., Urman, A. *et al.*, (2023). Mar. Drugs, 21(12), 644.

^a Adverse effect: $1 \supseteq at -10.4\%$.

^b Decrease of 0.8 ± 0.2 °C at 100 μg kg⁻¹ defined as a NOEL (no effect level) because the decrease is of less than 1 °C.

Objectif Plancton: a citizen science program to assess small-scale phytoplankton variability in a macrotidal environment (Bay of Brest, France)

Laura Schweibold^{1*}, Cécile Klein¹, Mathilde Cadier², Marc Sourisseau², Martin Plus², Marine Le Moal³, Céline Liret³, Philippe Pondaven¹

¹Université de Brest, Institut Universitaire Européen de la Mer, IUEM, Univ Brest, CNRS, IRD, Ifremer, LEMAR, Rue Dumont d'Urville, 29280, Plouzané, France.

² DYNECO/Pelagos, Ifremer-Centre de Brest, Technopôle Brest Iroise, Plouzané 29280, France

³Océanpolis, Port de plaisance du Moulin Blanc, 29200, Brest, France

*Corresponding author's email: laura.schweibold@gmail.com

Abstract

Synoptic observations of small-scale (<1 km) variability in phytoplankton community composition based on *in situ* sampling are rare. Thanks to a citizen science program called "*Objectif Plancton*," such sampling of phytoplankton communities has been performed in a macrotidal environment (the Bay of Brest, Brittany, France) since 2014. Using a predefined protocol and a simplified plankton sampling kit, 17 volunteer boaters sample simultaneously at distinct geolocated sites thrice a year. Collected samples are returned to the laboratory for subsequent analysis of phytoplankton community composition and other environmental variables. Recent results from sampling performed in April 2021 and 2022 are presented and compared, including measurements of abiotic parameters and light microscopy counts. Phytoplankton community compositions differ between 2021 and 2022, with the 2021 one consisting of a monospecific bloom of the diatom *Cerataulina pelagica* and the 2022 one being more diverse and evenly distributed. Despite strong tidal currents in the Bay of Brest, the data reveal a non-uniform spatial structuring of phytoplankton communities at small scales, with distinct clusters dominated by different phytoplankton communities. These clusters' cores are close to river estuaries, suggesting that these tributaries significantly impact the spatial distributions of phytoplankton.

Keywords: phytoplankton monitoring, community, synoptic observations, citizen science

Introduction

Citizen science has the potential to make valuable contributions to marine science in situations where the resources available for professional scientific activities are limited. For instance, when there is a shortage of marine scientists and/or scientific vessels, citizen science can provide an opportunity to conduct such scientific studies and enhance their potential (Garcia-Soto et al., 2017). Many marine citizen science monitoring programs have been ongoing for years, ranging from reporting incidental observations to advanced scientific projects requiring special training (Thiel et al., 2014). Concerning the study of planktonic communities, some successful examples exist, thanks to the possibilities given by the participatory approach to extend, for example, spatial and temporal resolution (Esenkulova et al., 2021; Siano et al., 2020).

The French program "Objectif Plancton", launched in 2014 and operational in 2021, aims to study spatial and temporal variability in phytoplankton community composition in a coastal ecosystem facing natural and anthropogenic disturbances. Its originality lies in its innovative sampling protocol, which enables the collection of synoptic observations of phytoplankton community composition and environmental variables on a small scale.

This study compares April 2021 and 2022 samplings to evaluate potential small-scale spatial variability in phytoplankton community compositions in the Bay of Brest and, if it exists, highlight potential underlying mechanisms.

Materials and Methods

Study area

The Bay of Brest is a shallow (8 m on average), semi-enclosed basin of ~180 km², located on the

west coast of Brittany (France; Fig.1) and open to the west on the Iroise Sea by a 1.8 km wide gullet (Fouillaron et al., 2007). This macro-tidal environment is characterized by a short residence time of water masses (~7-25 days; Poppeschi et al., 2021). It has two main tributaries flowing into the bay, the Elorn in the north and the Aulne in the southeast. The combination of strong tidal currents, shallow depths, and short residence time of water masses results in low vertical stratification and significant exchanges with the adjacent Iroise Sea, which limit, to a certain extent, the accumulation of nutrients from river inputs (Le Pape et al., 1999). In this environment, the anthropogenic impact is significant through different activities in the watersheds and bay, such as agriculture, fisheries, and aquaculture (Laruelle et al., 2009; Siano et al., 2021).

Field sampling program

The field sampling program is based on the citizen science program "Objectif Plancton" (hereafter called OP). Using a standardized protocol, it associates scientific institutions, a scientific mediation structure (Océanopolis, Brest), and citizens (boaters) to collect water samples. The project's originality is to collect plankton samples simultaneously in various locations (17 stations; see a map in Fig.1), thus providing a synoptic view of the distribution of plankton in the bay. This program occurs thrice a year (April, June, and Sept.). A complete description and yearly activity reports are available online (https://www.oceanopolis.com/objectifplancton/).

This study analyzed the results from samples collected in the Bay of Brest on April 24, 2021, and April 30, 2022. At each station, 10 L of seawater was sampled 1.5 m below the sea surface. A 250 mL aliquot was immediately fixed with acidic Lugol (~1%) in a brown polyethylene bottle to quantify phytoplankton taxa by optical inverted microscopy. On shore, 1 L of seawater was filtered (©Whatman GF/F 47 mm, porosity: 0.7 um), and three vials (V=15 mL) were filled with the filtered sample and kept for further analysis of dissolved inorganic nitrate and nitrite (DIN), phosphate (DIP), and silicate (DSi) concentrations.

Samples processing and analysis

The temperature and salinity for each station were extracted from the MARS 3D model (Model for Applications at Regional Scales, Lazure & Dumas, 2008). Dissolved inorganic nutrient analyses were measured by colorimetry, using an Autoanalyzer III (©AXFLOW/SEAL), following Aminot & Kérouel method (2007). Phytoplankton taxa in the Lugol-fixed samples were identified following Utermöhl's method (Edler & Elbrächter, 2010).

Data analyses

All statistical analyses and figures were processed using R (version 4.1.3, R Core Team, 2022). Shannon's diversity index (Shannon, 1948) and related Pielou's evenness index (Pielou, 1975) were calculated for each sample. Hierarchical clusterings were conducted using minimum Ward's variance method Hellinger-transformed abundance data to assess the presence or absence of spatial patterns in phytoplankton community composition and possible environmental influences (Borcard et al., 2011). Then, principal component analysis (PCA) was conducted using Hellingertransformed abundance data, and a posteriori projection of significant explanatory variables was added to the plot.

Results and Discussion

Temporal and small-scale variability in phytoplankton community composition In 2021, a monospecific bloom of the diatom Cerataulina pelagica was recorded in all OP stations; this species constituted up to 89% of the total microphytoplankton abundances (ranging from 427 to 940 cells mL⁻¹, Table 1). Including this bloom-forming species, 25 different taxa constituted the top ten most abundant species among 79 identified taxa in the 17 OP stations, with taxon-specific differences in relative abundance between stations. In 2022, a diatom-dominated community was also recorded, multi-specific this time, mainly composed of C. pelagica, Chaetoceros cf. compressus and Dactyliosolen fragilissimus. The total abundances ranged from 313 to 715 cells mL⁻¹. Among the 105 taxa counted, 14 were in the top ten most abundant. Shannon's and Pielou's indexes were higher in 2022 than in 2021, suggesting more diverse and evenly distributed phytoplankton communities (Table 1).

Hierarchical clustering, based on abundance data, revealed three main clusters of stations - showing similar phytoplankton community composition – which were detected in both years (Fig.1, blue, red, and green colors). They were located downstream of the Aulne River (E1), close to the entrance of the Bay (N5, N4), and in the middle of the bay (C2, C3). Cluster configuration differs between 2021 and 2022, with eight out of 17 stations changing groups. These changes occurred mainly in the center of the bay, while stations close to river estuaries

remain in their respective clusters (i.e., N1, N2; E2, E3; E1).

Beyond differences between years - with 2021 showing a community dominated by a monospecific bloom and 2022 being more heterogeneous - a small-scale spatial variability in phytoplankton community composition was detected in the Bay of Brest.

Influence of hydrodynamics

Table 1. Taxa richness (Rich), Shannon's index (H'), Pielou's index (E), and abundance (A,10³cell.L⁻¹) for each *OP* station and their total on April 24, 2021, and April 30, 2022

Statio	ons	C1	C2	C3	C4	E1	E2	E3	E4	N1	N2	N3	N4	N5	S1	S2	S3	S4	Total
2021	Rich	27	23	25	31	30	36	31	40	35	36	32	29	36	26	37	38	33	79
	H'	0.78	0.74	0.8	1.12	0.74	0.76	0.79	1.14	0.96	1.17	1.01	0.91	1.13	0.98	1.19	0.60	0.89	1.01
2021	E	0.24	0.24	0.25	0.33	0.22	0.21	0.23	0.31	0.27	0.33	0.29	0.27	0.31	0.30	0.33	0.17	0.25	0.23
	A	539	634	560	545	832	776	801	822	940	902	641	503	480	769	521	511	427	11204
2022	Rich	54	55	48	58	55	50	48	54	56	54	57	53	51	54	55	56	59	105
	H'	1.91	2.25	1.94	2.11	2.56	1.85	1.83	1.99	1.93	2.15	1.98	1.95	2.08	1.85	2.21	2.09	2.18	2.15
	E	0.48	0.56	0.50	0.52	0.64	0.47	0.47	0.50	0.48	0.54	0.49	0.49	0.53	0.46	0.55	0.52	0.53	0.46
	A	634	568	473	560	313	552	644	642	380	684	715	665	450	671	591	702	620	9862

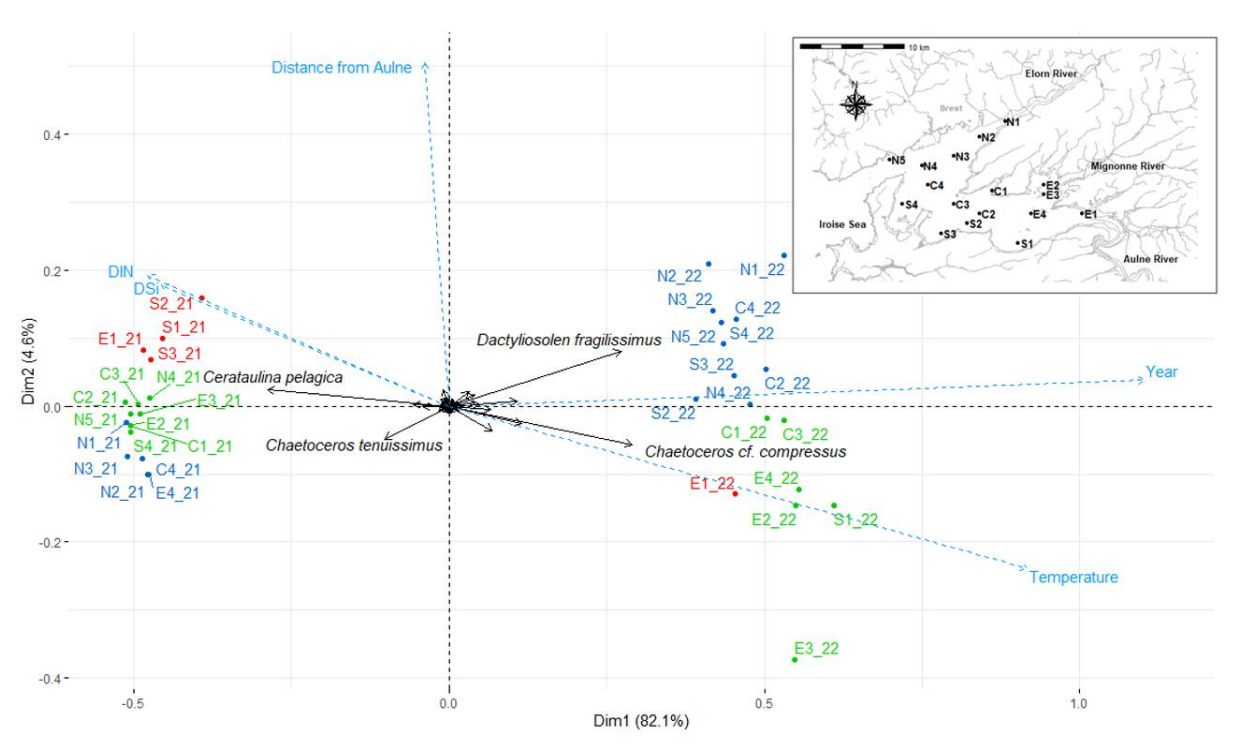


Fig. 1. Principal component biplot of phytoplankton abundances in April 2021 (left) and April 2022 (right), with the four most impactful taxa (solid arrows, active variables) and five supplementary variables (dotted arrows, illustrative variables). The stations were indicated by color (blue, red, green) according to their clusters, obtained *via* hierarchical clustering

Figure 1 shows that the first two axes of the PCA explain 86.69% of the total dataset inertia. The first axis - which accounts for ~82% of the total inertia - separates the two years, which distinct phytoplankton community compositions; the years also differed regarding temperature surface and nutrient concentrations. On the second axis representing 4.6% of total inertia – the stations are closer in 2021 than 2022 because their compositions are less differentiated. For 2022. the grouping is looser, implying more differentiated compositions, and stations are aligned according to a distance gradient from the Aulne's estuary (southeast). So, as seen with clustering, the detected small-scale variations in phytoplankton community composition seem to be linked to river influence.

While proximity to river mouths seems to influence community composition, currents can also interfere with this influence, particularly in the middle of the bay. A comparison of the clusters obtained in 2021 and 2022 further suggests that the alternation of spring and neap tides periods modulates the relative influence that the North-East versus Western boundaries conditions exert on spatial heterogeneity in phytoplankton species assemblages within the Bay. In 2021, the tidal coefficient was lower (value: 67), which may explain the westward extension of the North-East cluster compared to 2022. Conversely, in 2022, the tidal coefficient was higher than in 2021 (value: 88), and the cluster influenced by the Iroise Sea on the western boundaries extends further eastward.

In conclusion, this preliminary analysis confirms the presence of clear spatial patterns despite a macro-tidal environment with short residence times. Further studies are planned to assess the possible influence of hydrodynamics on observed spatial patterns in phytoplankton community composition in the Bay of Brest.

Acknowledgments

This study was funded by *Brest Metropole*, the *ARED* project, the *Fondation de France*, and *Brothier* Laboratories. Special thanks to the team Discovery from *LEMAR* laboratories, Sebastien PETTON and the *IGN* for providing model outputs for map creation, and all

volunteer boaters from the *Objectif Plancton* program.

References

- Aminot, A., and Kérouel, R. (2007). *Editions Quae*, 188pp.
- Borcard, D., Gillet, F., Legendre, P. (2011). New York: Springer, 688pp.
- Edler, L. and Elbrächter, M., (2010). Manuals and guides, IOC, Unesco Paris 110: 13–20.
- Esenkulova, S., Suchy, K. D., Pawlowicz, R., Costa, M., Pearsall, I. A. (2021). Front. Mar. Sci., 8, 725092.
- Fouillaron, P., Claquin, P., L'Helguen, S., Huonnic, P. *et al.*, (2007). J. Exp. Mar. Biol., 351, 188-198.
- Garcia-Soto, C., and van der Meeren, G. I. (2017). European Marine Board IVZW, 114pp.
- Laruelle, G. G., Regnier, P., Ragueneau, O., Kempa, M. *et al.*, (2009). Mar. Ecol. Prog. Ser., 385, 15-32.
- Lazure, P., and Dumas, F. (2008). Adv. Water Resour., 31(2), 233-250.
- Le Pape, O., Jean, F., Ménesguen, A. (1999). Mar. Ecol. Prog. Ser., 189, 135-147.
- Pielou, E. C. (1975). Wiley, 188pp.
- Poppeschi, C., Charria, G., Goberville, E., Rimmelin-Maury, P. *et al.*, (2021). Front. Mar. Sci., 8, 705403.
- R Core Team (2022). R Foundation.
- Shannon, C. E., (1948). Bell Syst. Tech. J., 27, 379-423.
- Siano, R., Chapelle, A., Antoine, V., Michel-Guillou, E. *et al.*, (2020). Mar. Policy, 117, 103039.
- Siano, R., Lassudrie, M., Cuzin, P., Briant, N. *et al.*, (2021). Curr. Biol., 31(12), 2682-2689.
- Thiel, M., Penna-Diaz, M. A., Luna-Jorquera, G., Sellanes, J. *et al.*, (2014). Oceanogr. Mar. Biol., 52, 257-314.

Saxitoxin dynamics underlying bloom development and persistence in the bioluminescent HAB species *Pyrodinium bahamense*

Kathleen D. Cusick^{1*}, Bofan Wei², Nicole L. Brown¹, Edith A. Widder³, Gregory L. Boyer²

¹University of Maryland Baltimore County, Dept. of Biological Sciences, Baltimore, MD, USA ²State University of New York College of Environmental Science and Forestry, Syracuse, NY, USA ³Ocean Research and Conservation Association, Vero Beach, FL, USA. *corresponding author's email: kcusick@umbc.edu

Abstract

Pyrodinium bahamense is a saxitoxin (STX)-producing bioluminescent dinoflagellate that blooms in the Indian River Lagoon (IRL), Florida, the bioluminescent bays in Puerto Rico, and the Indo-Pacific. STX is a potent neurotoxin that binds with high affinity to the voltage-gated sodium channel in humans and causes Paralytic Shellfish Poisoning. Its role in the ecology of P. bahamense remains unknown. While P. bahamense previously existed in Florida with no known record of toxicity, toxic blooms have emerged in the IRL over the past 20 years. The core STX biosynthetic pathway genes have been identified. SxtA4 is essential for toxin synthesis and so serves as a molecular proxy for toxicity. Our lab developed a single-cell multiplex PCR assay targeting the 18S rRNA and sxtA4 genes in P. bahamense and found that some cells within the same sub-populations lack sxtA4. In this work, we examine these genotype dynamics in relation to cell abundance and toxicity in spatially and temporally separate populations in the IRL. Our toxin data, normalized as toxin quota per cell, show that toxin content changes substantially both (1) temporally within the same sub-populations and (2) among sub-populations. Assimilating the collective data among sites revealed a significant negative correlation (Spearman Correlation, -0.434; p = 0.02) between toxin quota per cell and cell abundance: toxin quota decreased with increased cell abundance. The potential ecological link between toxicity and bioluminescence is discussed based on these findings.

Keywords: saxitoxin, Pyrodinium bahamense, Indian River Lagoon, harmful algal bloom

https://doi.org/10.15027/0002041265

Introduction

Pyrodinium bahamense is a saxitoxin (STX)-producing, bioluminescent dinoflagellate that occurs in both the Atlantic-Caribbean and the Indo-Pacific (Phlips et al., 2011; Usup et al., 2012). Humans know saxitoxin (STX) as a potent neurotoxin. It is the causative agent of the human illnesses paralytic shellfish poisoning (PSP) and saxitoxin pufferfish poisoning (SPFP) (Landsberg et al., 2006). Its eco-evolutionary role in the lifecycle of dinoflagellates, however, remains unknown. While multiple hypotheses have been put forward (Cusick and Sayler, 2013), the leading theory is that it functions as a predator deterrent, protecting the cells from copepod grazers.

Toxic outbreaks are well-documented from *P. bahamense* in the Indo-Pacific (Azanza and Taylor, 2001; Llewellyn et al., 2006). In contrast, *P.*

bahamense bloomed in the Indian River Lagoon (IRL), along the east coast of Florida, for years with no known record of STX production. Indeed, it is blooms of *P. bahamense* that are a source of the bioluminescence found along the Florida coast. However, in the mid-2000s, SPFP outbreaks across the US were traced back to Florida, and *P. bahamense* was identified as the source (Bodager, 2002; Landsberg et al., 2006), marking the first occurrence of toxin production by *P. bahamense* in the Western Atlantic.

P. bahamense forms annual recurring blooms in the northern IRL. It is worth noting that *P. bahamense* blooms have been increasing in both duration and intensity (Florida Wildlife Commission HAB reports, Cusick pers. obs.). To gain insights on toxin dynamics among populations, we sampled four spatially distinct areas over the

course of a year. All populations were bioluminescent. Here we present results of cell abundances, toxin dynamics, and genotype frequencies among populations over time and present a hypothesis as to how STX may function in conjunction with bioluminescence to faciliate bloom success.

Materials and Methods



Figure 1. Four sampling sites in the Indian River Lagoon, FL.

Whole water samples were collected from the surface to a depth of 0.5 m. Samples were collected by size-fractionating 10 – 25 L water through 20micron mesh and the biomass rinsed into a sterile 500 ml Nalgene bottle using filtered water from that site. Water samples were collected from four sites (Figure 1) in the IRL over the course of one year (2021-2022). The four sites are distributed among the three water bodies that comprise the IRL: 1. "Diamond Bay" (DB, Banana River); 2. "Haulover Canal" (HC, Indian River); 3. "Kelly Park" (KP, Banana River); and 4. "Beacon 42" (B42, Mosquito Lagoon). Individual cells from each site for genotype analysis were isolated, prepared, and analyzed using a single-cell sxtA4/18srRNA gene multiplex PCR assay as described in our previous work (Cusick and Duran 2021). Samples for toxin analysis were collected onto Whatman AE filters under low vacuum and stored at -20°C until extraction. Samples for cell enumeration were preserved with formaldehyde and stored at 4°C. Cell counts were performed under 100-400X magnification using standard light microscopy with a Sedgewick Rafter counting chamber. Toxicity was determined using the commercial Saxitoxin (PSP) ELISA kit (Eurofins Abraxis LLC, Warminster, PA, USA). STX was extracted with milli-Q water containing 1% acetic acid (v/v). The filter was combined with 5mL extraction solvent. The combined solution was freeze-thawed three times to extract STX. The supernatant was analyzed in duplicate using the STX (PSP) ELISA kit to determine STX concentration according to the manufacturer's instructions.

Results and Discussion

Cell Abundance. Some consider the emergence of *P. bahamense* in the late Spring as one extended bloom in the northern IRL. FWC considers 5,000 or more cells L⁻¹ a bloom (FWC, pers. comm.). Our results indicate these should be considered discrete bloom events, as sampling at four sites within the northern IRL found great variability in both presence and abundance, most notably early in the season. Overall,

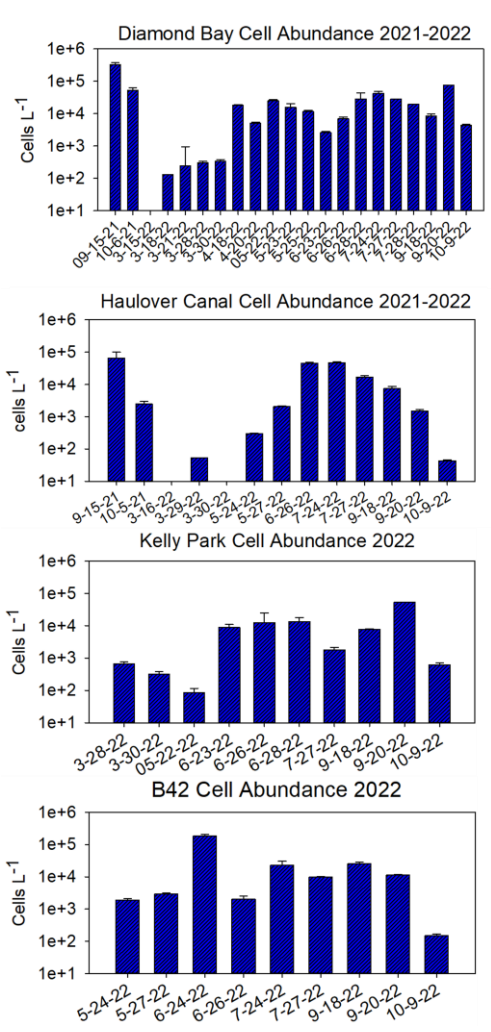


Figure 2. *P. bahamense* abundance over time at four sites in the IRL.

when present, abundances at all sites ranged from ca. 100-100,000 cells L⁻¹. In general, cell abundances at all sites were lowest in the Spring, and increased in the summer and fall. However, averages are not an accurate reflection of dynamics. For example, at DB, cells were not detected on 3/15/2022 but were present three days later. At HC, presence and abundance were very sporadic in March in comparison to DB (Figure 2). Sampling nearly consecutive days in June further underscored this variability, as cell concentrations were nearly identical over 3 samplings over a 5-day span for KP, while B42 showed a decline by nearly two orders of magnitude over that same span. Collectively, it is worth noting that a general trend among all sites showed while cell abundance was fairly consistent in the summer and fall, toxin quota was decreased in the summer in comparison to fall (Figure 4).

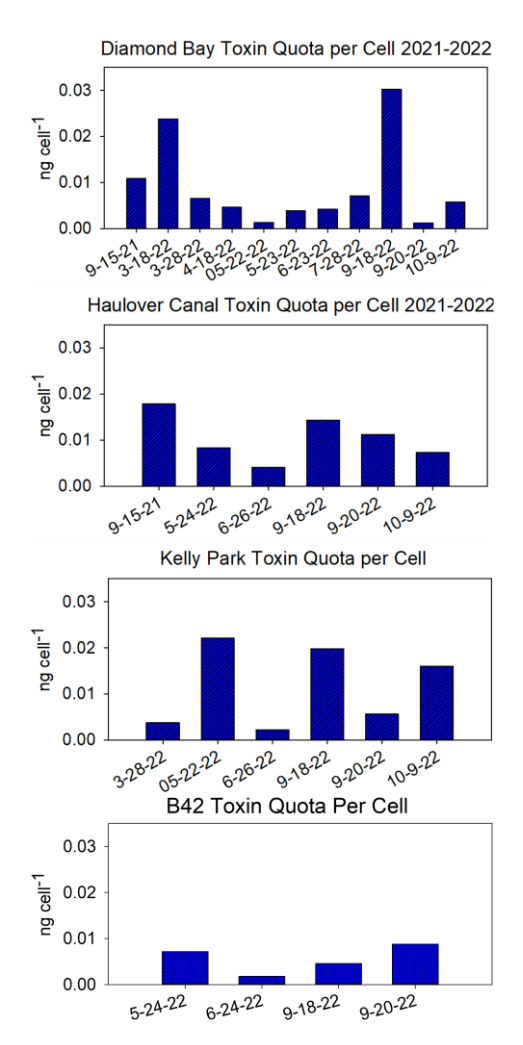


Figure 3. Toxin quota normalized to a per cell basis among populations in the IRL.

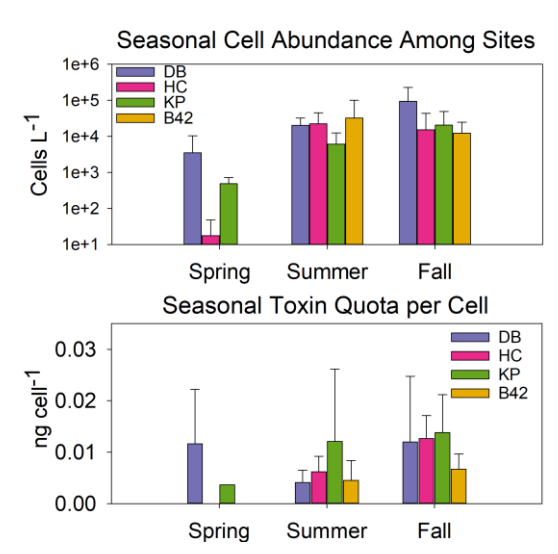


Figure 4. Seasonal average cell abundance and toxin quotae per cell among sites. A lack of bar indicates no samples were collected during that time frame. "Season" was defined as: Spring, March-late May; Summer, late May-Aug; Fall, Sept-Oct. No statistically significant difference was found among sites for either parameter (t-test or Mann-Whitney Rank Sum).

Toxin Dynamics. Toxin quota per cell varied substantially both spatially and temporally. At DB, toxicity fluctuated greatly (Figure 3), with a general trend of lower during summer (average of $0.004 \pm .002$), which is typically peak bloom season, and higher in early spring and fall (averages of .012 $\pm .01$ and $.012c\pm .012$, respectively) (Figure 4). Temporally, toxin quotas among HC populations were more consistent than at DB, typically ranging between 0.1-0.15 ng cell-1 (Figure 3), but displaying the same trend of lower in the summer (average .006 \pm .003) than fall (0.013 \pm .004) (Figure 4).Of all sites, KP displayed the highest averages per summer and fall, 0.012+0.014 and 0.014+0.007, respectively, (spring had only a single sample), but also showed decreased toxin in summer than fall. Of all populations, toxicity was lowest at B42 throughout the season (Figure 3) and remained relatively constant, with averages of 0.004+0.004 and 0.006+0.003 (Figure 4). Here again, toxicity was lower in the summer than fall. When combining all dates and sites, a general trend was observed in that toxin quota per cell decreased as cell abundance increased. The Spearman Correlation confirmed this, with a significant (p = 0.02) negative correlation coefficient of -0.434.

Dinoflagellate species that form some of the most extensive toxic harmful algal blooms (HABs) are also bioluminescent, yet these two traits (toxin production and bioluminescence) are rarely linked when considering the ecological significance of either. A general trend seems to be that the smaller, "dim emitters" such as Lingulodinium polyedra and P. bahamense, are also toxic, while the larger, "bright emitters" such as *Pyrocystis* spp. are not (Cusick and Widder, 2020). Since many bloomforming species are also toxic one hypothesis is that the bioluminescent flash in toxic species functions as an aposematic warning, signaling unpalatability to grazers (Cusick and Widder, 2020). Our work with toxic dim-emitter species showed it functioned as an aposematic signal at low cell concentrations, and a burglar alarm, in which the flash alerts visual predators to the dinoflagellate grazers, at high (Cusick and Widder, 2014; Hanley and Widder, 2017). An extension of aposematism is Batesian mimicry. Strong support for Batesian mimicry in dinoflagellates has come from experiments in the Widder lab that looked at copepod grazing on toxic and non-toxic bioluminescent dinoflagellates (Hanley Widder, 2017). Automimicry is Batesian mimicry within the same species.

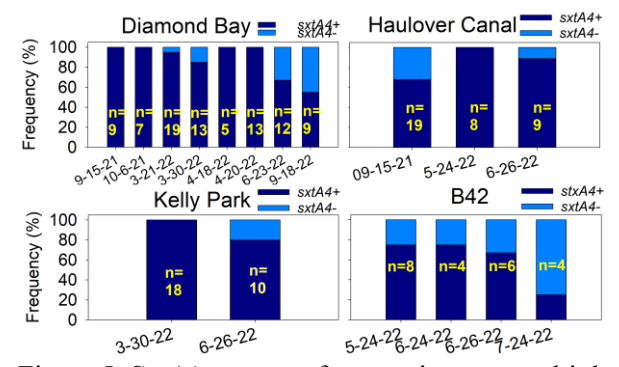


Figure 5. *SxtA4* genotype frequencies over multiple dates from the four sites in the IRL. *n* indicates number of cells analyzed.

Our previous field data with *P. bahamense* indicate an automimicry-like process may be occurring during bloom development: applying a mutliplex PCR on individual *P. bahamense* cells from the same population showed that a small percentage of the cells lacked a key gene (*sxtA4*) for toxin biosynthesis, lending support to the possibility of auto-mimics within the bloom (Cusick and Duran, 2021). We used this assay to analyze single cells

from the four sites in 2022, and our results confirmed the presence of both genotypes, though frequencies varied both spatially and temporally (Figure 5).

The trend in our recent field samplings of toxicity decreasing as cell abundance increased is an intriguing find. It supports the hypothesis that the population is initially comprised of nearly all toxic cells, but a portion of the population then "lose" their toxicity, enabling more rapid growth. However, the underlying molecular mechanism by which toxicity decreases remains to be determined: it may be an increase in sxtA4- cells; a decrease in sxtA4 transcription in sxtA4+ cells; or a combination of both. The inverse correlation between cell density and cell toxin quota has been observed with other HAB species and may simply reflect a concentrating or diluting factor when populations are growing slowly or quickly, respectively, and so must also be considered as an alternative to explain the trend in P. bahamense bloom toxicity recorded here.

Acknowledgements

This research and KC's travel to ICHA was supported by internal funding from UMBC to KC.

References

Azanza, R.V., Taylor, F.J.R., (2001). Ambio 30(6), 356-364.

Bodager, D., (2002). Fl J Environ Health 179, 9-13. Cusick, K., Duran, G., (2021). Microorganisms 9(6), 1128.

Cusick, K.D., Sayler, G.S., (2013). Mar. Drugs 11, 991-1018.

Cusick, K.D., Widder, E.A., (2014). Bull. Mar. Sci. 90, 797-811.

Cusick, K.D., Widder, E.A., (2020). Harmful Algae 98, 101850.

Hanley, K.A., Widder, E.A., (2017). Photochemistry and photobiology 93(2), 519-530.

Landsberg, J.H., Hall, S., Johannessen, J.N., White, K.D., et al (2006). Environ. Health Persp. 114(10), 1502-1507.

Llewellyn, L., Negri, A., Robertson, A., (2006). Toxin Reviews 25(2), 159-196.

Phlips, E.J., Badylak, S., Christman, M., Wolny, J., et al (2011). Harmful Algae 10, 277-290.

Usup, G., Ahmada, A., Matsuoka K., Lim P.T., Leaw, C.P., (2012). Harmful Algae 14, 301-312.

Investigating contributing sources to background domoic acid levels in mussels from Monterey Bay, California

Aubrey Trapp*, Raphael M. Kudela

University of California Santa Cruz, Dept. of Ocean Sciences, 1156 High St, Santa Cruz, California, 95064 United States of America, * Corresponding author: ajtrapp@ucsc.edu

Abstract

On the central California coast, toxigenic populations of *Pseudo-nitzschia* sp. cause near annual harmful algal blooms (HABs) related to upwelling-favorable winds in the spring and summer. This leads to ecological and economic losses from domoic acid toxin. Between bloom events, sentinel mussels at the Santa Cruz Municipal Wharf (SCW) show continuous low-level contamination with domoic acid. Chronic, low dose domoic acid exposure is difficult to regulate and is an emerging health risk for coastal communities. Here we investigate two potential contributing sources to background domoic acid in mussels. The first is the accumulation of dissolved domoic acid. Due to its chemical stability, domoic acid has been shown to persist in marine environments long after causative blooms dissipate. In addition, sampling for dissolved domoic acid via solid phase adsorption toxin tracking (SPATT) from SCW suggest bloom de-coupled toxin events and rising concentrations of dissolved domoic acid in recent years. We use experiments with dissolved domoic acid and California mussels to elucidate dissolved toxin accumulation from the water. The second potential source is slow depuration by mussels after consuming toxic cells. We fit 1-box exponential models to timeseries data from the SCW, tracking depuration months after a bloom event. Results suggest that slow depuration is a good fit for data at this site, although slight uptake of dissolved domoic acid and transient *Pseudo-nitzschia* populations may also bolster background levels between large bloom events.

Keywords: domoic acid, dissolved toxin, sentinel mussels, Pseudo-nitzschia, SPATT

https://doi.org/10.15027/0002041266

Introduction

Domoic acid (DA) is the main toxin threat on the central coast of California. Sentinel mussels collected weekly from the SCW consistently contain low levels of DA. While background toxin levels ($<< 20 \mu g g^{-1}$) are often too low to concern regulators of acute poisoning, new work showing cellular impacts of chronic, low-level DA exposure is an emerging environmental health issue (Petroff et al., 2021). The SCW is a long-running, colocated weekly timeseries including mussels, direct water analysis for particulate domoic acid (pDA), and solid phase adsorption toxin tracking (SPATT). SPATT adsorbs dissolved toxin, representing a quasi-time-integrated sample from 3-7 days prior to deployment (Lane et al., 2010; MacKenzie et al., 2004). SPATT, like mussels, regularly detect DA at the SCW when pDA via direct water analysis does not. In addition, recent work by Trapp et al. (2023) has shown that dissolved domoic acid (dDA) circulates into the Northern part of the bay outside the traditional spring bloom season. This reasoning along with previous experimental work with dDA and shellfish (Novaczek et al., 1991), leads us to propose the accumulation of dDA as one potential source contributing to background DA in sentinel mussels. The second potential source, slow depuration after consumption of toxic cells, has been extensively explored in experimental and field settings (Álvarez et al., 2019; Blanco et al., 2002). To our knowledge, depuration models have not yet been applied to multiple toxic events at one sample site. Here we observe depuration patterns over 12 years of monitoring.

Material and Methods

Experiment with dissolved domoic acid Four tanks, each containing 3 mussels and 500 mL filtered seawater were set-up as follows: 1) Control with filtered seawater, 2) dDA (25 μg DA L^{-1}) , 3) dDA acid (25 μg DA L^{-1}) and Pseudo-nitzschia pungens as a nontoxic food source (8.6 \pm 1.9 ng

Chl mL⁻¹), and 4) Toxic *Pseudo-nitzschia* multiseries $(8.5 \pm 1.8 \text{ ng Chl mL}^{-1}, 6.7 \pm 1.6 \text{ µg DA} \text{ mL}^{-1})$ for two hours at 15 °C with air bubbling. Each tank had 3 replicates. After 2 hours, mussels were opened and rinsed to remove residual tank water. The gills and digestive gland were carefully dissected from the remaining tissue. Samples were homogenized, extracted in 1:10 tissue to volume 50% MeOH, and analyzed by LCMS. Additional extraction details can be found in Peacock et al. (2018) and Lane et al. (2010). ANOVA and Tukey multiple comparisons of means were used to determine statistical significance.

Data acquisition from the Santa Cruz Wharf Time series data for sentinel mussels, pDA, and SPATT were accessed from the online repository (https://erddap.sccoos.org). Data included weekly measurements from 2010-2022. Background DA was calculated from the mean value in mussels when there were no toxic cells in the water column, or when pDA was below the method detection limit (MDL, 0.91 ng DA L⁻¹).

1-Box models Exponential decay with the equation:

$$T(t) = A_o e^{-bt}$$

Where T is the concentration of DA at time, t. A_o is the starting DA concentration and b is the depuration rate was used for 1-box model construction as in Blanco et al. (2002). Mussel data was ln transformed with zero values replaced by the MDL (0.38 ng DA g tissue⁻¹). Then an event threshold of 4 μ g g⁻¹, 20% of the regulatory max, was set to tabulate individual toxic events in the timeseries. Events spanning 0-10 consecutive weeks were included (n = 9). Logged data were fit to a linear model using the least squares method. All statistics and data analysis were performed in R and R studio (v4.2.2; R Core Team, 2022).

Results and Discussion

Background DA was determined from the detection limit up to $0.19 \mu g g^{-1}$, or about 10% of the overall mean value for SCW mussels. Approximately 55% of mussel samples between 2010-2022 were found to contain background levels of DA (Fig. 1A). These samples were distributed across all seasons and all years of the

study period, which contrasts with the traditional spring bloom pattern observed in mussel samples containing higher toxin levels (Fig. 1B). The lack of seasonal pattern suggests that depuration of background DA is slow, though DA uptake may prevent levels from falling below detection limits between bloom periods. A study of chronic exposure to DA by razor clam consumers found that memory could be impaired after consuming 219 µg DA per meal, which translates to approximately 1.8 µg g⁻¹ shellfish (Stuchal et al., 2020). Assuming the same results in mussels, about 15% percent of the samples from SCW would be toxic enough to cause neurological symptoms in humans.

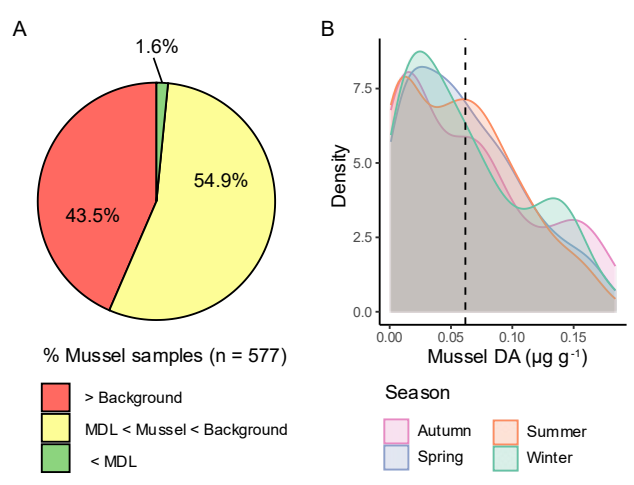


Fig. 1. A) Percent distribution of DA levels in mussels from SCW. B) Temporal distribution of samples containing background DA ($< 0.19 \mu g g^{-1}$). The vertical dashed line represents the mean.

Source 1: Accumulation of dissolved domoic acid To investigate the contribution of dDA to the background levels observed in SCW mussels, an experiment was conducted with wild California mussels and dDA. Mussels cleared most cells from tanks 3 and 4 after two hours, however there was significantly more chlorophyll remaining in the toxic Pseudo-nitzschia treatment than the nontoxic treatment (p < 0.01). Selective feeding of domoic acid producing cells by bivalves is consistent with other work (Mafra et al., 2010). There was no significant difference in dDA in tanks 2 and 3 before and after the experiment. In the digestive gland, there was approximately 50 times more accumulation of pDA from tank 4 than dDA from tanks 2 and 3 (Fig. 2A). With tank 4 excluded, tanks 2 and 3 were significantly different than the

control and from each other. Gill tissue also showed significant accumulation in all three tanks, but the dDA tanks were not significantly different from each other (Fig. 2B). Gill tissue has previously been identified as a primary adsorptive site for DA and amino acids (Novaczek et al. 1991; Manahan et al., 1982). dDA did not appear to be exported to remaining tissues. Taken together, experiments with dissolved DA show that California mussels did not accumulate significant amounts of dDA relative to pDA. This presents evidence that mussels are not an effective sentinel for dDA. Though the environmental effects of dDA are still largely unknown, detrimental effects on zooplankton, such as reduced feeding rates by krill have been observed (Bargu et al., 2006).

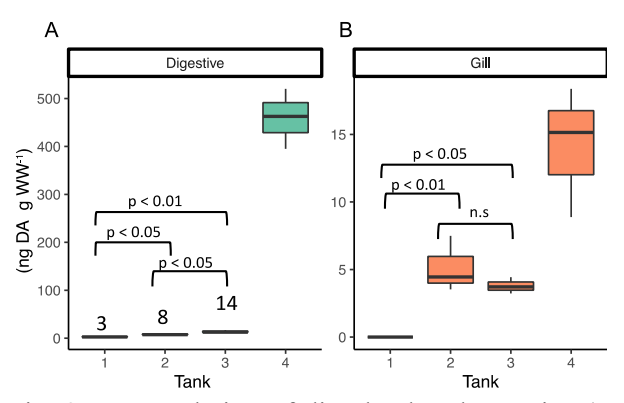


Fig. 2. Accumulation of dissolved and pDA in A) digestive gland and B) gill tissue. Tank conditions are described in methods.

Source 2: Depuration of particulate domoic acid Slow depuration of pDA was investigated through multiple minor toxic events in the SCW timeseries. There were 39 toxic events reaching 4 μg g⁻¹ in mussels between 2011-2022 with 9 events including 10 consecutive weeks of measurements. The event distribution ranged from spring to autumn throughout the study period (Table 1). When a linear model was fit to each event individually, depuration rates ranged from 0.118 μg DA g⁻¹ week⁻¹ to 0.542 μg DA g⁻¹ week⁻¹. Seven events had a good fit to the model (R² > 0.5 and p < 0.05). Using each event as an independent replicate gives a mean depuration rate of 0.36 μg g⁻¹ week⁻¹ (Fig. 3A).

Table 1. Linear model parameters for individual toxic events in SCW mussels. * p < 0.05.

Event No.	Date	A_o (ppm)	b (week ⁻¹)	R^2
1	Aug-2010	4.423	-0.408	0.53 *
2	Mar-2011	4.228	-0.506	0.79 *
3	Aug-2011	6.946	-0.447	0.61 *
4	Aug-2012	6.415	-0.542	0.73 *
5	Aug-2015	1.307	-0.118	0.18
6	Sep-2016	3.904	-0.204	0.72 *
7	Jun-2017	2.211	-0.368	0.64 *
8	May-2019	0.724	-0.238	0.28
9	Jun-2020	0.496	-0.442	0.70 *

This is much lower than reported literature values, however mussels in the field accumulate patchy pDA, which would decrease the effective depuration rate. Residuals were greater than predicted values during the first two weeks (Fig. This indicates that a 1-box model underestimates the true toxin levels at the start of a toxic event and suggests that a variable depuration rate would be more suitable. Other works have resolved the time dependence of residuals by applying a 2-box model, including a fast depuration box (box 1), a slow depuration box (box 2), and a transfer rate from box 1 to box 2 (Blanco et al. 2002). Future work modeling the depuration of mussels in the field may have success conducting experiments to determine depuration of box 1 on the order of days and using a long-term monitoring timeseries to determine the depuration rate of box 2 on the order of weeks or months. Events 5 and 8, which had the worst model fits, were punctuated by small increases in DA that did not meet the threshold for a new event. Thus, adding a third box for short-term accumulation of pDA from transient populations of Pseudonitzschia sp. may better represent real-world processes.

In conclusion, this work is consistent with previous studies showing that mussels accumulate small amounts of dDA primarily through the digestive system and gills. We also show that persistent background DA in the SCW mussels can be explained by slow depuration following a toxic event. In the natural environment, background DA levels are most likely affected by a combination of depuration and intermittent accumulation from dDA and ephemeral toxic cells. This work encourages the application of monitoring systems to investigations of long-term toxin dynamics in shellfish over timescales that exceed most experimental studies.

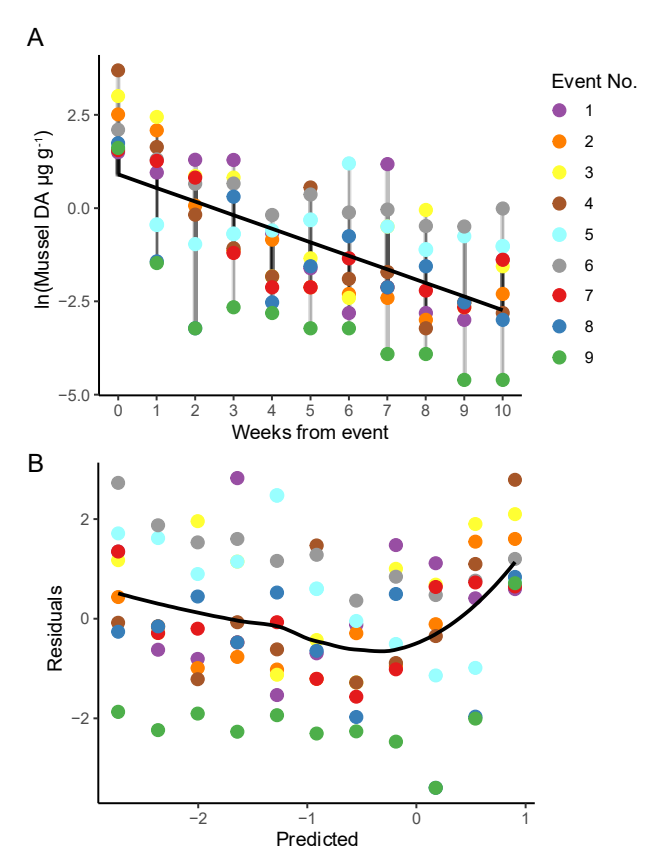


Fig. 3. A) Average linear model parameters for nine toxic events in SCW mussels. B) Residuals vs. predicted plot.

Acknowledgments

The authors give thanks to Kendra Hayashi and others who contribute to the SCW data collection effort. Funding support was provided by NOAA MERHAB award NA18NOS4780174. Travel funding to present this work at ICHA 2023 was provided by NOAA's National Centers for Coastal Ocean Science (NCCOS).

References

- Álvarez, G., Díaz, P., Godoy, M., Araya, M., Ganuza, I. et al., (2019). Toxins 11, 188.
- Bargu, S., Lefebvre, K., Silver, M.W. (2006). Mar. Ecol. Prog. Ser. 312, 169-175.
- Blanco, J., Salgado, C., Moroño, Á., (2002). Aquat. Living Resour. 15, 53-60.
- Lane, J., Roddam, C., Langlois, G., Kudela, R., (2010). Limnol. and Oceanogr: Methods 8, 645–660.
- MacKenzie, L., Beuzenberg, V., Holland, P., McNabb, P., et al., (2004). Toxicon 44, 901–918.
- Mafra, L., Bricelj, V., Fennel, K., (2010). Aquat. Toxicol. 100, 17–29.
- Manahan, D., Wright, S., Stephens, G., Rice, M., (1982). Science, New Series 215, 1253–1255.
- Novaczek, I., Madhyastha, M., Ablett, R., Johnson, G., et al., (1991). Aquat. Toxicol. 21, 103–118.
- Peacock, M., Gibble, C., Senn, D., Cloern, J., Kudela, R., (2018). Harmful Algae 73, 138–147.
- Petroff, R., Hendrix, A., Shum, S., Grant, K.S., *et al.*, (2021). Pharmacol. Ther. 227, 107865.
- Stuchal, L., Grattan, L., Portier, K., Kilmon, K., *et al.*, (2020). Regul. Toxicol. Pharmacol. 117, 104759.
- Trapp, A., Hayashi, K., Fiechter, J., Kudela, R.M., (2023). Harmful Algae 129, 102

Thymine Dioxygenase as a Proposed Enzyme for the Synthesis of 5-Hydroxymethyl Uracil in Dinoflagellates

Emily Jolly¹, Tsvetan Bachvaroff¹, Allen R. Place^{1*}

¹Institute of Marine and Environmental Technology, University of Maryland Center of Environmental Sciences, Baltimore, Maryland, USA.

*corresponding author's email: place@umces.edu

Abstract

Core dinoflagellate genomes contain a fifth nucleotide base, 5-hydroxymethyl uracil (5hmU). While there are several hypotheses for how this base is synthesized or how it gets incorporated into the genome, the exact synthetic mechanism has yet to be determined. We identified a transcript for a hypothetical thymine dioxygenase enzyme in the dinoflagellate *Amphidinium carterae* that could possibly combine thymine, 2-oxoglutarate, and oxygen to produce 5hmU, succinate, and carbon dioxide. In addition, the predicted protein structure and function of the transcript are consistent with other dioxygenase enzymes. Results generated in this study suggest that this transcript is highly conserved across core dinoflagellates as well as the broader Dinoflagellate phylum. Our findings ultimately introduce the possibility for algal bloom mitigation strategies highly specific to dinoflagellate targets should the knockdown or inhibition of thymine dioxygenase prove lethal in dinoflagellates.

Keywords: Dinoflagellate, 5-hydroxymethyl uracil, thymine dioxygenase

https://doi.org/10.15027/0002041267

Introduction

Erwin Chargaff famously established that DNA consists of four nitrogenous bases: adenine, thymine, guanine, and cytosine (Chargaff and Vischer, 1948). In 1973, however, Peter Rae found that about forty percent of the thymines in the dinoflagellate (Crypthecodinium) Gyrodinium cohnii were replaced by a fifth base, 5hydroxymethyl uracil (5hmU) (Rae, 1973). The 5hmU is distributed non-randomly in other core dinoflagellate species and strains, although the percentage at which it replaces thymine in the genome varies (Rae and Steele, 1978). 5hmU incorporation is extremely uncommon outside of Dinophyceae, making this largely a unique trait among core dinoflagellates but not necessarily the broader alveolate lineage (Place et al., 2020). While the function of 5hmU in the dinoflagellate genome is still unknown, it is hypothesized that this fifth base either plays some role in the regulation of gene expression or is a vestigial structure from an ancestral genome (Janoušková et al., 2017; Olinski et al. 2016; Rae and Steele, 1978).

The evidence suggests that incorporation of 5hmU occurs during DNA polymerization rather than as a

post-synthetic modification because i) 5hmU exists both within the deoxyribose and ribose nucleotide pools and ii) the DNA polymerase is not able to distinguish thymine from 5hmU (Galleron, 1984; Mehta et al. 2016: Place et al., 2020). Currently, there are two hypotheses for how 5hmU might be synthesized. The first assumes that 5-methyl cytosine is oxidized to form 5-hydroxymethyl cytosine which then undergoes deamination to produce 5hmU, resulting in a 5hmU:guanine pair. The problem with this hypothesis is that 5-methyl cytosine is only known to exist in higher eukaryotes and Rae's findings established that 5hmU in the dinoflagellate genome replaces thymine and therefore pairs with adenine (Boorstein et al., 1989). Thus, the second hypothesis— which assumes thymine is first oxidized and then hydrolysed to form 5hmU and a 5hmU:adenine pair is more (Rusmintratip and Sowers, 2000). The exact mechanism for this reaction, however, has yet to be discovered.

Previous transcriptomic annotations of *Amphidinium carterae* revealed the presence of a Fe(II)/2-oxoglutarate oxygenase that we hypothesize could combine thymine, 2-

oxoglutarate, and oxygen to produce 5hmU, succinate, and carbon dioxide (Fig. 1). The aim of this study was first to assess whether the sequence for this hypothetical protein is present in all dinoflagellates that incorporate 5hmU into their genomes. The second objective was to elucidate the

H0 -
$$C_{H_2}$$
 OH + 0 OH + 0 = $C = 0$

5-Hydroxymethyluracil succinate CO2

evolutionary origin for this proposed enzyme.

Fig. 1. The predicted reaction mediated by the hypothesized thymine dioxygenase enzyme.

Materials and Methods

Phylogenetic analysis of dinoflagellate transcripts A BLAST search using the A. carterae query sequence was performed against a database comprised of transcripts spanning 42 thecate, 9 naked, 3 non-core, and 2 syndinean dinoflagellates, as well as a single apicomplexan published in previous studies (Bachvaroff, 2019; Bachvaroff et al., 2014, 2011; Kohli et al., 2017; Van Dolah et al., 2017; Williams et al., 2017) as well as NCBI and CAMERA (Sun et al., 2011). Results from this search with an e-value lower than 1e-50 were then used to create a set of potentially homologous amino acid sequences across dinoflagellates. To see whether certain regions of these sequences were highly conserved, the data were imported into MacVector (18.5.0) and aligned via Multiple Sequence Comparison by Log-Expectation (MUSCLE). These aligned sequences were also used to construct a phylogeny with Robust Phylogenetic Analysis for the Non-Specialist (www.phylogeny.fr) which was then reconfigured in FigTree v1.4.4 to root the tree at the midpoint and order the nodes by most recent divergences. From the amino acid dataset, the corresponding nucleotides were recovered and analysed for the presence of the highly conserved spliced-leader sequence 5'-CCGTAGCCATTTTGGCTCAAG-3' and poly-A tail as indicators of completeness since dinoflagellate transcripts start and end with these sequences respectively (Zhang et al., 2007).

Protein structure prediction

The protein structures of amino acid sequences from *A. carterae* and *Oxyrrhis marina* were predicted using Phyre² to compare proposed 3D models and functions across distantly related taxa. The search produced a summary of results ranked by alignment, confidence, and percent identity.

Phylogenetic analysis of outgroup transcripts
Since the origin of the query transcript— and consequently the dinoflagellates' ability to produce 5hmU— is unknown, a second BLAST search was performed against the NCBI nt database. The top 10 hits that did not originate from a dinoflagellate species were then used to create a second dataset to represent an outgroup. With these sequences, a reciprocal BLAST was performed to confirm they are orthologous to the original query. A MUSCLE alignment of this second dataset was also performed against the original dinoflagellate dataset to identify highly conserved regions in the amino acid sequences.

Results and Discussion

The Fe(II)/2-oxoglutarate oxygenases perform a wide variety of biochemical reactions using a shared double-stranded β -helix fold. Roles for this class of enzymes include chromatin modifications, transcriptional regulation, and protein stability (Simmons et al., 2008). InterPro Scan and NCBI revealed that there were two domains in the query sequence that were highly conserved: a non-haem dioxygenase (pfam14226) and an oxoglutarate/ iron-dependent dioxygenase (pfam03171), both of which are classified as Fe(II)/2-oxoglutarate oxygenases. According to Phyre², these two domains produce a series of β -pleated sheets that fold to form a hollow opening of a possible active site. In addition, one of the top hits in the Protein Data Bank matched to a fungal thymine dioxygenase from Neurospora crassa. These results are consistent with our hypothesis that this transcript, originally annotated as a Fe(II)/2oxoglutarate oxygenase, has the potential to use oxygen and thymine to produce 5hmU.

The initial BLAST search against dinoflagellate transcripts returned 91 transcripts 43 species or strains. The average sequence length was 330 amino acids, the average percent identity was 56%, and the median e-value was 9.00e-127. Of all the dinoflagellate transcripts identified, 36 contained

the highly conserved spliced leader sequence while another 10 were complete because they contained both the spliced leader and a poly-A tail. In addition, the phylogenetic tree (Fig. 2) was consistent with general, multiprotein dinoflagellate phylogenies reported in the literature (Janouškovec et al., 2017). Transcripts that contained a spliced leader sequence and/or poly-A tail were evenly distributed across the phylogeny. Hematodinium sp., which are not core dinoflagellates but are syndineans do contain low levels of 5hmU in their genomes, was the most distantly related species (Place et al., 2020). These results suggest that the transcript is highly conserved dinoflagellates. Moreover, the ubiquity of the transcripts across the dinoflagellate phylogeny also lends itself to possible pathways for mitigation strategies highly specific to dinoflagellate blooms.

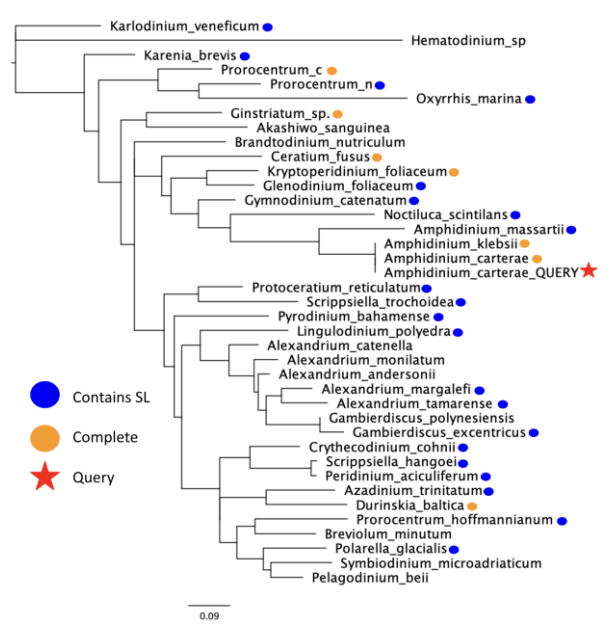


Fig. 2. Phylogeny of dinoflagellate thymine dioxygenase transcripts. Complete transcripts are transcripts that contained both the spliced leader and poly-A tail.

Interestingly, the transcript also appears to be present in a non-core, non-5hmU-producing dinoflagellate. *Oxyrrhis marina* is not a core dinoflagellate and does not contain 5hmU in its genome, but produced a hit against the query sequence (47% identity, 2.00e-115 e-value). The predicted protein structures for *A. carterae* and *O. marina* were similar, both having almost identical 3D models and predicted functions (Fig. 3). These results further support that this sequence is highly conserved across the broader dinoflagellate clade.

Dinoflagellates rely heavily on translational control rather than transcriptional regulation (Roy et al., 2018). Thus, it is possible that while *O. marina* does appear to have a homologous transcript, the resulting protein is never produced.

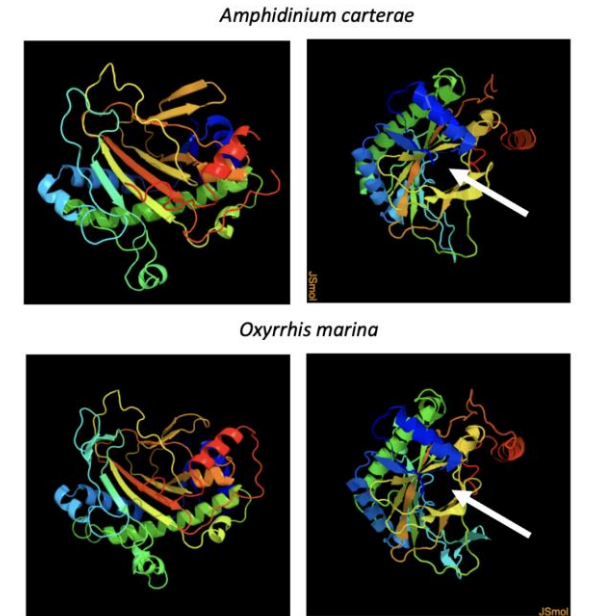


Fig. 3. Predicted protein structure for *A. carterae* and *O. marina*. Left images are oriented to provide better visibility of the beta-pleated sheets that appear to make up the active site as seen in the right images. Color of the model describes the direction of the amino acid sequence starting with red (the N terminus) and ending with blue (the C terminus).

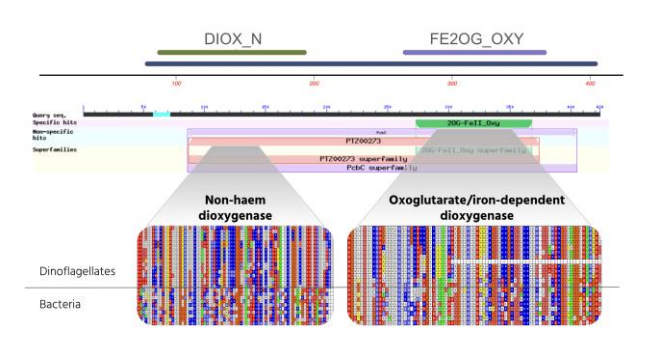


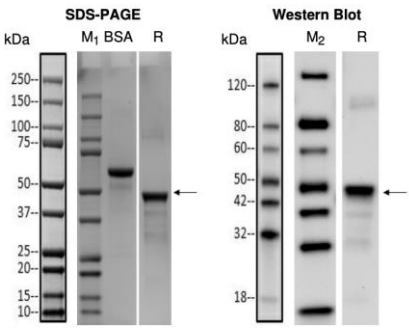
Fig. 4. Domain mappings of non-haem dioxygenase and oxoglutarate/iron-dependent dioxygenase. MUSCLE alignments for dinoflagellate and bacterial transcripts are provided for each domain.

To assess where this hypothetical thymine dioxygenase transcript may have originated, an outgroup was constructed from the top ten, non-dinoflagellate hits of the BLAST search. These ten hits were all bacterial transcripts encoding an

isopenicillin N synthase, another Fe(II)/2oxoglutarate oxygenase. The MUSCLE alignments revealed the iron-dependent dioxygenase domain is much more conserved between dinoflagellates and bacteria (Fig. 4). Events of horizontal gene transfer have been recorded between bacteria and dinoflagellates and it is possible that this domain was derived from a bacterial ancestor (Wisecaver et al., 2013).

We had GenScript synthesize an optimized open reading frame from A. carterae containing a Nterminus His-tag for recombinant protein expression and purification. E. coli BL21 StarTM (DE3) competent cells were transformed with the recombinant plasmid and a single colony was inoculated into auto-induction medium containing kanamycin. Cultures were incubated in 37°C at 200 rpm. SDS-PAGE and Western blot were used to monitor the expression (Fig. 5). As clear from Fig. 5, expression of the dinoflagellate gene is possible in bacteria.

SDS-PAGE & Western blot Analysis:



Lane M1: Protein Marker, Bio-rad, Cat. No. 1610374S, refer to annotated key on the left for size Lane M2: Protein Marker, GenScript, Cat. No. M00673, refer to annotated key on the left for size BSA: 2.00 µg R:Reducing condition Primary antibody: Mouse-anti-His mAb (GenScript, Cat.No. A00186)

Fig. 5. Recombinant protein production of the A. carterae putative thymine dioxygenase enzyme in E. coli

To summarize, these results suggest that the A. carterae query transcript for a hypothetical thymine dioxygenase enzyme is present in all core dinoflagellates that contain 5humU in their genomes as well as dinoflagellate species that do not. This work also demonstrates that the predicted structure and function of the enzyme are consistent with our hypothesis regarding the synthetic pathway of 5hmU. Future work will need to confirm that the enzyme performs its hypothesized function by synthesizing recombinant proteins, quantifying enzyme kinetics and substrate

specificity, and analysing products formed. Should interruption of 5hmU synthesis be lethal in dinoflagellates, this unlocks a pathway toward highly targeted mitigation strategies for harmful algal blooms.

Acknowledgements

This research was funded by the Institute of Marine Technology's Environmental Innovations in Science Program Grant. Attendance to ICHA was funded by the University of Maryland College Park, the University of Maryland Center for Environmental Science, and NOAA's National Centers for Coastal Ocean Science.

References

Bachvaroff, T.R. (2019). PLOS ONE 14, e0212912.

Bachvaroff, T.R., Gornik, S.G., Concepcion, G.T., Waller, R.F. et al., (2014). Mol. Phylogenet. Evol. 70, 314–322.

Bachvaroff, T.R., Handy, S.M., Place, A.R., Delwiche, C.F. (2011). J. Eukaryot. Microbiol. 58, 223–233.

Boorstein, R.J., Chiu, L.-N., Teebor, G.W. (1989). Nucleic Acids Res. 17, 7653-7661.

Chargaff, E. and Vischer E. (1948). J. Biol. Chem. 176, 703-714.

Galleron, C. (1984). Orig. Life 13, 195–203.

Janoušková, M., Vaníková, Z., Nici, F., Boháčová, S. et al., (2017). ChemComm 53, 13253-13255.

Kohli, G.S., Campbell, K., John, U., Smith, K.F. et al., (2017). J. Eukaryot. Microbiol. 64, 691–706.

Mehta, A.P., Li, H., Reed, S.A., Supekova, L. et al., (2016). J. Am. Chem. Soc. 138, 7272–7275.

Olinski, R., Starczak, M., Gackowski, D. (2016). Mutat. Res. Rev. Mutat. Res. 767, 59-66.

Place, A.R., Williams, E., Bachvaroff, T.R., Sabatini, R. (2020). In: Hess. P. (Ed.), Proc: Harmful Algae 2018--from ecosystems to socio-ecosystems, Nantes, France, pp.181–184.

Rae, P.M.M. (1973). Proc. Natl. Acad. Sci. 70, 1141-

Rae, P.M.M. and Steele, R.E. (1978). Biosystems 10, 37-53.

Rusmintratip, V. and Sowers, L.C. (2000). Proc. Natl. Acad. Sci. 97, 14183-14187.

Simmons J.M., Muller T.A., Hausinger R.P. (2008). R. Soc. Chem. 38, 5132-5142.

Sun, S., Chen, J., Li, W., Altintas, I. et al., (2011). Nucleic Acids Res. 39, D546-D551.

Van Dolah, F.M., Kohli, G.S., Morey, J.S., Murray, S.A. (2017). J. Phycol 53, 1325–1339.

Williams, E., Place, A.R., Bachvaroff, T.R. (2017). Mar. Drugs 15, 125.

Zhang, H., Hou, Y., Miranda, L., Campbell, D.A. et al., (2007). Proc. Natl. Acad. Sci. 104, 4618–4623.

Impact of drought and wildfires in recent trends of Diarrhetic Shellfish Toxins in cockles from northwest Portugal and its similarities with sardine stock trends in the period 2001-2023

Paulo Vale1*

¹ The Portuguese Sea and Atmosphere Institute, I.P. (IPMA, IP), Sea and Marine Resources Department (DMRM); R. Alfredo Magalhães Ramalho 6, 1495-165, Algés, PORTUGAL

*corresponding author's email: pvale@ipma.pt

Abstract

In mainland Portugal, the occurrence of diarrhetic shellfish poisoning toxins (DSTs) from *Dinophysis* in spring and early summer has been positively related to precipitation. Continental runoff supplies regularly nutrients to the marine food chain. A northwest to the south coast decreasing gradient in DSTs is commonly found, similar to the latitudinal decrease in precipitation and of macronutrients (N, P and Si). A decrease in average precipitation after 2003 led to a reduction in the interannual average concentration of DSTs after 2008 on the NW coast and the S coast. However, the accumulation of DSTs on the NW coast increased in the period 2019-2022. In the last two decades, extensive forest wildfires were recurrent, but the area burned reduced sharply after 2017 following tighter fire control measures. Low levels of DSTs or a low percentage of weeks with samples above the regulatory limit from the NW coast were related to high burned areas in the previous year. The recent increase in 2019-2022 of DSTs, a planktonic biomarker in bivalves, was also coincident with the similar temporal increase in either the recruitment or the biomass of *Sardina pilchardus*, a small pelagic planktivorous fish in decline after 2005-2006. Low sardine recruitment or low sardine biomass were coincident with low precipitation or high burned areas. Wildfires degrade coastal water quality, as seems reflected both in the bivalve DSTs and the sardine stock time series.

Keywords: diarrhetic shellfish toxins; cockles; Ria de Aveiro; drought; wildfires; global change; water quality; sardine recruitment; time-series

https://doi.org/10.15027/0002041268

Introduction

The occurrence of Diarrhetic Shellfish Toxins (DSTs), originating from *Dinophysis* spp in spring and early summer, has been related to precipitation in Portuguese bivalves (Vale, 2012). Continental runoff regularly supplies nutrients to the marine food chain. Toxic Dinophysis are mixotrophs and require a two-level food chain of other microalgae in order to thrive: a ciliate (Mesodinium rubrum), which in turn is required to supply plastids from a cryptophyte (Teleaulax sp.) (Park et al., 2006). Precipitation is highest on the northwest (NW) than on the southwest (SW) or south (S) coasts. A NW to S decreasing gradient in DSTs is commonly found as well as in macronutrients (N, P and Si) (Nogueira et al., 2016; Vale, 2022). A decrease in average precipitation after 2003 (Fig. 1), led to a reduction in the interannual average concentration of DSTs after 2008 on the NW coast as well as in the S coast (Vale, 2022).

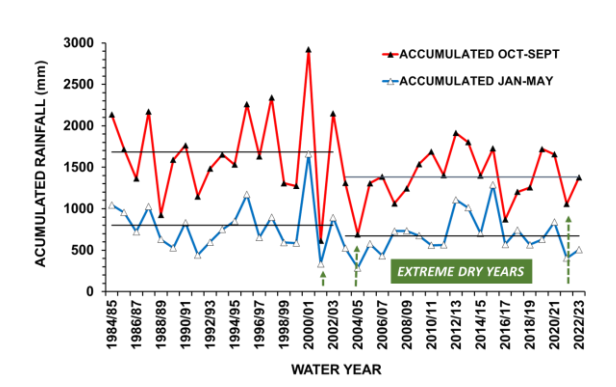


Fig. 1. Precipitation at Castelo de Burgães station, in the Vouga basin (NW Portugal). Red line depicts annual precipitation for the water year (Oct-Sep), and blue line depicts precipitation accumulated during Jan-May. Lines represent the averages for selected periods and dashed arrows extremely dry years.

However, the annual percentage of weeks with toxins above the regulatory limit (RL) on the NW

coast presented an increasing trend in the period 2019-2022. As this was unexpected, other environmental variables (severe drought and wildfires), were explored here to understand these opposite trends in the bivalve *Cerastoderma edule* (cockle) from Ria de Aveiro, which accounts for 90% of the annual cockle catch in Portugal (DGRM, 2023) (Fig. 2). These trends were further compared with data from another filter-feeder, *Sardina pilchardus* (sardine), a small pelagic fish, whose main spawning area is within the coastal area off Aveiro (ICES, 2021), and accounts for 25% of annual fish captures (DGRM, 2023).

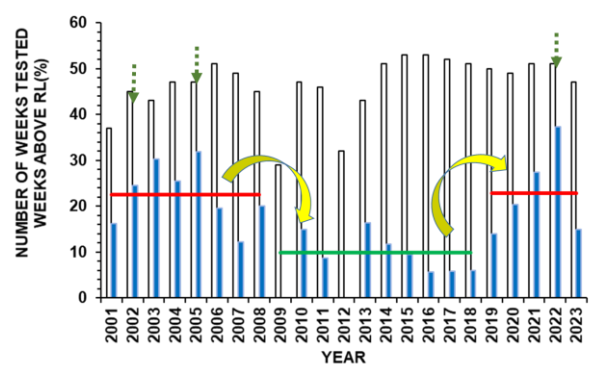


Fig. 2. Number of weeks tested annually for DSTs in Ria de Aveiro's cockle between 2001-2023 (white bars), and the percentage of those weeks with samples exceeding the regulatory limit (blue bars). Lines depict interannual average of weeks with cockles above the RL.

Materials and Methods

Cockles were collected weekly from Ria de Aveiro, Portugal, as part of the ongoing monitoring programme. DSTs were extracted with methanol and analysed by LC-MS until 2011 (Vale and Sampayo, 2002) and LC-MS-MS from 2013 forward (EURLBM, 2015).

Monthly precipitation data was from the National Water Resources Information System (SNIRH, 2024). The total burned area from wildfires was from the Institute for Nature and Forest Conservation (ICNF, 2024; former DGRF). Official statistics on sardine abundance were retrieved from ICES (2023).

Precipitation from Castelo de Burgaes station or other nearby stations in the Vouga river basin was analysed here. For comparison with DSTs, rainfall accumulated between January and May was taken into account. For sardines, cumulative precipitation was calculated between March of year N-3 and February of year N. The annual sardine stock

assessment is carried out annually by IPMA usually each March-April.

The total area burned by wildfires which took place in the Aveiro district in the year N-1 were related to DSTs. The total area combined burned in the districts of Viana do Castelo, Aveiro, Viseu and Coimbra in year N-1 were related to the abundance of sardine recruits (age-0 individuals) and in year N-2 to the biomass of sardines (age 1+ individuals). The number of symbols on top of each box-whisker plot, denotes significant differences at p<0.05, p<0.01 or p<0.001 level, respectively.

Results and Discussion

In severe dry years (2002, 2005 and 2022, arrows in Figs. 1 and 2), the average annual percentage of weeks above the regulatory limit in cockle samples surpassed (31%) both the low (14.3%) and high (17.8%) precipitation years (Fig. 3a). The same was observed for the mean DST's levels in samples above the RL (Fig. 3b).

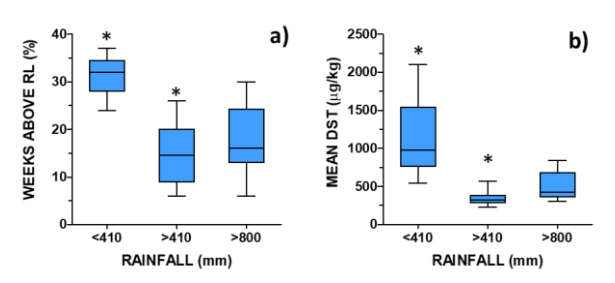


Fig. 3. Relationship between: a) the number of weeks above the RL; b) average DST levels, with precipitation of the preceding January through May for the years 2001-2023.

In severe dry years, toxicity originated mainly from monospecific blooms of *D. acuta* (e.g. 2005, 2022) or *D. acuminata* (2002), instead of the spring-summer *D. acuminata* - *D. acuta* species succession (Fig. 4). While *D. acuminata* grows after the abundant river discharges in spring, *D. acuta* is capable of growing in summer during upwelling favourable conditions, circumventing a poor terrestrial runoff year (Moita el a., 2006).

Nevertheless, this does not explain the continuous increase during 2019, 2020 and 2021, leading to the search for other environmental variables. Although wildfires have been increasing in recent decades (DGRF, 2005), the severe wildfire season of 2017 and its associated fatalities swiftly prompted the implementation of harsher wildfire control measures nationwide, which resulted in a

significant reduction of the area burnt annually immediately in the year 2018 (ICNF, 2024; Fig. 5a).

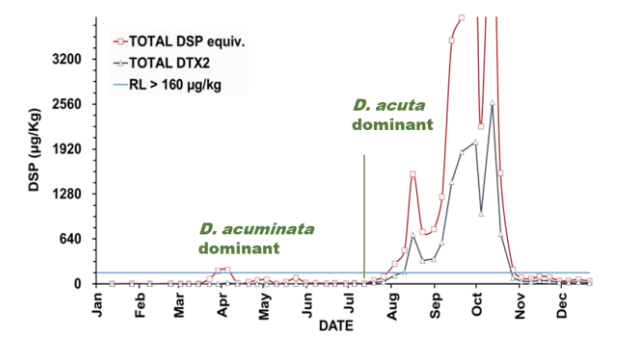


Fig. 4. Evolution in Ria de Aveiro's cockle of total toxicity (in μ g AO+DTX2/Kg) and the *D. acuta* marker toxin, DTX2 (in μ g/Kg) alone, during the dry year of 2005.

Wildfires take place mainly in mountainous areas with steep slopes. The ash layer is prone to postfire mobilization and export by water, particularly in steep slopes. Raoelison et al. (2023) compared preand post-fire freshwater quality, revealing that wildfire could increase the concentration of many pollutants by two orders of magnitude. After the wildfire, nutrients, suspended solids and polycyclic aromatic hydrocarbons (PAHs) concentrations increased within a year and heavy metals within 1-2 years.

Analysis of water courses affected by distinct fires in several regions of central Portugal showed an increase in the total mineralization of water, N and P, the cations Ca, Na, Mg and Mn, and of polycyclic aromatic hydrocarbons (PAHs) (Costa et al., 2014; Ferreira et al., 2016; Mansilha et al., 2019).

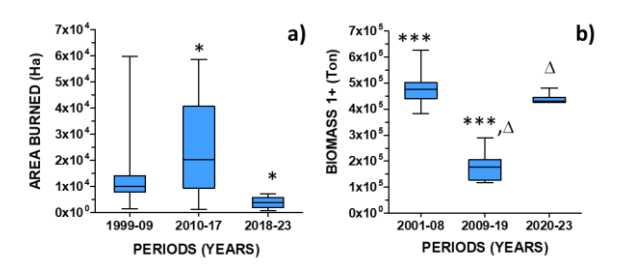


Fig. 5. a) Distribution of the annual areas burned in the districts of Aveiro and Viseu combined for selected years. b) biomass of sardine specimens aged +1 years during selected time periods.

A high number of weeks above the regulatory limit or a high concentration of DSTs took place mainly when the burned area in the Aveiro district alone was below 4000 hectares in the previous year (year N-1) (Fig. 6). The Aveiro district covers most of the Vouga river basin and its delta (Ria de Aveiro). The abundance of sardine recruits suffered a strong reduction after 2005, and sardine biomass reduced progressively after 2006 (ICES, 2023; Fig. 5b). Recruits recovered starting in 2019 and biomass in 2020 (ICES, 2023; Fig. 5b).

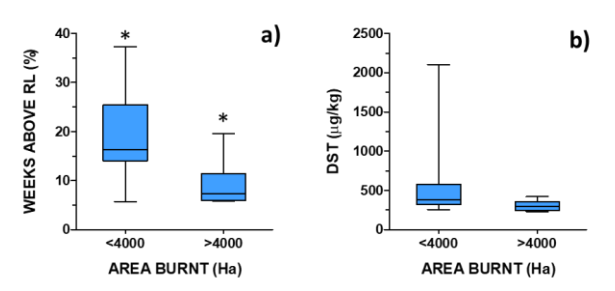


Fig. 6. Distribution between the a) the number of weeks with toxins above the RL and b) average toxin levels with the area burned in the Aveiro district in the previous year.

The abundance of this small filter-feeder pelagic fish increases with rainfall (Fig. 7), reflecting also the relevance of runoff nutrients to boost the marine food chain.

However, its abundance suffered a drastic reduction when burned areas were above 40,000 hectares in coastal districts in the year N-1 for recruits (Fig. 8a) or in the year N-2 for biomass (Fig. 8b).

Conclusions

Global change is affecting terrestrial inputs into the ocean, directly by reducing precipitation and indirectly by favouring forest fires all across the Mediterranean area (WMO, 2022). This research highlights that alterations in river runoff are already more impacting than an increase in water temperature, as the Western Iberian coast has not been warming in recent decades (WMO, 2022).

Wildfires degrade coastal water quality, maybe through the increase in PAHs and other toxics, as seems reflected in the cockle's DSTs and the sardine stock time series. These results oppose the plankton stimulation by ashes found in oligotrophic coasts, such as Australia (Liu et al., 2022), because the Western Iberian waters are not oligotrophic in nutrients such as Fe, N and P (Nogueira et al., 2016).

Despite the lower precipitation trend, improvement in coastal water quality allowed a recovery in plankton in 2019, as one year seems enough for the recovery of water quality, even after severe wildfire years.

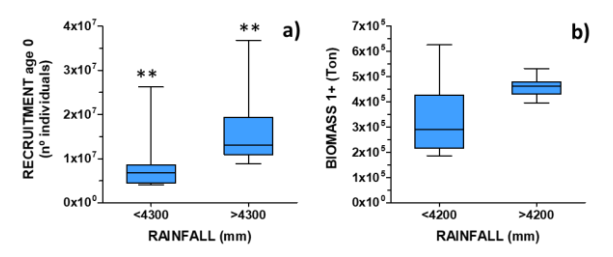


Fig. 7. a) distribution of sardine: a) recruitment and b) biomass, with rainfall.

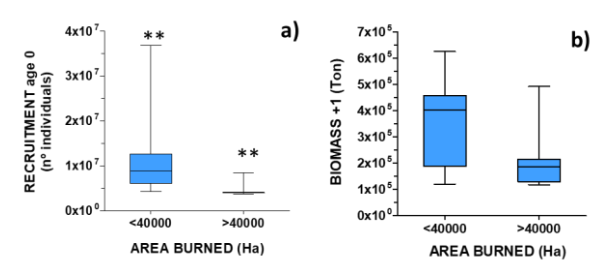


Fig. 8. a) distribution of recruitment with the area burned in the year N-1; b) distribution of biomass with the area burned in the year N-2.

The most relevant driver considered for sardine recruitment has been water temperature around 15 °C or lower during the spawning season of October-April (Ferreira et al., 2023). Temperatures during Oct-Dec of year N-1 (data not shown) were above optimal between 2007 and 2016, coinciding with the continuously low recruitment period (Fig. 5b). However, the presence low temperatures in Oct-Dec of 2005 or in 2017, failed to explain the low abundances of recruits found in the spring assessment of 2006 and 2018, respectively (ICES, 2023). The repercussions of the strong wildfire seasons of 2005 and 2017 in the marine environment must be taken into consideration for understanding the decline in recruit numbers in 2006, their failure to recover in 2018, as well as in the reduction of DST's levels. Keeping the areas burnt by wildfires to a minimum, seems to be of utmost importance to both terrestrial, freshwater and marine ecosystems.

Acknowledgements

The author acknowledges the EU Fisheries Operational Program 2020, FEAMP - Mar2020 (SNMB-Monitor programmes), which funds the National Bivalve Mollusc Monitoring System (SNMB) conducted by IPMA in Portugal. EU

funding also supports the National Biological Sampling Programme (PNAB) conducted by IPMA. Other institutions supplied raw data for this study: APA (SNIRH) and ICNF.

References

Costa, M.R., Calvão, A.R., Aranha, J. (2014). Appl. Geochem. 44, 93-102.

DGRF (2005). Direcção Geral dos Recursos Florestais (Ed.), Lisboa, Portugal, 28 pp.

DGRM (2024). Recursos da Pesca. Série Estatística, vol. 36 A-B, ano 2023.

Ferreira, A., Garrido, S., Costa, J.L., et al. (2023). Sci. Total Environ. 881, 163421.

Ferreira, R.V., Serpa, D., Machado, A.I., et al. (2016). Sci. Total Environ. 572, 1281–1288.

ICES (2021). ICES Scientific Reports 3, 108. 57 pp. https://doi.org/10.17895/ices.pub.8144

ICES (2023). ICES Advice 2023, pil.27.8c9a. https://doi.org/10.17895/ices.advice.21975209

ICNF (2024). Instituto da Conservação da Natureza e das Florestas, I.P., Lisboa, Portugal. https://www.icnf.pt/florestas/gfr/gfrgestaoinformacao/grfrelatorios/areasardidaseocorrencias

Liu, D., Zhou, C., Keesing, J.K., et al. (2022). Nat. Commun. 13, 1348.

Mansilha, C., Duarte, C.G., Melo, A. et al. (2019). Sustain. Water Resour. Manag. 5, 319-331.

Moita, M.T., Sobrinho-Gonçalves, L., Oliveira, P.B., et al. (2006). Afr. J. Mar. Sci. 28, 265-269.

Nogueira, M., Vale, C., Caetano, M., et al. (2016). Relatório Científico Final. IPMA, Lisboa, 45 pp.

Park, M.G., Kim, S., Kim, H.S., et al. (2006). Aquat Microb Ecol 45(2), 101-106.

Raoelison, O.D., Valenca, R., Lee, A., et al. (2023). Environ. Poll. 317, 120713.

SNIRH, 2024. Agência Portuguesa do Ambiente, Lisboa, Portugal. https://snirh.apambiente.pt/index.php?idMain=1.4 1&idItem=1.1

Vale, P. (2012). Estuar. Coast. Shelf Sci. 98, 94-100

Vale, P. (2022). Reg. Environ. Change 22, 116.

Vale, P. (2023). Estuaries and Coasts 46, 1792–1807.

Vale, P., Sampayo, M.A.M. (2002). Toxicon 40, 33-42.

WMO (2022). World Meteorological Organization (Ed.), Geneva, Switzerland, 52 pp.

Investigation of Limit of Detection and Quantification for digital PCR assays: the case study of *Azadinium spinosum* (Dinophyceae) in Irish waters

Nicolè Caputo¹, Dave Clarke², Francesca Cucchi¹, Fiona Kavanagh¹, Luca Mirimin^{1*}

¹Marine and Freshwater Research Centre, Atlantic Technological University, Galway, Dublin Road, H91 T8NW Galway, Ireland.

²Marine Environment and Food Safety, Marine Institute, Rinville, Oranmore, H91 R673 Galway, Ireland. *Corresponding author: Luca.Mirimin@atu.ie

Abstract

Azaspiracids (AZAs) are a group of lipophilic toxins associated with Azaspiracid Poisoning (AZP) in humans following consumption of contaminated shellfish. AZA toxins are produced by some species of marine nano dinoflagellates from the cosmopolitan family Amphidomataceae. Ireland is one of the countries most affected globally by AZA events, where blooms of toxigenic Azadinium spinosum have been leading to prolonged closures of shellfish farms. DNA-based techniques such as quantitative PCR (qPCR) and digital PCR (dPCR) are extremely sensitive methods that have shown great potential for routine screening of environmental samples, with the former being successfully applied in the detection and relative quantification of some species of Amphidomataceae in Irish waters. In contrast, dPCR has been used to a lesser extent despite its ability to enable absolute quantification of low-copy targets and potential to mitigate enzymatic inhibitory effects. Thus, the present study tested the accuracy of two dPCR systems (Standard BioTools' BiomarkHD and QIAGEN's QIAcuity Four) using a TaqMan probe-based assay targeting the LSU-rDNA gene in samples of known target concentration. Limit of Detection (LOD) and Quantification (LOQ) thresholds were defined to infer transferability, repeatability, and reproducibility of the assay across the different systems. Both dPCR methods showed a positive correlation between and within platforms, and high sensitivity and accuracy in detecting and quantify low-copy targets. These are promising results especially in view of implementing these platforms into National Monitoring Programmes for monitoring harmful phytoplankton.

Keywords: Azadinium spinosum, azaspiracids, quantitative PCR, digital PCR, LOD, LOQ, monitoring.

https://doi.org/10.15027/0002041269

Introduction

Azadinium spinosum Elbrächter et Tillmann is a photosynthetic marine nano-dinoflagellate of the cosmopolitan family Amphidomataceae, responsible for the production of azaspiracids (AZAs), a group of lipophilic toxins associated with Azaspiracid Poisoning (AZP) in humans following consumption of contaminated shellfish (Tillmann et al., 2009). AZAs are a major problem in Ireland, where toxin concentrations in shellfish often exceed the EU regulatory limit (160 µg/kg AZA equivalents), resulting in prolonged closures of shellfish farms, predominantly around the West coasts (Salas et al., 2011; Clarke, 2020). The Marine Institute is the National Reference Laboratory for monitoring of marine biotoxins phytoplankton in Ireland. From 2007, it has been implementing DNA-based methods for the simultaneous identification and enumeration of harmful species, overcome microscopy to limitations and improve species identification. A quantitative PCR (qPCR) TaqMan probe assay highly specific for the toxigenic ribotype A of Az. spinosum was developed by Toebe et al. (2013). The relative quantification in qPCR is based on pre-calibrated standard curves of the target gene and the technique is sensitive to environmental inhibitory effects which may generate false negatives (Kavlick, 2018). Digital PCR (dPCR) is a third-generation PCR method that enables absolute quantification of gene copies without calibration curves, based on the binomial response of a random distribution (Dorazio & Hunter, 2015). It boasts its high resilience to PCR inhibition effects thanks to the partitioning of the samples into thousands of single reactions, allowing a wide range of applications (i.e.: Yarimizu et al., 2021; Tiwari et al., 2022). The aim of this study is to test the transferability and sensitivity of the assay

developed by Toebe et al. (2013) in two dPCR platforms. This was done by investigating (i) its quantitative linear dynamic range, (ii) the Limits of Detection (LOD) and Quantification (LOQ), and (iii) potential PCR inhibitory effects.

Materials and Methods

Reference materials

Prior to DNA extraction, samples were prepared spiking monospecific cell culture of Az. spinosum (3D9 strain) into sterile seawater, in triplicate, along with a negative control (sterile seawater). DNA lysis and extraction were conducted following a modified the protocol of **DNeasy** Plant Mini manufacturer's instructions (QIAGEN), previously described by Lefran et al. (2020), excluding the liquid nitrogen cell disruption step. DNA extraction was performed using a QIAcube automated nucleic acid isolation system (QIAGEN). Amplification of the 28S ribosomal DNA (72 bp) was performed in triplicate, using species-specific primers Asp48F/120R (Toebe et al., 2013). PCR reaction included 1X AccuStartII PCR ToughMix (Quantabio), primers at a final concentration of 500 nM each, 3 µL of DNA template and molecular grade water for a final volume of 25 µL. PCR thermal cycling profile was: 3 min at 94°C, followed by 40 cycles of 30s at 94°C, 30s at 56°C and 60s at 72°C. The quality of the PCR products was examined on a 1.5% agarose gel stained with SYBRSafe (Invitrogen). Quantification performed using a Qubit fluorometer with a dsDNA HS Assay Kit (Invitrogen). A 10-fold standard dilution series of known concentration was prepared in TE buffer, ranging from 10⁹ to 10⁰ copies/μL. Standards were aliquoted and stored at - 20°C until analysis.

Real-time quantitative PCR (qPCR)

Standard curve construction was performed in triplicate for each dilution point, to identify the dynamic range. The lowest 4 points of the curve before the concentration plateau were tested to identify the LOD and LOQ, in 20 replicates each. Negative and No Template Controls (NTC) were included in every run. PCR reaction contained 1X EagleTaq Universal Master Mix (Roche), primers Asp48F/120R at a final concentration of 900 nM each and TaqMan FAM-MGB probe Asp77T at 200 nM (Toebe et al., 2013), 2 μL of DNA template and molecular grade water, for a final volume of 20 μL . The assay was run on the real-time PCR instrument Roche LightCycler 480 II with the following

cycling parameters: 2 min at 50°C; 10 min at 95°C; 40 cycles of 15s at 95°C, 60s at 60°C.

Digital PCR (dPCR)

The Az. spinosum probe-based assay was run on two dPCR platforms: BiomarkHD (Standard BioTools) and QIAcuity Four (QIAGEN). The BiomarkHD platform relies on a chip-based microfluidic technology and it is composed by two different systems of workflow operation. The partitioning takes place on the central array of the qd37k 48-inlets Integrated Fluid Circuit (IFC) plate in 770 partitions per inlet (36,960 single reactions of 0.84 each). Following manufacturer's recommendations, PCR pre-mix was carried out in an excess final volume of 6 µL per sample, of which 4 μL were loaded into each inlet. The standards were performed in triplicate to identify the dynamic range, while the lowest 4 points were tested in 10 replicates to identify LOD and LOQ.

The QIAcuity Four platform relies on a nanoplate microfluidic technology where the partitioning takes place on-plate in a fully integrated system with partitioning, thermocycling and imaging. The nanoplate used was the 26k 24-wells (624,000 single reactions of 0.91 nL each). Following manufacturer's recommendations, PCR pre-mix was carried out in a final volume of 40 µL. The standards were performed in triplicate to identify the dynamic range, while the lowest 4 points were tested in 5 replicates to identify LOD and LOQ. For both platforms, NTCs were included in every run to control any false positive amplifications, primers/probe concentrations and PCR cycling followed the same conditions as previously described for the qPCR.

Inhibition control

For the inhibition control, environmental samples resulted positive to qPCR inhibition test using an Internal Positive Control (IPC) standardized method (Kavlick, 2018) (data available upon request), were tested on both dPCR platforms with a spike of known standard concentration into respective PCR mixtures.

Statistical analysis

Prior to analysis, DNA concentrations measured with dPCR were corrected by the respective effective reaction sizes (Whale et al., 2020). All statistical analysis were performed with RStudio Software; the linearity between expected and estimated concentrations was analysed by Pearson's correlation test. LOD and LOQ were calculated with

two different R-script models developed for eDNA studies in combination with the discrete threshold method (Coefficient of Variation, CV=35%) (Forootan et al., 2017; Hunter et al., 2017; Klymus et al., 2019). The relationship between dPCR data obtained was assessed by Spearman's rank correlation test. The quantitative variable of spiked environmental samples in dPCR was analysed with a two-sided Student *t* test. A *p* value lower than 0.05 was considered statistically significant.

Results and Discussion

aPCR and *dPCR*

Results for both PCR platforms are summarized in Table 1. The consistency of the 10-fold dilution series was assessed with the qPCR, as gold-standard technique. Efficiency (E)=100%, r^2 =0.99, slope=-3.315 were obtained. As DNA approach concentrations zero. measured concentrations are higher than expected resulting in a concentration plateau, a fixed instrument response, which produce nonlinear standard dilution series and higher standard deviations (Hunter et al., 2017). The Pearson's coefficient between nominal concentration and estimated response showed a high linearity within each dPCR platform (r=0.99), highlighting the accuracy of quantifying gene copy number without calibration curve. However, the linear interval where nucleic acid can be quantified with accuracy, the dynamic range (Bustin et al., 2009), is limited (towards higher concentrations) compared to the qPCR, due to the incapability of dPCR to quantify many gene-copies within one partition, resulting in a saturated signal. This outlines an important aspect to consider when choosing this method to obtain the desired precision. reproducibility and repeatability measured with the CV% variation of the single dilution points and qPCR showed a wider range, mostly when approaching lower concentrations, the uncertainty of the detection increases resulting in a higher variability.

Table 1. Summary results (copies per μL, cp/μL) obtained for qPCR (Roche LightCycler) and dPCR (¹: BiomarkHD; ²: QIAcuity).

	qPCR	dPCR1	dPCR ²
Dynamic Range	10 ¹ -10 ⁹	10 ¹ -10 ⁴	10^{1} - 10^{5}
CV range (%)	1-63%	4-40%	3-34%
LOQ (cp/μL)	21±NA	10.6±3.0	14.3±1.4
LOD (cp/µL)	0.5	0.6	0.2
95% CI (cp/μL)	0.1-1	0.3-1.6	0.1-0.4

The LOD is needed to determine the lowest concentration above the plateau that can be estimated reliably. LOD and LOQ for qPCR data were analysed as described by Klymus et al. (2019); while for dPCR, LOD was investigated using the model developed by Hunter et al. (2017), (Fig 1). These models are less stringent than theoretical threshold of 95% positive replicates, because of the stochastic variability of trace DNA. Both qPCR and dPCR showed high sensitivity in controlled environments, giving responses in the same order of magnitude, with respective 95% Confidence Interval (CI) (Table 1). Digital PCR's LOQs $(CV \le 35\%)$ identified the dilution point 10^1 as an accurately quantifiable concentration BiomarkHD and 10⁰ for QIAcuity. Nevertheless, a large uncertainty in the binomial distribution was estimated for that point and it was rejected from quantification. Thus, 10¹ was accepted as LOQ.

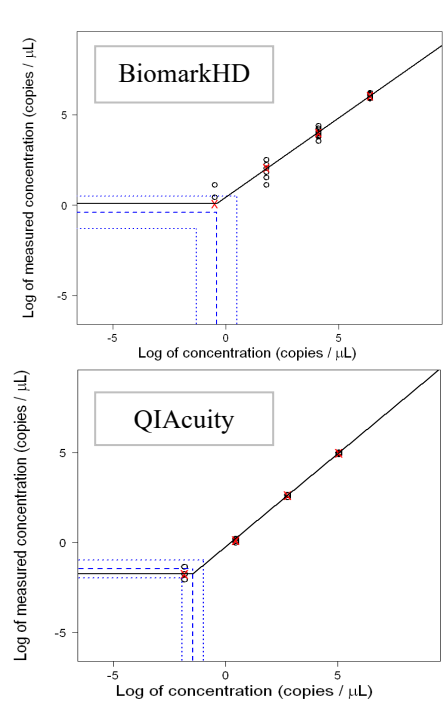


Fig 1. Limit of Detection (LOD) assessment on dPCR. Replicate averages are denoted by a red X. The estimated LOD is the intersection between the concentration linearity (solid line) and concentration plateau (dashed line). Upper and lower 95% confidence limits in dotted lines.

The Spearman's rho test showed a positive conformance between the two dPCR methods with a correlation coefficient of r=1, p<0.05. Az. spinosum TaqMan probe-assay was successfully transferred from the qPCR to the two dPCR instruments, without generating any assay artifacts.

This is a promising result, in view of using these platforms for other species-specific PCR assays.

Inhibition control

Az. spinosum DNA was detected reliably and consistently across environmental samples, with no significant differences with the controls (p>0.05). This is especially important to overcome the loss of trace levels of target DNA from environmental samples, due to potential PCR inhibitors or dilution of the DNA template (Tiwari et al., 2022).

Advantaged and Disadvantages of dPCR

Given the projection of future implementation of dPCR into routine monitoring programs, the results of this preliminary study were also used to address benefits and limitations of this technique.

Benefits of dPCR – Provides absolute quantification without standard curves, enhancing consistency over time. Analytically sensitive and highly accurate. Detection of rare targets in complex backgrounds. Mitigation of PCR inhibition effects. Transferability, repeatability, and reproducibility of assays between and within platforms.

Limitations of dPCR – Narrow quantitative dynamic range. Demands more precautions in loading the sample into the wells/inlets. Relatively more preparation and processing time. Amplicons cannot be always recovered for sequencing.

In conclusion, reliable quantitative data is crucial for HABs monitoring and risk assessment, especially for regulatory purposes. The positive performance characteristics of dPCR (i.e.: inhibition resilience and independence from calibration curves) suggest this technology is suitable for applications in shellfish food safety management, which often requires the measurement of rare targets in complex environmental matrices. Further studies are needed to investigate the reliability of multi-species dPCR assays. Overall, dPCR shows a remarkable potential for the assessment of low-copy targets for routine screening of environmental samples and early warning strategies.

Acknowledgments

This project (Grant-aid Agreement No. CS-21-007) is carried out with the support of the Marine Research Programme by the Irish Government. Mobility grants support: Paul C. Silva Student Grant funded by the International Phycological Society; Networking and Marine Research

Communication Award funded by the Marine Institute under the Marine Research Programme with the support of the Irish Government. Dr. Urban Tillmann, Alfred Wegener Institute (AWI), Germany, for kindly providing *Az. spinosum* 3D9 strain. Marine Institute's staff who works in the Phytoplankton Unit. Dr. Ferrante Grasselli for proofreading and statistical advice.

References

- Bustin, S. A., Benes, V., Garson, J. A., Hellemans, J., *et al.*, (2009). Clin. Chem., 55(4), 611–622.
- Clarke, D., (2020). Proc. 11th Irish Shellfish Safety Workshop, Athlone, Ireland, pp. 3-10.
- Dorazio, R. M., & Hunter, M. E., (2015). Anal. Chem. 2015, 87, 10886–10893.
- Forootan, A., Sjöback, R., Björkman, J., Sjögreen, et al., (2017). Biomol. Detect. Quantif., 12(April), 1–6.
- Hunter, M. E., Dorazio, R. M., Butterfield, J. S. S., Meigs-Friend, G., *et al.*, (2017). Mol. Ecol. Resour., 17(2), 221–229.
- Kavlick, M. F., (2018). Biotech. 65(5), 275–281.
- Klymus, K. E., Merkes, C. M., Allison, M. J., Goldberg, C. S., *et al.*, (2019). Environ. DNA, 2(3), 271–282.
- Lefran, A., Siemering, B., Cusack, C., Silke, J., Salas, R., (2020). Proc. 18th Int. Conf. on Harmful Algae, Nantes, France, pp. 87-90.
- Salas, R., Tillmann, U., John, U., Kilcoyne, J., et al., (2011). Harmful Algae, 10(6), 774–783.
- Tillmann, U., Elbrächter, M., Krock, B., John, U., & Cembella, A., (2009). Euro. J. Phycol., 44(1), 63–79.
- Tiwari, A., Ahmed, W., Oikarinen, S., Sherchan, S. P., Heikinheimo, *et al.*, (2022). Sci. Tot. Environ., 837(March), 155663.
- Toebe, K., Joshi, A. R., Messtorff, P., Tillmann, U., Cembella, A., & John, U., (2013). J. Plankton Res., 35(1), 225–230.
- Whale, A. S., De Spiegelaere, W., Trypsteen, W., Nour, A. A., *et al.*, (2020). Clin. Chem., 66(8), 1012–1029.
- Yarimizu, K., Sildever, S., Hamamoto, Y., Tazawa, S., et al., (2021). Harmful Algae, 103(March), 102008.

Using particle size distribution (PSD) to automate imaging flow cytobot (IFCB) data quality in coastal California, USA

Kendra Hayashi^{1*}, Jamie Enslein^{1,2}, Alle Lie³, Jayme Smith³, and Raphael M. Kudela¹.

¹Ocean Sciences Department, University of California, Santa Cruz, 1156 High Street, Santa Cruz, CA 95064, United States

²University of California, Berkeley, 306 Stanley Hall MC #1762, Berkeley, CA 94720, United States ³Southern California Coastal Water Research Project, 3535 Harbor Blvd., Suite 110, Costa Mesa, CA 92626, United States

*corresponding author's email: khayashi@ucsc.edu

Abstract

The use of imaging flow cytobots (IFCBs) for plankton research is increasing worldwide and coordinated IFCB networks are being developed to monitor harmful algal blooms (HABs) in several coastal regions. Monitoring programs with IFCBs designed to run continuously can generate up to 70 samples per day creating a wealth of image data. Ideally, data streams are monitored daily (real-time) for data quality assurance and quality control (QA/QC). However, front end data QA/QC can be cumbersome for personnel and is often left for a later date once thousands of data files have accumulated. Particle size distribution (PSD) is used to inform food web dynamics, calculate total community biomass, and calculate radiative transfer in ocean remote sensing. PSD can be generated from equivalent spherical diameter (ESD), a measure derived from IFCB image processing, and in previous work, anomalous IFCB generated PSDs identified bloom events in San Francisco Bay, CA. We propose that variations in PSDs also reveal "bad" data to allow for some automation in backend QA/QC procedures. As more and larger IFCB networks come online worldwide, the use of automated data QA/QC is prudent to increase the efficiency of working with these datasets. While full automation of IFCB data QA/QC is unlikely, using PSD to automatically flag data allows users to focus their efforts on a reduced number of data to determine whether they are questionable or reflect shifts in community structure.

Keywords: imaging flow cytobot (IFCB), particle size distribution (PSD), data QA/QC

Introduction

Imaging flow cytobots (IFCBs; McLane Research Laboratories, Inc., USA) are plankton imagers designed to autonomously collect samples in the environment. The high-resolution collected at high temporal frequency result in a powerful tool being employed by monitoring networks worldwide. When sampling continuously, a single IFCB has the potential to collect >10,000 sample files per year creating a wealth of data needing quality assurance and quality control (QA/QC). Ideally each file would be manually checked real-time to ensure the IFCB was operating correctly, however this is time consuming, inefficient, and not a standard practice, so users are left with thousands of files to QA/QC after the fact, resulting in a need to automate the QA/QC process.

Particle size distribution (PSD) is a critical component to understanding the optical properties

of the water column. It is used to inform food web dynamics, calculate total community biomass, and calculate radiative transfer in ocean remote sensing (Reynolds et al. 2010). PSD can be generated by plotting estimated spherical diameter (ESD), a measurement calculated during the post-processing of IFCB images, against particle concentration (Fig. 1). Previous work demonstrated that variations from theoretical PSD, specifically an increased number of particles of a certain size, revealed phytoplankton blooms in San Francisco Bay, California (Hayashi and Kudela 2022). Here we developed code using PSD to QA/QC IFCB data and evaluated its performance at 3 sites in the California (CA) IFCB Network.

Materials and Methods

Site Information

Three datasets from the CA IFCB Network were used to evaluate the automated data QA/QC code: Newport Beach Pier (NBP), Santa Cruz Wharf

(SCW), and the Hog Island Oyster Company (HIOC). The SCW and HIOC deployments are above water using a peristaltic pump to bring water to the IFCB. Data from the SCW span a 4-month stretch (3969 files, 9Aug to 4Dec2016) and were used to build and set thresholds for the QA/QC code. The HIOC dataset spanned about a 1-month deployment period (1835 files, 20Apr to 25May2023). The NBP has an underwater IFCB deployment configuration and had the largest data set evaluated, collected over about 2 years (14,969 files, 9Jul2021 to 13Aug2023).

All datasets had a subset of data manually checked. Data files from NBP and HIOC were manually checked by someone not familiar with the IFCB, but followed a specific set of guidelines. SCW data were manually checked by someone familiar with the IFCB and phytoplankton and had an additional 'Bad XY' flag that was not included in the automated code.

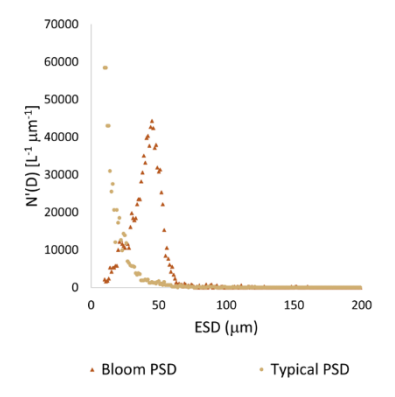


Fig. 1. PSDs generated from IFCB data. A typical PSD is represented by the tan dots and the dark orange triangles are the PSD of a sample with a 'Bloom' auto flag.

QA/QC code Information and Requirements

The QA/QC code was written in Python and the version used to evaluate the datasets in this study is download available to in GitHub (https://github.com/kudelalab/PSD). The code requires access to the IFCB's raw data files (.hdr and .adc) and corresponding v2 feature files generated from **MATLAB** code (https://github.com/hsosik/ifcb-analysis/; Sosik and Olson 2007). PSD was generated from 1 µm binned equivalent spherical diameter (ESD) and data were fit to a power law or Junge distribution. A total of 7 flags are available using the QA/QC code, their descriptions and thresholds are as follows:

- Beads File with 'sampleType: Beads' or a power fit constant greater than a user defined threshold (generally greater than 10[^]7)
- Bloom ESD difference between the maximum particle concentration and smallest ESD used in the curve fit is greater than 5 μm (Fig. 1)
- Bubbles ESD with the maximum particle concentration is greater than 150 μm
- Incomplete Run Runtime of a sample is less than half the expected runtime
- Low biomass Maximum particle concentration is less than 1000 L⁻¹ µm⁻¹
- Low $R^2 r^2 < 0.5$ and the poor fit is not associated with low biomass or bloom
- Missing Cells Image:Trigger count ratio is less than 0.8

It is important to note that the 'Bloom' and 'Low biomass' are not meant to denote bad data files. These flags are included because they explain why the power fit has a low r² value and to inform the users of unusual events.

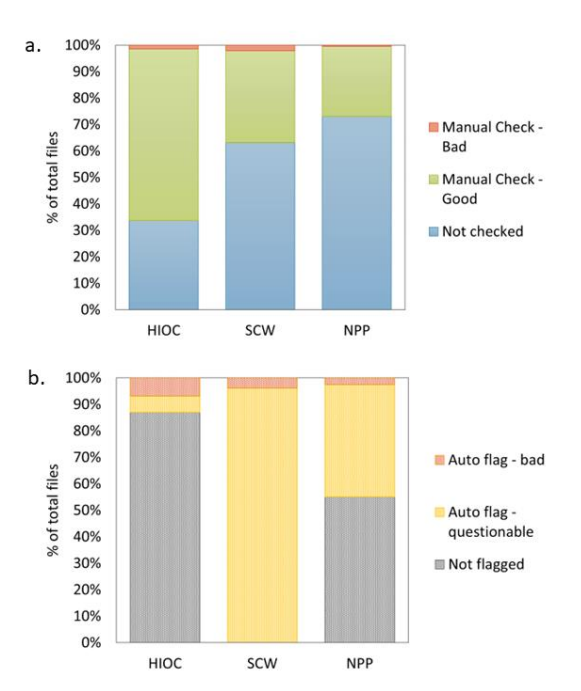


Fig. 2. Stacked bar graphs representing the distribution of bad data flags in manual checked (a) and auto flagged (b) datasets from the HIOC, SCW, and NBP. 'Bead,' 'Bubble,' 'Incomplete Run,' and 'Missing Cells' flags were combined into the 'Auto flag-bad' category. 'Auto flag-questionable' includes 'Low biomass,' 'Low R^2,' and 'Bloom' flags.

Results and Discussion

Overall Data Quality

A minimum of 27% of the data from each site was manually checked (Fig. 2a) using the online IFCB dashboard interface (https://ifcb.caloos.org/dashboard). Collectively this effort took over 300 hours, however, that estimate included the time for files to load. When webpage load times were removed, manual checking speeds ranged from 25-200 files per hour (depending on level of experience). Less than 2% of the manually checked files at all 3 sites were flagged as bad data and a majority of those flagged files (>70%) were bead samples.

The automated flags showed a similar result with 3-7% of the files in the dataset being flagged as bad data (Fig. 2b; bad data include the following flags: 'Bead', 'Bubble', 'Incomplete Run', and 'Missing Cells'). It should be noted that the proportion of data flagged by the QA/QC code varied widely between sites, ranging from 13% (at HIOC) to 100% (at SCW). However, when we look at the break down of flag type (Fig. 3), >78% of the automated flags in the SCW and NBP datasets were 'Bloom' and do not indicate bad data. At both sites, the 'Bloom' flagged files were collected during periods when Akashiwo sanguinea Lingulodinium dominated polyedra, the phytoplankton assemblage, indicating the flag's potential to identify HABs. Occasionally, the 'Bloom' flags were applied to files with peak size concentrations closer to the low end of the curve fit range (10 µm) and did not represent a bloom. While this is not ideal, it is not detrimental, as the intention of the flag was to indicate files with interesting community structure and not bad data.

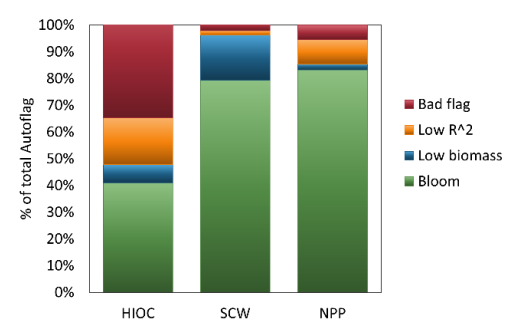


Fig. 3. Stacked bar graph representing the distribution of flag types (orange and yellow bars in Fig. 2b) in the QA/QC code generated flags for the HIOC, SCW, and NBP datasets. 'Bead,' 'Bubble,' 'Incomplete Run,' and 'Missing Cells' flags were combined into the 'Bad Flag' category.

Collectively, both the manual and automated flag results indicate that when IFCBs are deployed and operating, they are generating quality data over 95% of the time.

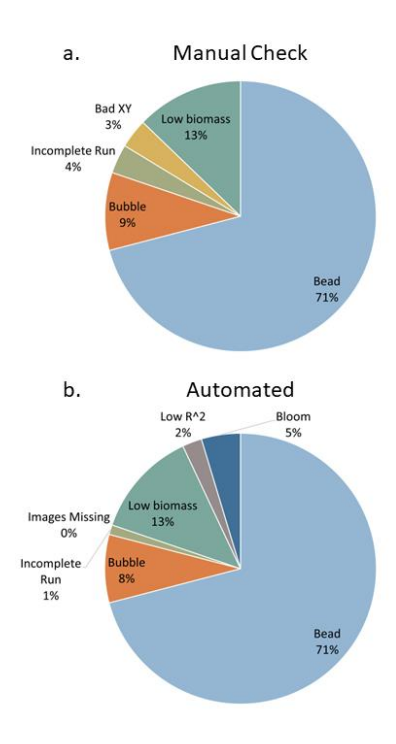


Fig. 4. Pie charts representing the distribution of flag types for the 86 matched manual check files (a) and the automated code flags (b) from the SCW dataset.

Automated vs Manual flags

To evaluate the QA/QC code performance, the manual and automated flags from the SCW dataset were directly compared by looking at the distribution of flag types (Fig. 4). Eighty of the 86 match ups had identical manual and automated flags. Of the 6 mismatches, 4 files were flagged as 'Bloom' and 2 files were flagged as 'Low R^2' by the code. The manual flag for 2 of the files (1 auto flagged 'Bloom', 1 auto flagged 'Low R^2') was 'Incomplete Run' and was likely miscategorized in the code due to an order of operations and can be fixed to elevate the 'Incomplete Run' flag, as it is more critical for data quality. The remaining auto flagged 'Bloom' samples correctly fell under the bloom criteria but were manually flagged for triggering too far to the left in XY space. The other incorrect 'Low R^2' file was manually flagged as 'Bubbles' (Fig. 5). The 'Bubbles' criteria were set based on the assumption that a sample would be composed primarily of large bubble images. This specific mismatched sample had some large bubble images, but most of the images had ESDs $<100~\mu m$ (real cells and partial bubbles) and we intend to change the criteria for the 'Bubble' flag to look for any particles with an ESD over 150 μm .

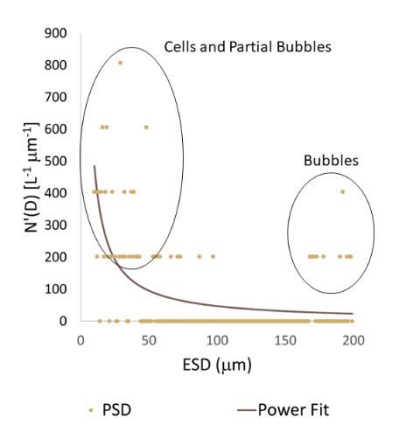


Fig. 5. An example PSD where full bubble images (circled on the right) were not the majority of the images collected in the sample. This file was auto flagged with a 'Low R^2' but should have a 'Bubble' flag.

Automated flags were manually spot checked to ensure the flags were working as expected in all 3 datasets and were found to consistently meet the flag criteria as the direct comparison revealed. More attention was directed towards the 'Low R^2' flag because goodness of fit is not something that can be manually assessed from raw images. The 'Low R^2' flag was generally assigned to files that did not have many images. A low biomass sample is not necessarily a bad sample, so care should be taken to not remove files during periods with low chlorophyll. 'Low R^2' and 'Low biomass' flags collectively made up 11-21% of the total automated flags (Fig. 3) and generally clumped together in time. We recommend files assigned these flags be manually checked before removing them from the dataset because most of the 'Low biomass' flagged files were considered good data.

A benefit to the automated code was that it was able to catch several legitimate bad data files that were missed by a human checker unfamiliar with the IFCB. For the NBP dataset, in addition to bead files caught by manual checking, the automated code caught 1 more bead file and 2 'Missing Cells' files than manual checking. The human checker and automated flags were more disparate for the HIOC dataset with the human checker missing most of the 'Missing Cells' files caught by the automated code and the automated code missing all the 'Bubble'

flags caught by the human checker. Human error increases with inexperience and increasing file number whereas the code cannot provide a nuanced evaluation of images. The discrepancies in the HIOC and NBP datasets represent the risks associated with relying on only 1 QA/QC method.

As IFCBs become more widely used and monitoring networks grow larger, the need for more automated data management increases. Combining information derived from the raw IFCB files (.hdr and .adc) and information from the PSD of the sample was the most successful approach to automating the QA/QC process. However, we believe manually checking files needs to be a part of the QA/QC process and the code generated in this project is best used as a screening tool, significantly reducing the number of files to be manually checked thereby focusing effort and reducing human error.

Acknowledgements

The authors thank L. Cruz Pascual and C. Park for performing manual checks for the NBP and HIOC datasets as a part of their California College Corps Fellowship. We also thank P. Daniel and G. Zirkel for their help with accessing data from HIOC. This work was supported by Cal-HABMAP which represents multiple organizations and partners who contribute to the operation and maintenance of the IFCB network. Support was also provided by SCCWRP JPA Research Funding. Core funding has been provided by NOAA, including the IOOS, ECOHAB, and MERHAB programs, NASA, California Sea Grant, California Ocean Protection Council, and numerous in-kind contributions from our partners and stakeholders. Initial purchase and development of the IFCBs was supported by NA16NMF4270263 (Saltonstall Kennedy) and NA14NOS0120148 (NOAA OTT).

References

Hayashi, K. and Kudela, R.M. (2022) U.S. Symposium on Harmful Algae. Albany, NY, United States. https://doi.org/10.5281/zenodo.11212206

Reynolds, R.A., Stramski, D., Wright, V.M., Woziak, S.B. (2010) J. Geophys. Res. 115, C08024.

Sosik, H. M. and Olson, R. J. (2007) Limnol. Oceanogr: Methods 5, 204–216.

In-situ segmentation and post-processing of phytoplankton image data suitable for an autonomous surface vehicle

Matias Haugum^{1*}, Glaucia M. Fragoso², Annette Stahl¹, Tor Arne Johansen¹

¹Department of Engineering Cybernetics, Norwegian University of Science and Technology, Trondheim, Norway

²Trondheim Biological Station, Norwegian University of Science and Technology, Trondheim, Norway *Email: matias.haugum@ntnu.no

Abstract

The utilization of autonomous surface vehicles (ASVs) for in-situ and real-time identification of phytoplankton species can provide early warning and thereby offer rapid solutions for mitigating the detrimental impacts of harmful algal blooms (HABs). Onboard imaging systems on mobile platforms, where in-situ images of main phytoplankton species are captured, and data are transmitted back to a taxonomist or fed into a machine learning model for inference, are promising technologies on the horizon. When the vehicle is in a remote location with limited connectivity, unnecessary data should be removed before transmitting, and prior to inference, the data must be segmented and processed. Here, methods for post-processing microscopic images of phytoplankton captured by a system built for autonomous operation are presented. Lightweight image manipulation methods with open-source software such as FIJI are used to remove clogged particles from the image sequence, as well as normalize the background and perform thresholding to generate binary masks well suited for inference in a machine learning model. A proof of concept is demonstrated and evaluated by feeding image data of phytoplankton into a neural network for classification.

Keywords: phytoplankton community composition, autonomous surface vehicles, flow-through microscope, computer vision.

https://doi.org/10.15027/0002041271

Introduction

There is a growing trend towards the utilization of autonomous surface vehicles (ASVs) for the purpose of collecting water samples and analyze aquatic environments. Depending on the platform, these vehicles can operate continuously, and cover a considerable range (many km) in aquatic systems. Furthermore, the unmanned nature of these vehicles results in significant time and cost savings, as one may omit the traditional collection and lab analysis of discrete water samples. Moreover, the advent of AI, computer vision and image analysis has brought powerful tools to enable near-real time analysis in remote locations.

Towards autonomous environmental monitoring, (Saad et al., 2020) propose a novel AI-driven mobile robotic platform with real-time plankton imaging capabilities. The silhouette camera system captures objects in the size range of $100~\mu m$ to 12~mm. The lightweight autonomous underwater vehicle (LAUV) employs a single-shot deep

learning method to process and classify plankton images directly onboard, enabling dynamic sampling based on the detected and predicted plankton distribution.

Several systems for in-situ imaging analysis of phytoplankton already exist. One example is the *Imaging FlowCytobot* (IFCB) developed by McClane Research Laboratories. The IFCB is combines flow-through cytometry and imaging of particles from a size range from ~10μm to 150μm and can be submerged to depths down to 40m. However, the IFCB comes at considerable cost, approximately USD 158,000 (Lombard et al., 2019).

The emergence of 3D printing and its accessibility to students and academics have facilitated the development of cheaper, DIY-systems such as the *PlanktoScope* (Pollina et al., 2022). The PlanktoScope is low-cost, flow through microscope that allows high throughput image data of plankton, with a price tag of approximately USD

500. Designed to enable citizen scientists to perform oceanographic activities, the PlanktoScope is capable of imaging suspended particles on a micrometer scale. However, the PlanktoScope was built for bench analyses and not for autonomous operation, and is, in its current form, unsuitable for remote missions.

This paper introduces a new version of the autonomous flow-through imaging (AFTI)-scope, a low cost, platform agnostic imaging system tailored for autonomous missions. The general design of the system is presented, and lightweight image manipulation methods using open-source software are used to illustrate how image data may be pre-processed prior to being fed into a convolutional neural network (CNN). Finally, a pre-trained CNN is trained on image data captured by the system to illustrate its capabilities for computer vision applications.

Materials and Method

The AFTI-scope is illustrated in figure 1.

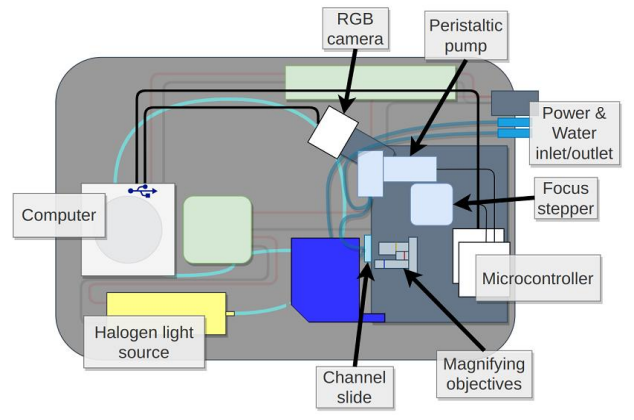


Fig. 1. Autonomous flow-through imaging -AFTI-scope. Water is pumped through the peristaltic pump from the inlet to the channel slide. An RGB camera captures images under magnification, which are saved to the computer. A halogen light source provides illumination, and a stepper motor allows for the focus to be adjusted.

The AFTI-scope can acquire images of suspended particles from net or water samples under 40x, 100x and 400x magnification, with a resolution of $0.41 \, \mu \text{m/pixel}$ at 100x magnification. The design of the system is described in Haugum et al. (2023). As the water sample is pumped through a microfluid flow cell situated underneath the magnifying

objectives, the RGB camera continuously captures images of the particles in the sample. The images are then saved to the computer. FIJI ("Fiji Is Just ImageJ") is an open-source image processing pipeline (Schindelin, 2012). Being highly customizable and scriptable, as well as capable of processing large batches of files, FIJI is well suited to processing the image data taken by the AFTIscope. This includes z-transforms to normalize the background of the data set, as well as subtracting the mean image to remove any stationary or "stuck" particles from the image frame. Furthermore, applying filters, such as gaussian blur can reduce noise in the image data, providing more consistent results when applying boundary detection and thresholding algorithms. Thresholding based on RGB or greyscale values can be applied to generate binary masks, producing images smaller in size with only one color channel. Finally, watershed algorithms may be applied to segment and quantify particles.

The image data used for this paper originate from Hopavågen, a semi-enclosed bay located in Agdenes, and the Trondheimsfjord, located in the coast of mid- Norway. A small phytoplankton net (20 µm mesh) was used to collect horizontal surface plankton samples, which were immediately transferred to a centrifuge tube and stored in the fridge for analyses in the same day. In the laboratory, an aliquot of the fresh net sample was inserted in the AFTI-scope, and the images were captured using under 100x magnification. The data set contains 271 JPG-images with a resolution of 1280x960p. An image frame from the dataset is shown in figure 2.



Fig. 2. Images containing the dinoflagellate *Tripos* spp. and the diatom *Coscinodiscus* spp.

Using FIJIs z-transform tools, a new frame containing the average value for every pixel in the data set is created. By converting to grayscale and subtracting the current frame by the average frame, particles stuck to the channel slide are effectively removed, as shown in figure 3.

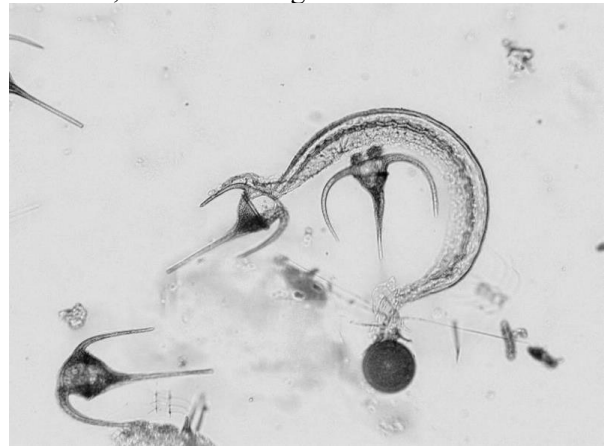


Fig. 3. Stuck particles shown as dark, blurry spots in figure 2 were removed through subtracting the average image.

As a proof-of-concept as well as a gauge of the system's ability to provide decent data for assessment by a CNN, a small batch of images were labeled and subsequently used to train the CNN. 27 images were annotated and divided into two classes, consisting of the most distinct phytoplankton genera in the dataset: *Tripos* and *Coscinodiscus*, as shown in figure 4.



Fig. 4. Frame containing *Tripos* and *Coscinodiscus*, the two categories used to train the network.

The objects were annotated if they were clearly visible in the frame and belonged to the categories mentioned above. The frames were then divided into 17 training images, 2 validation images and 8

test images. All the objects from all frames were cropped, resulting in 49 training objects, 6 validation objects as well as 29 test objects. The model used in this test is an Ultralytics nano-sized classification model (Jocher, 2023). The model was trained for 20 epochs. This network is a variant of the EfficientNet architecture, which is a CNN that scales uniformly along the depth, width, and resolution dimensions. (Tan et al., 2019)

The training data are augmented by the underlying Ultralytics-framework through random variations of rotation, translation, and brightness to increase the size of the training set.



Fig. 5. Cropped images of *Coscinodiscus* (left, valve view) and *Tripos* (right) used to train, validate, and test the neural network.

Results and Discussion

Pre-processing results

The processing methods presented in the paper are a lightweight way to improve and normalize imaging data prior to computer vision or any other image processing. By applying thresholding methods on the image in figure 3, binary masks can be created as shown in figure 6.



Fig. 6. Binary mask created from figure 3 by thresholding for specific greyscale values.

These binary masks can aid in segmentation in tandem with the original unprocessed pictures. Moreover, for algorithms and computer vision models that are invariant to color, the binary mask could be a faster, less storage-using alternative to the normal image data.

CNN results

Evaluating the neural network on the test set, an accuracy of 0.966 was achieved. A single error was observed, caused by a labelling error where a *Tripos* was mislabeled as a *Coscinodiscus*. The high accuracy rate is most likely due to the limited size of the data set. The *Coscinodiscus* were only imaged from their valve view, as this was their most common orientation in the flow cell. This is also the case for the *Tripos*, as their shape usually leads to them resting in the same manner against the channel slide. Figure 7 illustrates a girdle or "side view" of the *Coscinodiscus*, which was more uncommon to see in the image data.



Fig. 7. Coscinodiscus imaged from the girdle view.

In this setup, the AFTI-scope was oriented in a manner where particles would fall to the rear surface of the slide due to gravity. In future applications, the channel slide will be oriented vertically, allowing particles to flow in the same direction as gravity. Additional work with the CNN is expected, as multiple classes for the same particle may be needed, depending on their orientation in the channel slide.

The pre-processing methods were not applied on the images prior to inference in the CNN, as converting to greyscale may remove information contained in the natural color of the different classes.

Acknowledgements

Thanks to Espen Berntzen Høgstedt for assisting with all the computer vision related work within the context of the AILARON project (grant number 262741), which was supported by the Research Council of Norway.

This research was supported by the Research Council of Norway through MoniTARE project (grant number 315514), the IKTPLUSS project AWAS (grant number 327670)

References

- A Saad, A Stahl, A Våge, E Davies, T Nordam, N Aberle, M Ludvigsen, (2020). Advancing Ocean Observation with an AI-driven Mobile Robotic Explorer, Oceanography 33 (3), 50-59
- Lombard et al., (2019). Globally Consistent Quantitative Observations of Planktonic Ecosystems, Frontiers in Marine Science 6, 196
- Pollina, T. et al., (2022). PlanktoScope: Affordable Modular Quantitative Imaging Platform for Citizen Oceanography, fmars 9
- Schindelin, J., Arganda-Carreras, I., Frise, E., Kaynig, V., Longair, M., Pietzsch, T., ... Cardona, A. (2012). Fiji: an open-source platform for biological-image analysis. Nature Methods, 9(7), 676–682.
- Haugum, M., Fragoso, G., Henriksen, M.B., Zolich, A., Johansen, T.A. (2023). Autonomous Flow-Through RGB and Hyperspectral Imaging for Unmanned Surface Vehicles, Oceans, Limerick, Ireland
- Jocher, Chaurasia, Qui (2023). Ultralytics YOLOv8. Github.com/ultralytics
- Tan, M. & Le, Q. (2019). EfficientNet: Rethinking Model Scaling for Convolutional Neural Networks. *Proceedings of the 36th International Conference on Machine Learning*, 97:6105-6114

A mini-review on environmentally friendly strategies against HABs

Ichiro Imai¹, Keigo Yamamoto^{2*}, Nobuharu Inaba^{3, 4}

¹ Graduate School of Fisheries Sciences, Hokkaido University,
3-1-1 Minato-cho, Hakodate, Hokkaido 041-8611, Japan.

² Marine Fisheries research center, Research institute of Environment, Agriculture and Fisheries, Osaka
Prefecture. 2926-1 Misaki, Sennan, Osaka 599-0311, Japan.

³ Civil Engineering Research Institute for Cold Region, Public Work Research Institute,
Hiragishi 1-3-1-34, Toyohira-ku, Sapporo, Hokkaido 062-8602, Japan.

⁴ Centre for Marine Science and Innovation, University of New South Wales,
Sydney, NSW 2052, Australia,

*corresponding author's email: YamamotoKeig@knsk-osaka.jp

Abstract

Since there are currently no practical countermeasures for harmful algal blooms (HABs) other than passive measures such as stopping feeding and moving cages, there is an urgent need for effective and environmentally friendly strategies against HABs. Biological control strategies are considered to be more environmentally friendly than physicochemical methods. We propose that the development of seaweed and seagrass beds is effective against the occurrence of HABs through the activities of algicidal bacteria in the biofilm on the surface of seaweeds and seagrasses. As another strategy against HABs, we propose resuspending diatom resting stage cells (which require light for germination) from bottom sediments into the euphotic layer through sediment perturbation, thereby promoting the proliferation of vegetative cells after germination. Nutrients will be quickly consumed by growing diatoms, and HABs of flagellates would be prevented. *Chattonella* red tides were prevented by bottom sediment perturbation in Tomonoura. Toxic *Alexandrium* blooms have also been suppressed by bottom sediment perturbation in 2020-2024 in Osaka Bay.

Keywords: harmful algal blooms, environmentally friendly strategy, diatoms, resting stage cells, bottom sediment perturbation, algicidal bacteria, seaweeds, seagrasses

https://doi.org/10.15027/0002041272

Fisheries damage caused by HABs in Japan

Fisheries production through aquaculture is now critically important in food production. However, the history of aquaculture is also one of fighting against harmful algal blooms (HABs). The damage inflicted by the raphidophyte Chattonella is the most prominent, both in amount and frequency. In 1972. Chattonella antiqua killed 14.28 million farmed yellowtails in Harima-Nada, with extensive fishery damage of ~7.1 billion JPY (~50 million USD). This incident triggered the "Harima-Nada Red Tide Lawsuit", in which found that the eutrophication of the Seto Inland Sea was caused by industrial wastewaters. It triggered the enactment of the "Seto Inland Sea Environmental Conservation Temporary Measures Act" in 1973. Nevertheless, large-scale damages to fisheries caused by *Chattonella* continued to occur frequently. But from 1990 to 2002, damages to aquaculture fisheries of more than 100 million JPY per year were no longer recognized. After that period, damage amounted to 1.27 billion JPY in Harima-Nada in 2003. Later, in the Yatsushiro Sea in Kyushu, *Chattonella* red tides caused deaths of mainly yellowtail, reaching 3.3 billion JPY in 2009 and 5.3 billion JPY in 2010.

Since 1979, the dinoflagellate *Karenia mikimotoi* has been causing mortality damage to farmed fish and shellfish in the Seto Inland Sea, and in 2012, extensive damage was caused to red sea bream, amberjack, yellowtail, abalone, etc., totaling 1.53 billion JPY in the Bungo-Suido Channel. In the Kyushu area, red tides have also caused huge damage in Imari Bay and the Yatsushiro Sea by *K*.

mikimotoi. A new noxious dinoflagellate *Karenia selliformis* caused the first large-scale red tide in Hokkaido, and gave the largest damage (9.767 billion JPY) in the red tide history in Japan.

Other notable fisheries damage was observed in pearl oysters (3 billion JPY) and oysters (3.9 billion JPY) due to the dinoflagellate *Heterocapsa circularisquama*, and damage caused by the dinoflagellate *Cochlodinium* (currently *Margalefidinium*) *polykrikoides* in the Yatsushiro Sea amounted to 4 billion JPY. Diatom red tides have caused major bleaching damage to seaweed (Nori, *Pyropia*) cultivation, and in the winter of 2000, the most serious damage to Nori occurred in the Ariake Sea, with a decreased amount of 13.6 billion JPY compared to the previous year.

Environmentally friendly strategies for HABs

Since the mortality in aquaculture due to HABs increased in the 1960s, various countermeasures were proposed until the 1980s. However, there are almost no physicochemical methods that have been available for practical use other than the clay spraying. This is because no consideration was given to scale and cost, and there is a lack of care for the environment. Biological methods may be the most promising as environmentally friendly countermeasures (Imai et al. 2021).

The predation of HAB species by zooplankton (copepods and protozoa) and filtration by bivalves were once hoped for and studied for the prevention of HABs. However, zooplankton tend to avoid the predation of harmful algae (HA) as food (Uye and Takamatsu 1990). Considering the biomass of copepods and the water filtering rate, the ability to remove HA was estimated to be only a few percent per day, which is considered to be too little for the prevention of HAB occurrences (Uye 1986). Heterotrophic dinoflagellates (genus Gyrodinium and *Polykrikos*) have been observed in the seawater and have consumed Chattonella spp. and K. mikimotoi at the final stage of blooms (Nakamura et al. 1996). The grazing has also been confirmed in laboratory experiments. However, it is impractical to prepare large quantities of these highly predatory heterotrophic dinoflagellates for HAB control. Filter predation of HA by bivalves was anticipated to hold great promise for aquaculture. In northern Hiroshima Bay, where oyster farming is vigorously performed, the

amounts of suspended matter (phytoplankton and detritus) filtered by farmed oysters were estimated based on the annual average nitrogen balance, and it was reported that filtration amounts were equivalent to 26% of the primary production. (Sonsangjinda et al. 2000). Bivalves are also selective about their plankton prey. According to these facts, farmed oysters have a thinning effect phytoplankton communities, but it is questionable whether they contribute to the prevention of HAB occurrences. The frequent occurrence of red tides in Hiroshima Bay, where oyster farming is intense, indicates the limits of the abilities of bivalves for HAB control. Based on the results above, it is considered that controlling HABs using predators is not realistic (Pomeroy et al. 2006).

Table 1. Effective and promising countermeasures for harmful algal blooms (HABs).

Indirect method

· Legal regulation

Act on special measures concerning conservation of the environment of the Seto Inland Sea, Act on special measures concerning restoration of the environment of the Ariake Sea and Yatsushiro Sea, Water pollution control law, Marine pollution prevention law, Regulation law of agricultural chemicals, Sustainable aquaculture production assurance act, etc

- Forecasting by monitoring
 - Regular monitoring, Molecular monitoring Improvement of prediction accuracy by data analysis and modeling
- Fish culture technique
 - Improvement of feed (Moist pellet) Keeping proper scale and density of fish Large scale and deep pen cage
- Emergency procedures
 - Stop giving feed, Transfer of net cages (horizontal and vertical)

Direct method

· Physicochemical method

Clay dispersal

Disturbance of thin-layer orientation of population (*Karenia mikimotoi*, etc.)
Removal of bottom sediments containing dense cysts of HAB species located in the seed bed

· Biological control

Algicidal activity: Viruses, Algicidal bacteria, Parasitic protists (dinoflagellates, etc.)

Competitive overwhelming: Diatoms (Diatom growth after germination of diatom resting stage cells in sediments lifted to the euphotic layer with bottom perturbation by sea-bed tillage)

Currently effective and promising strategies for HABs are summarized in Table 1 (Imai 2023). Until now, indirect strategies appear to have contributed to reducing damage by HABs. In particular, legal regulations have greatly contributed to improving water quality in the Seto Inland Sea. Improvements in feed in aquaculture technology have also dramatically reduced water pollution during feeding. Currently, feed stoppage is the most commonly used emergency measure in the event of red tide outbreaks. Improvements in prediction accuracy for HAB occurrences and the model construction using data from the monitoring hold a great promise in the future. As a direct countermeasure, conventional clay spraying has been carried out in various ways. Since technology has improved significantly, such as in increasing the efficacy in aggregating HA cells (Yu et al., 2017). Therefore, spraying improved clay is an effective emergency measure on-site after a HAB outbreak. Expectations are higher than before.

Figure 1 summarizes HAB countermeasures that are considered effective or promising in the future, in relation to the stages of HAB occurrences. Monitoring needs to be carried out as a basis for countermeasures during the whole course of HAB from start to end.

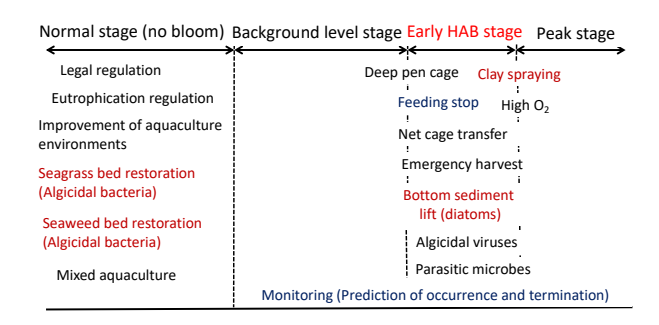


Fig. 1. Stages of HAB and countermeasures considered effective or promising in the future.

In the early stages of blooms, a physical countermeasure for K. mikimotoi is to disrupt the thin-layer orientation (Miyamura, 2017), whereas biological countermeasures include spraying bottom sediments containing algicidal viruses for H. circularisquama (Nakayama et al., 2020) and lifting bottom sediments into the euphotic layer by bottom plowing to promote the growth of diatoms (Imai. 2010). In Tomono-ura, Hiroshima Prefecture, sea-bottom plowings had been successful in preventing the occurrences of Chattonella red tides (Imai et al. 2017). The creation of seaweed and seagrass beds utilizing algicidal bacteria that live in biofilms on the surface of seaweeds and seagrasses is expected to prevent the mass proliferation of phytoplankton, including HA, in target water areas (Imai 2015, Inaba and Imai 2023). Above are thought to be environmentally friendly strategies to reduce the frequency of HAB occurrences.

Successful prevention of HAB occurrences by sediment perturbation

It is empirically known that when HABs of flagellates occur, there are very few diatoms in the water (Imai 2012). Huge numbers of diatom resting stage cells (DRSCs) lie in the bottom sediments in coastal areas. DRSCs usually require light for germination (Itakura 2000). Therefore, if DRSCs are suspended in the water column of the euphotic layer, the resultant diatom vegetative cells, through germination, will consume the nutrients in the water and proliferate extensively. Diatoms are expected to suppress the growth of harmful flagellates (Fig. 2).

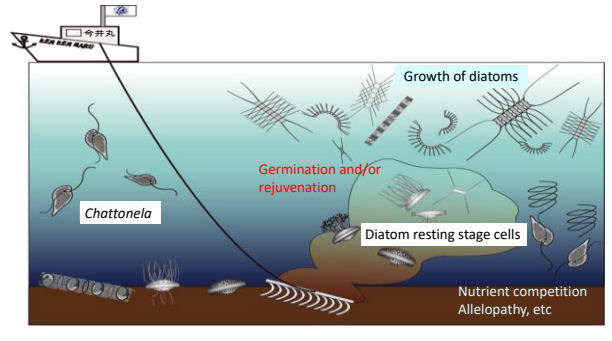


Fig. 2. Bottom sediment perturbation by using of bottom trawling fishing boat.

As an excellent example of HAB countermeasures taken in the field, we here show the results of sediment perturbation in Osaka Bay (Fig. 3)

(Yamamoto et al. 2023). Bottom sediment perturbations were carried out off the coast of Sakai City and Kishiwada City in the northern waters of Osaka Bay three times in an area of approximately 5 km², twice in late January and on February 10, 2020. The occurrence of the toxic dinoflagellate Alexandrium catenella (Group I) (hereinafter referred to as Alexandrium) had been expanding in Osaka Bay since 1994, and thereafter, and the highest density was well over 10³ cells/mL often passing over 10⁴ cells/mL in March or April of each year. As a result of bottom sediment perturbation, diatoms, mainly belonging to the genera Skeletonema, Chaetoceros, and Leptocylindrus, continuously showed high densities exceeding 10³ cells/mL. Alexandrium did not exceed the alarming density of 5 cells/mL set by Osaka Prefecture during February. The warning density (10 cells/mL) was exceeded in early March, more than 20 days after the last sea bottom perturbation (February 10), and the highest density of 31 cells/mL was recorded on March 23rd. Compared to the high-density occurrence of 10^3 – 10⁴ cells/mL over the past several years, this cell density has been reduced 100-fold. The above results are considered to be an ideal phenomenon in which diatoms frequently occur due to bottom sediment perturbation, and toxic Alexandrium populations are suppressed. After that, bottom sediment perturbations have been performed in the same manner from January to March in 2021 to 2024, and diatoms have been similarly prevalent in the water columns, and there were no outstanding blooms of Alexandrium. It is thought that the lowered level of toxins of the bivalves resulted in the increase in the survival rate of aquatic resources such as octopuses that prey on the bivalves. The toxin of Alexandrium usually accumulates in zooplankton such as copepods, and the toxin is transferred through the food chain, and will cause mortalities in fish and other higher marine organisms (White 1981). If non-toxic diatoms consistently predominate in coastal ecosystems, biological production will be positively stimulated, leading to increased yields of higher organisms such as fish and mollusks.

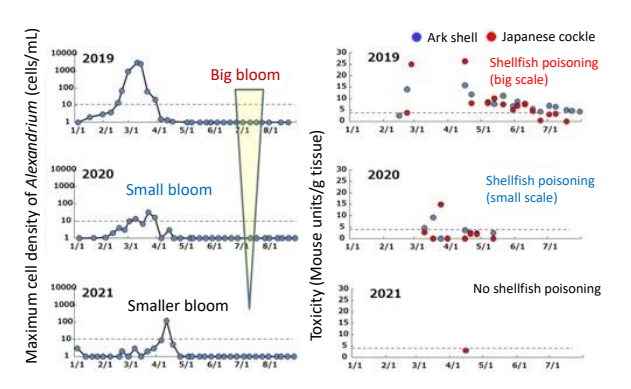


Fig. 3. Maximum cell densities of *Alexandrium catenella* (Group I) (left) and toxicity of bivalves in 2019 to 2021 (right) (Yamamoto et al., 2023). Timing and location of sediment perturbations were good in 2020 and 2021, and bad in 2019.

References

Imai, I. (2010) Aquabiology 32, 378-379.

Imai, I. (2012) Biology and ecology of Chattonella red tides. Seibutsu-Kenkyusha, 184 pp.

Imai, I. (2015) In: Ohtsuka, S., Suzaki, T., Horiguchi, T., Suzuki, N., Not, F. (eds) Marine Protists. Springer Japan; Tokyo, pp.597-619.

Imai, I. (2023) Kaiyo Monthly 55, 497-507.

Imai, I., Kakumu, A., Ohara, S., Yuki, T., et al. (2017) Bull Fish Sci Hokkaido Univ 67, 57-66.

Imai, I., Inaba, N., Yamamoto, K. (2021) Fisheries Science 87, 437-464.

Inaba, N. and Imai, I. (2023) Kaiyo Monthly 55, 532-538.

Itakura, S. (2000) Bull Fish Environ Inland Sea 2, 67-130.

Miyamura, K. (2017) Aqua Culture Business 54 (12), 49-52.

Nakamura, Y., Suzuki, S., Hiromi, J. (1996) Aquat Microb Ecol 10, 131-137.

Nakayama, N., Hamaguchi, M., Yamaguchi, H., Masuda, K., Fujiwara, M. (2020) Aquaculture 529, 735625.

Pomeroy, L.R., D'Elia, C.F., Schaffner, L.C. (2006) Mar Ecol Prog Ser 325, 301-309.

Sonsangjinda, P., Matsuda, O., Yamamoto, T., Rajendran, N., et al. (2000) J Oceanogr 56, 223-231

Uye, S. (1986) Mar Biol 92, 35-43.

Uye, S. and Takamatsu, K. (1990) Mar Ecol Prog Ser 59, 97-107.

White, A. (1981) Limnol Oceanogr 26, 103-109.

Yamamoto, K., Okamoto, H., Imai, I. (2023) Kaiyo Monthly 55, 526-531.

Yu, Z., Song, X., Cao, X., Liu, Y. (2017) Harmful algae 69, 48-64.

Branched-chain fatty acids in 7-O-acyl okadaite esters from bivalves

Paulo Vale^{1*}, Hajime Uchida², Toshiyuki Suzuki²

*corresponding author's email: pvale@ipma.pt

Abstract

The okadaites, a group of polyether compounds involved in the human syndrome diarrhetic shellfish poisoning (DSP), include three major parent toxins (okadaic acid and the analogues DTX1 and DTX2) which in bivalves are mostly esterified at C7 with fatty acids (FA). Most of these esters include common saturated and unsaturated FA. Others involve odd FA and multi-branched FA. The major unidentified 7-O-acyl esters with the okadaites in Portuguese bivalves were confirmed here, by high-resolution mass spectrometry (HRMS), to present a side chain with the same exact mass as the OA and DTX2 palmitoyl esters (isopC16:0). A common chain with this exact mass, and abundant in the marine environment, is 4,8,12-trimethyltridecanoic acid (TMTD), which is a chlorophyll degradation product. Although all bivalves assayed contain the isopC16:0 ester, the unknown peaks were more abundant in sand-dwelling bivalves (clams, cockles) than in suspension-feeding bivalves (mussels). In addition to the high abundance of isopC16:0 combined with OA and DTX2 in natural samples, the isopC16:0 ester was also obtained by feeding bivalves with Prorocentrum lima containing DTX1. If this metabolization is attributable to the bivalves themselves, to a particular bacterial flora in sand-dwelling bivalves, or both, is a question that remains open.

Keywords: okadaic acid, branched chain fatty acids; 7-O-acyl esters, dinophysistoxins, 4,8,12-trimethyltridecanoic acid

https://doi.org/10.15027/0002041273

Introduction

The okadaites are a group of polyether compounds involved in the human syndrome diarrhetic shellfish poisoning (DSP), and include okadaic acid (OA), the dinophysistoxins (DTX1, DTX2) and, several esters at C1 or C7 of these three parent toxins. Esters at C1 are found in microalgae while esters at C7 are found in predators, such as bivalves (Torgersen et al., 2008; Hu et al., 2017).

Contamination with okadaites in bivalves from Portuguese production areas derives commonly from predating upon *Dinophysis acuminata* and *D. acuta*, which are planktonic microalgae recurrently found at the Atlantic Iberian coast. These two species produce only the parent toxins OA and DTX2 (Pizarro et al., 2009).

In many bivalve species, okadaite's esters at C7 with fatty acids (FA) are largely dominant over free okadaites, with blue mussel and donax clams as an exception (Vale, 2006; Torgersen et al., 2008).

The 7-O-acyl esters of okadaites include common FA, but may include other less typical acids. The most prominent unknown ester found in Portuguese bivalves elutes closely to 7-O-palmitoyl-OA and -DTX2, respectively (Vale, 2006, 2010).

Unknown FA esters have been found also with spirolides (at C16:0; Aasen et al., 2006), pinatoxins (at C20:2 and C22:5; McCarron et al., 2012) and gymnodimines (at C19:0; de la Iglesia et al., 2013).

These uncommon 7-O-acyl esters were studied here in more detail by artificially feeding bivalves

¹ The Portuguese Sea and Atmosphere Institute, I.P. (IPMA, IP), Sea and Marine Resources Department (DMRM); R. Alfredo Magalhães Ramalho 6, 1495-165, Algés, PORTUGAL

² Environment and Fisheries Applied Techniques Research Department, Fisheries Technology Institute, Japan Fisheries Research and Education Agency; 2-12-4 Fukuura, Kanazawa-ku, Yokohama-city, Kanagawa, JAPAN, 236-8648.

with a cultured *Prorocentrum lima* strain in order to additionally obtain esters with the parent toxin DTX1. Natural esters with OA and DTX2 were studied here in more detail resorting to high-resolution mass spectrometry (HRMS).

Materials and Methods

Artificial feeding experiments were carried out with a toxic *P. lima* strain (Vigo #PL3) in the common cockle *Cerastoderma edule* and the blue mussel *Mytilus galloprovincialis* from the Portuguese coast. Digestive glands (DG) were dissected and extracted with MeOH. The hexane sub-fraction was analysed in an Agilent 1946A single quadrupole LC-MS as described in Vale (2006).

Mussels, cockles and the clam *Ruditapes decussatus* were collected from Ria de Aveiro in October 2019, during a double contamination with OA and DTX2 derived from naturally feeding upon *D. acuta*. Methanolic extracts of DG were analysed in a Bruker micrOTOFQII ESI-HRMS by the negative ion mode. A full scan was acquired in the range of m/z 100–1500 for HRMS. Separation was performed on a Hypersil Gold C8 (2.1 x 100 mm, 1.9 μ m) as described in Suzuki et al. (2009), with a modified linear gradient from 20%B to 90%B for 10 min, and 90%B for 25 min. The extracted ion chromatograms were obtained to ± 0.05 m/z units from the theoretical value of [M-H] of 7-O-acyl esters.

Results and Discussion

The *P. lima* strain used produced a double contamination with two parent toxins, similar to natural contamination. In cockles, esters with palmitic acid (C16:0) either with OA or DTX1, were much less abundant than those with the isoprenoid isomer (isopC16:0) eluting before (Fig. 1a and 1b, respectively). In mussels, the situation was reversed, and both OA and DTX1 esters were dominated by palmitic acid, but the isopC16:0 isomer was nevertheless present (Fig. 1c).

Overall, the putative branched FA with the pair OA/DTX1 were more common in sand-dwelling bivalves than in suspension-feeding bivalves (Fig. 1d), similar to the previous findings with natural contamination by the pair OA/DTX2 (Vale, 2006; 2010).

High-resolution mass spectrometry confirmed that the signal for natural esters with palmitic acid comprised an extra pair of unknown peaks with the same exact mass but eluting before the expected retention times for the respective palmitic esters of OA and DTX2 (Fig. 2; Table 1). The unknown peaks were more abundant in sand-dwelling bivalves (clams, cockles) than in suspension-feeding bivalves (mussels) (Fig. 2), confirming the previous findings with natural contamination by the pair OA/DTX2 (Vale, 2006).

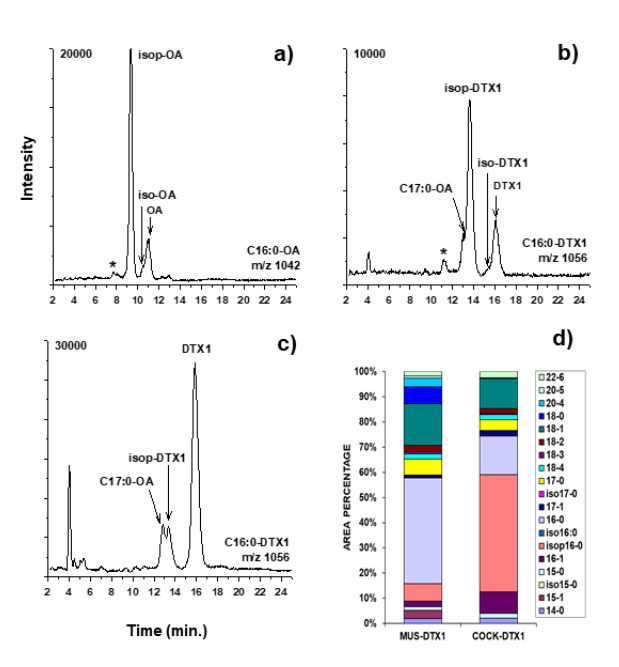


Fig. 1. LC-MS chromatograms of 7-*O*-acyl esters in DG with palmitic acid of: a) OA and b) DTX1 in cockle; c) DTX1 in mussel (* denotes interfering signals from ¹³C isotope peaks of lower molecular weight esters, namely the C16:1 esters); d) distribution of FA combined with DTX1 forming 7-*O*-acyl esters in mussel (MUS) and cockle (COCK).

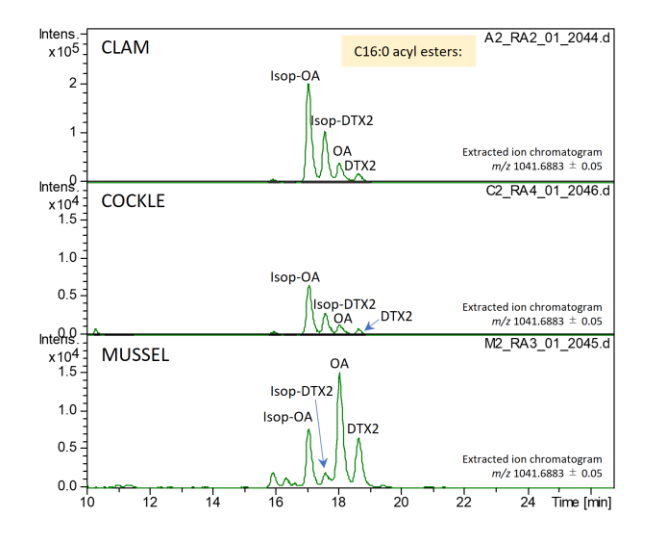


Fig. 2. LC-HRMS chromatograms for 7-*O*-acyl esters with palmitic acid (C16:0) in the DG of bivalves from Ria de Aveiro during a double contamination with OA and DTX2. The isoprenoid attached to both okadaites corresponds putatively to TMTD (see Fig. 6).

Other signals with this double pair of peaks were found corresponding to the 20:1 fatty acid ester (Fig. 3, Table 1). The putative isoprenoid esters presented similar abundance than with the 20:1 fatty acid ester in all bivalve species.

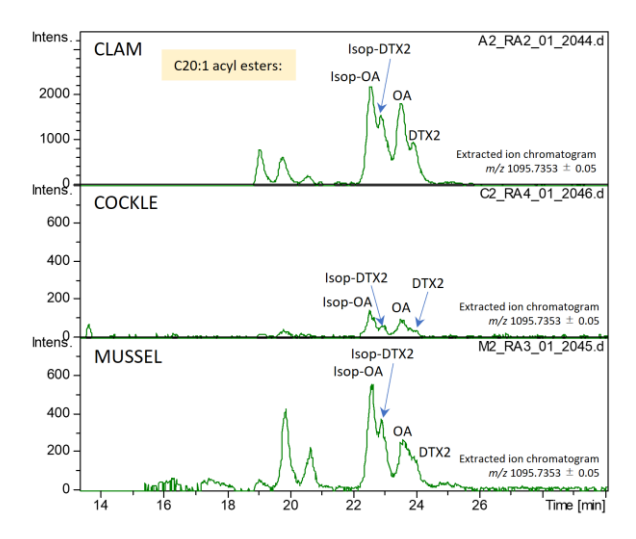


Fig. 3. LC-HRMS chromatograms for 7-*O*-acyl esters with eicosenoic acid in the DG of bivalves from Ria de Aveiro during a double contamination with OA and DTX2. The isoprenoid attached to both okadaites corresponds putatively to phytenic acid (see Fig. 6).

The major unidentified 7-O-acyl esters with the okadaites were confirmed to present a side chain with the same exact mass as the linear 16:0 or the 20:1 ester (Table 1). The mass spectra also presented similar abundances of M+1, M+2 and M+3 ions (Fig. 4).

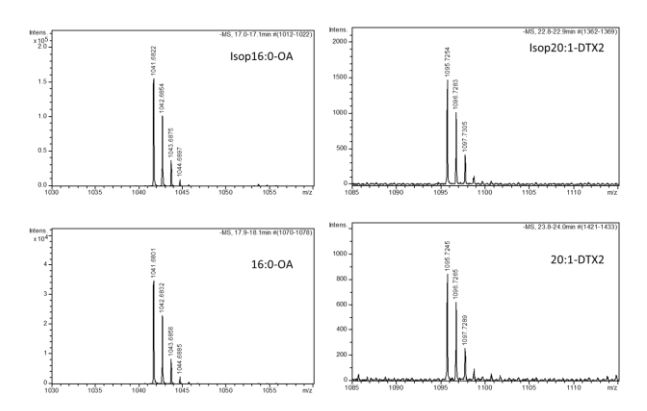


Fig. 4. Selected HRMS spectra of esters with OA and DTX2 in clams.

The chromatographic properties of the 7-O-acyl esters were studied by calculating the dependence of the elution order (retention time) with the number of carbon atoms for saturated (SFA) and mono-unsaturated (MUFA) conjugates with okadaites in clams. The elution order fitted a second degree polynomial curve, with $R^2 \geq 0.99$ (Fig. 5). The isoprenoid conjugates eluted before the respective SFA ester but after the MUFA ester with the same carbon number, in accordance with the behaviour of a branched FA in reversed phase columns (Fu et al., 2023).

Table 1. The error values of 7-O-acyl esters with C16:0 and 20:1 were calculated from measured accurate masses by Data Analysis software (Bruker, Germany).

Compounds	Molecular Formula [M-H] // Calculated	Measured accurate mass	Error (ppm)
16:0-OA	exact mass m/z	m/z 1041.6801	6.9
10.0-OA	$C_{60}H_{97}O_{14}$	1041.0601	0.9
Isop16:0-OA	// 1041.6883	1041.6822	4.9
16:0-DTX2		1041.6804	7.7
Isop16:0-DTX2		1041.6822	4.9
20:1-OA	$C_{64}H_{103}O_{14}$	1095.7255	9.0
Isop20:1-OA	// 1095.7353	1095.7266	8.0
20:1-DTX2		1095.7245	9.9
Isop20:1-DTX2		1095.7254	9.1

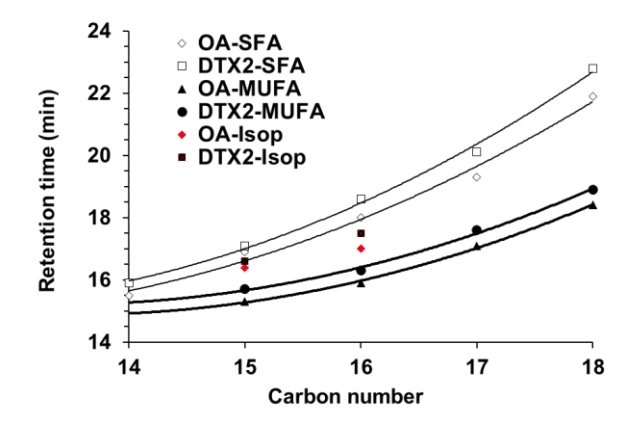


Fig. 5. Dependence of elution order with the number of carbon atoms for SFA and MUFA conjugates with okadaites in clams. Isoprenoid conjugates elute before the respective SFA, but after MUFA with the same carbon number. Lines represent polynomial fittings.

High abundance of odd FA are characteristic of bacteria (Harvey and Macko, 1997), and multi-branched FA (with isoprenoid skeleton) are

characteristic of chlorophyll degradation products (Rontani and Volkman, 2003).

Several phytol degradation products have been identified during marine invertebrate feeding, including pristane, isomeric pristenes, isomeric phytadienes, dihydrophytol and phytanic, pristanic, 4,8,12-trimethyltridecanoic and isomeric phytenic acids (Rontani and Volkman, 2003).

A chain with the exact mass of palmitic acid and also quite abundant in the marine environment is 4,8,12-trimethyltridecanoic acid (TMTD) (Fig. 6). The other acid found in okadaite's esters at lower levels might be phytenic acid (Fig. 6). This one presents an extra branch and has more four carbons in length. Phytenic acid precedes TMTD in the degradation cascade of phytol (Fig. 6).

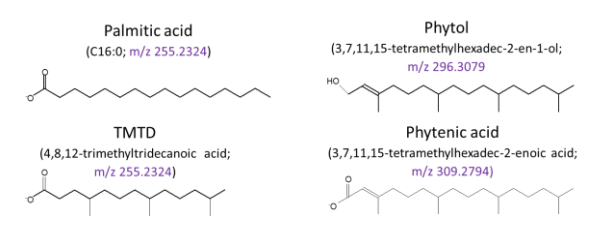


Fig. 6. Examples of chains linked to okadaites. The phytol moiety from chlorophyll a or b degrades to a series of isoprenoid analogues.

The esterification is much more active in sand-dwelling bivalves, and promotes their fastest depuration of these toxins (Vale, 2004). In mussels, esterification is less active, and protein-binding seems to be responsible for its longest depuration times (Vale, 2004; Rossignoli and Blanco, 2010).

Nevertheless, mussels are capable of performing esterification of okadaites by themselves. Treating with antibiotics did not have any significant effect on the acylation of the OA supplied to mussels, suggesting that bacteria do not play any significant role in this process (Rossignoli et al., 2011), as opposed to the hypothesis of a much deeper bacteria role in sand-dwelling bivalves, attributed to their high acylation rate and high percentage of odd FA plus isoprenoid FA in their 7-O-acyl esters (Vale, 2006, 2010).

Whether this particular acylation profiles found in Portuguese bivalves is attributable to the bivalve's metabolism, to the respective particular bacterial flora of sand-dwelling bivalves, or both, is a question that remains open.

Acknowledgements

The Portuguese authors acknowledge the EU Fisheries Operational Program 2020, FEAMP - Mar2020 (SNMB-Monitor programmes), which funds the National Bivalve Mollusk Monitoring System (SNMB) in Portugal.

References

- Aasen, J., MacKinnon, S.L., LeBlanc, P. et al. (2006). Rapid Commun. Mass Spectrom. 20, 1531-1537.
- de la Iglesia, P., McCarron, P., Diogène, J., Quilliam, M.A. (2013). Rapid Commun. Mass Spectrom. 27, 643-653.
- Fu, X., Hafza, N., Götz, F., Lämmerhofer, M. (2023). J. Chrom. A 1703, 464111.
- Harvey, H.R. Macko, S.A. (1997). Org. Geochem. 26, 531-544.
- Hu, T., LeBlanc, P., Burton, I.A. et al. (2017). Harmful Algae 63, 85-93.
- McCarron, P., Rourke, W.A., Hardstaff, W. et al. (2012). J. Agric. Food Chem. 60, 1437-1446.
- Pizarro, G., Paz, B., Gonzalez-Gil, S. et al. (2008). Harmful Algae 8, 926-937.
- Rontani, J.F., Volkman, J.K. (2003). Org. Geochem. 34, 1-35.
- Rossignoli, A.E., Fernández, D., Regueiro, J. et al. (2011). Toxicon 57, 712-720.
- Rossignoli, A.E., Blanco, J. (2010). Toxicon 55, 221-226.
- Suzuki, T., Kamiyama, T., Okumura, Y., et al. (2009). Fish. Sci. 75, 1039-1048.
- Torgersen, T., Wilkins, A.L., Rundberget, T., Mile, C.O. (2008). Rapid Commun. Mass Spectrom. 22, 1127-1136.
- Vale, P. (2004). Toxicon 44, 123-134.
- Vale, P. (2006). J. Chromatogr. A 1128, 181-188.
- Vale, P. (2010). Comp. Biochem. and Physiol. Part C 151, 18-24.

New azaspiracid analogues produced by *Azadinium spinosum* isolated from Japanese coastal waters

Mayu Ozawa¹, Hajime Uchida¹, Satoshi Numano¹, Ryuichi Watanabe¹, Ryoji Matsushima¹, Hiroshi Oikawa¹, Kazuya Takahashi², Mitsunori Iwataki², Toshiyuki Suzuki^{1,3*}

¹Fisheries Technology Institute, Japan Fisheries Research and Education Agency, 2-12-4 Fukuura, Yokohama, Kanagawa 236-8648, Japan.

²Graduate School of Agricultural and Life Sciences, University of Tokyo, 1-1-1 Yayoi, Bunkyo, Tokyo 113-8657, Japan.

³Kitasato University School of Marine Biosciences, 1-15-1 Kitazato, Minami-ku, Sagamihara, Kanagawa 252-0373, Japan

*Corresponding author's email: suzuki.toshiyuki@kitasato-u.ac.jp

Abstract

Azaspiracids (AZAs) are one of marine toxins that cause food poisoning with a primary syndrome of diarrhea. They are produced by toxic dinoflagellates belonging to the genera *Amphidoma* and *Azadinium*. *Azadinium* spinosum is known to produce AZA1, AZA2, AZA11 and AZA51 as the dominant toxins. There have been few investigations on AZA profiles in *A. spinosum* isolated in coastal waters in Japan. To investigate AZA profiles in *A. spinosum* isolated from Japan, a methanolic extract of a culture strain was analyzed by several LC/MS/MS techniques. Although known AZA analogues were not detected in the *A. spinosum* strain, four new AZA analogues were detected in the strain. Three of the four new AZA analogues have a structure lacking one methyl group attached to the cyclic amine.

Keywords: azaspiracid, AZA, LC/MS/MS, Azadinium spinosum (maximum 10 keywords)

https://doi.org/10.15027/0002041274

Introduction

The first human poisoning case associated with azaspiracids (AZAs) was reported by the consumption of mussels (Mytilus edulis) cultivated in Killary Harbour of Ireland (McMahon and Silke, 1996). AZAs causes gastrointestinal symptoms including nausea, vomiting, severe diarrhea, and stomach cramps. AZA1, AZA2, and AZA3 are regulated with the regulatory levels of 160 µg AZA1 equivalents kg-1 edible shellfish meat (EFSA Panel on Contaminants in the Food Chain, 2008). Four AZA-producing species have been reported: Azadinium spinosum, A. poporum, A. dexteroporum and Amphidoma languida (Tillmann et al., 2009, 2011, 2012; Percopo et al., 2013). A. spinosum was originally isolated from European coastal waters and ribotype A has been known to produce mainly AZA1 and AZA2. Recently, ribotype B producing AZA11 and AZA51 as dominant toxins was reported (Tillmann et al., 2018). AZA11 and AZA51 were tentatively determined as 3-hydroxylated analogues of AZAs by LC/MS/MS analyses (Tillmann *et al.*, 2019). More than 60 AZA analogues have currently been reported from toxic dinoflagellates and bivalves. Although azaspiracid shellfish poisoning (AZP) had not occurred in Japan, we recently reported several strains of *A. poporum* producing AZA2 along with other minor AZAs isolated from the coastal waters of Japan (Ozawa *et al.*, 2021; Takahashi *et al.*, 2021).

In our present study, we analyzed *A. spinosum* isolated in Japanese coastal water in the first case by using liquid chromatography-tandem mass spectrometry (LC/MS/MS). Precursor ion scan and neutral loss scan modes of LC/MS/MS for comprehensive search for AZA analogues in *A. spinosum* were carried out. Four novel AZAs were unambiguously identified by the LC/MS/MS analyses in our present study.

Group 1: [M+H]*
$$R_2$$
 Group 2: m/z 641+ R_3 + R_4 + R_5 H R_3 Group 3: R_4 Group 3: R_5 Group 3: R_5 Group 4: R_4 Group 4: R_5 Group 4: R_5 Group 5: R_7 R_7 Group 5: R_8 Group 5: R_8 Group 6: R_8 Group 7

Fig. 1. The chemical structure of AZAs and the fragmentation diagram by positive ion mode LC/MS/MS.

Materials and Method

Static culture and large-scale culture with aeration A. spinosum strain HrAz562 was isolated from Hiroshima Bay, Japan. The strains were maintained in 50 mL flasks at 24°C, 35 µmol m⁻² s⁻¹ ¹ under a 16:8 h light: dark photocycle in a growth chamber. Cells on static culture and aerated culture were maintained for 2 weeks in 25 mL and 1L modified f/2-medium, respectively. 100 µL aliquots of the cultures were collected and fixed with 2.5% glutaraldehyde (final concentration), and cells were counted using a microscope. Cells in 50 mL tubes were harvested by centrifugation at $1200 \times g$ for 3 min, and the pellets were stored at -20°C. The thawed cells were extracted twice with 2 mL, and residues after removing the methanolic solvent were dissolved in 0.2 mL. For the largescale aerated culture, cells and medium were stored frozen. thawed cells were extracted twice with methanol as above and redissolved in 10 mL. The thawed medium was loaded onto Sep-pak C18 (5g) pre-conditioned with 50 mL methanol and 50 mL water, then desalted with 50 mL water, and eluted with 50 mL metanol. The eluate was dried by a rotary evaporator, and dissolved in 5 mL methanol.

AZAs analyses

In the LC/MS/MS, selected reaction monitoring (SRM) analysis using Q1 > Q3 parameters described in previous report (Ozawa *et al.*, 2021) was performed to detect known AZAs, and precursor ion scan or neutral loss scan analyses were performed to search for new AZAs. Compounds I, II, III and IV were quantified using the AZA1 standard by SRM LC/MS/MS analysis with [M+H]⁺ set in Q1 and Group3 ions set in Q3.

The accurate mass and composition formula of AZAs were obtained by survey scan analysis using LC/QTOFMS carried out as previous report (Ozawa *et al.*, 2021).

Results and Discussion

Detection of AZAs

Although no known AZAs were detected from the extract of A. spinosum strain HrAz562 by LC/MS-SRM, four ion peaks were found by precursor ion scan using the fragment ions observed commonly in AZAs. Ion peaks corresponding to m/z 774.5, m/z 860.5 and two of m/z 874.5 showed the characteristic MS/MS fragment ions of AZAs. Extracted ion chromatograms of AZA1, 2, 3 in the standard mixture and four compounds (compounds I-IV) in the strain HrAz562 extract are shown in Fig. 2. Because the MS/MS fragment ions were not matched to those of known AZAs, four compounds were suggested as novel AZA analogues. Cellular contents of compounds I, II, III and IV calculated from cell numbers and quantification were 0.8, 2.7, 15.0 and 8.6 fg cell⁻¹, respectively.

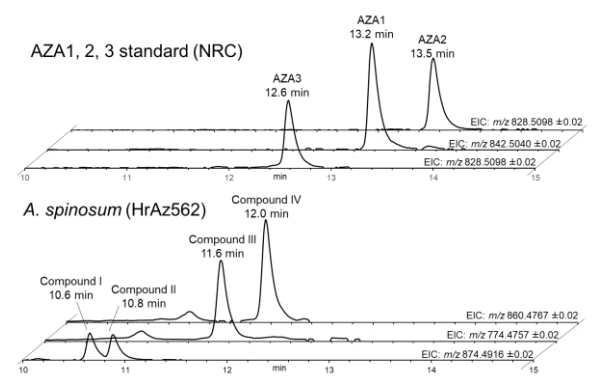


Fig. 2. Extracted ion chromatograms of AZA1, 2, 3 and four AZA analogues in the strain HrAz562 extract.

Structural Analysis of AZAs

Chemical structures of four new compounds were estimated by positive ion mode MS/MS fragmentations. The *m/z* and composition formulas of [M+H]⁺ and their MS/MS product ions derived from major cleavages of AZAs are shown in Table 1. The LC/MS/MS fragmentation diagrams of four new AZA analogues with the assignments of MS/MS product ions are shown in Fig. 3. The composition formulas of both compounds I and II were identified as having two more oxygen atoms than AZA1, whereas product ions derived from the

major cleavage in compound I were shifted -14 m/z units compared to those of compound II (Table 1). Detection of the product ion at m/z 154.1 in compounds I and III suggests a loss of one methyl group in the I-ring (Fig. 3). Compound III with m/z774.5 corresponding to [M+H]⁺ had a relatively small molecular weight. AZA33, an AZA analogue of a small molecular weight of 715.5 without the A, B and C ring moieties, was reported in a previous study (Kilcoyne et al., 2014). On the other hand, it is presumed that compound III retains these rings structures (Fig. 3). This is the first report of this kind of structure losing the carboxy side chain. In compound IV, a loss of one methyl group in the Iring was suggested from the characteristic ion m/z154. Furthermore, the product ion shifted by -44 m/z units from $[M+H]^+$ of m/z 860.5 was detected, supporting the addition of an oxygen atom to C3 in compound IV (Fig. 3).

Table 1. MS/MS product ions derived from major cleavages of four new AZAs.

	AZA1		Cor	mpound I	Compound II		
	m/z	Composition	m/z	m/z Composition		Composition	
Group 1	842.5	$C_{47}H_{72}NO_{12}$	874.5	$C_{47}H_{72}NO_{14}$	874.5	$C_{47}H_{72}NO_{14}$	
Group 2	672.4	$C_{38}H_{58}NO_9$	690.4	$C_{37}H_{54}NO_{10}$	704.4	$C_{38}H_{56}NO_{10}$	
unknown	_	_	540.3	$C_{31}H_{42}NO_7$	554.3	$C_{32}H_{44}NO_7$	
unknown	_	_	480.3	$\mathrm{C}_{29}\mathrm{H}_{38}\mathrm{NO}_{5}$	494.3	$C_{30}H_{40}NO_5$	
Group 3	462.3	$\mathrm{C}_{27}\mathrm{H}_{44}\mathrm{NO}_{5}$	464.3	$C_{26}H_{42}NO_{6}$	478.3	$C_{27}H_{44}NO_6$	
Group α^*	_	_	394.3	$\mathrm{C}_{22}\mathrm{H}_{36}\mathrm{NO}_5$	408.3	$C_{23}H_{38}NO_5$	
Group 4	362.3	$C_{22}H_{36}NO_3$	348.3	$\mathrm{C}_{21}\mathrm{H}_{34}\mathrm{NO}_3$	362.3	$C_{22}H_{36}NO_3$	
Group 5	262.2	$C_{16}H_{24}NO_2$	248.2	$C_{15}H_{22}NO_2$	262.2	$C_{16}H_{24}NO_2$	
Group 6	168.1	C ₁₀ H ₁₈ NO	154.1	$C_9H_{16}NO$	168.1	C ₁₀ H ₁₈ NO	

	Con	npound III	Cor	npound IV
	m/z	Composition	m/z	Composition
Group 1	774.5	C ₄₃ H ₆₈ NO ₁₁	860.5	$C_{46}H_{70}NO_{14}$
Group 2	644.4	$\mathrm{C}_{36}\mathrm{H}_{54}\mathrm{NO}_{9}$	644.4	$C_{36}H_{54}NO_9$
unknown	_	_	_	_
unknown	_	_	_	_
Group 3	434.3	$\mathrm{C}_{25}\mathrm{H}_{40}\mathrm{NO}_5$	434.3	$C_{25}H_{40}NO_5$
Group α^*	_	_	_	_
Group 4	348.3	$\mathrm{C_{21}H_{34}NO_3}$	348.3	$C_{21}H_{34}NO_3$
Group 5	248.2	$C_{15}H_{22}NO_2$	248.2	$C_{15}H_{22}NO_2$
Group 6	154.1	$C_9H_{16}NO$	154.1	$C_9H_{16}NO$

*The product ions derived from group α are detected in AZAs with an oxygen atom added to C23 (Rehmann *et al.*, 2008).

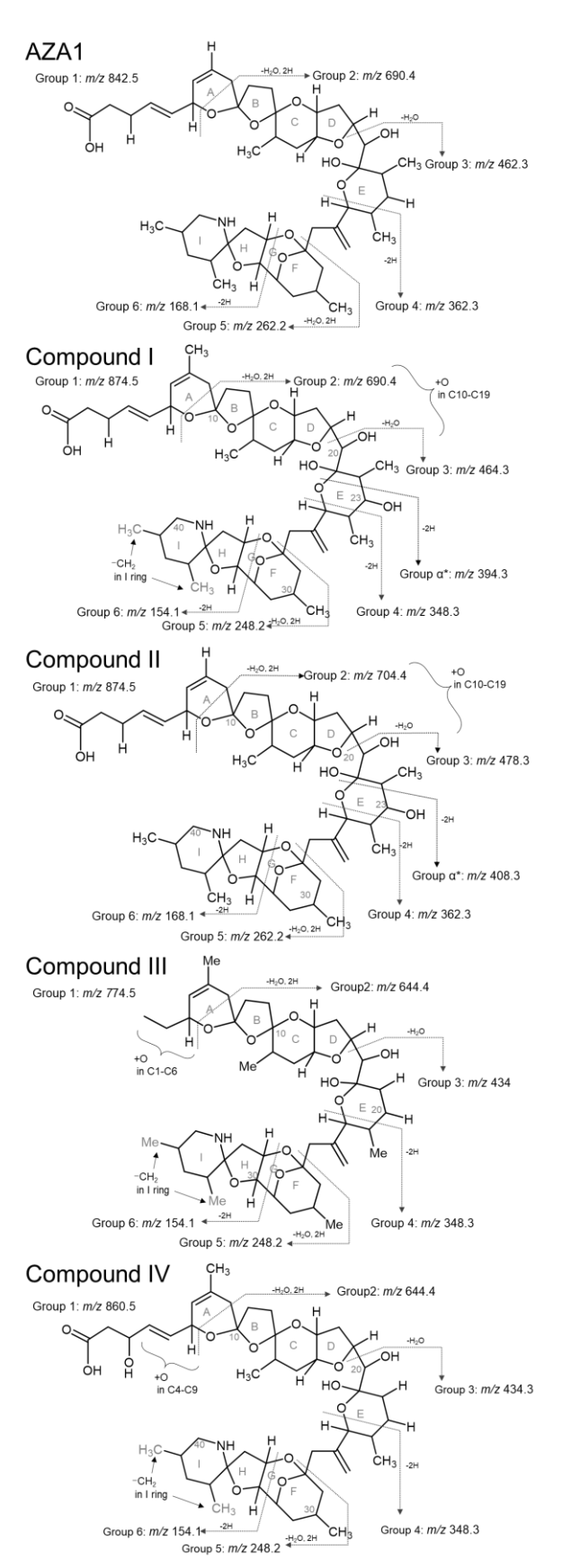


Fig. 3. Fragmentation diagrams of AZA1 and four new AZAs.

Toxin distributions in the cells and medium obtained from the large scale culture

Contents of the four new AZAs obtained from the large cultivation of the strain HrAz562 are shown in Table 2. The highest amount of compound IV was exclusively confirmed under the aeration conditions. The percentages of AZAs in the cells and the medium showed that AZAs were highly distributed in the medium. In the A. poporum previously reported (Ozawa et al., 2021), more than 95% of AZAs were detected in the cells under the same aeration culture conditions. No cells were observed in the medium after centrifugation of the strain HrAz562 cultures. Therefore, it was suggested that this strain tends to excrete AZA extracellularly. The aeration culture produced less amounts of compounds I and II compared to static culture. It was reported that aeration during incubation affected the toxin profiles of A. poporum (Ozawa et al., 2023).

Table 2. Distributions and amounts of AZAs in large cultivation of the strain HrAz562 cultures.

AZAs .	Distribu	ıtions (%)	3L culture		
7273	Cells	Medium	medium (ng)	(ng)	
Compound I	29.4	70.6	228	3.5	
Compound II	21.8	78.2	179	9.6	
Compound III	21.2	78.8	1384	1.1	
Compound IV	42.1	57.9	3598	3.2	

This is the first reported of the toxin profile of *A. spinosum* isolated from Japanese coastal waters. Three of four AZAs found from the strain HrAz562 were analogues lacking one methyl group attached to the I-ring. Compound I is the isomer of compound II, and the position of one methyl group is different. The molecular phylogeny, detailed toxin profiles of this strain and complete elucidation of chemical structures will be discussed in the future.

Acknowledgements

This work was partially supported by the research project on Regulatory research projects for food safety, animal health and plant protection (JPJ008617, 18064849) funded by the Ministry of Agriculture, Forestry and Fisheries of Japan, and JSPS KAKENHI 22H02416 and 23KK0117 (MI).

References

- EFSA J. 723 (2008) Marine biotoxins in shellfish-Azaspiracid group-Scientific Opinion of the Panel on Contaminants in the Food chain, 1–52.
- McMahon, T. and Silke, J. (1996). *Harmful Algae News* 14, 2.
- Ozawa, M., Uchida, H., Watanabe, R., Matsushima, R., Oikawa, H., Takahashi, K., Iwataki, M., Suzuki, T. (2021). *Toxicon* 199, 145-155.
- Ozawa, M., Uchida, H., Watanabe, R., Matsushima, R., Oikawa, H., Takahashi, K., Iwataki, M., Suzuki, T. (2023). *Toxicon* 226, 17069.
- Percopo, I., Siano, R., Rossi, R., Soprano, V., Sarno, D., Zingone, A. (2013). *J. Phycol.* 49, 950-966.
- Rehmann, N., Hess, P., Quilliam, M.A. (2008). *Rapid Commun. Mass Spectrom.* 22, 549-558.
- Takahashi, K., Lum, W.M., Benico, G., Uchida, H., Ozawa M., Oikawa, H., Suzuki, T., Nguyen, V.N., Dao, V.H., Iwataki, M. (2021). *Phycol. Res.* 69, 175-187.
- Tillmann, U., Elbrächter, M., Krock, B., John, U., Cembella, A. (2009). *Eur. J. Phycol.* 44, 63-79.
- Tillmann, U., Elbrächter, M., John, U., Krock, B. (2011). *Eur. J. Phycol.* 46, 74-87.
- Tillmann, U., Salas, R., Gottschling, M., Krock, B., O'Driscoll, D., Elbrächter, M. (2012). *Protist* 163, 701-719.
- Tillmann, U., Edvardsen, B., Krock, B., Smith, K.F., Paterson, R.F., Voß, D. (2018). *Harmful Algae* 80, 15-34.
- Tillmann, U., Wietkamp, S., Gu, H., Krock, B., Salas, R., Clarke, D. (2021). *Microorganisms* 9, 134.

Toxin analysis of Kareniaceae cultures isolated from the northern coastal waters in Japan

Hajime Uchida^{1*}, Koki Yuasa¹, Tomoyuki Shikata¹, Mayu Ozawa¹, Satoshi Numano¹, Ryuichi Watanabe¹, Ryoji Matsushima¹, Hiroshi Oikawa¹, Koyo Kuwata², Wai Mun Lum^{1,2}, Kazuya Takahashi², Mitsunori Iwataki², Toshiyuki Suzuki¹

¹ Fisheries Technology Institute, Japan Fisheries Research and Education Agency, 2-12-4 Fukuura, Kanazawa, Yokohama 236-8648, Japan.

*corresponding author's email: uchida hajime03@fra.go.jp

Abstract

Unarmored dinoflagellates in the Kareniaceae are known to be harmful to a variety of marine organisms due to their toxicity. In 2021, a red tide dominated by *Karenia selliformis*, along with a few occurrences of *K. mikimotoi*, *K. longicanalis*, and *Takayama* spp., caused the death of fish and sea urchins along the Pacific coast of Hokkaido, Japan. In our present study, brevetoxins (PbTxs) and cyclic imines (CIs) in kareniacean culture strains collected from the Pacific coast of Hokkaido and Mutsu Bay in northern Japan were analyzed using selected reaction monitoring (SRM) liquid chromatography-quadrupole tandem mass spectrometry (LC/MS/MS). PbTxs and CIs were not detectable in the kareniacean cultures collected from the red tide along the Pacific coast of Hokkaido in 2021. The *K. selliformis* strains isolated from Hokkaido in 2021 were closely related to those isolated from the coasts of Kamchatka and Chile based on molecular phylogenetic analysis. Interestingly, *K. selliformis* from Kamchatka and Chile exhibited high toxicity to some marine organisms. On the other hand, *K. selliformis* cultured strain MoKr600 from the Mutsu Bay produced GYM-A and B/C of CIs. This strain belonged to the same intraspecific phylogenetic group of *K. selliformis* that produces GYM in New Zealand. Our findings suggest that toxin production and intraspecific phylogeny are closely related in *K. selliformis*.

Keywords: Kareniaceae, Karenia selliformis, Cyclic imines, Brevetoxins, LC/MS/MS

https://doi.org/10.15027/0002041275

Introduction

The dinoflagellates of Kareniaceae formed a massive red tide in the Pacific coast of East Hokkaido in 2021, and caused extensive damage to fishes, sea urchins, and other marine organisms. This red tide was dominated by *Karenia selliformis*, along with a few occurrences of *Karenia mikimotoi*, *Karenia longicanalis*, *Karlodinium* sp. and *Takayama* spp. (Iwataki *et al.*, 2022).

K. selliformis could be distinguished into two subclades by the ITS phylogeny, group-I and -II (Mardones et al., 2020). The group-I was reported from Chile in 1999 (Clément et al., 2001) and Kamchatka, Russia in 2020 (Orlova et al., 2022). This group has high toxicity for marine organisms and cytotoxicity, and the bloomed strain occurred

in the Pacific coast of East Hokkaido in 2021 also belonged to the group-I. On the other hand, *K. selliformis* group-II has productivity of gymnodimines (GYMs) in New Zealand and Tunisia (MacKenzie *et al.*, 1996; Ben Naila *et al.*, 2012).

The GYMs (Fig. 1) are marine biotoxin of cyclic imines (CIs) isolated from New Zealand oysters and dinoflagellate (Seki *et al.*, 1995; Miles *et al.*, 2000, 2003). The GYMs are neurotoxins acting on the muscle nicotinic acetylcholine receptor (Kharrat *et al.*, 2008).

² Graduate School of Agricultural and Life Sciences, University of Tokyo, 1-1-1 Yayoi, Bunkyo, Tokyo 113-8657, Japan.

Fig. 1. Chemical structures of gymnodimines. (A) gymnodimine-A (GYM-A), (B) 17-exocyclic methylene and 18-hydroxyl group (GYM-B/C).

Karenia brevis and Karenia papilionacea produce brevetoxins (BTXs) among ladder-like polyether compounds (Fig. 2). The BTXs are known as fish-killing toxins and the cause of the neurotoxic shellfish poisoning.

Fig. 2. Chemical structures of brevetoxins. BTXs have two backbone types. (A) A-type back bone; PbTx-1, PbTx-7 and PbTx-10. (B) B-type backbone; PbTx-2 and PbTx-3.

The occurrence of toxic kareniacean species imposes concerned risk of industrial damage for fisheries and human food poisoning. A red tide caused by Kareniaceae brought the first case of fisheries damage in the Pacific of East Hokkaido in 2021, however, the toxin production capability of the culture strains from the northern coastal waters in Japan is unclear. In this study, the LC/MS/MS and quadrupole-time of flight mass spectrometry (QTOF) were performed to analyze known toxins produced by the kareniacean culture strains obtained from the northern coastal waters in Japan.

Materials and Methods

Culture conditions

The Kareniaceae cultures of 15 strains were maintained in 1/2 Daigo's IMK medium (Wako, Tokyo, Japan) or modified K/2 medium, under the conditions of $18-20^{\circ}\text{C}$, 30 psu, and 16:8 h light and dark cycle with 60-100 µmol photons m⁻² s⁻¹ light illumination for 14-21 days. 10 mL of the cultured solutions were separated into harvested cells and cultured supernatants by centrifugation ($1,200 \times g$, for 3 min). The harvested cells and cultured supernatant were stored at -30°C in freezer until analyses.

Sample preparation for LC/MS/MS

The cultured cells were extracted twice with methanol (MeOH) 300 μ L, and centrifuged (5,000 \times g, for 5 min). The MeOH extract was transferred to 1 mL volumetric flask, and made up to 1 mL with MeOH. This MeOH extract of harvested cells were analyzed for GYMs and BTXs.

The toxins in the cultured supernatant were retained in a solid phase extraction (SPE) column Sep-Pak C18 plus cartridge (340 mg, Waters, UK). A SPE column was conditioned with 5 mL MeOH and 5 mL distilled water (D.W). A supernatant was applied for SPE column, and washed with 5 mL D.W. The elution was performed with 10 mL MeOH. An eluate was evaporated, and dissolved in 1 mL MeOH.

LC/MS/MS analyses

The toxin analyses were carried out with two LC/MS/MS systems. A triple quadrupole mass spectrometer 4500Qtrap (Sciex, Canada) coupled with liquid chromatograph LC-20XR series (Shimadzu, Japan) was used for the quantitative analysis using selected reaction monitoring (SRM) analysis. A QTOF micrOTOF QII (Bruker, Germany) coupled with liquid chromatograph ultimate3000 (Thermo Fisher Scientific, USA) was used for the analysis of high-resolution mass spectrometry (HRMS) and product ion scan.

The LC separation of GYMs was carried out using a Waters Acquity BEH C8 (2.1 mm I.D. \times 50 mm, 1.7 μ m, Waters, UK) column with mobile phase (A) D.W. and (B) MeCN:D.W, (95:5, v/v) both containing 50 mM formic acid and 2 mM ammonium formate. Linear gradient performed from 5%B to 100%B for 20 min, and 100%B for 10 min. Flow rate and column temperature were 0.3 mL min⁻¹ and 25°C, respectively. Injection volume was 5 μ L. CIs (GYM-A, SPX-1, PnTX-E, PnTX-F, and PnTX-G standards were purchased from

Sigma-Aldrich and National Research Council Canada.

The LC separation of BTXs was carried out on a L-column2 C6-phenyl (2.1 mm I.D. \times 150 mm, 3 μ m, CERI, Japan) column with mobile phase (A) D.W. and (B) MeCN both containing 0.1 vol% formic acid. Linear gradient: 20%B to 100%B for 15 min, and 100%B for 5 min. Flow rate: 0.3 mL min⁻¹, column temperature: 40°C, injection volume: 5 μ L. BTXs standards (PbTx-1, PbTx-2, and PbTx-3) were purchased from Sigma-Aldrich.

Results and Discussion

SRM chromatograms of BTXs standards and *K. selliformis* group-I and -II are shown in Fig. 3. BTXs were below the limit of detection (LOD) by SRM analysis in all samples.

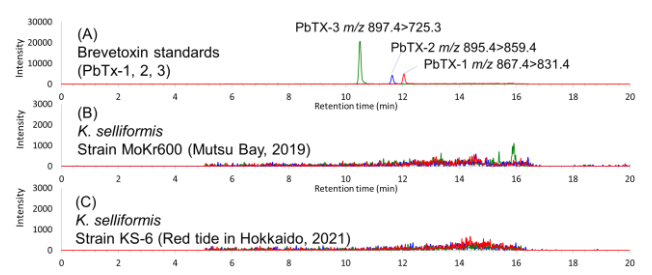


Fig. 3. SRM chromatograms of brevetoxins. (A) BTXs standards (PbTx-1, PbTx-2 and PbTx-3). (B) MeOH extracts of *K. selliformis* group-II from Mutsu Bay, 2019. (C)The representative chromatogram of MeOH extract of *K. selliformis* group-I from the Pacific coast of Hokkaido, 2021.

Karenia brevis CCMP2228 strain has been reported to produce BTXs (PbTx-2 and PbTx-3) at a level of 9.6 pg cell⁻¹ (Hardison *et al.*, 2012). On the other hand, *K. selliformis* group-I from the Pacific coast of Hokkaido showing high toxicity for marine organisms (Hasegawa *et al.*, 2022) had few BTXs less than PbTx-2 20 fg cell⁻¹ in concentrated cells extracts of KKsKs74 strain (Table 1), and BTXs-like compounds giving characteristic MS spectra of BTXs were not detected by extracted ions of the LC/QTOF analysis.

SRM chromatograms of CIs standards and *K. selliformis* MoKr600 strain of the group-II are shown in Fig. 4. GYM-A and putative GYM-B/C/D (*m/z* 524.3>506.3) were detected from cell extract of *K. selliformis* MoKr600 strain. GYM-A content of MoKr600 strain was 54 pg cell⁻¹ in cell quota. GYM-A was detected with 21.4 ng mL⁻¹ in

cultured supernatant, approximately 20% of the total GYM-A produced by the culture.

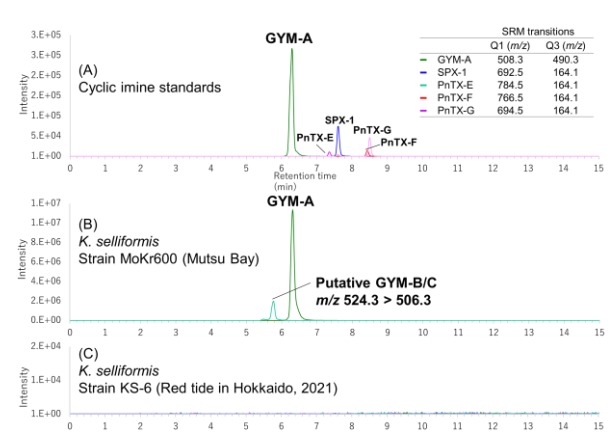


Fig. 4. SRM chromatograms of cyclic imines. (A) CIs standards (GYM, SPX-1, PnTX E, PnTX F and PnTX G). (B) MeOH extracts of *K. selliformis* group-II from Mutsu Bay, 2019. (C)The representative chromatogram of MeOH extract of *K. selliformis* group-I from the Pacific coast of Hokkaido, 2021.

CIs were not detected in the Kareniaceae samples from the Pacific coast of Hokkaido as shown in Table 1. In previous reports, the group-I Chilean *K. selliformis* did not produce GYM. On the other hand, *K. selliformis* group-II from New Zealand produced GYMs (Mardones *et al.*, 2020). The culture strains of *K. selliformis* from Northern coastal waters in Japan also supported this molecular phylogeny and capability of producing CIs.

Table 1. Brevetoxins and cyclic imines (CIs) analyses from Japanese Kareniaceae. N.D.: Not detected. The limit of detection (LOD:S/N =3) of CIs in the extracts were GYM-A 0.1 ng mL⁻¹, SPX-1 and PnTX-G 0.3 ng mL⁻¹, PnTX-E and PnTX-F each 0.6 ng mL⁻¹. The LOD of BTXs in extracts were PbTX-1 and PbTx-2 each 2.0 ng mL⁻¹ and PbTx-3 0.6 ng mL⁻¹.

Source	Strain	Species	Cells ×10 ³ mL ⁻¹	Toxins contents Cell Quota		
			in MeOH	BTXs	CIs	
Mutsu Bay (2019)	MoKr600	K. selliformis (Group II)	10.0	N.D.	GYM-A 54 pg cell ⁻¹	
	LK2Ks306		14.0	N.D.	N.D.	
	LK2Ks307	K. selliformis	3.0	N.D.	N.D.	
	KKsKs74	(Group I)	125.0	N.D.	N.D.	
	KS-6		100.0	N.D.	N.D.	
	KKsKm70		22.0	N.D.	N.D.	
	KKsKm71	K. mikimotoi	8.5	N.D.	N.D.	
Red tide in	KKsKm72		6.5	N.D.	N.D.	
Hokkaido	KKsKm73		50.0	N.D.	N.D.	
(2021)	LAkKL297	K. longicanalis	3.4	N.D.	N.D.	
	LAkKL300	k. longiculuis	11.2	N.D.	N.D.	
	KKsTk68		18.2	N.D.	N.D.	
	KKsTk69	Takayama sp.	0.6	N.D.	N.D.	
	LK929Tak330		4.1	N.D.	N.D.	
	KKsTk67	Takayama cf. acrotrocha	9.8	N.D.	N.D.	

GYM-A was detected at m/z 508.3411 trace as $[M+H]^+$ (C₃₂H₄₆NO₄⁺, calculated mass m/z508.3421) in the HRMS for GYMs by the LC/QTOF. Putative GYM-B/C was detected at m/z 524.3350 trace as $[M+H]^+(C_{32}H_{46}NO_5^+, calculated)$ mass m/z 524.3471). GYM-D has the same molecular formula with GYM-B/C but different MS/MS spectra (Harju et al., 2016). GYM-B/C exhibited the characteristic product ions at m/z 488 and m/z 320, whereas this ion was not detected from GYM-D. The MS/MS spectra obtained from K. selliformis MoKr600 strain exhibited the specific production m/z 488 and m/z 320 (Fig. 5). The characteristic ions at m/z 346 and m/z 316 of GYM-D were not detected from putative GYM-B/C (Fig. 5). In our present study, it was demonstrated that Japanese K. selliformis group-II produced GYM-A as the dominant toxin, along with small amounts of GYM-B/C.

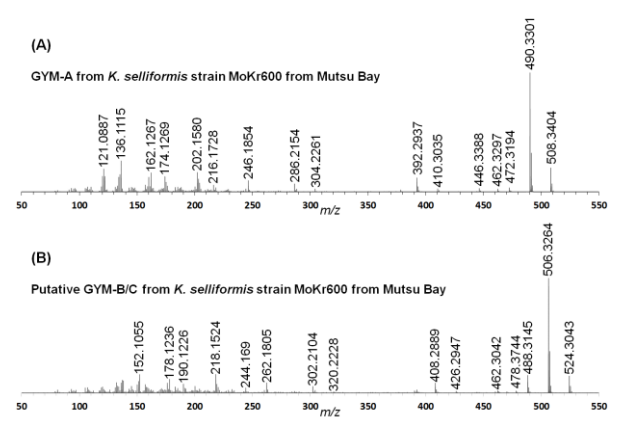


Fig. 5. MS/MS spectra produced from [M+H]⁺ of gymnodimines in Japanese *K. selliformis* group-II. (A) GYM-A, (B) Putative GYM-B/C.

We report that *K. selliformis* group-II collected from the coast of Japan has GYM production. The small amount of CIs including GYMs were detected from Japanese bivalves in our previous studies (unpublished data). Microalgae that produce CIs such as *K. selliformis* group-II could be the causative species on the contaminations of bivalves in Japan.

The BTXs and CIs were not detected in all the strains of Kareniaceae from the 2021 Hokkaido red tide. The Hokkaido *K. selliformis* belonged to the phylogenetic clade group-I with Chile and Kamchatka strains. These red tides were highly toxic to marine organisms, and this phylogenetic clade has cytotoxicity (Mardones *et al.*, 2020). Therefore, *K. selliformis* group-I is considered to

have some novel toxins. Further investigation to clarify the causative toxins will be required.

Acknowledgements

This work was partially supported by Japanese JSPS Kakenhi 19KK0160, 21H02268, and the Fisheries Agency of Japan.

References

Clément, A., Seguel, M., Arzul, G., et al., (2001). In: Hallegraeff, G.M., Blackburn, S.I., Bolch, C.J., Lewis, R.J. (Eds.), HABs, IOC, UNESCO, Paris, pp. 66–69.

Ben Naila, I., Hamza, A., et al., (2012), Harmful Algae 18, 56–64.

Hardison, D.R., Sunda, W.G., Litaker, R.W., *et al.*, (2012). Journal of Phycology, 48(4), 844–858. Harju, K., Koskela, H., *et al.*, (2016), Toxicon 112, 68–76.

Hasegawa, N., Watanabe, T., Unuma, T., Yokota, T., *et al.*, (2022) Fish. Sci. 88, 787–803.

Iwataki, M., Lum, W.M., Kuwata, K., Takahashi, K., *et al.*, (2022). Harmful algae, 114, 102204 Mardones, J.I., Norambuena, L., Paredes, J., *et al.*, (2020). Harmful Algae 98, 101892.

Kharrat, R., Servant, D., Girard, E., Ouanounou, G., et al., (2008). Journal of Neurochemistry, 107(4), 952–963.

MacKenzie, L., Haywood, A., *et al.*, (1996) In: Yasumoto, T., Oshima, Y., Fukuyo, Y. (Eds.), Harmful and Toxic Algal Blooms, IOC of UNESCO, Sendai, pp. 97–100.

Miles C.O., Wilkins A.L., *et al.*, (2000), J. Agric. Food Chem. 48, 1373–1376.

Miles C.O., Wilkins A.L., *et al.*, (2003), J. Agric. Food Chem. 51, 4838–4840.

Orlova T.Y., Aleksanin A.I., *et al.*, (2022), Harmful Algae, 120, 102337

Seki, T., Satake, M., Mackenzie, L., *et al.*, (1995), Tet. Lett. 36, 7093–7096.

The magical mystery tour that is the dinoflagellate sterolysin biosynthesis some assembly (correction) required

Allen R. Place^{1*}, Ernest P Williams^{1,2}, Saddef Haq^{1,3}, Tsevtan R. Bachvaroff¹

²Current address: ESR's Enteric Reference laboratory (ERL), 27 Creyke Road, Ilam, Christchurch 8041, PO Box 29181, Christchurch 8540, Aotearoa New Zealand;

³Current address: FDA/ CDER/ OND, Building 22, 10903 New Hampshire Ave, White Oak, MD USA 20903.

*corresponding author's email:place@umces.edu

Abstract

We have uncovered a single transcript (>14 Kb) with three consecutive KS modules, that are conserved across three species of dinoflagellates (Karlodinium veneficum and Amphidinium carterae, have known toxins, and Akashiwo sanguinea, which is non-toxic), as well as many single module KS subunits using RNA sequencing analysis. When comparing the three species, the acyl transferase (AT) subunit in the triple module KS was present only in the non-toxic species and missing in the toxin producing species. To test the functionality of PKS in these species, we added cerulenin, an inhibitor that covalently binds to the KS subunits (Funabashi et al, 1989), to an exponential phase culture of A. carterae and A. sanguinea. Using ¹⁴C labeled acetate and liquid chromatography mass spectrometry (LC/MS), we found that cerulenin inhibition resulted in the reduction of both fatty acid and toxin production. This shows KS plays a role in both fat and toxin synthesis leading us to our hypothesis: The triple module KS acts as a scaffold for both toxin and fatty acid production where the final product is mediated by accessory trans-AT subunits, which exist in parallel with the KS. To substantiate that the triple KS transcript produces a protein, we have generated an antibody to an epitope in the TE domain. We clearly have evidence that a partial multi-module protein (~285,000 daltons) is expressed and is predicted to catalyze two carbon additions to a growing fatty acid/polyketide chain. However, an antibody to KS1 domain found a discrete protein containing the KS1 and KS2 domains but not the KS3 domain indicating posttranslational processing. We are currently investigating the interacting partners with these two protein scaffolds.

Keywords: Dinoflagellate; PKS; Fatty acids, Cerulenin; Transcript

Introduction

Dinoflagellates are unicellular protists often implicated in harmful algal bloom (HAB) events that result in fish kills and human illnesses worldwide as a result of potent toxin production consistent with a polyketide origin of biosynthesis based on ¹³C acetate labelling [1–3]. Polyketide synthases (PKS) are similar to fatty acid synthases (FAS), where individual domains sequentially add activated acetate-derived 2-C units to a growing carbon chain [4,5]. The PKS process begins when acvl monomer is loaded phosphopantetheine "arm" of the acyl carrier protein (ACP) by acyl transferase (AT) domains. The ACP is the site of monomer attachment as well as the site of condensation and reduction reactions that occur during PKS biosynthesis.

Condensation reactions are carried out by ketosynthase (KS) domains while reduction reactions are mediated by ketoreductase (KR), dehydratase (DH), and enoylreductase (ER) domains. At the end of product synthesis the thioesterase (TE) domain is responsible for the release of the finished product.

In addition to PKSs, non-ribosomal peptide synthetases (NRPS) and NRPS/PKS hybrids are also present in dinoflagellates [6]. These synthases have a mechanism similar to PKSs, but amino acid residues are incorporated into the product. Adenylation (A) domains recognize specific amino acids for incorporation. The thiolation (T) domains form an aminoacylthioester intermediate while the condensation (C) domains form the peptide bond between substrates. Finally, the thioesterase (TE) domain releases the final product. PKS/NRPS

^{1*}Institute of Marine and Environmental Technology, University of Maryland Center for Environmental Science, Baltimore, U.S.A.;

hybrids combine domains from both of these pathways.

In this paper we will focus on one multimodular PKS, as described by Williams *et al.*, which contained three KS domains [6]. We are focusing on this triple module PKS because transcriptome data have shown this domain arrangement is found in all dinoflagellates studied to date. The AT domain is missing in toxin producing species and must be supplied by a *trans single module* AT. In the non-toxic species, *Akashiwo sanguinea*, a *cis* AT found within the transcript making it a strong candidate for involvement in fatty acid synthesis in this species (Figure 1) [6].

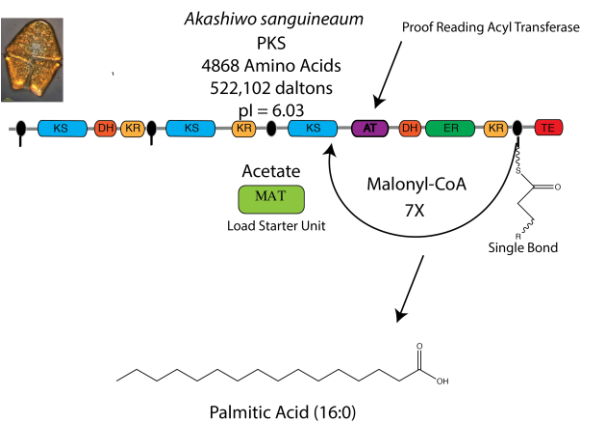


Figure 1. The "Triple KS" gene is shown as a multi-modular polyketide synthase (PKS) in *Akashiwo sangineaum*. Resultant products based on a purely processive synthesis

Materials and Method

Generation and validation of affinity-purified antibodies The amino acid sequence of the AT and TE domain in multi-modular polyketide synthase (PKS) of Akashiwo sangineaum was submitted to the Genscript Optimum AntigenTM Design Tool to determine the optimal antigenic regions to use for immunization. Genscript synthesized the antigenic peptides and added an additional cysteine residue (AT domain: VDMGKQLYDKEPVFC & TE domain: GVSWPRGSGPSAWC) to allow for conjugation to the KLH adjuvant. These were used for immunization of New Zealand white rabbits. Specific antibodies were isolated from the resulting serum by affinity purification using the synthesized peptide as bait. Antibodies were tested for reactivity by an ELISA assay with the peptide used to generate the antibody as the target coating the wells of a 96-well plate. Protein concentrations were determined using a QubitTM protein assay kit (Life Technologies) and approximately 250 ng of each

protein loaded per lane. Samples were analyzed using a 4-12 % BisTris NuPAGE SDS- PAGE gel (Life Technologies) and separated by molecular weight using denaturing electrophoresis. Proteins were transferred to PVDF 0.2 µM membrane (BioRad) using the Bolt Mini Blot Module (Life Technologies) and western blot carried out using the iBind Western Blot Apparatus (Life Technologies). Affinity-purified rabbit polyclonal antibodies specific to AT domain were used as the primary probe in western blotting. An anti-rabbit IgG (H&L) (GOAT) antibody that was peroxidase conjugated (BioRad) was used as the secondary probe. Luciferase signal was visualized by incubation in Clarity Enhanced Chemiluminescent (ECL) substrate (BioRad) and imaged using a FluorChem E (Protein Simple). Quantification of band intensities was performed using Imageview software (Protein Simple).

Cell Culture Conditions for A. carterae and A. sanguinea Amphidinium carterae (CCMP 1314) was grown in ESAW medium modified to contain 10 mM of HEPES in polystyrene culture flasks from Corning (Corning NY) [39]. The cultures were maintained under constant light at 150µm cm² s⁻¹ with a 14:10 light:dark schedule. Akashiwo sanguinea was grown in the same conditions; however, the ESAW medium was used at a salinity of 15 parts per thousand.

¹⁴C Acetate Labeling of A. carterae and A. sanguinea. The cultures of A. carterae and A. sanguinea were cultured as described above. Cells were counted using a Coulter counter and had cell densities of 79,000 cells mL⁻¹ for A. carterae and 1000 cells mL⁻¹ for A. sanguinea. All experiments were conducted in a light room that had a light intensity of 100 µmol cm⁻² s⁻¹. For each experiment, 2 mL of the culture was aliquoted to a clean test tube, and experiments were conducted in triplicate. Treatment groups received cerulenin (Sigma-Aldrich, Saint Louis, MO, USA) at a concentration of 100 µM for A. carterae and 45 µM for A. sanguinea at 3 time points: 0 h, 1 h, and 2 h. Control groups received 11 µL of DMSO at the same 3 time points: 0 hours, 1 hour, and 2 hours. Samples were incubated with cerulenin and DMSO for 5 min prior to acetic acid $[1-^{14}C]$ with a specific activity of 55.2 mCi mmol-1 (Lot# 184901) (Perkin Elmer, Waltham, MA) addition. A total of 10 µCi of 14C acetic acid was added to each sample and was inverted three times until mixed. Initially, T0-hour test tubes were immediately placed in an ice bath to stop the reaction. The T1 h and T2 h test tubes were placed in ice baths after 1 and 2 h incubations were complete, respectively. After the cessation of all the reactions, the test tubes were spun down at $800 \times g$

for 20 min. The supernatant was poured into a clean test tube and stored at 4 $^{\circ}$ C. The pellet was stored at -20 $^{\circ}$ C.

Lipid and Toxin Extraction from Cell Pellets of A. carterae and A. sanguinea Lipid extraction followed the protocol as described by Adolf et al. [2007]. In total. 1 mL of methylene chloride:methanol at a 2:1 ratio was added to the pelleted samples and vortexed for 10 seconds. In total, 1 mL of methylene chloride at a ratio of 1:1 and 1 mL of methylene chloride at a ratio of 1:2 were added, and the samples were vortexed for 10 seconds. Test tubes were placed in a rack until phase separation occurred. Aqueous phases, which contained the toxins, and organic phases, which contained lipids, were separated and placed in clean test tubes for further analysis.

Results and Discussion

In Akashiwo sanginea, two "triple KS" transcripts have been recovered (Contig38980 & Contig65906) with 69% amino acid identity. As shown in **Figure 2 & 3**, we were not able to observe the full predicted size of the Triple KS protein but only something slightly larger than the predicted proof reading AT module. It is unclear whether post translation processing is responsible for this finding or not. Addition of cerulenin resulted in a 50% reduction of ¹⁴C acetate incorporation in total lipids at 2 hours for Akashiwo sanginea (**Figure 4**)

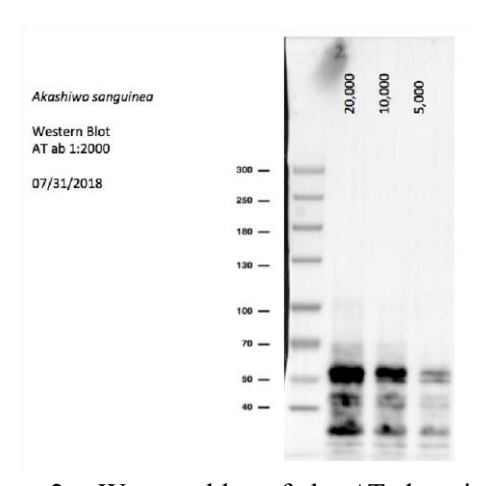


Figure 2. Western blot of the AT domain from whole cell extracts of the multi-modular polyketide synthase (PKS) in *Akashiwo sanginea*. The observed band (55 kD) is larger than the expected AT module (34 kD) but much smaller than the 522 kD full length multi-modular PKS.

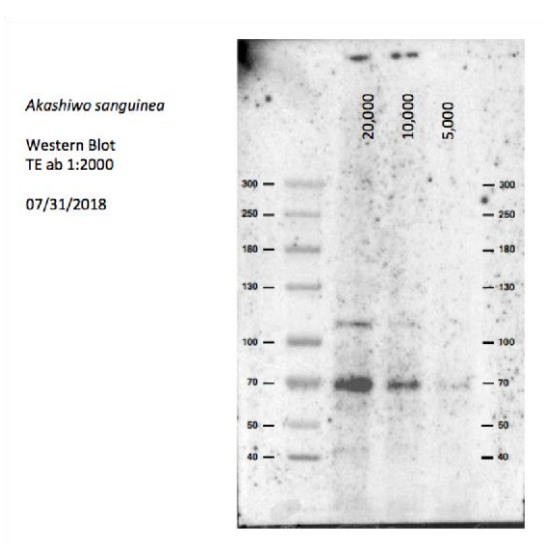
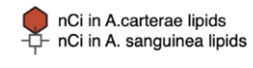


Figure 3. Western blot of the TE domain from whole cell extracts of the multi-modular polyketide synthase (PKS) in *Akashiwo sanginea*. The observed band (110 kD) is smaller than the 522 kD full length multi-modular PKS.



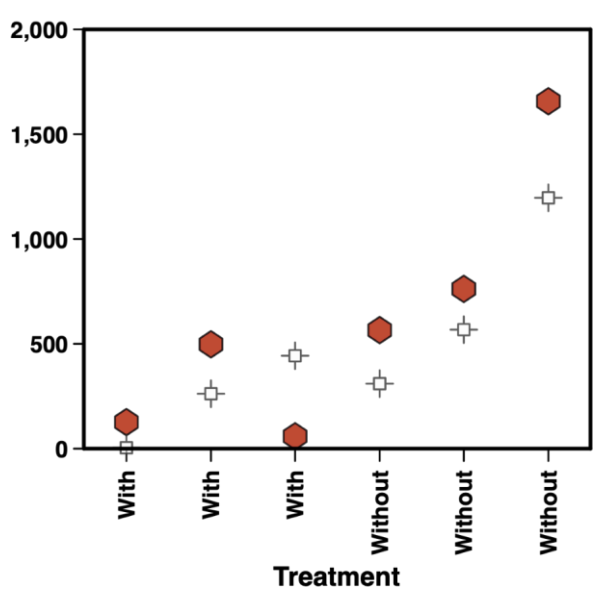


Figure 4. Quantitation of 14C acetate incorporation into lipids over a 2-hour period after cerulenin addition. Error bars (within the symbol widths) show one standard deviation for triplicate samples.

The third module of the multi-domain PKS (**Figure 1**) has the same domain arrangement as a traditional fatty acid synthase (FAS), namely KSDH-ER-KR-TE, with only the AT domain missing in *A. carterae*. However, this arrangement is different from the arrangements observed in marine γ -proteobacteria PUFA synthases that also make some of the same PUFA compounds as dinoflagellates (Yazawa, 1996). This leaves the possibility that dinoflagellates are able to synthesize both of these

products using the same machinery, and AT domains could be acting in trans configuration with the machinery in a noniterative fashion. *Trans-ATs* are able to synthesize diverse bioactive polyketide products and, while still an emerging field, have been studied more thoroughly in bacterial and fungal systems to date. Previous works that have identified trans ATs and multi-modular PKSs in dinoflagellates have hypothesized that multiple **PKSs** work together, and the trans-AT configuration could be a way to increase the diversity in the metabolites being synthesized. Kohli et al. (2017) showed how fatty acid synthase genes in dinoflagellates have been observed to be more conserved, while PKSs tend to be more variable. This fits well with our observation of a cis AT in A. sanguinea, while trans ATs are observed in A. carterae. The AT domain could be mediating product specificity in this scaffold, allowing for the production of both fatty acids and toxins. We envision the "Triple KS" multi-modular polyketide synthase in Akashiwo sanginea exists as a dimer transferring two carbon units across the chains to complete fatty acid synthesis.

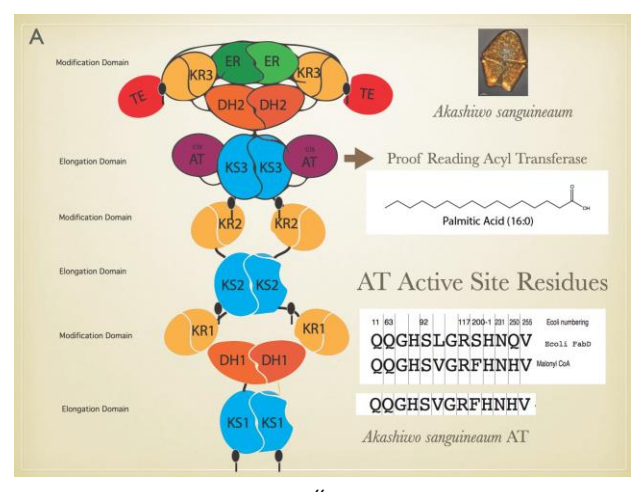


Figure 5. Model of the "Triple KS" protein shown as a multi-modular polyketide synthase (PKS) from *Akashiwo sanginea*. The active site residues in the *cis* AT module are nearly identical with those *E. coli* Fab D and Malonyl CoA.

Acknowledgments: We would like to acknowledge Sabeena Nazar at the BASlab for sequencing support.

Conflicts of Interest: The authors declare no conflict of interest.

References

Bachvaroff, T. R., and Place, A. R. (2008). From stop to start: Tandem gene arrangement,

- copy number and splicing sites in the dinoflagellate Amphidinium carterae. PLos One 3(8):e2929
- Bachvaroff, T. R., Williams, E. P, Jagus, R., and Place, A. R. (2015). A Noncryptic Noncanonical Multi-module PKS/NRPS Found in Dinoflagellates. 16th ICHA Proceedings 101-105, Wellington, New Zealand.
- Haq, S., Oyler, B. I., Williams, E., Khan, M. M. Goodlett, D. R., Bachvarof, T., and Place, A. R. (2023). Investigating A MultiDomain Polyketide Synthase in *Amphidinium carterae*. Mar. Drugs, 21, 425. https://doi.org/10.3390/md21080425 https://www.mdpi.com/journal/marinedrugs.
- Kohli, G.S., Campbell, K., John, U., Smith, K.F., Fraga, S., Rhodes, L.L., Murray, S.A., 2017. Journal of Eukaryotic Microbiology 64, 691–706.
- Mehta, A.P., Li, H., Reed, S.A., Supekova, L., Javahishvili, T., Schultz, P.G., 2016. J. Am. Chem. Soc. 138, 7272–7275.
- Olinski, R., Starczak, M., Gackowski, D., 2016. Mutation Research/Reviews in Mutation Research 767, 59–66.
- Place A.R., Williams, E., Bachvaroff, T.R., Sabatini, R., 2020. Harmful Algae 2018from ecosystems to socio-ecosystems 181–184.
- Rusmintratip, V., Sowers, L.C., 2000. Proceedings of the National Academy of Sciences 97, 14183–14187.
- Simmons, J., Müller, T.A., Hausinger, R.P., 2008. R. Soc. Chem. 0, 5132–5142.
- Yazawa, K. Production of eicosapentaenoic acid from marine bacteria. Lipids 1996, 31 Pt 2, S297–S300. https://doi.org/10.1007/ BF02637095.
- Sun, S., Chen, J., Li, W., Altintas, I., Lin, A., Peltier, S., Stocks, K., Allen, E.E., Ellisman, M., Grethe, J., Wooley, J., 2011. Nucleic Acids Research 39, D546–D551.
- Van Dolah, F.M., Kohli, G.S., Morey, J.S., Murray, S.A., 2017. Journal of Phycology 53, 1325–1339.
- Williams, E., Place, A. R., and Bachvaroff, T. (2020). A Global Approach to Estimating the Abundance and Duplication of Polyketide Synthase Domains in Dinoflagellates. Evolutionary Bioinformatics 17; 1-24.

Translational costs and regulation in *Amphidinium carterae*: Insights from synchronized cultures with a novel quantification method

Miranda Judd^{1*}, Rosemary Jagus¹, Allen R. Place¹

¹Institute of Marine and Environmental Technology, University of Maryland Center for Environmental Science – 701 E. Pratt Street, Baltimore, MD 21202 *corresponding author's email: mjudd@umces.edu

Abstract

In dinoflagellates, translation regulation plays a crucial role in regulating gene expression, where transcript levels remain constant. We hypothesize that dinoflagellate expression is regulated through protein translation, specifically by a diverse pool of eIF4E translation factors. *A. carterae* cultures were synchronized followed by quantification of translation rates and eIF4E translation factor abundance. Puromycin-incorporation (SUnSET method) was used as a measure of translation rates and Western blots were used to quantify translation factor abundance. We found that maximum rates of translation occurred during the light period, peaking just before lights-off, followed by decreasing translation during the dark period. The pattern of abundance for translation factors eIF4E-1a and eIF4E-2a correlated positively with translation rates, whereas abundance of eIF4E-1d did not correlate as well. Here we begin to summarize patterns associated with the cell cycle, diel translation rates, and eIF4E abundances in order to see how these translation factors potentially effect differential expression.

Keywords: dinoflagellate, translation, transcription, regulation

https://doi.org/10.15027/0002041277

Introduction

Dinoflagellates are ubiquitous in marine environments and are known to cause 75% of marine harmful blooms; an issue that is increasing in prevalence with climate change conditions (Gobler, 2020; Griffith and Gobler, 2020; Verma et al., 2019; Wells et al., 2015). Knowledge on dinoflagellate biosynthetic pathways adaptations is stunted by the lack of research into their regulation. Such investigations are hindered by difficult genetic features such as unusually large genomes, permanently condensed liquid crystalline chromosomes, and the presence of multiple copies of tandem repeats throughout the genome (Brayton et al., 2007; Debarry and Kissinger, 2011; Jones et al., 2015; Verma et al., 2019). One of the largest obstacles to studying dinoflagellate genomcis is their apparent lack of transcriptional regulation (Van Dolah et al., 2007; Haq et al., 2017; Jones et al., 2015; Morey et al., 2011; Morse et al., 1989; Roy et al., 2018). Constitutive transcription of the mRNA pool does not allow for significant inferences into differential expression. Because of this, post-transcriptional regulation must be further studied to understand how dinoflagellates regulate and adapt.

Amphidinium carterae is one of the most basal of the photosynthetic dinoflagellates, and it is notably also a toxin-producer among some strains (Hieda et al., 2021; Morales-Amador et al., 2021; Tango et al., 2004). A full transcriptome is also available for this species (*BioProject:* PRJNA257290). This strain can also be grown to high densities with antibiotics, making Amphidinium a good candidate for regulation studies (Liu et al., 2017).

Materials and Method

Cell synchronization

Three 50mL flasks of *Amphidinium carterae* (Herbert 1314) were grown in ESAW artificial marine media at salinity 32 supplemented with f/2 nutrients without silicates at a starting concentration of 10³ cells mL⁻¹. Culture were acclimated for 5 days in 14:10 hour light:dark regime at 100 µmole photons m⁻² sec⁻¹ at 25°C (Berges et al., 2001). They were then kept in the dark for 48 hours to synchronize before being

reintroduced to the previous light phases for sampling over 24 hours (Leighfield and Van Dolah, 2001).

Cell counts and cycling

Cells were counted using a ScepterTM 2.0 Handheld Automated Cell Counter equipped with a 40 µm sensor. To measure DNA content per cell, triplicate aliquots of 1mL of culture were centrifuged at 2000 x g for 10 minutes and the medium was discarded. The cell pellet was resuspended in -20°C methanol and stored at -20°C. Once all samples were collected over the diel cycle, they were centrifuged at 2000 x g for 10 minutes, the methanol was discarded, and the cell pellet was resuspended in 500 μL of PI base intercalating dye solution (10 μg mL⁻¹ propidium iodide in phosphate buffered saline containing 40 units mL⁻¹ RNase and 0.5% Tween 20) (Leighfield and Van Dolah, 2001). The nucleistained sample was then analyzed via flow cytometry with a BD AccuriTM C6 Flow Cytometer.

Translation measurements: SUnSET method Incorporation of puromycin, an aminonucleoside structural analog to tRNA, was used as a proxy measurement for translation rates for one flask culture by a surface sensing of translation (SUnSET) method (Goodman & Hornberger, 2013). Puromycin incorporation into growing peptide chains halts translation, resulting in a released truncated peptide. Abundance of these neosynthesized peptides directly translation rates. At each sampling point, aliquots of the culture were incubated with 1 mM puromycin for exactly 45 min to allow detectable incorporation. Aliquots were then centrifuged at 10,000 x g and stored in SDS-PAGE buffer at -20°C before immunoblot analysis. Detection of incorporated puromycin was measured in triplicate on an immunoblot using a monoclonal mouse antipuromycin antibody (Sigma Aldrich, MO, USA) and a secondary goat anti-mouse HRP monoclonal (Invitrogen, antibody California, Normalization was done with No-StainTM Protein Labeling Reagent (Invitrogen, California, USA) to visualize the total protein in each lane.

Translation factor abundance:

Aliquots of 30 mL cell culture was taken at each sampling point and centrifuged at 2000 x g for 10 min. The medium was discarded, and the cells were resuspended in SDS-PAGE buffer and stored at

-20°C. Abundance of known translation factors from the *A.carterae* eIF4E family were measured via immunoblot using custom monoclonal rabbit anti-eIF4E antibodies (Genscript, New Jersey, U.S.A) as a primary and goat anti-rabbit HRP-conjugated antibodies as a secondary (Invitrogen, California, U.S.A) (Jensen et al., 2021; Jones et al., 2024). Abundances for 3 of the *A.carterae* eIF4E family members were measured as they are the 3 most abundant eIF4Es found in *A.carterae*; in decreasing order of abundance: eIF4E-1a, -1d, and -2a, respectively. Normalization was done using No-Stain™ Protein Labeling Reagent (Invitrogen, California, U.S.A) to visualize the total protein in each lane.

Lastly, potential modification of eIF4E-1a was measured over the diel cycle. eIF4E-1a has a phosphorylation site equivalent to the Ser209 site found in mouse/human eIF4E1A (Jagus et al., 2012; Joshi et al., 1995). Phosphorylation of Ser209 changes eIF4E-mRNA association. Therefore, non-phosphorylated eIF4E-1a in *Amphidinium* may result in greater or differential translation. Double-bands appear when using a specific antibody of eIF4E-1a in immunoblots, which may allude to a modification such as phosphorylation.

Results and Discussion

Cell cycling

The cell density of the *A.carterae* cultures remained relatively constant over the light period. During the dark period, the cultures observed an average population increase of 43%, which remained relatively consistent into the next light period (Fig. 1). This aligned well with the nuclei staining, which showed synchronized cells in G1 at the beginning of the light period (Fig. 2). This was followed by the beginning of DNA synthesis 12 hours into the light period (observed as the beginning of a second larger peak in Fig. 2). Finally, a peak level of DNA per cell was observed during the dark period. DNA content per cell reverted back to its original G1 state by the end of the dark period.

Translation rate

As a proxy for translation rates, we found that most puromycin-incorporation occurred right before the end of the light period (Fig. 3). During the light period, translation rates increased up to at least 2 hours before the end of the light phase. At the end

of the dark period, the amount of puromycin incorporated fell back to minimum levels.

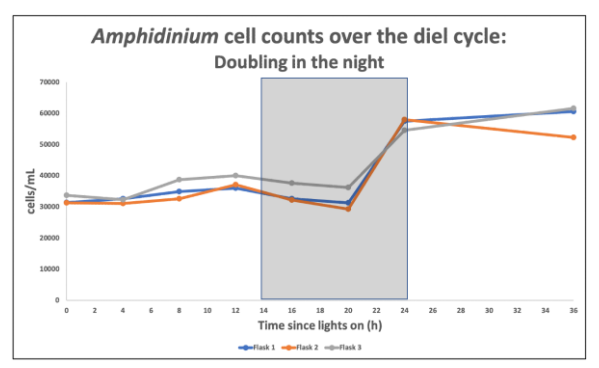


Fig. 1. Cell counts of *A. carterae* cultures over a diel cycle.

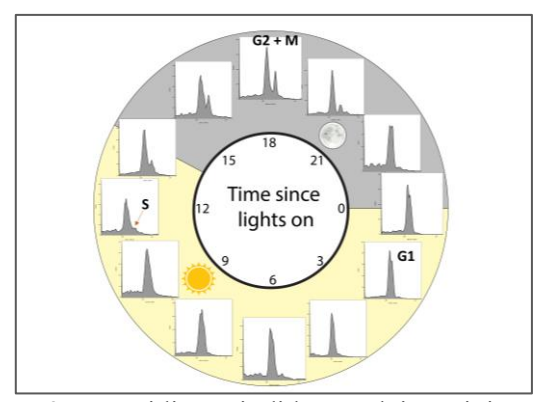


Fig. 2. Propidium iodide nuclei staining of *A.carterae* over the diel cycle. Two peaks represent haploid and diploid cells as they synthesize DNA and eventually replicate. Peak DNA per cell was observed at mid-dark period.

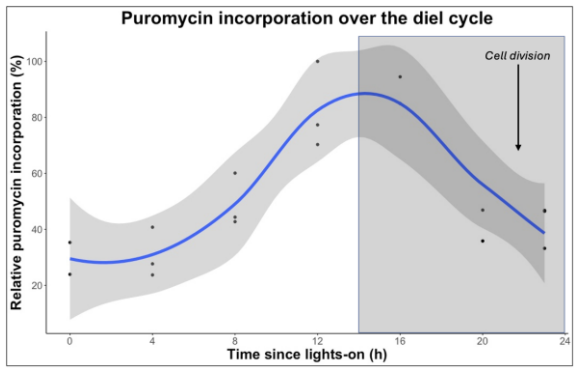


Fig. 3. Relative puromycin incorporation over the diel cycle. Timepoints were normalized by total protein. Puromycin incorporation is presented as a percentage of the maximum observed within the immunoblot lanes, with 100% being the largest amount of incorporated puromycin detected during the light period. Triplicates graphed in R with a local regression trendline.

eIF4E translation factor abundance

Translation factor immunoblots showed that eIF4E-1a abundance increased slightly over the light period, peaking at the end of the light period at least 2 hours before the end of the light phase. The eIF4E-1a abundance then decreased over the dark period to 65% of the max level, followed by a slight uptick before the beginning of the next light phase (Fig. 4). The eIF4E-1d abundance remained relatively consistent over the experiment with a slight peak before the end of the light period, followed by a decrease as during the beginning of the dark period, which then began to increase during the middle of the dark period through to the morning. eIF4E-2a abundance increased over the day, peaking around the end of the light period, and decreasing back to initial levels during the dark period.

The pattern of abundance for translation factors eIF4E-1a and eIF4E-2a correlated with the relatively well with translation rates, whereas abundance of eIF4E-1d did not.

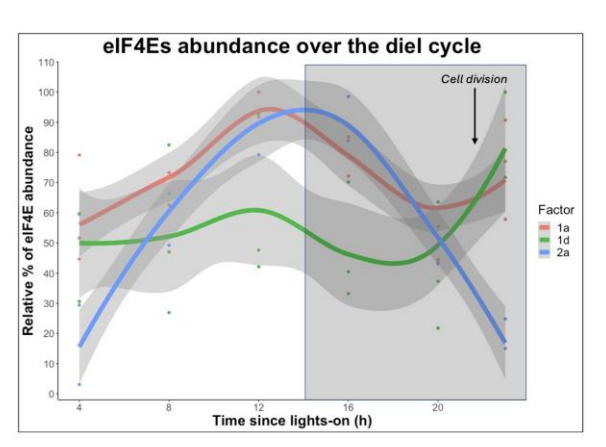


Fig. 4. Relative abundances of translation factor eIF4E family members in *A.carterae* over the diel cycle. Protein abundance is presented as a percentage of the maximum observed within the immunoblot lanes, with 100% being the largest amount of specific factor detected. Triplicates graphed in R with a local regression trendline.

Modified eIF4E-1a

The percent of the potentially modified eIF4E-1a based on observed double-banding was found to increase over the light period and subsequently decrease at dark period (Fig. 5). This pattern appeared to correlate well with translation rates over the light period.

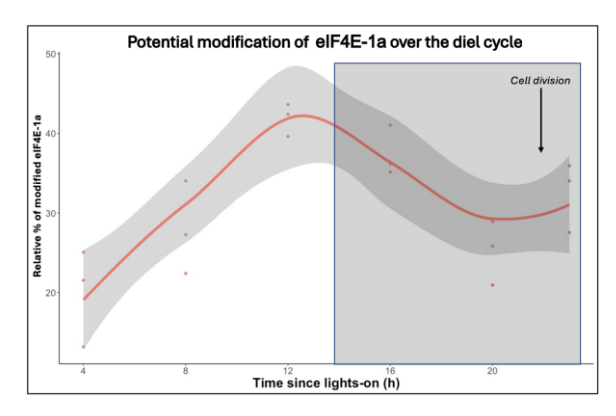


Fig. 5. Percentage of modified eIF4E-1a over the diel cycle as measured by immunoblot abundance. Triplicates graphed in R with a local regression trendline.

The abundance of the eIF4E translation factors found in A. carterae provides a preliminary insight into which factors may play a role in dinoflagellate differential translation. The translation rates appear to increase as the cell populations begin synthesizing DNA and drops off once the cells divide (Fig 1, 2, & 3). Both eIF4E factors 1a and 2a appear to follow a similar trend in abundance as the translation rates throughout the day, showing there may be a correlation to the two processes (Fig 3 & 4). Further work needs to be done to qualify which pathways are regulated by the various eIF4Es, and to understand which exogenous conditions and endogenous factors transcription the diel cycle. Future work will also include determination of modifications of eIF4E-1a such as the phosphorylated states.

Acknowledgements

Attendance to ICHA 2023 was funded by the University of Maryland Center for Environmental Science and NOAA's National Centers for Coastal Ocean Science.

References

Berges, J.A., Franklin, D.J., Harrison, P.J., 2001. J Phycol 37, 1138–1145.

Brayton, K.A., Lau, A.O.T., Herndon, D.R., Hannick, L., Kappmeyer, L.S., Berens, S.J., Bidwell, S.L., Brown, W.C., Crabtree, J., Fadrosh, D., Feldblum, T., Forberger, H.A., Haas, B.J., Howell, J.M., Khouri, H., Koo, H., Mann, D.J., Norimine, J., Paulsen, I.T., Radune, D., Ren, Q., Smith, R.K., Suarez, C.E., White, O., Wortman, J.R., Knowles,

D.P., McElwain, T.F., Nene, V.M., 2007. PLoS Pathog 3, e148.

Debarry, J.D., Kissinger, J.C., 2011. Mol Biol Evol 28, 2855–2871.

Van Dolah, F.M., Lidie, K.B., Morey, J.S., Brunelle, S.A., Ryan, J.C., Monroe, E.A., Haynes, B.L., 2007. J Phycol 43, 741–752.

Gobler, C.J., 2020. Harmful Algae 91, 101731.

Goodman, C.A., Hornberger, T.A., 2013. Exerc Sport Sci Rev 41, 107–115.

Griffith, A.W., Gobler, C.J., 2020. Harmful Algae 91, 101590

Haq, S., Bachvaroff, T.R., Place, A.R., 2017. Mar Drugs 15, 1–10.

Hieda, M., Sorada, A., Kinoshita, M., Matsumori, N., 2021. Biochem Biophys Rep 26, 100941.

Jagus, R., Bachvaroff, T.R., Joshi, B., Place, A.R., 2012. Comp Funct Genomics 2012.

Jensen, K.B., Dredge, B.K., Toubia, J., Jin, X., Iadevaia, V., Goodall, G.J., Proud, C.G., 2021. Nucleic Acids Res 49, e105–e105.

Jones, G.D., Williams, E., Haq, S., Bachvaroff, T.R., M. Basanta, S., Place, A.R., Jagus, R., 2024. Elife.

Jones, G.D., Williams, E.P., Place, A.R., Jagus, R., Bachvaroff, T.R., 2015. BMC Evol Biol 15, 1–12.

Joshi, B., Cai, A.-L., Keiper, B.D., Minich, W.B., Mendez, R., Beach, C.M., Stepinski, J., Stolarski, R., Darzynkiewicz, E., Rhoads, R.E., 1995. Journal of Biological Chemistry 270, 14597– 14603.

Leighfield, T.A., Van Dolah, F.M., 2001. J Exp Mar Biol Ecol 262, 177–197.

Liu, C.L., Place, A.R., Jagus, R., 2017. Mar Drugs 15.
Morales-Amador, A., Molina-Miras, A., López-Rosales,
L., Sánchez-Mirón, A., García-Camacho, F.,
Souto, M.L., Fernández, J.J., 2021. Mar Drugs 19.

Morey, J.S., Monroe, E.A., Kinney, A.L., Beal, M., Johnson, J.G., Hitchcock, G.L., Van Dolah, F.M., 2011. BMC Genomics 12, 346.

Morse, D., Milos, P.M., Roux, E., Hastings, J.W., 1989. Proc Natl Acad Sci U S A 86, 172–176.

Roy, S., Jagus, R., Morse, D., 2018. Microorganisms 6, 1–25.

Tango, P., Butler, W., Wazniak, C., 2004. Maryland's Coastal Bays Ecosystem Health Assessment 2–8.

Verma, A., Barua, A., Ruvindy, R., Savela, H., Ajani, P.A., Murray, S.A., 2019. Microorganisms 7, 1–29

Wells, M.L., Trainer, V.L., Smayda, T.J., Karlson, B.S.O., Trick, C.G., Kudela, R.M., Ishikawa, A., Bernard, S., Wulff, A., Anderson, D.M., Cochlan, W.P., 2015. Harmful Algae 49, 68–93.

Diversity of HABs from the Texas coast (Gulf of Mexico) with a focus on extreme events: a full length 18S rDNA metabarcoding approach

Lisa Campbell^{1*}, Chetan C. Gaonkar¹

¹Department of Oceanography, Texas A&M University, College Station, TX 77843 USA *corresponding author's email: lisacampbell@tamu.edu

Abstract

More than half of the 153 documented toxic harmful algal bloom species (HABs) are found in the Gulf of Mexico and most of these HABs are observed on the Texas coast. Using a metabarcoding approach, samples from the Texas Observatory for Algal Succession Time series (TOAST) were examined for the presence of HABs. Metabarcoding is a rapid and effective means to investigate microplankton community composition and species diversity. In this study we compared HAB diversity estimated from 18S long-read sequences obtained from the minION with diversity estimated from MiSeq short sequences using V4 and V8-V9 markers of 18S rDNA. Seasonal variation in diversity over the four-year period 2019-2022 at TOAST was compared with results from a 1-day cruise along the Texas coast one month after the extreme flooding event following Hurricane Harvey (2017) and a sample collected one month after Hurricane Nicholas (2021). Results show that full-length sequences provide improved discrimination among closely related species and that the diversity of HAB species increases after an extreme event. Given the anticipated increase in the number and intensity of hurricanes with climate change, it is important to determine how this will impact the diversity and potential for blooms of harmful algae in the Gulf of Mexico as well as other parts of the world.

Keywords: amplicon sequence variants (ASVs), community diversity, diatom, dinoflagellate, minION

https://doi.org/10.15027/0002041278

Introduction

Of the 153 documented toxic HAB species, more than half of these (83) are found in the Gulf of Mexico (Anderson et al., 2023). Historically, HAB monitoring has been conducted using light microscopic analysis. Such morphology-based observation and enumeration requires taxonomic expertise and is therefore labor-intensive; cryptic species can confound these analyses as well. To overcome these obstacles, DNA-based molecular approaches, such as metabarcoding, have been employed (e.g., Liu et al., 2020; Huang et al., 2021; Funaki et al., 2022).

Many previous applications of metabarcoding have focused at the level of major domain or phylum level. Here the focus was on species, which is essential for HAB detection and early warning. In using the full-length 18S rDNA gene sequence, which includes all conserved and variable regions, detailed taxonomic identification at the species-level is possible, even among the closely related species. Using this approach we asked: (1) Would full-length 18S rDNA metabarcode sequencing

increase estimates of HAB diversity? (2) Can this approach be used to distinguish species that are indistinguishable with either the V4 or V8-V9 marker? and (3) How does seasonal variation in HAB diversity compare with HAB diversity after an extreme storm event?

Materials and Method

Sample collection

Samples were collected on a cruise from along the coast of Texas during a 24-hr period one month after Hurricane Harvey in 2017 and at the TOAST Surfside Beach site from 2019 -2022 (Fiorendino et al., 2023). All HAB results were binned into monthly totals.

Primers

Primers for the V4 and V8-V9 short reads (Table 1) were used for Illumina MiSeq sequencing. For the full-length 18S rDNA of the microbial community, a primer pair that had been designed and tested for sequencing the complete full-length 18S rDNA gene in a mock community (Gaonkar and Campbell, 2024) were used for the field

samples in this study (Table 1).

Primer	Primer sequence
V4f	CCAGCASCYGCGGTAATTCC
	(Stoeck et al. 2010)
V4r	ACTTTCGTTCTTGAT
	(Bradley et al. 2016)
V8f	ATAACAGGTCTGTGATGCCCT
	(Bradley et al. 2016)
V8/9r	CCTTCYGCAGGTTCACCTAC
	(Amaral-Zettler et al. 2009)
SSUF	AACCTGGTTGATCCTGCCAGT
	(Medlin et al. 1988)
ITS-1dr	CCTTGTTACGACTTCACC
	TTCC (Edgar and Theriot 2004)

Table 1. Primers used for comparison of full-length 18S rDNA sequencing with minION vs. short-reads with MiSeq sequencing.

Sequencing

Full-length 18S rDNA sequencing was performed using the minION Mk-1C (Oxford Nanopore Technologies [ONT]) (Gaonkar and Campbell, 2024). Short reads (V4 and V8-V9) were sequenced using Illumina MiSeq (Gaonkar and Campbell, 2023).

Data analysis

Base calling for minION data was conducted using "guppy" (software provided by ONT) and the results were BLAST'ed against the PR² database v.5.0.0 (Guillou et al., 2013). To confirm the identity of HAB species in the field data, the following criteria were used. Only ASV sequences ≥250 bp and ≥98% similarity to references in PR² were retained.

The Jaccard Index (defined as the number of species common to both samples divided by the total number of species in the 2 samples) was used to assess the significance of the diversity estimates for the 2017 field results after Hurricane Harvey and the 2019 results after Hurricane Nicholas compared to monthly totals at the TOAST Surfside Beach time series station from 2019-2022.

Results and Discussion

Would full-length 18S rDNA metabarcode sequencing increase estimates of HAB diversity? The total number of HAB species identified in this study from the Hurricane Harvey cruise and the

TOAST time series was 44. After Hurricane Harvey, the HAB species diversity observed was higher with the full-length 18S rDNA gene sequencing than with the V4 marker, but the same as V8-V9 (Table 2). Note that both the number of diatoms and dinoflagellates detected is higher with full-length 18S rDNA sequencing than with V4. Of the 34 HAB species identified with either the full-length 18S or the V8-V9 marker, only 26 were identified with both and each identified 8 unique species.

The high number of species observed with the V8-V9 marker is possibly the result of artifacts. Because MiSeq sequencing generates thousands of short-read sequences, some of the resulting ASVs can be artifacts of heterogeneity, PCR amplification, or sequencing error. In addition, since the resolution power of short reads is low, BLAST results for sequences with only a few bp difference, may inflate the actual number of different ASVs by erroneously hitting closely related species, e.g. reference sequences for *Karenia mikimotoi* and *K. selliformis* are identical in V8-V9 region (Gaonkar and Campbell, 2023).

Group	18S	V4	V8-V9
Diatoms	7	5	8
Dinoflagellates	21	17	19
Haptophytes	2	2	3
Raphidophytes	4	4	4
Dictyophytes	0	0	0
Total	34	28	34

Table 2. HAB species diversity compared using different metabarcode sequencing methods.

Can this approach be used to distinguish species that are indistinguishable with either the V4 or V8-V9 marker?

At the genus level, the ASV results from 18S, V4 and V8-V9 sequencing are similar; however, for species level delineation, the full-length 18S rDNA sequence is more informative than the short-read markers. Previously it was noted that within several dinoflagellate genera, e.g., *Alexandrium, Karenia, Prorocentrum,* and *Heterocapsa,* it was not possible to distinguish all species using V4 or V8-V9 markers (Gaonkar and Campbell, 2023). Thus, because no single short marker (V4 or V8-V9) can delineate all species, we proposed instead to use metabarcoding with the full-length 18S rDNA sequence as a marker.

We observed that the full-length 18S marker does provide better resolution compared to the shorter markers for a number of HAB species. For example, the improved discrimination among closely related species is seen for the genus *Alexandrium* (Fig. 1) and *Chaetoceros* (Gaonkar et al., 2018). Using a full-length 18S rDNA phylogenetic approach,

HAB species can be differentiated within the genera *Karenia, Prorocentrum,* and *Heterocapsa* (Fig. 2). Recommendations for future HAB studies include using full-length 18S rDNA sequences with super high accuracy basecalling tools (Dorado, ONT, UK). Additionally, a more complete curated database for gene markers will improve HAB identification for better monitoring practices.

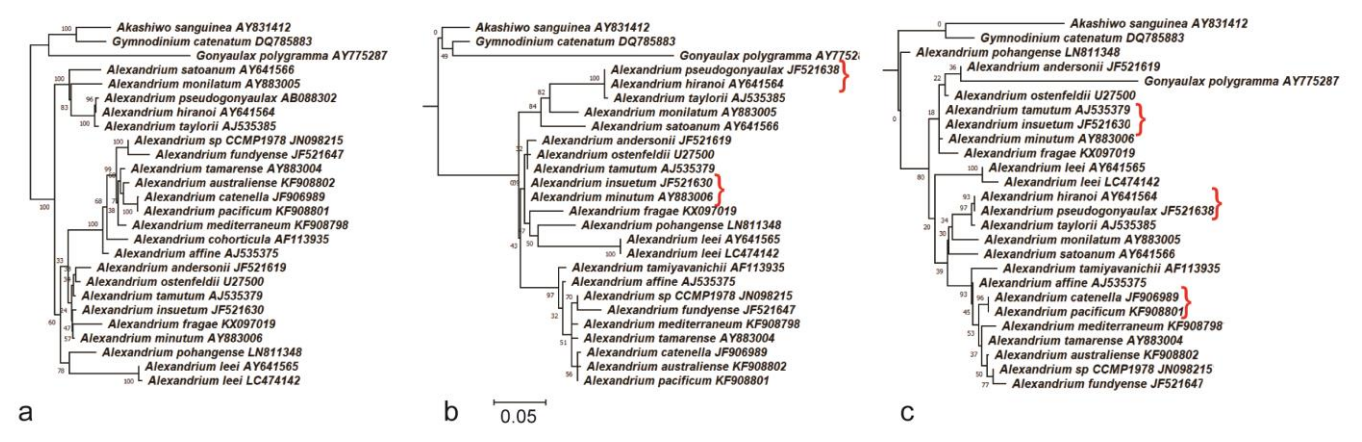


Fig. 1. Maximum likelihood phylogeny of *Alexandrium* using (a) 18S; (b) V4 rDNA gene region; (c) V8-V9 rDNA gene region markers constructed with raxmlGUI (1000 iterations) (see Gaonkar et al., 2018).

How does the seasonal variation in HAB diversity compare with HAB diversity after an extreme storm event?

Based on full-length 18S results, the HAB diversity was much higher in the month post-Hurricane Harvey, with 34 HAB species identified; 13 of these were not found at any other time point at TOAST. Not only was the number of HABs detected exceptionally large, from the Jaccard results, the diversity of the HAB community in 2017 post-Hurricane Harvey was unlike the typical composition of the August-September period observed at the TOAST site (Fig. 3). Note that the months of January-March, when Dinophysis blooms occur in Texas, were more similar (Campbell et al., 2010). Similarly, post-Nicholas, the diversity was unlike the August-September period (Fig. 3). In contrast to 2017, the number of HABs detected was much fewer post-Nicholas. The difference in these observations can be explained by the difference in severity of the events. Hurricane Harvey was a category 4 cyclone that stalled over the TX coast and delivered more than 1500 mm of rain that had lasting impacts on the coastal environment. Nicholas was a category 1 cyclone, with only 200-

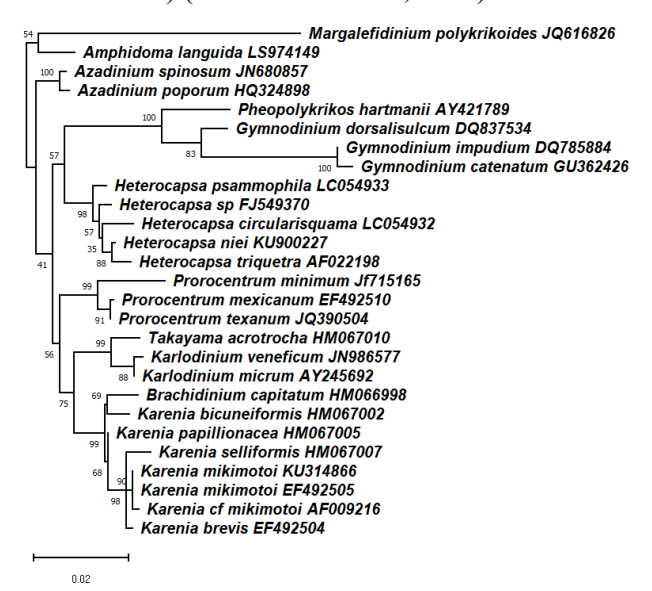


Fig. 2. Phylogeny based on full-length 18S rDNA shows that HAB species in the genera *Karenia*, *Prorocentrum*, and *Heterocapsa* can be distinguished. Phylogeny generated similarly to Fig. 1 (Gaonkar et al., 2018).

300 mm of rain and it made landfall farther east, in Louisiana, so potentially had less impact on the TOAST site in TX. Unfortunately, few samples were collected during the month of October over the time series, so reliable estimates of diversity for

that time period coinciding with the month post-Nicholas in 2021 are lacking.

In summary, full-length 18S rDNA sequencing provides improved resolution among closely related species within many HAB genera and has

provided increased HAB species diversity estimates. The diversity of HAB species increased dramatically after Hurricane Harvey, which has also demonstrated the importance of time series for assessing impacts of climate change on coastal ecosystems.

_	Jan	Feb	Mar	Apr	May	June	July	Aug	Sept	Oct	Nov	Dec	Harvey	Nicholas
	(16)	(17)	(18)	(13)	(10)	(11)	(8)	(2)	(5)	(7)	(12)	(7)	(34)	(7)
Jan	*	0.57	0.48	0.38	0.24	0.42	0.26	0.06	0.17	0.28	0.33	0.35	0.25	0.28
Feb		*	0.52	0.43	0.35	0.47	0.39	0.06	0.22	0.26	0.38	0.33	0.38	0.26
Mar			*	0.48	0.27	0.38	0.30	0.05	0.21	0.19	0.30	0.32	0.27	0.19
Apr				*	0.35	0.50	0.24	0.00	0.29	0.33	0.32	0.43	0.24	0.33
May					*	0.31	0.38	0.00	0.07	0.31	0.22	0.21	0.26	0.31
June						*	0.36	0.08	0.23	0.38	0.64	0.38	0.29	0.38
July							*	0.25	0.08	0.25	0.33	0.25	0.24	0.25
Aug								*	0.00	0.00	0.17	0.00	0.06	0.00
Sept									*	0.20	0.31	0.33	0.08	0.20
Oct										*	0.36	0.40	0.17	*
Nov											*	0.36	0.28	0.36
Dec												*	0.17	0.40
Harvey													*	0.17
licholas														*

Fig. 3 HAB diversity for samples collected over a four-year period (2019-2022) at TOAST binned monthly (total number of HAB species is indicated for each month) compared with results from a 1-day cruise along the Texas coast the month after the extreme flooding event post-Hurricane Harvey (8/2017) and a sample from the month post-Hurricane Nicholas (9/2021). Red indicates samples are more similar; Blue indicates samples are less similar.

Acknowledgements

This project was supported by funds from the National Science Foundation (OCE-1760620) and NOAA Ocean Service NCCOS Competitive Research Program (NA17NOS4780168). Any opinions, findings and conclusions or recommendations expressed in this material are those of the authors and do not necessarily reflect the views of the NSF or NOAA. This is ECOHAB Publication number 1092.

References

Amaral-Zettler, L. A., McCliment, E. A., Ducklow, H. W., and Huse, S. M., (2009) PLoS One 4, e6372

Anderson, D. M., Fensin, E., Gobler, C. J., Hoeglund, A. E., *et al.*, (2021). Harmful Algae 102, 101975.

Bradley, I. M., Pinto, A. J., and Guest, J. S. (2016) Appl. Environ. Microbiol. 82, 5878-5891.

Campbell, L., Olson, R. J., Sosik, H. M., Abraham, A., *et al.*, (2010). J. Phycol. 46, 66-75.

Edgar, S. M., and Theriot, E. C. (2004). J. Phycol. 40, 772-788.

Fiorendino, J. M., Gaonakar, C. C., Henrichs, D. W., Campbell, L. (2023). J. Plankton Res. 45, 205-220.

Funaki, H., Gaonkar, C. C., Kataoka, T., Nishimura, T., *et al.*, (2022). Harmful Algae 111, 102163.

Gaonkar, C. C., Piredda, R., Minucci, C., Mann, D. G., et al., (2018). PLoS One 13, e0208929

Gaonkar, C. C., and Campbell, L. (2023). Harmful Algae 121, 102368.

Gaonkar, C. C., and Campbell, L. (2024). Ecol. Evol. 14, e11232.

Huang, H., Xu, Q., Gibson, K., Chen, Y., and Chen, N. (2021). Harmful Algae 106, 102066.

Liu, S., Gibson, K., Cui, Z., Chen, Y. *et al.*, (2020). Harmful Algae 92, 101772.

Medlin, L., Elwood, H. J., Stickel, S., and Sogin, M. L. (1988). Gene 71, 491-499.

Stoeck, T., Bass, D., Nebel, M., Christen, R. *et al.*, (2010). Mol. Ecol. 19, 21-31.

Microbiomes of *Gambierdiscus lewisii* from the Great Barrier Reef, Queensland, Australia

Shikder Saiful Islam^{1,2}*, Andrew Bridle¹, Shauna Murray³, Christopher Bolch¹

¹Institute for Marine and Antarctic Studies, University of Tasmania, Hobart, Tasmania, Australia ²Fisheries and Marine Resource Technology Discipline, Khulna University, Khulna, Bangladesh ³University of Technology Sydney, School of Life Sciences, Sydney, NSW, Australia. *Corresponding author's email: shikdersaiful.islam@utas.edu.au

Abstract

The microbiomes associated with algae can have a substantial influence on host algal cell physiology and health. We examined the relative abundance and core microbiomes of the toxic dinoflagellate *Gambierdiscus lewisii* cultured from inner (Palm Islands) and outer (Bramble Reef) reef locations on the Great Barrier Reef (Queensland, Australia). Cell-associated (attached) and culture medium-associated microbiomes (unattached) were compared. Both attached and unattached microbiomes of inner reef cultures were dominated by Proteobacteria (Gammaproteobacteria and Alphaproteobacteria) whereas outer reef culture microbiomes were dominated by Gammaproteobacteria and Flavobacteriia. Core attached microbiomes of outer reef cultures were more diverse, including *Varunaivibrio sulfuroxidans*, *Thalassospira povalilytica*, *Marinobacter salarius* and *Labrenzia aggregata* as additional taxa. In conclusion, this study indicated that microbial community within species may differ due to variations in geographical distribution or ecosystem structure.

Keywords: microbiomes, Gambierdiscus lewisii, microalgae

Introduction

Microbiomes are microorganisms that share the space and products of host environment (Ho & Bunyavanich, 2018). In the ocean, organic host substrates, physical contact of algae, and their close association often create an opportunity for ecological and chemical interactions (Tarazona-Janampa et al., 2020). The diversity and structure of microbiomes are shown to affect the physiology and health of the host by providing, competing for, or exchanging micronutrients, vitamins, and minerals (Amin et al., 2012; Croft et al., 2005). Microbiomes also change in response to changes in nutrients and organic matter exuded by different species (Park et al., 2017).

A wide range of studies also indicate that microbiomes exhibit species-specificity (Jackrel et al., 2021; Martin et al., 2021), and those biological interactions are a stronger determinant of aquatic microbial community environmental structure than factors (Pushpakumara et al., 2023). These hostmicrobiome interactions are often obligatory for the host alga and may contribute to bloom formation (Bolch et al., 2011; Bolch et al., 2017; Grossart et al., 2005).

Microbiomes of many planktonic harmful algal bloom (HAB) causing dinoflagellates are relatively well characterised, however those of epiphytic dinoflagellates remain documented. In this study, we use Oxford Nanopore amplicon sequencing of near fulllength 16S rRNA genes to compare microbiome diversity among cultures of four cultures of the toxic dinoflagellate Gambierdiscus lewisii from tropical waters of the Great Barrier Reef (GBR), Australia.

Materials and methods

Gambierdiscus isolates culture, sample collection and processing

Clonal cultures of *G. lewisii* were isolated in Sept. 2019 from mixed macroalgal substrates collected at two reef locations on the mid-GBR region. Cultures OIRS33 and OIRS57 from Little Pioneer Bay, Orpheus Island (75 km north-northwest of Townsville, Queensland), and OIRS413 and OIRS438 from the outer reef atoll Bramble Reef (30km north-west of Orpheus Island. All strains were cultured in 75 ml cell culture flasks with 40 ml of 35 ppt f/10 medium (+L1 trace metals) at 25°C and 70 µmol photons m⁻² s⁻¹ (14h:10h L:D), and microbiome DNA extracted from mid-log phase samples (day 12-15). The phycosphere of

algal cells has no distinct boundary but cellassociated bacteria can be defined as those in the diffusive boundary layer (DBL), a zone resistant to turbulent mixing but which can be distorted by cell motion (Seymour et al., 2017). Any separation method will distort/disturb the DBL and potentially dislodge cells from the phycopshere. To minimize dislodgement, we used low-speed centrifugation (400 g, 5 mins) to gently remove "unattached" bacteria with the culture medium (CM), leaving firmly attached DBL-associated bacteria Gambierdiscus cell pellet. Culture medium (CM) microbiomes in the supernatant were transferred to separate clean tubes. The CM samples were centrifuged at high-speed (12,000g, 15 min.) to pellet bacteria, the supernatant carefully removed, and pellets retained for DNA extraction. Gambierdiscus cell pellets with attached microbiomes were washed with an equal volume of sterile seawater, centrifuged at 400g for 5 min., supernatants removed, centrifuged at 1,000 g for 5 min, medium removed, and cell pellets extracted as below.

DNA extraction, PCR, library preparation and sequencing

Total nucleic acid was extracted by an ammonium acetate-based protocol modified from Ooi et al. (2020). Briefly, 400 µl of lysis buffer (4 M urea, 0.5% SDS, 10% glycerol, and 0.2 M NaCl) and 5.0 µl of proteinase K were added, the sample heated at 55°C for 30 min and vortexed for 5 sec. Tubes were incubated on ice for 5 mins, 210 µl 7.5M ammonium acetate added, tubes vortexed for 20 sec and centrifuged at 14,000 g for 5 mins at 18°C. Supernatants were transferred to a new 1.5 ml microtube, an equal volume of isopropanol added, mixed by inversion (40×) and centrifuged at 14,000 g for 10 min. Supernatants were decanted, the pellet washed twice with 500 µl of 70% molecular grade ethanol, and resuspended in 50 µl of molecular grade water.

An initial PCR was carried out using primers 27F-1492R in 20 μ l reaction volumes, using MyTaq HS mix (Bioline, Australia), and primers at 0.5 μ M. PCR cycling comprised: denaturation at 95°C for 3 mins, then 25 cycles of denaturation at 95°C for 15 sec, annealing at 50°C for 30 sec, and extension at 72°C for 45 sec, followed by extension at 72°C for 3 mins.

A second PCR was performed in 50 µl volumes, consisting of 25 µl LongAmp Hot Start Taq 2X Master Mix, 10 µl of each 16S barcode-tailed primers, 14 µl molecular grade water, and 1 µl first-round PCR product. Thermal cycling comprised denaturation at 95°C for 1 min, then 15 cycles of: denaturation at 95°C for 15 sec, annealing at 55°C for 30 sec and extension at 72°C for 60 sec, and a final extension at 72°C for 3 mins. PCR products were purified using an AMPure XP kit (Beckman-Coulter, Aust.), quantified using a Qubit4 Fluorometer, and used for Oxford Nanopore library preparation Oxford (SQK-16S024, Nanopore Technologies, UK). Sequencing was performed on the MinION R9.4.1 flow cell (Oxford Nanopore, UK) according to the manufacturer's protocols.

Bioinformatics

Sequencing data acquisition used MinKNOW core software (v. 4.0.5) and Guppy (v. 4.4.2) for base-calling, demultiplexing and removal of adapter sequences (Wick et al., 2019). Microbiome composition was determined using Emu (ver. 3.4.5; Curry et al., 2022) with a species detection threshold of 0.01%. Microbiome taxon relative abundance analyses were computed using marker data profiling module of MicrobiomeAnalyst (Chong et al., 2020). Data were normalized using total sum scaling to address the variability in sampling depth. Core microbiomes of the attached and unattached microbiomes were determined using 75% prevalence and 0.01% detection thresholds for bacterial taxa.

Results and Discussion

Proteobacteria dominated microbiomes, (attached, 78%-87%; unattached, 66%-82%) of all *G. lewisii* strains except the unattached microbiome of OIRS413 (Bacteroidetes 53%, Proteobacteria 44%; Fig. 1).

At class level, γ - and α -proteobacteria (mean value; 60% and 25%) dominated the attached microbiome of inner reef and outer reef (47% and 33%) *G. lewisii* cultures (Fig. 2). Unattached microbiomes of inner reef cultures comprised 58% γ -proteobacteria and 6% Flavobacteriia, compared to 36% and 30% in outer reef *G. lewisii* microbiomes (Fig. 2).

Both the attached and unattached core microbiomes of *G. lewisii* shared 7 and 9 taxa,

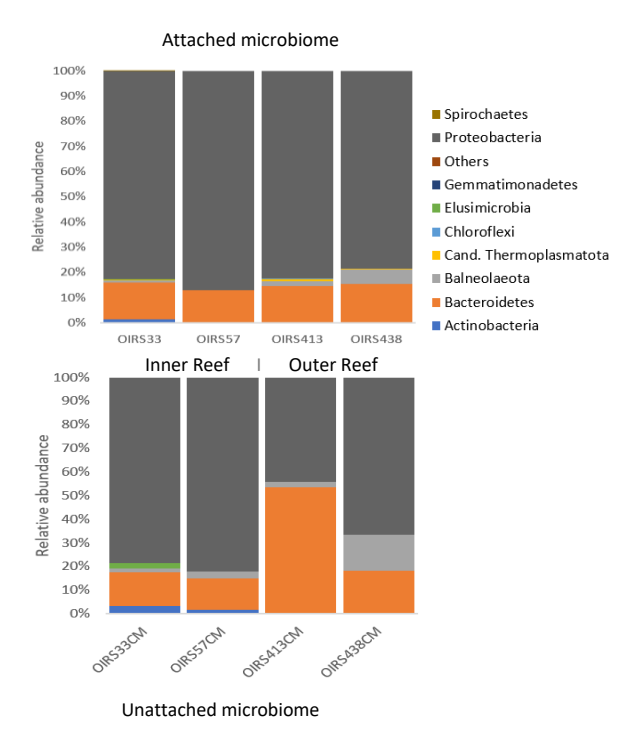


Fig. 1. Phylum relative abundance of attached and unattached microbiomes associated with *G. lewisii* strains.

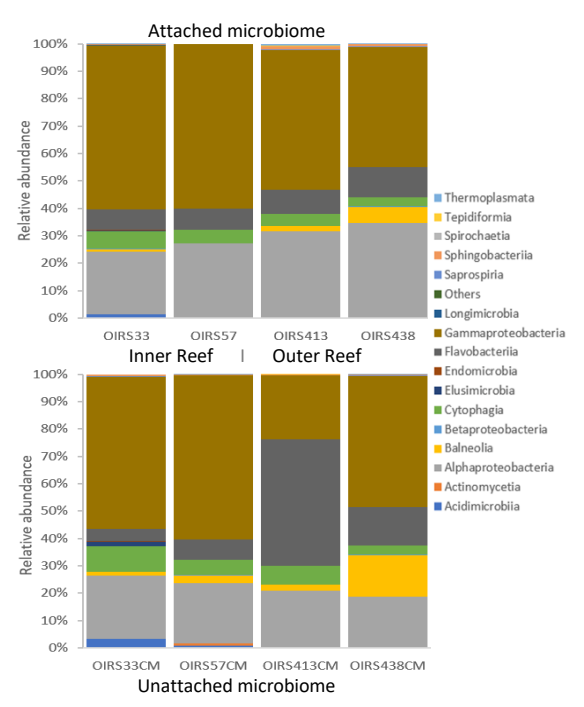


Fig. 2. Class relative abundance of attached and unattached microbiomes of cultured *G. lewisii* strains.

respectively (Figs. 3 and 4), indicating that the majority of more abundant bacteria were associated both with *G. lewisii* cell surfaces and

the surrounding medium. However, *Gambierdiscus* cultures exude considerable amounts of extracellular polysaccharides (EPS) that likely contributed to inefficient partitioning of the unattached versus attached components of the microbiome during our extraction process.

Despite the similarities, there were clear differences in composition and rank order of prevalence of core microbiome taxa. Attached microbiomes of inner reef cultures were predominantly a subset of the unattached core microbiome of inner reef samples except for Pontibacterium granulatum, Labrenzia aggregata and Magnetospira thiophila, and thus appear to be primarily cell or EPSassociated using our conservative prevalence (75%)/abundance thresholds (0.01) for core taxa. In contrast, outer reef cultures retained a much higher attached core microbiome diversity (18 taxa) compared to core unattached (11 taxa); all but three (Thalassopsira australica, Methylobacter marinus, Spongibacter marinus) were also part of the core offshore unattached microbiome (compare Figs. 3 & 4).

Of particular note is the presence of *Marinobacter* and *Labrenzia* as part of the core attached microbiome of *G. lewisii*. Both bacteria are known to be growth-supporting associates of dinoflagellates (Bolch et al., 2017) and other phytoplankton (Green et al., 2015).

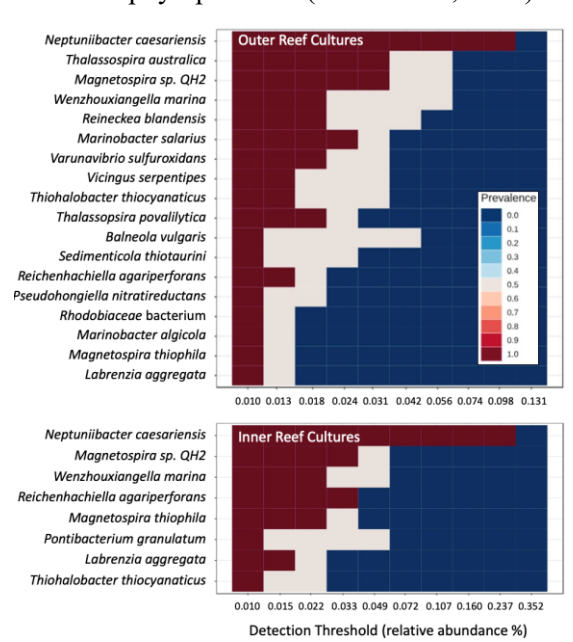


Fig. 3. Core attached microbiomes (\geq 75% sample prevalence; \geq 0.01% rel. abund.) of cultured *G. lewisii* strains.

Bacterial species

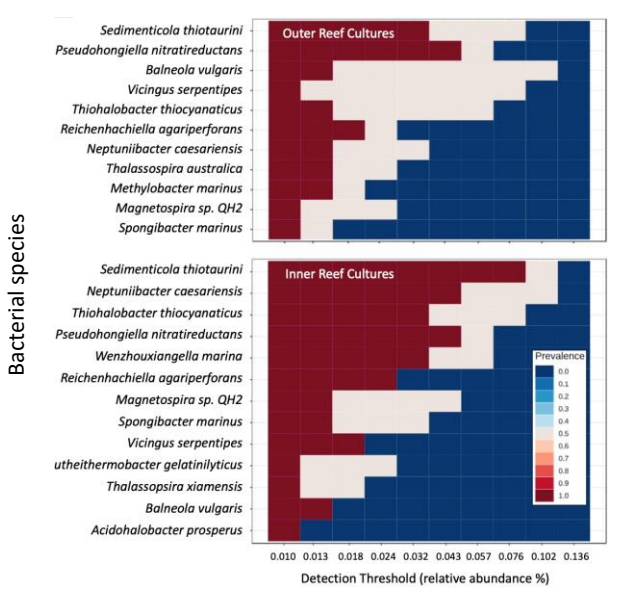


Fig. 4. Core unattached microbiomes (\geq 75% sample prevalence; \geq 0.01% rel. abund.) of cultured *G. lewisii* strains.

Labrenzia aggregata has also been shown to increase bleaching resilience of corals (Doering et al., 2023), and may perform a similar oxidative stress management function for *G. lewisii*.

The overall similarity of the community structure of the four G. lewisii microbiomes from the inner and other fringing reefs, is indicative of a certain level of speciesspecificity. However, changes in dominance, the higher diversity of core microbiomes at Bramble Reef indicate that the environment also partly shapes the microbiome (Pushpakumara et al., 2023). The observed differences in microbiomes between inner and outer reef locations may arise from different physiochemical conditions at inner and outer reef sites. For example, inner mid-GBR reef waters have higher dissolved nitrate, ammonium and phosphorous, and are subject to larger seasonal changes in salinity and turbidity than atolls on the outer reef (Uthicke et al., 2014). Alternatively, the physiological influence of these differences on G. lewisii, and/or the macrophyte host substrate may, inturn, modify selection and recruitment to the G. lewisii microbiome.

Acknowledgements

This study was funded through the Australian Research Council (ARC) Linkage Project,

DP1800001 to SM & CB, and Discovery Project DP210102493 to CB. We thank Sam Murray of the Cawthron Institute (Nelson, New Zealand) for assistance with epiphyte and coral sample collection.

References

- Amin, S.A., Parker, M.S., Armbrust, E.V. (2012). Microbiol. Mol. Biol. Rev., 76(3), 667-684.
- Bolch, C.J., Subramanian, T.A., Green, D.H. (2011). J. Phycol, 47(5), 1009-1022.
- Bolch, C.J.S., Bejoy, T.A., Green, D.H. (2017). Front. Microbiol., 8, 670.
- Chong, J., Liu, P., Zhou, G., Xia, J. (2020). Nat. Protoc., 15(3), 799-821.
- Croft, M.T., Lawrence, A.D., Raux-Deery, E., Warren, M. J., *et al.*, (2005). Nature, 438(7064), 90-93.
- Curry, K.D., Wang, Q., Nute, M.G., Tyshaieva, A., *et al.*, (2022). Nat. Methods, 19(7), 845-853
- Doering, T., Maire, J., van Oppen, M. J., Blackall, L. L. (2023). Microbiol. Aust., 44(1), 36-40.
- Green, D.H., Echavarri-Bravo, V., Brennan, D., Hart, M.C. (2015). Biomed Res. Int., 2015, 194540.
- Grossart, H.P., Levold, F., Allgaier, M., Simon, M., *et al.*, (2005). Environ. Microbiol., 7(6), 860-873.
- Ho, H.E. and Bunyavanich, S. (2018). Curr. Allergy Asthma Rep., 18(4), 1-11.
- Jackrel, S.L., Yang, J.W., Schmidt, K.C., Denef, V.J. (2021). ISME J., 15(3), 774-788.
- Martin, K., Schmidt, K., Toseland, A., Boulton, C.A., *et al.*, (2021). Nat. Commun., 12(1), 5483.
- Ooi, M.C., Goulden, E.F., Trotter, A.J., Smith, G.G., *et al.*, (2020). Front. Microbiol., 11, 573588.
- Park, B.S., Guo, R., Lim, W.A., Ki, J.S. (2017). Mar. Ecol., 38(6), e12474.
- Pushpakumara, B.L.D.U., Tandon, K., Willis, A., Verbruggen, H. (2023). Sci. Rep., 13(1), 2743.
- Seymour, J.R., Amin, S.A., Raina, J.B., Stocker, R. (2017). Nat. Microbiol., 2(7), 17065.
- Tarazona-Janampa, U.I., Cembella, A.D., Pelayo-Zárate, M. C., Pajares, S., *et al.*, (2020). Front. Mar. Sci., 7, 569.
- Uthicke, S., Furnas, M., Lønborg, C. (2014). PLoS ONE, 9, e109092.
- Wick, R.R., Judd, L.M., Holt, K.E. (2019). Genome Biol., 20(1), 129.

Genomics and eco-active organic matter in the oceans: the roles of harmful and other algae, with emphasis on physical effects

Ian R. Jenkinson^{1*}, N.M.Aiswararya², Elisa Berdalet³, Wei-Chun Chin⁴, Igor Emri^{5,6}, Oscar Guadayol⁷, Rodrigo Gonçalves^{8,9}, Santosh Karn^{10,11}, Xavier Mari¹², Magdalena Mrokowska¹³, Janina Rahlff^{14,15}, Pablo Sánchez-Puga¹⁶, Jun Sun¹⁷, Oliver Wurl¹⁸, Tim Wyatt¹⁹

¹Agency for Consultation and Research in Oceanography, Lavergne, La Roche Canillac 19320, France; ²Birla Institute of Science and Technology, Pilani, Hyderabad Campus, Telangana, India; ³Institute of Marine Sciences (ICM-CSIC), Barcelona, Catalonia, Spain; ⁴Department of Bioengineering, University of California, Merced, CA USA; ⁵Department of Mechanics, Polymers and Composites, Ccentre for Experimental Mechanics, University of Ljubljana, Kongresni trg 12, Ljubljana, Slovenia; ⁶Zhejjang Tiantai Industry Co., Ltd., 92B, Renmin East Road, Tiantai, China; ⁷School of Life Sciences, Joseph Banks Laboratories, Univ. Lincoln, Lincoln LN6 7DL,UK; 8Departamento de Ecologia, Universidad de Granada, Granada, Spain; ⁹CONICET at CESUMAR, Puerto Madryn, Argentina; ¹⁰Department of Biochemistry and Biotechnology, Sardar Bhagwan Singh University, Balawala, Dehradun, Uttarakhand 248161, India; 11Key Laboratory of Environmental Corrosion and Biofouling, Institute of Oceanology, Chinese Academy of Sciences, 7 Nanhai Road, Oingdao, China; ¹²Aix-Marseille Université, CNRS/INSU, Université de Toulon, IRD, Mediterranean Institute of Oceanography, UM 110, Marseille, France; ¹³Institute of Geophysics, Polish Acad. Sciences, Ks. Janusza 64, Warsaw, Poland; ¹⁴Aero-Aquatic Virus Research Group, Faculty of Mathematics and Computer Science, Friedrich Schiller University Jena, Jena, Germany; ¹⁵Centre for Ecology and Evolution in Microbial Model Systems (EEMiS), Department of Biology and Environmental Science, Linnaeus University, Kalmar, Sweden; ¹⁶Departamento de Fisica Fundamental, Universidad Nacional de Education a Distancia (UNED), Las Rozas, Spain: ¹⁷College of Mar. Sci. Technol., China Univ. Geosciences (Wuhan), Wuhan, China: ¹⁸Institute for Marine Chemistry and Biology, Carl von Ossietzky University Oldenburg, Wilhelmshaven, Germany; ¹⁹Borreiros, Gondomar, Pontevedra, Galicia, Spain. *Corresponding author's email: ian.jenkinson@ocean-expert.org

Abstract

Dissolved organic matter (DOM) in the ocean represents approximately 662 billion tons of carbon, about 200 times more than the living biomass. It is produced mainly by microbial primary production. The largest fraction of this DOM is old (>weeks to months) and both chemically and biologically recalcitrant. The remaining fraction is young (seconds to weeks), more labile, surface-active, and powerfully changes the rheological properties in the bulk water and bordering interfaces, including the sea surface microlayer. Correlations have been observed between in situ phytoplankton concentrations and rheological thickening, with the greatest viscosity increases measured in blooms of harmful algae such as *Phaeocystis* spp., Karenia mikimotoi, K. selliformis, and Margalefidinium polykrikoides. Surface foams and increased viscosity and elasticity also occur in blooms of other microalgae and cyanobacteria. Living microplankton genomes (PGs) control the production and release of the main DOM molecules, largely polymeric complexes. The properties of ocean water and its interfaces and its biogeochemical fluxes may thus be engineered by PGs. These fluxes influence ocean and atmospheric climate. Viral infection may modify prokaryotic and eukaryotic genes and their expression. Therefore, these ocean PGs and the fluxes and microclimates they influence may be subject to Darwinian-type selection. Research programs need to integrate ocean ecology, rheology, biogeochemistry and genomics, to find the associations among them. High-biomass harmful algal blooms may be notable ecoengineers, where the effects of eco-engineering, exopolymers and causative DNA are likely to be spatially associated and thus easy to study.

Keywords: ocean; phytoplankton; bacteria; viruses; biogeochemistry; rheology; genomics

https://doi.org/10.15027/0002041280

Introduction

Dissolved organic matter (DOM) in the ocean repre-

sents about 662 billion tons of carbon (Hansell et al. 2009), approximately 200 times more than the living

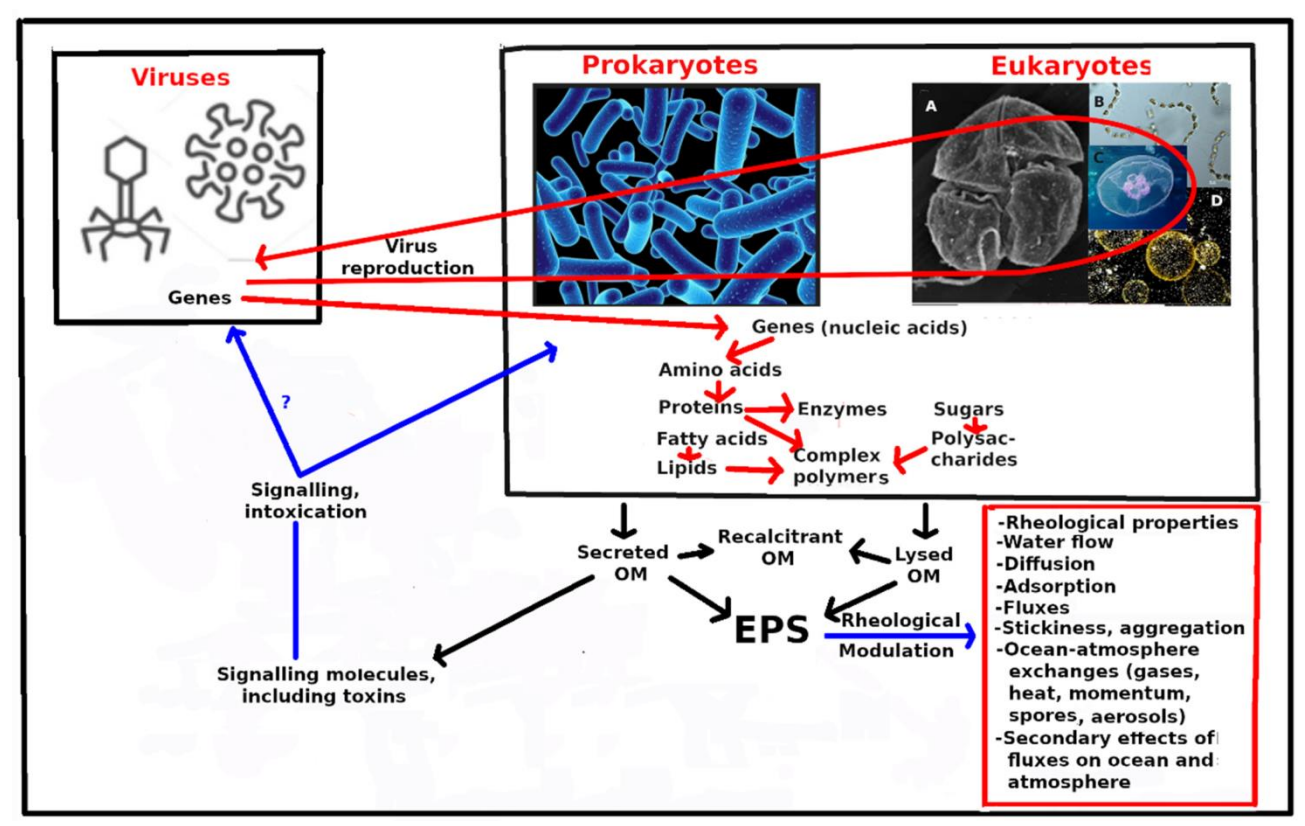


Figure 1. Hypothetical sketch of the eco-activity of extracellular biomolecules. From Jenkinson (2023).

biomass. It is primarily produced by the primary production (PP) of the microbial prokaryotes and eukaryotes. The most labile fraction of this DOM is young (seconds to weeks) and it is the most rheologically and surface-active.

The plankton genomes (PGs) in these microbes affect the quality and quantity High algal biomass, traditionally referred to as "red tides") thus tends to be associated with high production and local abundance of rheologically active OM, often manifesting as slimy water and foam.

When abundant, this OM significantly alters the rheological properties (viscosity, elasticity, plasticity) of bulk-phase water (Jenkinson et al. 2010), biofilms at interfaces (Ardekani 2022; Fang et al. 2012; Karn et al. 2020), marine organic aggregates (Guadayol et al. 2020 and the sea surface microlayer (SML) (Jenkinson et al. 2018).

Eco-active plankton genomes (PGs) and extracellular molecules

Figure 1 illustrates a hypothesis of signaling by extracellular molecules in natural waters. Prokaryotes and eukaryotes both have their own machinery to form amino acids and proteins (including

enzymes) from genetic instructions. Viruses, however, insert their genes into prokaryotes or eukaryotes, commandeering these cells to reproduce viral genes and outer casings. Some rheologically active exopolymeric substances (EPS) modulate physical and physicochemical processes in the ocean and at the ocean—atmosphere interface (inside red box). The blue arrows in the figure show potential signaling and intoxication pathways induced by signaling molecules, some of which are toxins.

Eco-activity of PGs

1. PGs modulate on how Physics controls Biology in the ocean.

Physical constraints like light, turbulence, and physical contact control all organisms. These constraints affect inert particles and organisms similarly. However, organisms' responses to these constraints are modulated by reception organelles, membranes, armor, and motility, all governed by PGs, which build and activate these structures and functions.

2. PGs are the architects of cell structure and function in the plankton.

Inside microbial cells, their genomes interact with viral genomes to produce and control microorganisms' enzymes, internal structures, and metabolic and mechanical functions (Banas et al. 2023; Biddanda et al. 2021). PGs also control immunological and sensory organelles, including uptake and secretory channels, thereby influencing cellular perception and response to the environment. They govern the production and secretion of signaling molecules, including toxins (Fig. 1) (Ianora et al. 2011).

3. PGs modulate how Biology changes Physics in the ocean.

Seawater viscosity is sometimes statistically correlated with chlorophyll content (a proxy for phytoplankton content) (Jenkinson and Biddanda 1995; Seuront et al. 2007). Microbial plankton, controlled by their genomes, microbial plankton produces and then secretes organic molecules, some of which are polymeric and act rheologically to thicken water, decreasing mechanical dispersion of water and solutes. These molecules aggregate and form structures, adding granularity to seawater (Guadayol et al. 2020). Some of these structures are sticky and trap objects, acting as mucous feeding traps and webs (Tillman et al. 2023; Reguera et al. 2024). Other polymers are hydrophobic and may decrease drag at surfaces that they coat.. These exopolymers are important for niche engineering, especially in organic aggregates, at subsurface density discontinuities and the sea-air interface (Jenkinson and Sun 2010). Such gene-influenced change in physical properties may impart Darwinian-type natural selection to control the the ocean physical environment (Jenkinson e tal., 2015).

4. PGs affect the sea surface microlayer (SML). The SML contains high abundances of virus-like particles, prokaryotic cells, and dissolved organic matter compared to non-slick SML and underlying water. The SML is thickened by EPS (Wurl et al. 2008), and it reduces exchange of materials including greenhouse gases (Jenkinson et al. 2018). Specific metabolic profiles of bacterial metagenome-assembled genomes and isolates in the slick SML included a prevalence of genes encoding motility and carbohydrate-active enzymes (CAZymes) (Rahlff et al. 2023).

5. PGs stabilize sea-surface foam (whitecaps). Ocean foams, such as whitecaps, play a crucial role in regulating Earth's temperature. The propor-

tion of incident solar radiant energy that is reflected, known as albedo, is typically ~ 0.05 for a foam-free ocean surface, whereas foam, often white in appearance, exhibits a much higher albedo of ~ 0.5 . When algal DOM increases foam stability, the proportion of foam cover increases, leading to greater reflection of solar energy back into space. This reflective property helps mitigate solar heating of the Earth (Stabeno et al. 1986; Evans et al. 2010).

The decay of ocean foams occurs through the coalescence of their constituent bubbles as interbubble water drains, causing the surfaces of adjacent bubbles to touch and eventually burst. This drainage process is slowed down when the liquid contains surfactants that bind to bubble surfaces or when it is more viscous, or both, resulting in a prolonged foam lifetime. The duration of ocean foam presence is notably extended in regions with high primary production (PP) or phytoplankton biomass (PB) compared to areas with lower PP or PB (Callaghan 2018). High foam occurrence is often associated with harmful algal blooms (HABs), including those dominated by *Phaeocyst*is spp., Margalefidinium polykrikoides, or Karenia spp. (e.g., K. selliformis). Additionally, blooms of the fish-killing dinoflagellate Alexandrium monilatum have been linked to foams causing intense itching. This species also produces goniodomines. Further investigation is warranted into the chemistry of the extracellular polymeric substances (EPS) of these organisms, which frequently contribute to increased viscosity and foam stabilization (Jenkinson 2023).

Conclusions and recommendations

The DOM in the oceans is produced, secreted, consumed and altered mostly by microbial cells under the control of their genomes. Some of this DOM is eco-active, and influences physical processes, including diffusion and exchange, by its rheological and surface properties. In future oceanographic sampling and archiving of egenomes, it is important to include associated physical, chemical and biological data, the polymeric and surfactant OM as well as measured rheological and surfactant properties of whole seawater at different scales. HABs would seem a promising place to start.

References

- Ardekani, A. M. (2022). Motile microorganisms in complex fluids. Science Talks 3, 100048.
- Banas, I. et 11 al. (2023). Spatio-functional organ ization in virocells of small uncultivated archaea from the deep biosphere. ISME Journal 17, 1789-1792.
- Biddanda, B., Dila, D., Weinke, A?n Marcuso, J., Villar-Agaiz, M., Medina S ánchez, J.M., Gonzalez-Olalla, J.M., Carillo, P. (2021). House-keeping in the hydrosphere: microbial cooking, cleaning, and control under stress. Life 11, 152.
- Callaghan, A.H. (2018). On the relationship between the energy dissipation rate of surface-breaking waves and oceanic whitecap coverage. J. Phys. Oceanogr. 48, 2609-2626.
- Evans J.R.G., Stride E.P.J., Edirisinghe M.J., An drews D.J., Simon R.R. (2010). Can oceanic foams limit global warming? Climate Res. 42, 155-160.
- Fang, H., Zhao, H., Shang, Q., Chen, M. (2012). Effect of biofilm on the rheological properties of cohesive sediment. Hydrobiologia 694, 171-181.
- Guadayol Ó. et 5 al. (2020). Microrheology re veals microscale viscosity gradients in planktonic systems. Proc. natl Acad. Sci. USA 118(1).
- Hansell, D.A., Carlson, C.A., Repeta, D.J., Schlitzer, R. (2009). Dissolved organic matter in the ocean: a controversy stimulates new insights. Oceanography 22, 202-211.
- Ianora A. et 16 al. (2011). The relevance of ma rine chemical ecology to plankton and ecosystem function: an emerging field. Mar. Drugs 9, 1625-1648.
- Jenkinson, I.R. (2023). Plankton genes and extra cellular organic substances in the ocean. J. mar. Sci. Eng. 11, 783.
- Jenkinson; I.R., Biddanda, B.A. (1995). Bulk-phase viscoelastic properties of seawater: relationship with plankton components. J.Plankton Res. 17, 2251-2274.
- Jenkinson, I.R., Seuront, L., Ding, H., Elias, F. (2018). Biological modification of mechanical properties of the sea surface microlayer, influ-

- encing waves, ripples, foam and air-sea fluxes. Elementa Sci. Anth. 6, 26.
- Jenkinson, I.R., Sun, J. (2010). Rheological properties of natural waters with regard to plankton thin layers. A short review. J. Mar. Sys. 83, 287-297.
- Jenkinson, I.R., Sun, X.X, Seuront, L. (2015). Thalassorheology, organic matter and plankton: a more viscous approach to plankton ecology.J. Plankton Res. 37, 1100-1109.
- Karn, S.K., Bhambri, A., Jenkinson, I.R., Duan, J., Kumar, A. (2020). The roles of biomolecules in corrosion induction and inhibition of corrosion: a possible insight. Corrosion Rev. 38, 403-421.
- Rahlff, J. et 13 al. (2023). Ecogenomics and culti vation reveal distinctive viral-bacterial communities in the surface microlayer of a Baltic Sea slick. ISME Comm. 3(1).
- Reguera, B., Garcia-Portela, M;, Velasco-Senovilla, E., Rial, P., Escalera, L., Diaz, P.A., Rodriguez, F. (2024). *Dinophysis*, a highly specialized plankton protist. Front. Protistol., 1.
- Seuront, L, et 7 al. (2007). The influence of *Phae ocystis globosa* on microscale spatial patterns of chlorophyll a and bulk-phase seawater viscosity. Biogeochem. 83, 173-188.
- Stabeno, P.J., Monahan, E.C. (1986). In: Monahan, E.C., Mac Niocaill, G. (ed.), Oceanic Whitecaps and their Role in Air-Sea Exchange Processes, Springer, Dordrecht, Netherlands, pp. 261-266.
- Tillmann, U., Mitra, A., Flynn, K.J., Larsson, M.E. (2023). Mucus-trap-assisted feeding is a common strategy of the small mixoplanktonic *Prorocentrum pervagatum* and *P. cordatum* (Prorocentrales, Dinophyceae). Microorganisms 11, 1730
- Verdugo, P. (2021). Marine biopolymer dynamics, gel formation, and carbon cycling in the ocean. Gels 7, 136.
- Wurl, O., Holmes, M. (2008). The gelatinous na ture of the sea-surface microlayer. Mar. Chem. 110, 89-97.

Citizen science participation can increase the coverage and speediness in harmful microalgae blooms detection

Magda Vila*, Laia Viure, Carlos Rodero, Jaume Piera, Elisa Berdalet

Institut de Ciències del Mar, ICM-CSIC, Pg. Marítim de la Barceloneta 37-49, 08003 Barcelona, Catalonia-Spain.

*corresponding author's email: magda@icm.csic.es

Abstract

Monitoring HABs requires a well established connection between scientists and environmental, food security and health authorities. It is a well-structured coalition whose central limitations are the lack of coverage of certain areas mainly due to budget-driven sampling constraints and, secondly, the slow response given the elapsed time since the problem is reported, the samplers arrive at the site, and the samples reach and are processed in the laboratory. Some of these difficulties could be overcome by the participation of the general public acquiring and transferring microphotographs of microalgae. The harmful benthic dinoflagellate *Ostreopsis* proliferates during summer months in Mediterranean beaches covering marine substrates (macroalgae, phanerogams, pebbles and sand) with a self-produced brown sticky mucilage. This mucus could be easily recognized by naked eye when people is trained to identify it. A pilot trial was developed in which volunteers were trained to recognize the mucilage containing microalgae and observe and photograph them using a cheap portable microscope. Citizen observations can increase the speediness in HAB detection and become a useful and complementary tool to established monitoring programmes.

Keywords: Citizen Science, Harmful Algal Blooms (HABs), Benthic Microalgae, Ostreopsis blooms, Mediterranean

https://doi.org/10.15027/0002041281

Introduction

Monitoring harmful algal blooms (HABs) requires established connection between scientists and environmental, food security and health authorities. It is a well-structured coalition whose main limitations are the lack of coverage of certain areas due to budget-driven sampling constraints and the elapsed time since the problem is reported, the samplers arrive at the site, and the samples reach and are processed in the laboratory. Overall, this often results in a relative slow response of the authorities to manage the HAB event.

The case of the harmful benthic dinoflagellate *Ostreopsis* is paradigmatic because it recurrently proliferates in summer (from the end of June to the end of September) in many Mediterranean beaches covering the seabed (macroalgae, phanerogams, pebbles and sand) with a sticky brown mucilage of its own production (Vila et al., 2001; Mangialajo et al., 2011; Tester et al., 2020). This mucilage is

abundant at shallow depths (<2m) and can be easily recognised with naked eye when people are trained to identify it.

The aim of this study was to develop a protocol to train citizens to recognise the benthic mucilage, collect samples and process them to acquire microphotographs with low-cost portable microscopes connected to their own smartphones that would be sent to the scientific team.

The implementation of a system with citizen participation would increase the spatio-temporal coverage of the blooms and obtain a quicker response about the specific microorganisms producing the events, improving Early Warning Systems of benthic harmful algal blooms (BHABs) already implemented (e.g. Vila et al., 2022). In addition, once the protocol is fine-tuned, it will be possible the identification of blooms by beach users in areas not systematically controlled by monitoring programmes.

Materials and Methods

Six volunteers, with ages ranging from 35 to 65 years were enrolled in this citizen science project. The first step in implementing volunteers' participation in the project was to develop a simple protocol of sample collection and observation using digital microscopes, model USB Digital Microscope (Bysameyee) and 4k Wifi Digital Microscope (Bysameyee) connected to a smartphone. The method feasibility was tested by the scientific team in the laboratory and on the beach; thereafter, it was tested with the volunteers.

Preliminary scientific tests

In the laboratory, several low-cost (less than 50 Euros) digital microscopes were tested to explore their capacity to observe *Ostreopsis*. Then, the common scientific procedure was adapted for easy use by the general trained public, as described next.

Observation protocol in field environment

The observation protocol (Fig. 1) consisted on the following steps:

- 1. Select, preferably, a rocky area with abundant macroalgae along the Catalan coast (within N 42° 25' 51.3"; E 3° 9' 57.88" and N 40° 31' 21.138"E 0° 31' 0.852") in the NW Mediterranean Sea.
- 2. Collect the macroalgae (about 5-8 g) from their base (avoid touching the bushy part containing the attached epiphyte organisms), place them in a plastic tube, fill it with seawater (50 mL) and close it. If the mucilage is observed on pebbles, rocks or sand, scrape these substrates with the tube and fill it with seawater up to 50 mL.
- 3. In the beach, shake the tube vigorously for about 60 seconds to detach the epiphyte organisms bound to the macroalgae, and remove the macroalgae with forceps.
- 4. With a plastic (Pasteur) pipette, fill a Sedgewick-Rafter counting chamber or an excavated slide with the seawater containing the detached microalgae. If using a Sedgewick-Rafter counting chamber, a semi-quantitative result of cell abundance can be obtained.
- 5. Observe the water sample using the digital microscope at two magnifications (general field and high magnification and take photos). Share the images with the scientific team, and the rest of the volunteer community, indicating site, date and, if possible, sampled macroalgae. Once observed, the

sample can be fixed with Lugol's solution and sent to the laboratory for precise cell counting.

6. Upload a picture of the macroalgae, as complementary shared observation, to be identified by the scientists or experts in the volunteer community. Then, wipe the macroalgae with paper towel and freeze them (in a regular freezer) if it cannot be sent in the same day to the laboratory. There, it will be identified and weighted for estimation of cells concentration per fresh weight.



Collect the macroalgae (5-8 g) from their base



Place it in a tube (50 mL) and fill it with seawater

Shake it vigorously for about 60"



Place the seawater containing the released microalgae in a Sedgewick-Rafter counting chamber or an excavated slide

Conduct the observation with the digital microscope and take pictures



Share the pictures with the scientific team and upload them to a citizen observatory

Take a picture of the macroalgae and share



Fig. 1. Observation protocol in field environment.

Test with volunteers

A pilot test was conducted with volunteers who were trained in the laboratory on the adapted protocol. The necessary material for sampling and the low-cost portable digital microscopes were provided. Tests included connection of the volunteer's smartphones with the microscopes.

In parallel, an experienced volunteer active contributor in citizen science projects, who had already been trained at the beach, performed his own observations using an optical microscope model Sk-T (Nikon). Photos were captured at low (100X) and high (400X) magnification attaching the smartphone camera to the ocular. Citizens' observations, in the form of microphotographs, were shared with the scientific team who could determine the presence, absence or high *Ostreopsis* abundances.

Results and Discussion

The potential of this study arises in that, by training non-academic volunteers equipped with low-cost microscopes, it is possible to collect geolocated samples at different locations along the coast to detect the presence of certain microalgae, some of them producing harmful algal events. Moreover, since the morphology of the genus *Ostreopsis* is easily recognizable, the *Ostreopsis* bloom detection by using low-cost digital microscopes is promising.

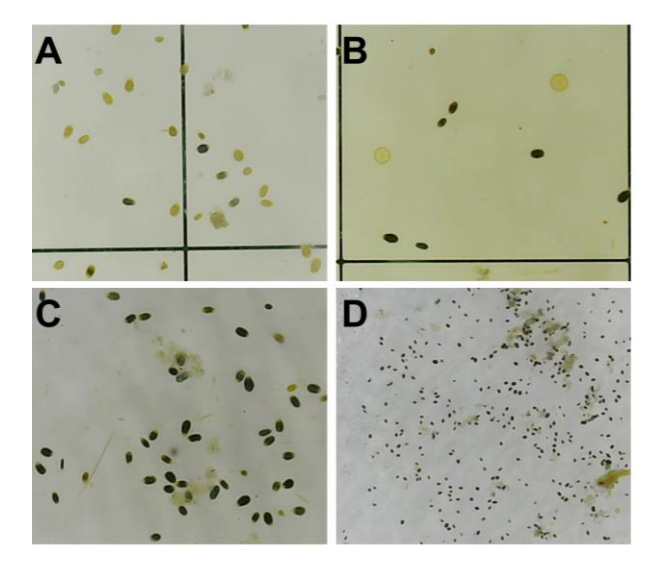


Fig. 2. Four examples of microphotographs taken during *Ostreopsis* blooms with a low-cost digital microscope. A-B. Samples in a Sedgewick-Rafter counting chamber. C. Sample in an excavated slide at high magnification. D. Sample in an excavated slide at low magnification.

The protocol designed is easy to apply and gives a qualitative information on the presence or absence of *Ostreopsis* blooms (Fig. 2). The time necessary to take the sample and obtain a photo is about 15-20 min. Moreover, if the weight of fresh macroalgae can be measured in the laboratory, semi-quantitative abundances could be inferred in most cases. As noted by different studies (e.g. Tester et al. 2020), *Ostreopsis* can attach to a diversity of macroalgae while no strict preference has been clarified. Thus, depending of the habitat and conditions, specific macroalgae or a mixture of the most abundant macroalgae present in the algal bed can be collected and this information is communicated to the scientists.

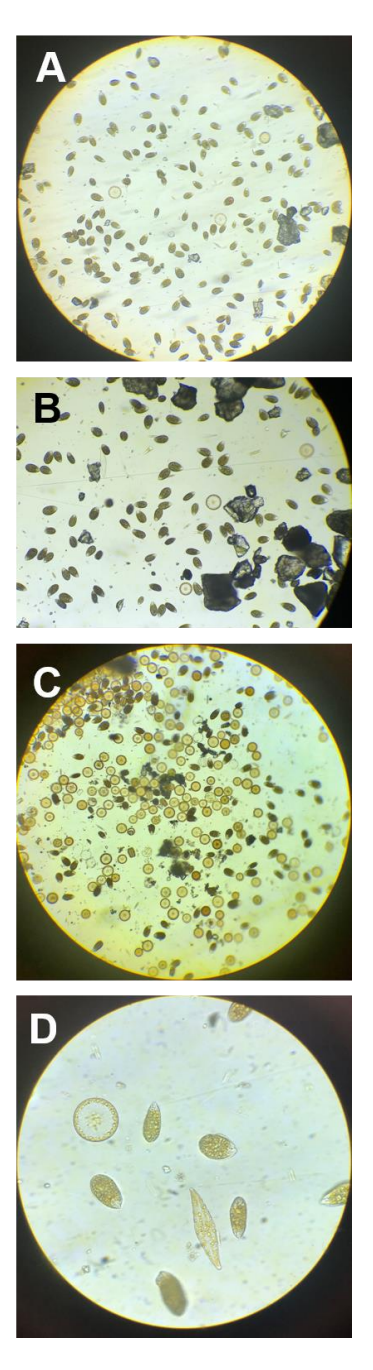


Fig. 3. Microphotographs taken by an experienced volunteer with an optical microscope. A-B. Communities dominated by *Ostreopsis* (almondshaped cells). C. Community dominated by diatoms. D. Mixed community of *Ostreopsis* and diatoms at higher magnifications (400X).

The protocol was proven satisfactory by an experienced volunteer, who obtained *Ostreopsis* microphotographs at low (100X) and high (400X) magnification using their own light Nikon microscope (Fig. 3). In turn, inexperienced

volunteers found some problems in sampling the correct site and macroalgae without a training in the field. In addition, we noticed that imaging apps (image capture applications), smartphones and microscopes are not always compatible. It was also encountered that the intensity of the sunlight intensity on the beach prevents a good vision of the smartphone screen; this is, however, an easily solvable issue.

The next step, before extending the protocol to the public or environmental associations, would be to train the sampling team of the surveillance programs, since they know what they are looking for and how it is sampled; they just need to learn how to use the device. Training people in the field when a bloom occurs is a crucial point. This allows to learn how to identify the correct macroalgae, recognize the mucilage and learning how to sample. Training using photographs is often not enough to recognize macroalgae covered by *Ostreopsis* mucilage. Other problems, such as usability issues (different smartphones, different applications) and payment for applications to obtain high-resolution images would be solved in the future.

The presented protocol is a good way to quickly detect *Ostreopsis* blooms and scientists can distinguish the three most common benthic dinoflagellates blooming in NW Mediterranean (*Ostreopsis, Coolia* and *Prorocentrum*) from the received microphotographs. Overall, sampling collection and observations by citizens can increase the speed of BHAB detection and become an useful and complementary tool for monitoring programs, including high-biomass phytoplankton blooms.

Finally, all this information can be combined with citizen science platforms, such as MINKA (https://minka-sdg.org/) and Observadores del Mar (https://www.observadoresdelmar.es/), to facilitate sharing this information to the general public. In addition, citizen participation in scientific projects increases their awareness of marine environmental issues and their ocean literacy.

In summary, a simple and easy-to-use protocol is described for non-academic users, who can collect useful data for early detection of HABs, thanks to the microalgae images that the volunteers would post on citizen science platforms. Speed gains because scientists receive the microphotograph few

minutes after the sample is taken in the field in contrast to the elapsed time in conventional monitoring programs, indicated above. In addition, as more trained volunteers are envolved, more coverage for the detection of HABs will be achieved. Therefore, if this voluntary system is applied on a large scale it can be a powerful tool used by the Administration and/or the scientific world, which could have quick information to take specific measures to manage the bloom.

Acknowledgements

This study was supported by the project "WHO IS THERE? New technological solutions for a better sampling experience when exploring the plankton community" funded by the Technological Development Projects grants of the AEI 'Severo Ochoa Centre of Excellence' accreditation (CEX2019-000928-S) of the Institute of Marine Sciences. We thank Pablo Ruiz and other five volunteers who share their time to this research.

References

Mangialajo, L., Ganzin, N., Accoroni, S., Asnaghi, V., et al., (2011). Toxicon 57, 408-420.

Tester, P.A., Litaker, W., Berdalet, E. (2020). Harmful Algae 91, 101655.

Vila, M., Garcés, E., Masó, M. (2001). Aquat. Microb. Ecol. 26, 51-60.

Vila, M., Viure, L., Lemée, R., Berdalet, E. (2022).
In: Band-Schmidt, C.J. and Rodríguez-Gómez,
C.F. (Eds.), Proc. Conference on Harmful Algae,
La Paz, B.C.S., Mexico, pp. 310-315.

Performance of high-throughput microfluidic real-time qPCR technology for the simultaneous detection of six *Alexandrium* species in environmental samples

Francesca Cucchi¹, Dave Clarke², Fiona Kavanagh¹, Amanda Curtin², Nicolè Caputo¹, Francis Butler³, Luca Mirimin^{1*}.

¹Marine and Freshwater Research Centre, Atlantic Technological University of Galway, Dublin Road, H91 T8NW Galway, Ireland.; ²Marine Institute, Rinville, Oranmore, H91 R673, Galway, Ireland; ³Biosystems Engineering, UCD School of Agriculture, Food Science and Veterinary Medicine, University College Dublin, Dublin, Ireland.

*Corresponding author's email: luca.mirimin@atu.ie

Abstract

Several species of the genus *Alexandrium* are associated with the production of Paralytic Shellfish Toxins (PSTs) causing the human illness known as Paralytic Shellfish Poisoning (PSP) through the consumption of contaminated filter-feeding molluscs. The threat to public health and the severe economic impact on shellfish industries that PST events constitute urge the development of rapid, efficient, and reliable monitoring tools. High-throughput qPCR systems such as the Standard BioTools' BiomarkHD have the potential to perform up to 9,216 reactions simultaneously, providing significant cost and time advantages. This study investigated the transferability of six previously published qPCR assays to the BiomarkHD real-time HT-qPCR system, for the simultaneous DNA detection of *Alexandrium minutum*, *A. tamarense*, *A. catenella*, *A. mediterraneum*, *A. tamutum*, and *A. ostenfeldii*. Double-stranded synthetic DNA fragments (dsDNA) and environmental samples were used to evaluate the platform performances in terms of efficiency of amplification (E), Limits of Detection (LOD), Limits of Quantification (LOQ), linearity (r²), dynamic range (DR), inhibition control, and taxonomical identification reliability. For dsDNA, BiomarkHD results were overall comparable to conventional qPCR, while on environmental samples the instrument showed better inhibition control. On the side of taxonomical identification, both platforms confirmed *Alexandrium minutum* as the species present in all the field samples analyzed.

Keywords: Alexandrium, HT-qPCR, Paralytic Shellfish Toxins, BiomarkHD, Surveillance and Management

https://doi.org/10.15027/0002041282

Introduction

Several genera of marine dinoflagellates are responsible for the occasional accumulation of biotoxins in shellfish resulting in significant impacts on human health and the blue economy. Species of the genus Alexandrium produce Paralytic Shellfish Toxins (PSTs) causing, through the consumption of contaminated filter-feeding molluscs, the human illness known as Paralytic Shellfish Poisoning (PSP). Since PST analysis in bivalve species commenced in Ireland in the mid 1990s, several PST events have been recorded. The important shellfish production area of Castlemaine Harbour, located on the Irish Southwest coast, has observed closures on mussel and oyster harvesting on an annual basis since 2019. Toxin concentrations in shellfish exceeded the PST regulatory limit as laid down in EU legislation (N. EU 853/2004, 0.8 mg Kg⁻¹ in shellfish meat). In 2021, the Irish Department of Agriculture, Food, and the Marine

(DAFM) funded a 4-year project (PSPSafe, www.pspsafe.ie), aimed at addressing knowledge gaps on causes, timing, environmental factors, and mechanistic pathways of PST occurrences in Castlemaine Harbour. The project includes the development and implementation of molecular tools to improve Alexandrium detection, surveillance, management, and early warning strategies. DNAbased multi-target technologies such as highthroughput qPCR (HT-qPCR) are promising in addressing the goal. The BiomarkHD is a chipbased automated HT-qPCR system, which uses microfluidics technology to process samples at nanolitre-scale volumes and allows the processing of up to 9,216 reactions in a single run. This promises to be an important time and cost-efficient instrument if its performances are comparable to that of qPCR (Miller et al. 2016, Olwagen et al. 2019). The aim of this preliminary study is to evaluate the transferability of six previously

published qPCR assays targeting *Alexandrium* species on the HT-qPCR system BiomarkHD.

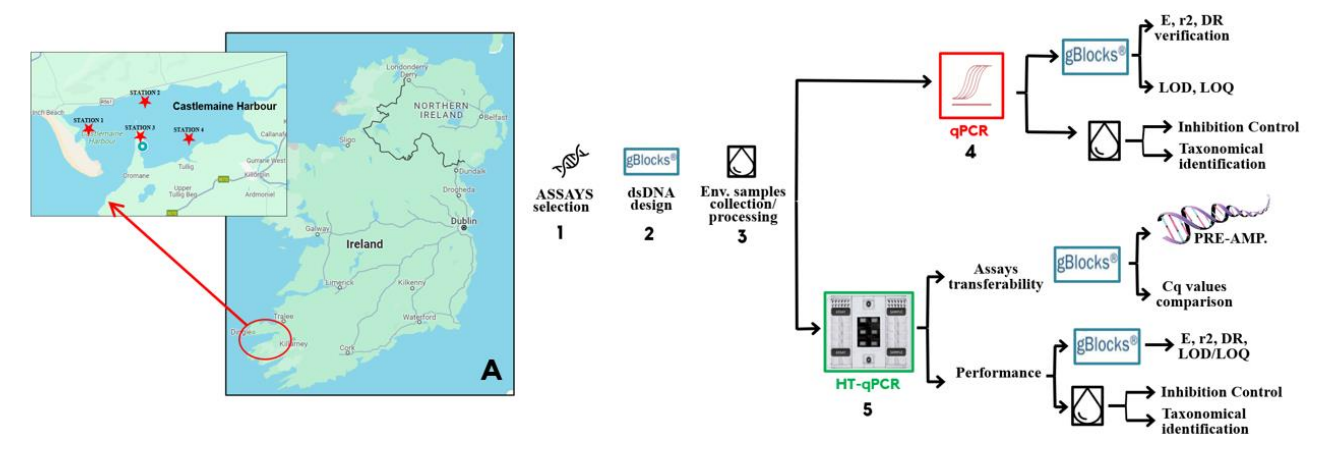


Fig. 1: Study workflow showing the main steps carried out in the present study and the sampling area (A).

Materials and Method

Study workflow and samples preparation

Fig. 1 describes the study workflow. In detail, (Step 1) six previously published qPCR species-specific assays were chosen to detect DNA of Alexandrium catenella, A. mediterraneum, A. minutum, A. ostenfeldii, A. tamarense, and A. tamutum, respectively (Collins et al. 2009, Toebe et al. 2013). (Step 2) Synthetic dsDNA fragments (gBlocks®, Integrated DNA Technologies Inc., USA) were specifically designed to match the target DNA region of each assay using the Geneious Prime® Software (version 2022.2.2). (Step 3) Environmental samples were collected Castlemaine Harbour during the Summer of 2022 over a seven-week period covering the onset and duration of an observed PST event. The water samples were collected from 4 sites (see Fig. 1A) through horizontal net tows for 4 meters using a 20 um-mesh plankton net with 30 cm diameter. The DNA was extracted from 50 mL of concentrated sample, pelleted by centrifugation (4200 rpm for 15 min), using the DNeasy Plant Pro Kit (Qiagen, Germany) following the manufacturer's instructions. (Step 4) The dsDNAs were first analysed by qPCR, to evaluate Limits of Detection (LOD) and Limits of Quantification (LOQ), and to confirm that efficiency of amplification (E), linearity (r²), and dynamica range (DR) values were as expected from previous publications and our prior analyses. (Step 5) Subsequently, to test the assays transferability and performance, samples were processed using the HT-qPCR platform.

Environmental samples were used to assess inhibition effects, due to potential presence of inhibiting substances often found in environmental

samples (Kavlick 2018), and to taxonomically identify *Alexandrium* using both qPCR and HT-qPCR techniques.

qPCR and HT-qPCR conditions

Conventional qPCR analyses were performed on a LightCycler 480 II Thermocycler (Roche Diagnostics, USA) as described by Toebe et al. (2013). For HT-qPCR analyses, the BiomarkHD instrument (Standard BioTools, USA) was used following the manufacturer's protocol for Gene Expression TaqMan Flex Six dynamic array with few modifications; primers/probes final concentrations (900 nM and 200 nM respectively) and annealing temperaature (59 °C) were as per Toebe et al. (2013).

Prior to assay runs on BiomarkHD, a preamplification step, consisting of an end-point multiplex PCR in which all the assays' primers are pooled together at the final concentration of 90 nM each, was performed on all the targets, using a Mini Amp Plus Thermal Cycler (Applied Biosystems, Thermo Fisher Scientific). Thermal cycling conditions were 95°C for 2 min, followed by 14 cycles at 95°C for 15 sec and 60°C for 4 min. After cycling, the reactions were diluted 1:5 in TE Buffer (Sigma-Aldrich, Germany). This step is required by the manufacturer for low-concentration targets (\le \) 800 copies ul⁻¹ in the final sample mix). A No Template Control (NTC, molecular grade water) was added to all the qPCR and HT-qPCR runs. For the analysis with BiomarkHD, both pre-amplified and pure NTCs were included in the final runs.

In transfering the assays from qPCR to HT-qPCR, it was first evaluated the effectiveness of the preamplification step using the assay targeting *A. minutum* as a case study. Briefly, 5 serial 100-fold

dilutions ranging from 10^8 to 1 copies μ l⁻¹ of both pre-amplified and not pre-amplified *A. minutum* dsDNA target were run on BiomarkHD in six technical replicates.

Assays transferability and performance

The technical performance of BiomarkHD was evaluated using dsDNA specific for each assay to construct standard curves. Ten serial 10-fold dilutions ranging from 108 to 10-1 copies µ1-1 were run in triplicate (qPCR) or 12 replicates (HT-qPCR). The reaction efficiency (E) was calculated as follows: $E = 100 \times 10^{-1/m} - 1$, where *m* is the slope of the standard curve for the respective assay. The slope and r² were determined from the linear regression of log versus values of the template concentration of the 10-fold standard dilution series cycle threshold. The DR was considered as the range of input template for which r^2 was ≥ 0.980 and efficiency ranged between 90 and 110%. The LOD and the LOQ on both qPCR and HT-qPCR of each assay were calculated considering the last 4 concentrations of the calibration curves in 12 technical replicates. The LOD was defined as the lowest standard concentration of template DNA that produced at least 95% positive replicates, while the LOO was the lowest standard concentration that could be quantified with a Coefficient of Variation (CV) value below 35% (Footoran et al. 2017, Kralik & Ricchi 2017, Klymus et al. 2019). The CV was calculated for each standard by the equation derived by Forootan et al. (2017):

$$CV_{\text{ln}} = \sqrt{(1+E)^{(SD(Cq))^2 * \ln(1+E)} - 1}$$

where E is the qPCR efficiency and SD(Cq) is the standard deviation of replicate Cq values.

When screening the environmental samples, an inhibition test was performed on both qPCR and HT-qPCR. Based on preliminary qPCR analysis of Castlemaine Harbour 2022 samples (data not shown), 3 selected samples were run in triplicates as neat as well as diluted (1/10 and 1/100). The result was confirmed by the use of an Internal Positive Control (IPC) spiked in the qPCR and HT-qPCR reaction mixes at known concentrations (10^3 and 10^4 copies μl^{-1} respectively). Once the best sample concentration was assessed for each instrument, 12 selected net samples were run in triplicate for all the six assays for the taxonomical identification.

Results and Discussion

Fig. 2 shows the effects of the pre-amplification step on serial dilutions of *A. minutum* dsDNA. On pre-amplified samples (Fig. 2A), there was

amplification in all the dilutions tested. A sigmoidal amplification curve was achieved from 10⁴ to 1 copies μl^{-1} , while the 10^8 and 10^6 copies μl^{-1} concentrations were too concentrated to be quantified. Without the pre-amplification step (Fig. 2B), there was amplification from 10^8 to 10^2 copies μl⁻¹; the dilution of 10⁸ copies μl⁻¹ resulted in a nonsigmoidal amplification curve, while the 10² and 1 copies µl⁻¹ were partially or completely missed. Preamplified NTCs resulted in negative for all 6 assays, indicating the absence of primer-dimer formation during the pre-amplification step. In conclusion, the pre-amplification step is required for transferring qPCR assays to the BiomarkHD, since it increases assavs' sensitivity on lower Consequently, the step was applied to all the samples analysed in this study.

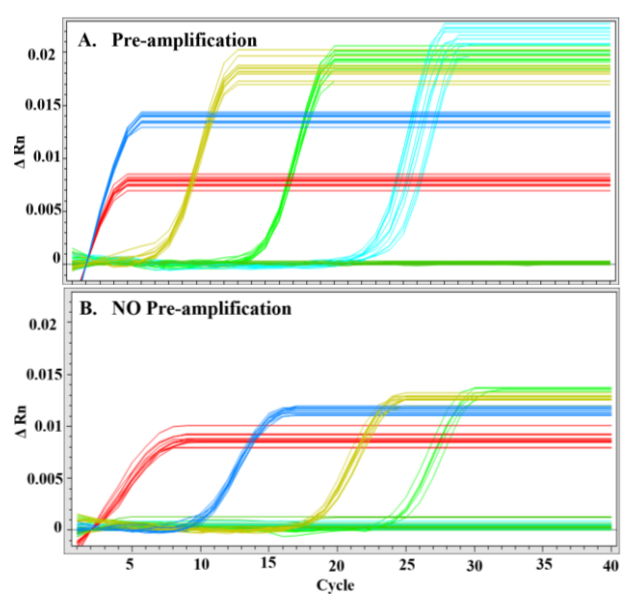


Fig. 2. Amplification curves of pre-amplified (A) and not pre-amplified (B) serial dilutions of A. minutum dsDNA. Used concentrations are 10^8 (red), 10^6 (blue), 10^4 (yellow), 10^2 (light green), 1 (light-blue) copies μl^{-1} , NTC (dark green).

In comparing the E, r^2 , LOD, LOQ, and DR range of values obtained with the six assays on qPCR and HT-qPCR it was noticed that overall, reflective of the literature (Miller et al. 2016, Olwagen et al. 2019), the performance of BiomarkHD is comparable with the one of qPCR. However, the HT-qPCR values resulted in a wider range than in qPCR. Reaction efficiencies ranged between 92 and 97% in qPCR and within 80 and 113% in HT-qPCR, with an average of 94 ± 2 and 99 ± 11 , respectively. The r^2 was always 0.99 in qPCR, and \geq 0.98 in HT-qPCR, except for the *A. catenella* (0.92) and the *A. tamarense* (0.93) assays. LOD ranges were similar

on both the instruments $(1-39 \text{ copies } \mu l^{-1})$, while LOQ was lower in qPCR than in HT-qPCR, ranging between 7-39 and 14-192 copies μl^{-1} , respectively. The DR was wider in qPCR than in HT-qPCR, ranging from 10^8 to 1 and from 10^6 to 1 copies μl^{-1} respectively. The BiomarkHD's results variability in this first preliminary study can be explained by the instrument sensitivity, the low reaction volumes, and the multiple steps required in samples preparation. Such variability is expected to decrease with further protocol optimization and routine processing.

The performance of BiomarkHD on field samples revealed good inhibition control. All the samples, as neat or diluted, were correctly amplified, and quantified, while in qPCR the neat samples gave false-negative results. These data were confirmed by the IPC test (Fig. 3). Accordingly, the remaining environmental samples were analyzed as neat on HT-qPCR and diluted 1/10 on qPCR.

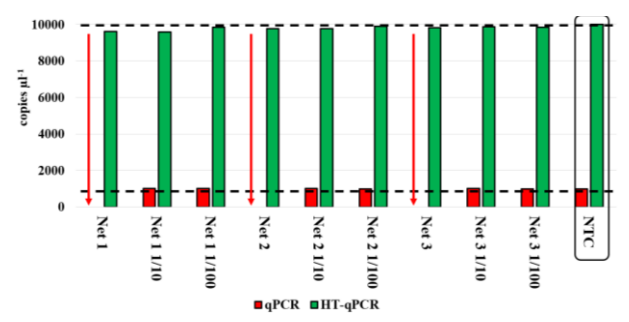


Fig. 3. IPC inhibition test results. Dashed lines indicate the IPC thresholds (copies μl^{-1}) detected in NTCs for respective platforms.

On the side of taxonomical identification, as expected, both the instruments confirmed *Alexandrium minutum* as the species present in all the 12 samples analyzed from the 2022 sampling campaign in Castlemaine Harbour (i.e. all other five assays were negative).

In conclusion, qPCR assays designed for conventional qPCR instruments can be readily transferred to the BiomarkHD instrument, with minimal optimization. This makes HT-qPCR not only a powerful tool for qPCR assays development but also a promising resource for the high-throughput screening of environmental samples, with lower risks of false negatives due to reaction inhibition. The potential of processing up to 9,216 reactions in a single run is attractive especially when the number of potential targets is high, hence providing a time and cost-effective alternative to other community-based approaches such as High

Throughput Sequencing-based metabarcoding (Esenkulova et al. 2020), and therefore increasing its applicability to the surveillance and management of toxic Harmful Algal Blooms events.

Acknowledgements

The PSPSafe Project is supported and funded by the Irish Department of Agriculture, Food and the Marine (DAFM, Project Ref 2021R578).

Thanks to the Networking and Marine Research Communication Award funded by the Marine Institute under the Marine Research Programme with the support of the Irish Government, and the ISSHA Travel Award, which enabled attendance of the first author to ICHA20.

Thanks to Castlemaine Harbour's shellfish producers and Patrick Costello (Marine Institute) for the fundamental support during the sampling operations.

References

Collins, C., Graham, J., Bresnan, Jennifer, G., Lyndsay, B., *et al.* (2009). In Proc. ICMSS09, Nantes, France.

Esenkulova, S., Sutherland, B.J.G., Tabata, A., Haigh, N., et al. (2020). FACETS 5, 784–811.

Forootan, A., Sjöback, R., Björkman, J., Sjögreen, B., *et al.* (2017). Biomol. Detect. Quantif. 12, 1–6.

Kavlick, M. F. (2018). BioTechniques 65(5), 275–280.

Klymus, K.E., Merkes, C.M., Allison, M.J., Goldberg, C.S., *et al.* (2020). Environ. DNA 2(3), 271–282.

Korenková, V., Scott, J., Novosadová, V., Jindrichová, M., *et al.* (2015). BMC Mol. Cell Biol, 16(1).

Kralik, P., and Ricchi, M. (2017). Front. Microbiol. 8(108).

Miller, K.M., Gardner, I.A., Vanderstichel, R., Burnley, *et al.* (2016). DFO Can. Sci. Advis. Sec. Res. Doc. 038, 282.

Olwagen, C. P., Adrian, P. V., and Madhi, S. A. (2019). Sci. Rep, 9(1).

Toebe, K., Alpermann, T. J., Tillmann, U., Krock, B., *et al.* (2013). Eur. J. Phycol, 48(1), 12–26.

Biotoxins profile in mussels of the north-western Adriatic Sea in the last decade (2012-2022): major contamination events and correlation with toxic phytoplankton

Giorgia Zoffoli¹, Franca Guerrini¹, Laura Pezzolesi¹, Monica Cangini², Sonia Dall'Ara², Silvana Vanucci³, Rossella Pistocchi¹

¹ Department of Biological, Geological and Environmental Sciences, University of Bologna Ravenna Campus, Via Sant'Alberto 163, 48123 Ravenna, Italy

Abstract

The north-western Adriatic Sea (above 43° N) is one of the most eutrophic areas of the Mediterranean Sea and represents an important aquaculture area, accounting for about 90% of the Italian shellfish production. Since the 1970s, HAB species have frequently occurred in this area, posing a serious health risk to consumers. Therefore, according to European legislation, seawater and shellfish in production and relaying sites are regularly monitored. This study presents an analysis of over 2000 samples collected from 2012 to 2022 as part of the official monitoring in ten production sites along the coast of the Emilia-Romagna region. During this decade, no PSP toxins were above the regulatory limit in mussels, despite the presence of Alexandrium spp. in seawater. Instead, several toxic events related to lipophilic toxins occurred, with a clear correspondence between the main phytoplanktonic species involved in the production of each toxin and the toxin presence in mussels. Yessotoxins were detected in mussels predominantly during the autumn and winter seasons from 2012 to 2015, exceeding the regulatory limit by a significant margin. Different toxin profiles related with the presence of the producing species Gonyaulax spinifera, Lingulaulax polyedra, and Protoceratium reticulatum have been observed. Diarrhoeic toxins levels increased in mussels together with the increase in cell density of several Dinophysis spp. in seawater, for which seasonal trends were observed. Multiple toxic events attributable to these toxins have been identified, each resulting in the temporary closure of shellfish production sites.

Keywords: Adriatic Sea, mussel farms, biotoxins, Dinophysis spp., Gonyaulax spinifera, Lingulaulax polyedra, Protoceratium reticulatum

https://doi.org/10.15027/0002041283

Introduction

The north-western Adriatic Sea (above 43° N) is among the most eutrophic regions in the Mediterranean Sea and serves as an important aquaculture zone, contributing to approximately 90% of Italy's shellfish production (Ciminiello and Fattorusso, 2006). Harmful algal species have been repeatedly emerging in this area since the 1970s, posing a significant health risk to consumers. Thus, according to EU Regulation 2019/627 (European Commission, 2019), seawater and shellfish in production sites are regularly monitored.

Along the Emilia-Romagna coastal region, in the north-western Adriatic Sea (Italy), the main algal

toxins responsible for shellfish contamination belong to the class of lipophilic toxins, primarily diarrhoeic shellfish toxins (DSTs), e.g., okadaic acid and derivatives (OAs), and yessotoxins (YTXs) (Pistocchi et al., 2012). The accumulation of these toxins above permitted levels has led to the closure of production sites on several occasions over the years. The first contamination event of mussels farmed in this area by OAs dates back to 1989 and was related to the presence in seawater of various species of *Dinophysis* (Boni et al., 1992), which are currently known to produce DSTs. Since that episode, OAs have been regularly found in mussels from the North-Western Adriatic Sea, always in association with low concentrations of

National Reference Laboratory for Marine Biotoxins (FCRM), Viale Vespucci 2, 47042 Cesenatico, Italy Department of Chemical, Biological, Pharmaceutical and Environmental Sciences (ChiBioFarAm), University of Messina, Viale Ferdinando d'Alcontres 31, 98166 Messina, Italy.
*corresponding author's email: giorgia.zoffoli3@unibo.it

Dinophysis spp. (Pistocchi et al., 2012) and Phalacroma spp., also known to produce DSTs. In June 1995, mussels were found to contain OAs and YTXs (Ciminiello et al., 1997); this was the first recorded instance of that class of lipophilic toxins in the Adriatic Sea. YTXs are now endemic (Rubini et al., 2021) and are produced by dinoflagellates belonging to genera within the order Gonyaulacales, which are quite common in this area, including Protoceratium reticulatum, Lingulaulax polyedra (= Lingulodinium polyedra), and Gonyaulax spinifera.

In the Emilia-Romagna region, the official laboratory for monitoring marine biotoxins in shellfish farms is the Italian Reference Centre for Marine Biotoxins (FCRM, Cesenatico, Italy). Based on the data obtained from FCRM, the present study aimed to establish a correlation between potentially toxic phytoplankton species and shellfish toxicity along the coast of this region between 2012 and 2022.

Materials and Method

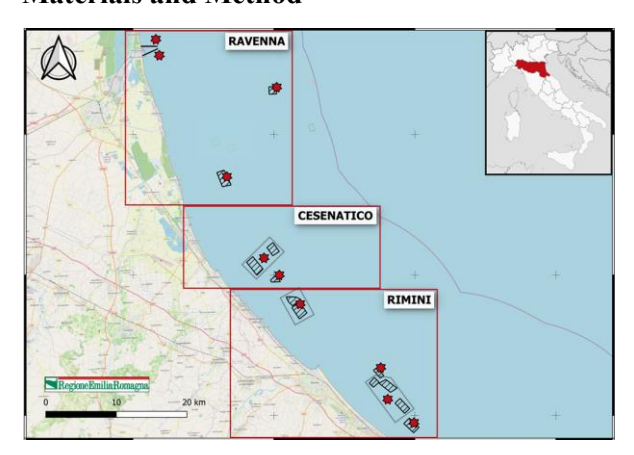


Fig. 1. Map of the production sites for *Mytilus* galloprovincialis in the north-western Adriatic Sea, from which samples were collected.

Samples of seawater and mussels (*Mytilus galloprovincialis*) were collected fortnightly from ten production sites along the Emilia-Romagna coast as part of the regional official monitoring program. According to the regional Official Gazette on "Classification of waters for the production of bivalve molluscs", these stations can be included into three main geographic areas: Ravenna, Cesenatico, and Rimini (Regional Regulation, 2021) (Fig. 1). The present work considered samples collected by the ASL

Romagna Veterinary Service between 2012 and 2022.

Phytoplankton

Until 2019, seawater samples for phytoplankton analysis were collected from production areas using plankton nets with a mesh size of 20 µm and a bucket on the surface. Beginning in August 2019, sampling using a hose sampler (Reguera et al., 2014) was implemented.

After collection, samples were preserved by adding neutral Lugol's solution, and toxic or potentially toxic species were counted following the Utermöhl method (European Standard, 2006).

Toxin analyses

In accordance with the EC Regulation 2074/2005 (European Commission, 2005), mussel samples were tested for the presence of lipophilic toxins (OAs, YTXs, PTXs, AZAs), domoic acid (DA) and saxitoxins (STXs). Quantification of lipophilic toxins was performed through LC/MS-MS analyses (EU-RL-MB, 2015). Samples were considered positive based on the criteria defined in EC Regulation 853/2004 (European Commission, 2004) and subsequent amendments. The regulatory limit for OAs is set at 160 μg kg⁻¹, while the limit for YTXs increased from 1 to 3.75 mg kg⁻¹ in 2013 (European Commission, 2013).

Data processing

The abundance of toxic phytoplankton in seawater (expressed as cell L^{-1}) and the concentration of biotoxins in mussels (expressed as μg or $mg kg^{-1}$) were grouped according to the Emilia-Romagna Official Gazette (Regional Regulation, 2021) and assigned to the ten main production sites (Fig. 1). Time series of cell abundance and biotoxin concentrations were plotted for all production sites over the decade considered.

Data were tested for normality (Shapiro-Wilks test) and homogeneity of variances (Leven's test), after assigning a random number between zero and the detection limit to samples with values below the detection limit itself. Multivariate correlation between potentially toxic phytoplankton species and biotoxins was then estimated using the non-parametric Kendall test after square root transformation of the dataset. All statistical analyses were performed using R software (R Core Team, 2022).

Results and Discussion

Saxitoxins and producing species

During the studied period from 2012 to 2022, cell densities of *Alexandrium* species ranging from approximately 10³ to 10⁴ cell L⁻¹ were detected in seawater along the coast of the Emilia-Romagna region in the north-western Adriatic Sea. Nevertheless, STXs in mussels never exceeded the regulatory limit. On the other hand, several toxic events related to lipophilic toxins were recorded, mainly due to OAs and YTXs (Fig. 2).

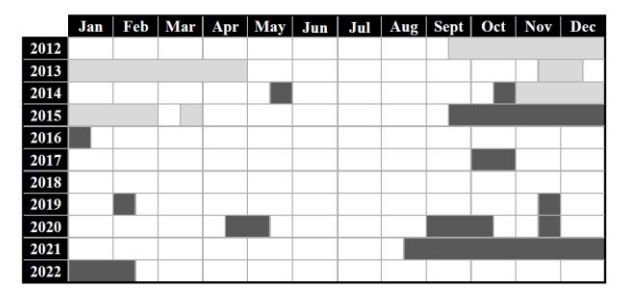


Fig. 2. Closure periods for *M. galloprovincialis* production areas along the Emilia-Romagna region coast from 2012 to 2022. Dark: closures due to the presence in mussels of OAs $> 160 \mu g kg^{-1}$ Light: closures due to the presence of YTXs in mussels > 1 or 3.75 mg kg⁻¹

Okadaic acid and derivatives and producing species

The dataset for OAs and potentially producing phytoplankton species contained 1892 records, of which 70 showed toxin concentrations above the regulatory limit. These toxic episodes, which resulted in the temporary closure of mussel farms, typically occurred from September to February, with two exceptions in May 2014 and April 2020 (Fig. 2). During those periods, several potentially OAs-producing phytoplankton species were detected in seawater, mainly belonging to the genus Dynophysis: D. acuminata complex, including D. acuminata, D. sacculus, and D. ovum, as well as D. fortii, D. caudata, and Phalacroma rotundatum. Graphs of cell counts of these potentially toxic species over the considered decade per production site, showed that in most years the highest cell counts were reached in spring by D. acuminata and D. sacculus, as also reported by Accoroni et al. (2024). Despite this, the presence of OAs in mussels at high concentrations often coexisted with the presence in seawater of D. fortii, D. caudata and P. rotundatum, albeit at low cell numbers (<10³ cell L⁻¹). Among the species

within the *D. acuminata* complex, the role of *D. acuminata* seemed unclear, as it did not consistently occur in spring and sometimes coexisted with OAs peaks, unlike other species within the same group (Fig. 3).

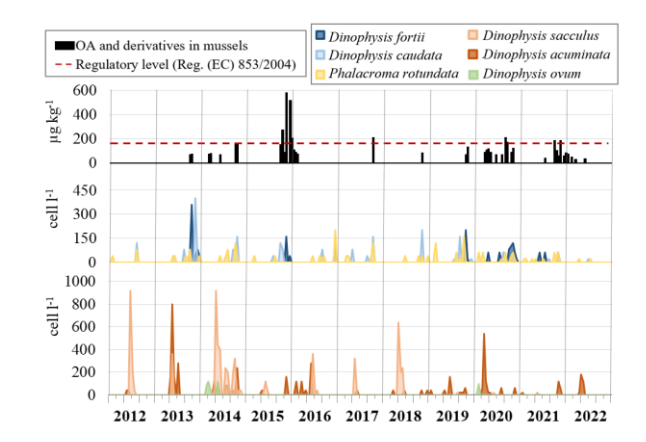


Fig. 3. Trends of OAs concentration in mussels and potentially producing phytoplankton species counts in seawater from 2012 to 2022 in the Cesenatico area.

The multivariate correlation analysis revealed a weak but positive association of OAs only with D. fortii (Kendall index 0.05). This finding can be supported by field data. For instance, over the period 2012-2022, the highest toxin concentration in mussels (941 µg OAs kg⁻¹), recorded in November 2015 in the Cesenatico area, corresponded to the presence of D. fortii in seawater, together with D. caudata and P. rotundatum, although the latter two were at extremely low concentrations (max 160 cell L⁻¹) (data not shown). In the rest of the Mediterranean Sea, the presence of OAs in bivalve molluscs typically occurs during warm seasons and is mostly associated with the *D. acuminata* complex (Reguera et al., 2014). This would indeed distinguish the north-western Adriatic Sea as a unique area compared to other Mediterranean regions, despite this assertion would require validation through further investigations.

Yessotoxins and producing species

YTXs and the list of potentially producing phytoplankton species consisted of 1829 records, of which only 35 exceeded the regulatory limit. High concentrations of YTXs in mussels leading to the closure of production areas occurred only from 2012 to 2015, mostly from early autumn to late spring (Fig. 2). During the same time periods,

various phytoplankton species that have previously been identified as YTXs producers in the northwestern Adriatic Sea were detected in seawater, i.e. *P. reticulatum*, *L. polyedra*, and *G. spinifera*. Pistocchi et al. (2012) reported that until the appearance of *G. spinifera* along the Emilia-Romagna region coasts, in 2004, YTXs detected in mussels were mostly associated with *P. reticulatum*. Since that date, the presence of YTXs in bivalve molluscs (mostly the homo-YTX analogue), has consistently coexisted with the presence in seawater of both *G. spinifera* and *L. polyedra*.

The time series of these potentially toxic species over the considered decade per production site showed that when the regulatory limit was exceeded, the highest cell counts were reached by *G. spinifera* and *L. polyedra*, with a slight delay between the peaks of cell abundance and those of toxins (Fig. 4). Correspondingly, the highest toxin concentration in mussels (8.44 mg YTXs kg⁻¹) over the period 2012-2022, recorded in November 2014 in the Cesenatico area, corresponded to the presence of 2000 cell L⁻¹ of *G. spinifera* and 120 cell L⁻¹ of *L. polyedra* in seawater (Fig. 4).

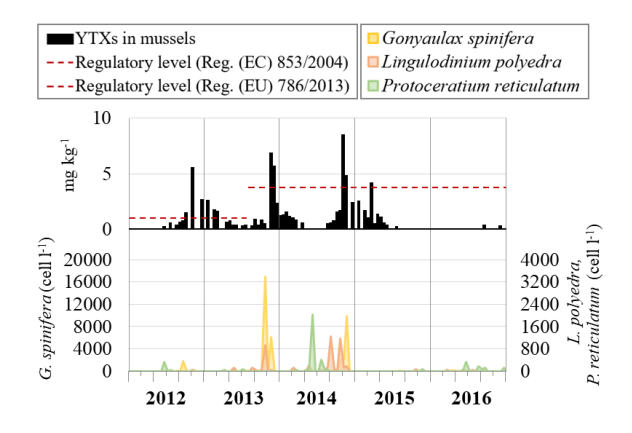


Fig. 4. Trends of YTXs concentration in mussels and potentially producing phytoplankton species counts in seawater from 2012 to 2016 in the Cesenatico area.

provide further confirmation of observations, a multivariate correlation analysis producing performed on the YTXs dinoflagellates dataset from 2012 to 2015, including the toxic profile highlighted in mussels (i.e. YTX, 45-OH YTX, homo YTX, 45-OH homo YTX). The results showed that YTX-contaminated mussels mainly contained homo YTX and 45-OH homo YTX (Kendall indexes 0.49 and 0.34 respectively). These analogues were found to be slightly but positively associated with both *G. spinifera* and *L. polyedra* (Kendall index 0.10 and 0.12 respectively), but not with *P. reticulatum* (Kendall index -0.01).

The present study is the first aimed to link toxins found in mussels to the specific presence of toxic phytoplankton species, using extensive field data from the North-Western Adriatic Sea. This holds particular significance for *Dinophysis* spp., as their toxicity could not be validated through laboratory cultures.

The results indicate an ever-changing toxic scenario in this area, both in terms of dominant toxic species and toxin production and highlights the need for a more continuous evaluation of this threat to human health and the shellfish industry.

References

Accoroni, S., Cangini, M., Angeletti, R., Losasso, C., et al., (2024). Harmful Algae 131, 102560.

Boni, L. (1992). G. Bot. Ital., 126, 229-236.

Ciminiello, P., Fattorusso, E., Forino, M., Magno, S., *et al.*, (1997). Toxicon 35, 177–183.

Ciminiello, P., Fattorusso, E. (2006). Progress in Molecular and Subcellular Biology, 53–82.

European Commission, (2004). Regulation (EC) No 853/2004 of 29 Apr 2004.

European Commission, (2005). Commission Regulation (EC) No 2074/2005 of 5 Dec 2005.

European Commission, (2013). Commission Regulation (EU) No 786/2013 of 16 Aug 2013.

European Commission, (2019). Commission Implementing Regulation (EU) 2019/627 of 15 Mar 2019.

Pistocchi, R., Guerrini, F., Pezzolesi, L., Riccardi, M., et al., (2012). Mar. Drugs 10, 140–162.

Regional Regulation, (2021). Determinazione del Responsabile del Servizio Prevenzione Collettiva e Sanità Pubblica 22 Febbraio 2021, n. 3077.

Reguera, B., Alonso, R., Moreira, A., Méndez, S., et al., (2014). Guide for Designing and Implementing a Plan to Monitor Toxin-Producing Microalgae, 2nd ed.; IOC: Paris, France, 2016.

Reguera, B., Riobó, P., Rodríguez, F., Díaz, P.A., *et al.*, (2014). Mar. Drugs 12, 394–461.

Rubini, S., Albonetti, S., Menotta, S., Cervo, A., *et al.*, (2021). Toxins 13, 634.

Pseudo-nitzschia blooms associated with rapid onset of amnesic shellfish toxin contamination in mussels from Scottish coastal waters

Sarah C. Swan, Shannon Lafferty

Scottish Association for Marine Science, Dunbeg, Oban, Argyll, Scotland, PA37 1QA, UK.

*corresponding author's email: sarah.swan@sams.ac.uk

Abstract

Pseudo-nitzschia is present in the coastal waters around Scotland throughout the year and despite the frequent occurrence of blooms, shellfish contamination with domoic acid is relatively rare. However, in the summer of 2022, blooms led to unusually high levels of amnesic shellfish toxins in mussels at four sites, with the highest concentration of 95 mg kg⁻¹ recorded in July at Braewick Voe. Pseudo-nitzschia australis was identified as the likely causative organism. Autumn blooms containing a mix of Pseudo-nitzschia species, including P. fraudulenta, occurred at some sites in the Shetland Islands in September, but were not associated with any toxicity. A regulatory monitoring programme is in place to safeguard public health, with no reported cases of human AST poisoning in the UK, although the potential for such an event exists.

Keywords: P. australis, ASTs, aquaculture, monitoring, phytoplankton, harmful algal bloom, HABs

https://doi.org/10.15027/0002041284

Introduction

The cultivation and harvesting of bivalve molluscs contribute to the Scottish economy, enabling sustainable growth in rural coastal regions (Whyte et al., 2023). In 2022, the farming of blue mussels (Mytilus edulis) directly for human consumption increased to a record high of 9,092 tonnes, with the Shetland Islands accounting for 79% of total production (Munro and Murphy, 2023). To safeguard public heath, a regulatory monitoring programme is in place with testing for biotoxin groups conducted weekly, fortnightly, or monthly, depending on the risk level (Potts et al., 2022). Amnesic shellfish toxins (ASTs) are typically monitored monthly throughout the year, but testing frequency can increase in response to a heightened risk identified through either routine shellfish phytoplankton analysis monitoring. Contamination of shellfish with domoic acid, the neurotoxin responsible for amnesic shellfish poisoning, is usually preceded by, or coincides with, an increase in the abundance of the marine pennate diatom Pseudo-nitzschia (Skov et al., 1999). While pronounced seasonal changes in density occur, the genus Pseudo-nitzschia is present in the waters around the coast of Scotland

throughout the year. Despite the frequent occurrence of blooms (defined as exceeding 50,000 cells L⁻¹), AST events are relatively rare (Rowland-Pilgrim *et al.*, 2019).

Although it is not possible to accurately identify Pseudo-nitzschia to species level using light microscopy for samples preserved with Lugol's iodine, cells may be split into size categories based on the width of the transapical axis (P. delicatissima complex <3 µm and P. seriata complex > 3 µm) (Skov et al., 1999). The P. seriata complex includes species that potentially contain a greater amount of domoic acid per cell (Trainer et al., 2012). The Pseudo-nitzschia spring blooms that occur around the Scottish coast during late March and early April are typically dominated by P. delicatissima complex cells. Bloom densities can reach several hundred thousand cells per litre and some shellfish contamination with ASTs may occur, but levels are usually below 5 mg kg⁻¹. Pseudo-nitzschia delicatissima complex cells are often abundant in mid summer (June/July), but an increasing number of P. seriata complex cells are found in the water column towards late summer and into autumn (August/September) (Brown and Bresnan, 2008; Whyte et al., 2023). This study investigated the relationship between some unusually high concentrations of ASTs detected in mussels during the 2022 regulatory monitoring, and the abundance of *Pseudo-nitzschia* in the water column.

Materials and Method

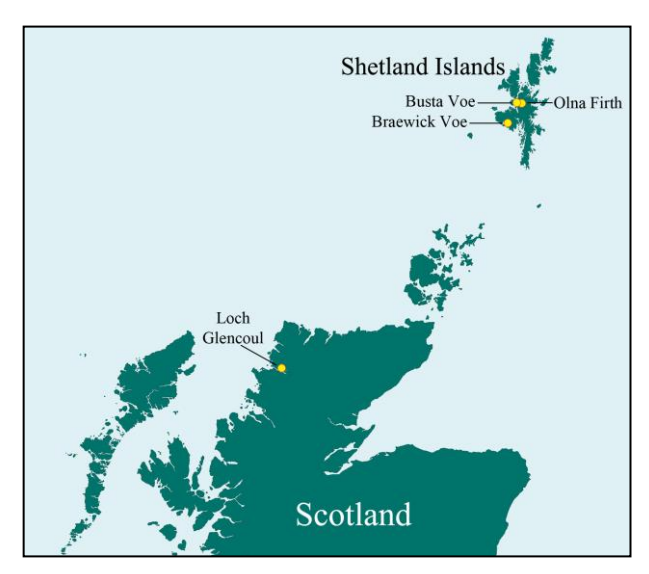


Fig. 1. Mussel harvesting sites in northern Scotland and around the Shetland Islands discussed in this study.

Seawater samples for phytoplankton analysis were collected weekly between March and mid October and at a reduced frequency over the winter months when there is less light available for growth. A well-mixed 500 mL sub-sample was fixed on site with acidic Lugol's iodine to obtain a final concentration of approximately 1%. Samples were processed following the Utermöhl method described in Andersen and Throndsen (2004), using a 50 mL sub-sample. An inverted light microscope was used to identify and enumerate the phytoplankton in the sub-sample and cell counts were converted to number of cells per litre. Seawater samples were prepared for scanning electron microscopy (SEM) analysis using the method described in Whyte et al. (2023). Pseudonitzschia was identified to species level using the fine structure measurements of individual cells.

Shellfish harvesting occurs throughout the year and shellfish samples were collected prior to and during periods of active harvesting and analysed by liquid chromatography with ultraviolet absorbance detection (Rowland-Pilgrim *et al.*, 2019). Sample

collection and analysis followed methods specified by the UK National Reference Laboratory (Marine Biotoxins), available at https://www.afbini.gov.uk/articles/nrl-marine-biotoxins-procedures-and-links.

Results and Discussion

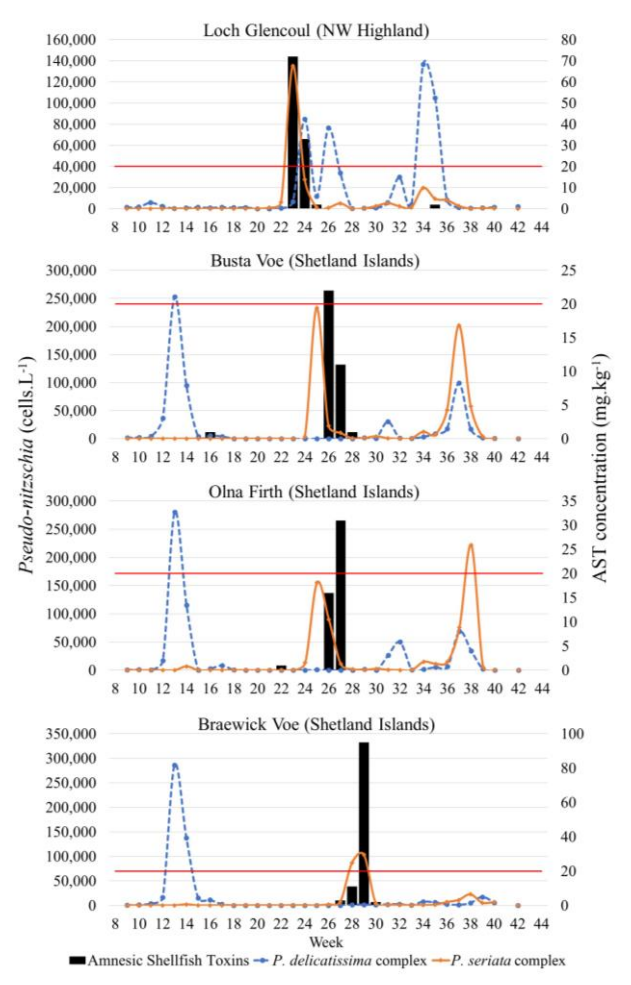


Fig. 2. *Pseudo-nitzschia* abundance and ASTs detected in mussels from four sampling sites. The red line indicates the regulatory limit for ASTs.

In 2022, regional differences were evident in the timing of *Pseudo-nitzschia* blooms, with events occurring earlier on the northwest mainland of Scotland (Loch Glencoul) compared to the Shetland Islands (Fig. 2). Spring *Pseudo-nitzschia* blooms were not observed in Loch Glencoul, but were recorded around the Shetland Islands between late March and early April (Weeks 13 and 14). *Pseudo-nitzschia delicatissima* complex cell counts reached in excess of 250,000 cells L⁻¹, whereas *P. seriata* complex cells were infrequently observed. There was little or no toxicity detected in

shellfish that was associated with these spring blooms. In contrast, *Pseudo-nitzschia* blooms observed in Loch Glencoul in June (Week 23 and 24) and around the Shetland Islands during June (Weeks 25 and 26) and July (Weeks 27, 28 and 29), were primarily composed of cells from the *P. seriata* complex. The blooms were brief in duration, with counts exceeding the threshold level of 50,000 cells L⁻¹ for only one or two weeks.

A maximum cell count for the *P. seriata* complex bloom in Loch Glencoul was recorded at 135,150 cells L⁻¹ in Week 23. In Week 25, cell counts reached 232,835 cells L⁻¹ and 155,223 cells L⁻¹ in Busta Voe and Olna Firth, respectively, whereas the bloom peak of 103,482 cells L⁻¹ was recorded slightly later (Week 29) in Braewick Voe. These short-lived blooms led to the rapid onset of AST contamination in mussels, exceeding the regulatory limit of 20 mg kg⁻¹ at the four sites. Amnesic shellfish toxin values in mussels, obtained as part of the regulatory monitoring, were reported at 33 mg kg⁻¹ in Loch Glencoul (Week 24), 22 mg kg⁻¹ in Busta Voe (Week 26), and 31 mg kg⁻¹ from Olna Firth (Week 27). Notably, mussels from Braewick Voe reached a maximum AST concentration of 95 mg kg⁻¹ (Week 29). One additional AST test on mussels from Loch Glencoul in Week 23 recorded a value of 72 mg kg⁻¹. Shellfish toxin levels decreased quickly, falling below the regulatory limit by the following week in most cases. Autumnal blooms containing a mix of Pseudonitzschia species occurred in Loch Glencoul in August (Weeks 34 and 35), and around the Shetland Islands in September (Weeks 36 to 38), with low levels of ASTs found in the mussels from Loch Glencoul.

Morphological and meristic characteristics were used to determine *Pseudo-nitzschia* cells to species level (Skov *et al.*, 1999). Identification was based on a combination of the overall dimensions and shape of the valve, the presence or absence of a central interspace in the raphe, the numbers of striae and fibulae in 10 μ m, the number of rows of poroids, and the number of poroids in 1 μ m. Analysis by scanning electron microscopy revealed the cosmopolitan highly toxic species *Pseudo-nitzschia australis* to be the likely causative organism of the AST contamination.

Pseudo-nitzschia fraudulenta and P. pungens were

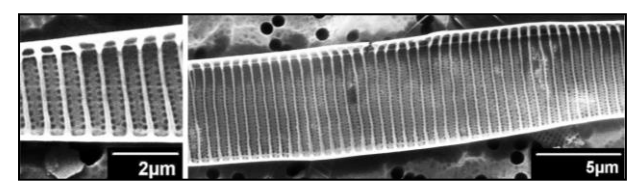


Fig. 3. SEM image showing *Pseudo-nitzschia* australis in a water sample collected from Olna Firth in June 2022 (Week 25).

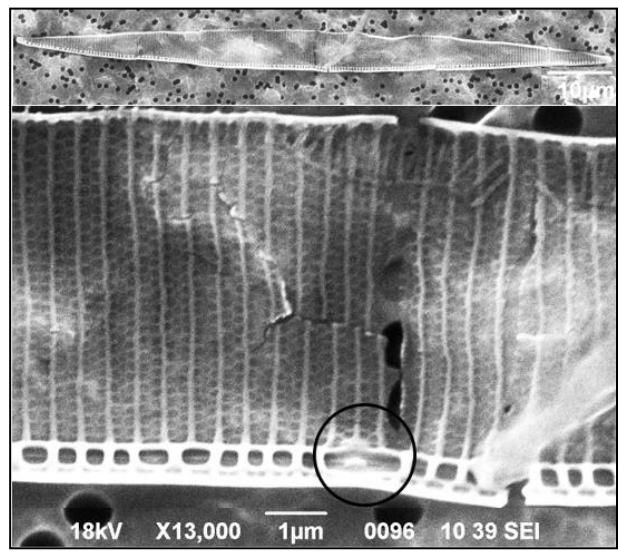


Fig. 4. *Pseudo-nitzschia fraudulenta* identified from Busta Voe in September 2022 (Week 37). The central interspace (circled) is clearly visible, along with 2-3 rows of poroids.

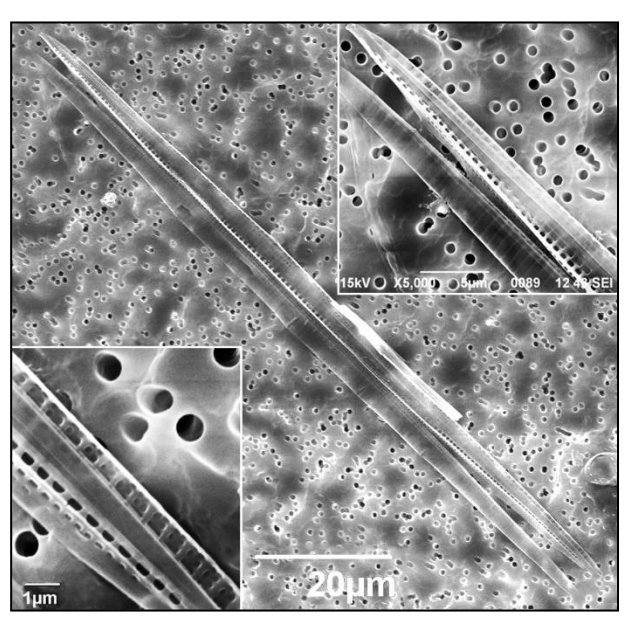


Fig. 5. *Pseudo-nitzschia pungens* from Braewick Voe in September 2022 (Week 38).

found in the autumnal blooms present around the Shetland Islands in September. Although some strains of these species are recognized as toxin-producers globally (Trainer *et al.*, 2012), there was little indication of domoic acid production by the strains found around the Scottish coast.

Amnesic shellfish toxicity in mussels exceeded the regulatory limit in another site in the Shetland Islands, Bunya Sand, in 2020 (Whyte *et al.*, 2023). This was also a rapid and short-lived event, with the causative organism again identified as *Pseudonitzschia australis*.

Mussels are known for their ability to rapidly absorb and eliminate toxins, including domoic acid, (Bresnan *et al.*, 2017; Rourke *et al.*, 2021). This can make them a valuable indicator species compared to other shellfish, although, as this study demonstrates, toxin spikes in mussels could easily be missed unless testing occurs frequently when *Pseudo-nitzschia* blooms are present.

Shellfish testing frequency is determined by risk assessment, and testing is seasonal and targeted at locations with a history of toxicity in shellfish. However, the relationship between a harmful algal bloom event and shellfish toxin contamination becomes less clear when testing does not occur, often the case when a harvesting site is closed due to the presence of other toxin groups. This can complicate future risk evaluations. The occurrence of ASTs around Scottish coastal waters is likely underestimated and even though no instances of human AST poisoning have been officially documented in the UK, the potential for such an event remains.

Acknowledgements

Food safety is regulated by Food Standards Scotland, following retained EU regulation 2019/627. Official control testing of shellfish tissue is carried out by the Centre for Environment, Fisheries and Aquaculture Science (Cefas). The Scottish Association for Marine Science (SAMS) monitors inshore coastal waters for potentially toxic phytoplankton. Data are available at https://www.foodstandards.gov.scot/business-and-industry/industry-specific-advice/shellfish/shellfish-results

References

- Andersen, P., Throndsen, J. (2004). Estimating cell numbers. In: Hallegraeff, G.M., Anderson, D.M., Cembella, A.D, Enevoldsen, H.O. (eds.). Manual on Harmful Marine Microalgae. 2nd revised edition. UNESCO, Paris, France, pp. 99-129. https://doi.org/10.25607/OBP-1370
- Bresnan, E., Fryer, R., Fraser, S., Smith, N., Stobo, L., Brown, N., Turrell, E. (2017). Harmful Algae, 63, 193-202.
- Brown, L., Bresnan, E. (2008). Proceedings of the 12th International Conference on Harmful Algae. Intergovernmental Oceanographic Commission of UNESCO, Copenhagen, pp. 165–167.
- Munro, L.A., Murphy J. (2023). Scottish Shellfish Farm Production Survey 2022. Marine Scotland. Available at https://www.gov.scot/publications/ 132 cottish-shellfish-farm-production-survey-2022/documents
- Potts, J., Mayer, C.-D., Horgan, G., Swan, S., Brook, T., Davidson, K. (2022). Risk assessment of the Scottish monitoring programme for marine biotoxins in shellfish harvested from classified production areas FSS/2020/042, 116 pp. Available at https://www.foodstandards.gov.scot/downloads/Biotoxin_risk_assessment_-FSS_2020-042.pdf
- Rourke, W.A., Justason, A., Martin, J.L., Murphy, C.J. (2021). Toxins, 13, 168. https://doi.org/10.3390/toxins13020168
- Rowland-Pilgrim, S., Swan, S.C., O'Neill, A., Johnson, S., Coates, L., Stubbs, P., Dean, K., Parks, R., Harrison, K. and Alves, M.T. (2019). Harmful Algae 87: 101623.
- Skov, J., Lundholm, N., Moestrup, Ø., Larsen, J. (1999). Potentially Toxic Phytoplankton, 4. The diatom genus *Pseudo-nizschia* (Diatomophyceae / Bacillariophyceae). In: Lindley J.A. (ed). ICES Identification Leaflets for Plankton, No. 185, 23 pp.
- Trainer, V.L., Bates, S.S., Lundholm, N., Thessen, A.E., Cochlan, W.P., Adams, N.G., Trick, C.G. (2012). Harmful Algae, 14, 271-300. https://doi:10.1016/j.hal.2011.10.025
- Whyte, C., Swan, S.C., Turner, A.D., Hatfield, R.G., Mitchell, E., Lafferty, S., Morrell, N., Rowland-Pilgrim, S., Davidson K. (2023). Toxins, 15, 554. https://doi.org/10.3390/toxins15090554

Official control protocol in the Canary Islands (Spain) for detecting CTXs in commercial fish from first sale points

Fernando Real*, Natalia García-Álvarez, Freddy Silva, María J. Ramos-Sosa, Yefermin Darias-Dágfeel, Paula Poquet, Daniel Padilla, Breixo Sánchez, Andres Sanchez-Henao

Address – University Institute of Animal Health and Food Safety (IUSA). University of Las Palmas de Gran Canaria. Carretera de Trasmontaña, s/n; 35416.- Arucas, Las Palmas (Spain)

*corresponding author's email: fernando.real@ulpgc.es

Abstract

Ciguatera poisoning (CP) has been known in the Canary Islands since 2004. To fight the disease, a control program is being carried out since 2011. The experience acquired in recent years through this program has made it possible to establish risk species in relation to minimum weights for all fish marketed, from which a sample must be analyzed and obtain a negative result, before being sold for human consumption. The current list contains the following species with weights equal to or greater than those indicated: island grouper (*Mycteroperca fusca*, 7 kg); amberjack (*Seriola* spp., 12 kg); dusky grouper (*Epinephelus marginatus*, 12 kg); bluefish (*Pomatomus saltatrix*, 9 kg) and wahoo (*Acanthocybium solandri*, 35 kg). The results of this program are very reliable and all fish with negative results are released to the market for consumption. No person has been poisoned during these years, and more than 15,000 fish have been evaluated. It must be highlighted that the proportion of CTX-positive fish detected (LOD: 0.003-0.008 ppb Eq. CTX1B) in the Canary Islands has risen from 9.9% in 2017 to 19.2% in 2023. The causes of the new outbreaks of CP detected are discussed in this work.

Keywords: Ciguatera poisoning, CTX, food safety, official control protocol, Canary Islands

https://doi.org/10.15027/0002041285

Introduction

The Canary Islands are a Spanish archipelago located in the northwest coast of Africa, approximately 100 km far from the Mauritanian coast. This location may be an important factor to be influenced by climate change, resulting in increased water temperature, which has facilitated favorable environmental conditions for the proliferation of different species of microalgae belonging to the genus *Gambierdiscus*.

In recent years, different outbreaks of ciguatera poisoning (CP) have occurred in the Canary Islands. The first case was detected in 2004 (Pérez-Arellano et al, 2005), in which two fishermen caught a 26 kg amberjack (medregal negro; *Seriola rivoliana*), which they consumed, resulting in the poisoning of five family members.

In the following years several CP outbreaks were recorded. Until now, more than 120 people have been poisoned in the Canary Islands for this cause,

corresponding to a total of 21 outbreaks (General Directorate of Public Health, 2022). For this reason, CP was included, in 2015, in the regional statement of notifiable diseases.

The Government of the Canary Islands has been involved by implementing an official control program since 2011 to prevent new CP cases. It consists of the detection of ciguatoxins (CTX) in samples of certain weights of some fish species, considered a potential risk in this region for transmitting the toxin to consumers (Table 1) (General Directorate of Fisheries, 2023).

At the same time, not all the specimens of a fish species mentioned in the protocol are considered, they also have to be greater than the established weight. Years of experience have made possible to establish certain fish species and weights that pose a risk for the consumers.

Materials and Method

Marine environment allows CTX accumulation in the trophic web, especially in carnivorous fish that are at the top. This is the reason why fish with certain weights are included in the official control protocol (Table 1). Each specimen that meets these conditions is individually subjected to CTX control in the laboratory.

Table 1.-Species and size of fish subjected to the

protocol

Common name	Scientific name	Limit weight (kg) *
Island- grouper	Mycteroperca fusca	7
Amberjack	Seriola spp.	12
Dusky grouper	Epinephelus marginatus	12
Bluefish	Pomatomus saltatrix	9
Wahoo	Acanthocybium solandri	35

^{*}Fish of this weight or greater are analyzed

There is a commission to update the species and size of fish that must be subjected to analysis. Sport fishing is not included in the official protocol because it is considered for self-consumption.

Protocol for CTX detection

Three hundred grams of flesh samples are taken from the tail of each fish specimen at the first sales points of each fish specimen that must be analyzed and are sent directly to the laboratory. The fish remain frozen in the meantime. Once the results are obtained, they are placed on an application, which automatically informs the first sales points.

Fish samples in which CTX is detected are marked as SANDACH for destruction, while the negative ones are released for human consumption (General Directorate of Fisheries, 2023).

The analysis method includes two phases: a) extraction of CTX from the sample, following the method described by Lewis (2003), this method describes the steps that need to be implemented to extract and clean CTX from fish muscle.

Briefly, to extract CTX from the flesh, the whole flesh sample received, without skin and connective tissue, is homogenized and a portion of 10 g of flesh is cooked at 70 °C for 10 min. Twenty mL of acetone is added at room temperature, mixed with an ultraturrax and centrifuged at $3000 \times g$ during 5 min at 4 °C. This last step is repeated twice, and both supernatants are pooled.

The resulting acetone is filtered through a 0.45 μm of PTFE filter and evaporated with a rotary evaporator at 55 °C. The dried extract is resuspended in methanol:water (9:1) and *n*-hexane for phase separation. The upper phase of n-hexane is discarded, and fresh n-hexane is added for a second liquid-liquid partition and discarded again, the methanol phase is dried under N₂ current at 40 °C for a subsequent partition with ethanol:water (1:3) and diethyl-ether (DEE). The DEE is reserved, then a fresh DEE is added to the ethanol:water phase, after phase separation, both DEE are pooled and evaporated under N₂ current to dryness. The final residue is resuspended in 4 mL of methanol and kept at -20 °C to be used in the cell-based assay (CBA).

b) The CBA with neuroblastoma (neuro-2A) cells, is performed following the method described by Caillaud et al. (2012).

In brief, neuro-2A cells are seeded in a 96-well flat bottom microplate (200 µL well-1) (RPMI medium supplemented with 5% of FBS). Density of 34,000 cells is placed per well. Cells are incubated for 24 h. Two solutions, ouabain (0.12 mM) and veratridine (0.012 mM), are added to half of the seeded wells. Mortality will be seen in the half of the pretreated microplate if there is presence of CTX in the sample. Due to the large number of fish samples received each week (aprox. 40) it is not able to perform a full dose-response curve per sample, a screening of two concentration is performed instead (100 and 50 mg TE·mL-1) (Fig. 1).

A dose-response curve with CTX1B standard (STD) is always performed as an internal control. Every sample extract and the STD were assayed in triplicate. After a 20 h-period of exposure to fish extracts and to CTX1B standard solution, cell viability is evaluated with MTT [3-(4,5-dimethylthiazol-2-yl)-2,5-diphenyltetrazolium] and DMSO (dimethyl sulfoxide) solutions.

Finally, absorbances are read at 570 nm by a multiwall spectrophotometer scanner and plotted into the Microsoft Office Excel 2016 and GraphPad Prism 9 softwares (GraphPad, San Diego, California, USA). Less than 20% of cell mortality is considered as a non-toxic effect (Caillaud et al., 2012).

The concentration of CTX1B STD causing 20% inhibition of cell viability (IC20) is set as the LOD and LOQ according to this concentration of fish extract used for testing. Maximum concentration of extracts set to avoid matrix effect (100 mg TE·mL¹), the LOD/LOQ ranges between 0.003 and 0.008 pg Eq. CTX1B/mg TE of sample (ppb Eq. CTX1B).

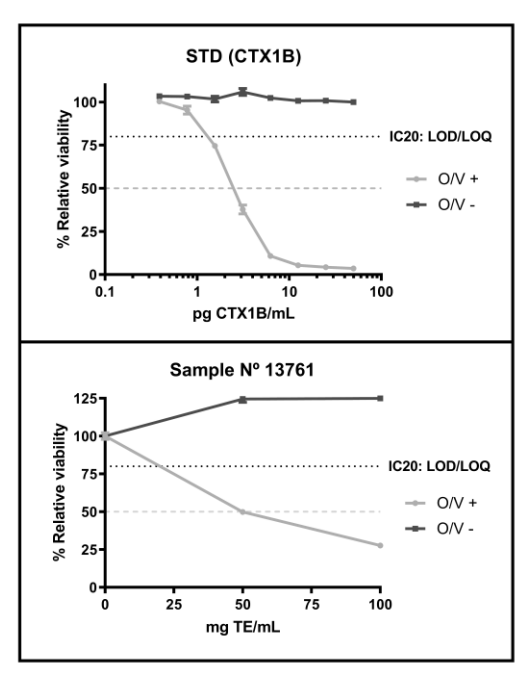


Figure 1. Representative dose-response curves obtained by neuro-2a CBA with a) CTX1B STD, and b) CTX detected in a fish sample from the official protocol.

Results and Discussion

Species and number of CTX-like positive samples The percentage of samples with CTX-like activity found in the official control protocol has varied slightly in recent years. Between 2012 and 2015, it reached a percentage of 12% (variation: 9.9-13.5%). However, in recent years the risk represented by specimens of less weight of the species considered at risk has increased the number of samples received at the laboratory. Therefore, the relative number of positive results has been

raised reaching 16.7% for the year 2022, while in 2023 this value has increased to 19.2% (Figure 2). This increase could be also related to climate change and rising seawater temperatures. Although it is noteworthy that this increase in toxicity was not gradual, as toxicity was 4.2% in 2020.

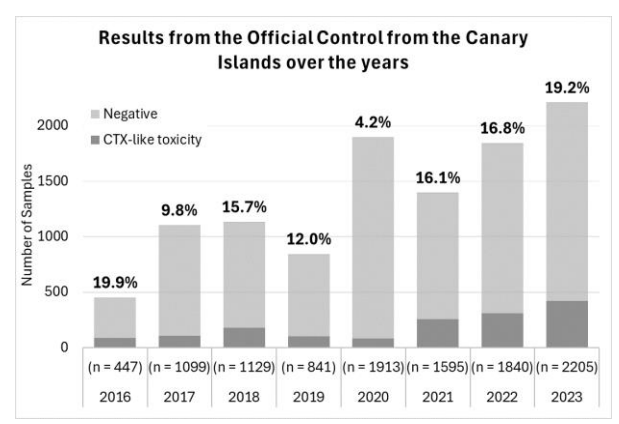


Figure 2.- Results of the number of samples analyzed in the official control protocol of CTX in the Canary Islands between 2016 and 2023.

In 2022, the islands with the greatest percentage of positives samples were El Hierro, La Palma, and Gran Canaria, with 48.2%, 44.4% and 36.5%, respectively (Table 2). These results varied with respect to 2017, when Lanzarote had the highest toxicity rate (52.9%), followed by Fuerteventura (21.0%), Gran Canaria (17.8%) and El Hierro (15%). Furthermore, La Palma was one of the islands with the lowest toxicity rate, with only 5.1% (Sanchez-Henao et al., 2019). These data have changed slightly in 2023, but it is important to check how its trend is increasing.

Table 2.- The number of positive and negative fish samples detected for CTX on the seven Canary Islands by CBA is shown, and the frequency of presentation for the year 2022.

	T . 1	N T	D '.'
Islands*	Total	Negatives	Positives
	(n)	(n) (%)	(n) (%)
LZ	414	324 (78.3%)	90 (21.7%)
FU	246	201 (81.7%)	45 (18.3%)
GC	96	61 (63.5%)	35 (36.5%)
TF	615	528 (85.8%)	87 (14.2%)
LG	381	370 (97.1%)	11 (2.9%)
LP	27	15 (55.6%)	12 (44.4%)
EH	54	28 (51.8%)	26 (48.2%)
TOTAL:	1833	1527 (83.3%)	306 (16.7%)

*LZ = Lanzarote; FU = Fuerteventura; GC = Gran Canaria; TF = Tenerife; LG = La Gomera; LP = La Palma; EH = El Hierro.

In general, the amberjack and dusky grouper were the species with the greatest representation in the official monitoring, accounting for more than 95% of the samples received. In fact, these two species of fish are also the ones most involved in causing CP outbreaks in this Region (General Directorate of Public Health, 2022).

Regarding fish species, in the last year, 2023, wahoo was the fish species with the highest relative number of positive samples (66.7%), followed by bluefish (21.4%), dusky grouper (20.3%), and amberjack (18.4%). None of the four island grouper samples analyzed showed toxicity.

CTX evaluation and control protocol

The establishment of an official protocol to control the spread of CTXs in the food safety of the region was a decisive factor in ensuring the continued safe consumption of fish. To the best of our knowledge, this preventive monitoring is unique to this area of the world.

When assessing the effectiveness of the official control protocol developed in this region, it is important to note that since 2011, year when tests to detect CTX began, more than 15,000 samples have been submitted for CTX detection in the laboratory. And there is a very important fact to highlight in terms of food safety: "no case of CP has been detected in all the fish without CTX-like activity obtained in the official protocol and released for human consumption".

From a public health perspective, it is important to remark that all current CP outbreaks in the Canary Islands are linked to illegal or sport fishing (General Directorate of Public Health, 2022).

Finally, some conclusions should be proposed from the results obtained in this work. The Canary Islands is an area of expansion of CP endemicity, therefore a monitoring of CTX accumulation in fish and the presence of *Gambierdiscus* spp. in Canary marine waters must be emphasized.

Official control protocol has demonstrated to be a safe and reliable tool for monitoring CTX in fish for consumption in this area. In order to enhance food safety for all consumers, sport fishing should be included in an official plan, allowing the control of CP cases in regions where this disease is endemic.

Acknowledgements

The authors thank the Directorate-General for Fisheries of the Canary Government as responsible of the official control program of ciguatera in the Canary Islands. A. Sanchez was funded by the research staff training aid program Catalina Ruiz from Canary Islands Research Agency (ACIISI, APCR2022010011), Y. Darias was funded by (ACIISI, TESIS2021010048) and P. Poquet by investigo program ULPGC (32/39/2022, Next Generation EU).

This work was also supported by the EuroCigua project, Spain ('Risk characterization of ciguatera poisoning food in Europe' [GP/EFSA/ AFSCO/2015/03]); CIGUARISK/CIGUAFOOD ('Food risks associated with ciguatoxins monitoring and tracking the toxins toxin/producing organisms in marine ecosystems' [PID 2019-108781RR-C21, PID 2019-108781RR-C22]); and RASPA ('Red Atlántica para la vigilancia Sanitaria de los productos Pesqueros y [INTERREG MAC Acuícolas' 2014–2020, MAC2/1.1A/305])

References

- Caillaud, A., Eixarch, H., de la Iglesia, P., Rodríguez, M. et al. (2012). Food Addit Contam Part A Chem Anal Control Expo Risk Assess, 29(6), 1000-1010.
- General Directorate of Fisheries (2023). Official control protocol for the detection of ciguatoxin in fish sampled at first sale points. Canary Government. Las Palmas de Gran Canaria.
- General Directorate of Public Health (2022). Summary of records from Epidemiological Surveillance System for Ciguatera Poisoning in the Canary Islands, period 2008–2022. Canary Government. Las Palmas de Gran Canaria.
- Lewis, R.J. (2003). In: Hallegraeff, G M; Anderson, D M; Cembella, and A D (ed). Manual on Harmful Marine Microalgae. UNESCO Publishing, Landais (France), pp. 267-277.
- Pérez-Arellano, J.L., Luzardo, O.P., Pérez Brito, A., Hernández Cabrera, M., et al. (2005). Emerg Infect Dis, 11(12), 1981-1982.
- Sanchez-Henao, J.A., García-Álvarez, N., Fernández, A., Saavedra, P, et al. (2019). Sci. Total Environ., 673: 576-584.

AUTHOR INDEX

Accoroni, S25	Haq, S 97
Aiswararya, N.M	Harman, T
Allen R. Place97	Hart, C
Arnich, N45	Haugum, M 77
Arima, D29	Hayashi, K
Bachvaroff, T61	Ikeda, C.E
Bachvaroff, T.R97	Imai, I29, 81
Band-Schmidt, C.J17	Inaba, N 81
Berdalet, E113, 117	Islam, S.S109
Bill, B.D37	Iwataki, M89, 93
Bolch, C109	Jagus, R101
Boyer, G.L53	Jenkinson, I.R113
Bridle, A109	Johansen, T.A
Brown, N.L53	Jolly, E
Butler, F	Judd, M101
Cadier, M49	Kanamori, M
Campbell, L	Karn, S113
Cangini, M	Kavanagh, F69, 121
Gaonkar, C.C	Keck, M 45
Caputo, N	Kibler, S 41
Chin, WC	Klein, C
Clarke, D69, 121	Kudela, R.M57, 73
Cochlan, W.P37	Kuroda, H29
Cucchi, F	Kuwata, K 93
Curtin, A121	Lafferty, S129
Cusick, K.D53	Leyva-Valencia, I17
Dall'Ara, S125	Lie, A
Darias-Dágfeel, Y133	Liret, C
Dreckmann, K.M33	Litaker, W 21
Emri, I 113	Lum, W.M 93
Fragoso, G.M77	Mari, X113
García-Álvarez, N133	Márquez, S.H
Gonçalves, R 113	Masura, J 41
Greengrove, C41	Matsushima, R89, 93
Guadayol, O113	Matweyou, J41
Guerrini, F125	Mirimin, L69, 121

Moal, M.L.	49	Sourisseau, M	49
Molgó, J	45	Stahl, A	
Mrokowska, M	113	Sun, J	113
Neri. F	25	Suzuki, T	85, 89, 93
Numano, S	89, 93	Swan, S.C	129
Núñez-Resendiz, M.L.	33	Takahashi, K	89, 93
Murray, S	109	Tester, P	21
Oikawa, H	89, 93	Totti, C	25
Okolodkov, Y.B	17	Trainer, V.T	37
Ozawa, M	89, 93	Trapp, A	57
Padilla, D	133	Trick, C.G	37
Pezzolesi, L	125	Ubaldi, M	25
Piera, J	117	Uchida, H	85, 89, 93
Pistocchi, R	125	Urman, A	45
Place, A.R	21, 61, 101	Vale, P	65, 85
Plus, M	49	Vandersea, M	41
Pondaven, P	49	Vanucci, S	125
Poquet, P	133	Vila, M	117
Rahlff, J	113	Viure, L	117
Ramos-Santiago, A.E	17	Walton, J	73
Ramos-Sosa, M.J	133	Watanabe, R	89, 93
Real, F	133	Wei, B	53
Rodero, C	117	Widder, E.A	53
Romagnoli, T	25	Williams, E.P	97
Sakamoto, S	29	Wira, J	21
Sánchez, B	133	Wurl, O	113
Sanchez-Henao, A	133	Wyatt, T	113
Sánchez-Puga, P	113	Yamamoto, K	81
Sato, M	29	Yasunaga, T	29
Schweibold, L	49	Yuasa, K	93
Sentíes, A	33	Zamudio-Resendiz, N	M.E33
Servent, D	45	Zoffoli, G	125
Shimada, H	29		
Shinada, A	29		
Shikata, T	93		
Silva, F	133		
Silva, F.O.T.	33		
Smith, J	73		

